(4)

AFGL-TR-88-0041



# SATELLITE INSTRUMENT DEVELOPMENT AND DATA ANALYSIS

Louise Gentile
Ernest Holeman
Alan Huber
Stephen Kahler
John Pantazis
David Webb
M. Patricia Hagan

The Trustees of Emmanuel College
400 The Fenway
Boston, Massachusetts 02115

Final Report
1 April 1982 - 30 June 1987

30 September 1987



Approved for public release; distribution unlimited

AIR FORCE GEOPHYSICS LABORATORY
AIR FORCE SYSTEMS COMMAND
UNITED STATES AIR FORCE
HANSCOM AFB, MASSACHUSETTS 01731

SATELLITE INSTRUMENT DEVELOPMENT AND DATA ANALYSIS

"This technical report has been reviewed and is approved for publication"

DAVID A. HARDY
Contract Manager

E.G. MULLEN
Branch Chief

FOR THE COMMANDER

RITA C. SAGALYN
Division Director

This report has been reviewed by the ESD Public Affairs Office (PA) and is releasable to the National Technical Information Service (NTIS).

Qualified requestors may obtain additional copies from the Defense Technical Information Center. All others should apply to the National Technical Information Service.

If your address has changed, or if you wish to be removed from the mailing list, or if the addressee is no longer employed by your organization, please notify AFGL/DAA, Hanscom AFB, MA 01731. This will assist us in maintaining a current mailing list.

Do not return copies of this report unless contractual obligations or notices on a specific document requires that it be returned.

Unclassified
SECURITY CLASSIFICATION OF THIS PAGE

## REPORT DOCUMENTATION PAGE

| | |
|---|---|
| 1a. REPORT SECURITY CLASSIFICATION: Unclassified | 1b. RESTRICTIVE MARKINGS: None |
| 2a. SECURITY CLASSIFICATION AUTHORITY: N/A | 3. DISTRIBUTION/AVAILABILITY OF REPORT: Approved for publication; distribution unlimited |
| 2b. DECLASSIFICATION/DOWNGRADING SCHEDULE: N/A | |
| 4. PERFORMING ORGANIZATION REPORT NUMBER(S): Technical Report - Final | 5. MONITORING ORGANIZATION REPORT NUMBER(S): AFGL-TR-88-0041 |
| 6a. NAME OF PERFORMING ORGANIZATION: Emmanuel College; 6b. OFFICE SYMBOL (If applicable): PRD | 7a. NAME OF MONITORING ORGANIZATION: Air Force Geophysics Laboratory |
| 6c. ADDRESS (City, State and ZIP Code): 400 The Fenway, Boston MA 02115 | 7b. ADDRESS (City, State and ZIP Code): Hanscom AFB MA 01731, ATTN: Dr. David Hardy |
| 8a. NAME OF FUNDING/SPONSORING ORGANIZATION: USAF AFSC ESD PKR; 8b. OFFICE SYMBOL (If applicable): | 9. PROCUREMENT INSTRUMENT IDENTIFICATION NUMBER: F19628-82-K-0039 |
| 8c. ADDRESS (City, State and ZIP Code): Hanscom AFB MA 01731 | 10. SOURCE OF FUNDING NOS. |

| PROGRAM ELEMENT NO. | PROJECT NO. | TASK NO | WORK UNIT NO |
|---|---|---|---|
| 62101F | 7601 | 12 | AN |

11. TITLE (Include Security Classification): Satellite Instrument Development and Data Analysis

12. PERSONAL AUTHOR(S): Louise Gentile, Ernest Holeman, Alan Huber, Stephen Kahler, John Pantazis, David Webb, M. Patricia Hagan

| 13a. TYPE OF REPORT | 13b. TIME COVERED | 14. DATE OF REPORT (Yr., Mo., Day) | 15. PAGE COUNT |
|---|---|---|---|
| Final | FROM 4/1/82 TO 6/30/87 | 87 September 30 | 116 |

16. SUPPLEMENTARY NOTATION

| 17. COSATI CODES | | | 18. SUBJECT TERMS (Continue on reverse if necessary and identify by block number) |
|---|---|---|---|
| FIELD | GROUP | SUB GR | DMSP, Auroral Boundary, Auroral Oval (continued on reverse) |
| | | | |
| | | | |

19. ABSTRACT (Continue on reverse if necessary and identify by block number)

This contract has supported research in the areas of Software, Hardware, Theory, and Modelling. Each of these four areas has been developed in concert with the other three. Consequently, the on-going effort has been totally integrated in its results, with changing emphases across these areas as work progressed. This report, therefore, treats each area separately, and consists - in large part - in the presentation of published reports which occurred during the lifetime of the contract.

| 20. DISTRIBUTION/AVAILABILITY OF ABSTRACT | 21. ABSTRACT SECURITY CLASSIFICATION |
|---|---|
| UNCLASSIFIED/UNLIMITED ☒ SAME AS RPT. ☐ DTIC USERS ☐ | Unclassified |

| 22a. NAME OF RESPONSIBLE INDIVIDUAL | 22b. TELEPHONE NUMBER (Include Area Code) | 22c. OFFICE SYMBOL |
|---|---|---|
| David Hardy | (617)377-3211 | AFGL/PHG |

DD FORM 1473, 83 APR EDITION OF 1 JAN 73 IS OBSOLETE.

Unclassified
SECURITY CLASSIFICATION OF THIS PAGE

18. cont.

CRRES
LEPA
Coronal Mass Ejections (CME)
Solar Filament
Interplanetary Shock
Ground Level Events (GLE)
Geomagnetic Field
Cosmic Ray Equator
Cut-off Rigidities
Solar Radio Bursts
Proton Emissions
SSJ4

TABLE OF CONTENTS


| | Page |
|---|---|
| DATA REDUCTION AND ANALYSIS | 1 |
| I. Introduction | 1 |
| II. Data Reduction | 1 |
| 1. DMSP F2 Satellite, J/3 Instrument | 1 |
| 2. DMSP F4 Satellite, J/3 Instrument | 2 |
| 3. P781 Satellite, J/3 Instrument | 2 |
| 4. DMSP F6 Satellite, J/4 Instrument | 2 |
| 5. DMSP F7 Satellite, J/4 Instrument | 2 |
| 6. DMSP F7 Satellite, J* Instrument | 2 |
| III. Data Analysis | 3 |
| 1. Auroral Boundary Studies | 3 |
| 2. Auroral Oval Maps | 4 |
| 3. Polar Rain Studies | 4 |
| HARDWARE | 6 |
| I. Laboratory | 6 |
| II. Electronics | 6 |
| III. CRESS/LEPA | 7 |
| IV. SSJ4 | 7 |
| THEORY | 8 |
| (Reprints) | |
| 1. Coronal Mass Ejections | 10 |
| 2. Characteristics of Solar Coronal Source Regions Producing $^3$He-Rich Particle Events | 23 |
| 3. Solar Filament Eruptions and Energetic Particle Events | 33 |
| 4. Interplanetary Shocks Preceded by Solar Filament Eruptions | 43 |
| 5. A Comparison of Solar $^3$Helium-Rich Events with Type II Bursts and Coronal Mass Ejections | 52 |
| 6. Characteristics of Coronal Mass Ejections Associated with Solar Frontside and Backside Metric Type II Bursts | 58 |
| 7. Gradual Hard X-Ray Events and Second Phase Particle Acceleration | 64 |
| MODELS AND DATA | 70 |
| (Reprints) | |
| 1. A Revised Standard Format for Cosmic Ray Ground-Level Events Data | 72 |
| 2. Estimating the Change in Asymptotic Direction Due to Secular Changes in the Geomagnetic Field | 76 |
| 3. The Use of the McIlwain L-Parameter to Estimate Cosmic Ray Vertical Cutoff Rigidities for Different Epochs of the Geomagnetic Field | 80 |
| 4. The Cosmic Ray Equator Determined Using the International Geomagnetic Reference Field for 1980.0 | 84 |
| 5. Vertical Cutoff Rigidities for Selected Cosmic Ray Stations for Epoch 1980.0 | 88 |
| 6. On the Correlation Between Asymptotic Directions of Cosmic Ray Particles and Cutoff Rigidities in the Evolving Geomagnetic Field | 92 |
| 7. Peak-Flux-Density Spectra of Large Solar Radio Bursts and Proton Emissions from Flares | 96 |

# DATA REDUCTION AND ANALYSIS

## I: INTRODUCTION

Emmanuel College has written software in support of various studies of magnetospheric particles using data from instruments flown on a series of Air Force satellites. We have designed data base structures suitable for detailed analysis of this data and have written support software for graphic presentation of the results of these studies.

## II: DATA REDUCTION

Satellite data is delivered to AFGL and the basic data reduction is done by AFGL personnel and other organizations under contract to AFGL. The result is a series of data base tapes sorted by time for each instrument flown. Emmanuel College has written programs to interface with these data base tapes for each of a series of six satellite instruments during the course of this contract as outlined below.

### II.1 DMSP F2 satellite, J/3 instrument

The J/3 instrument is a cylindrical plate electrostatic analyser which records precipitating electrons from 50 ev to 20 Kev over 16 channels. The DMSP satellite is a polar orbiting satellite and the data has been used in a series of statistical studies of auroral precipitation and polar rain. We wrote a program to interface with the data base for this instrument, designed the data structures for the statistical studies and

processed all the available data for these studies.

II.2 DMSP F4 satellite, J/3 instrument.

This instrument was almost identical to the above J/3 instrument and the interface program for it was modified to support both instruments. For most of the statistical studies, the data from the two instruments were merged.

II.3 P781 satellite, J/3 instrument.

The interface program for the F2 satellite was also modified to read data from this satellite data base. A limited set of this data was used in the statistical studies.

II.4 DMSP F6 satellite, J/4 instrument.

The J/4 instrument sampled both precipitating ions and electrons between 30 ev and 20 Kev with twenty channels for each species. We wrote a program to interface with this data base and designed data structures to allow statistical studies.

II.5 DMSP F7 satellite, J/4 instrument.

This instrument was almost identical to the one above and the F6 interface program was modified to read the F7 data base. Data from the two satellites was merged for most of the statistical studies.

II.6 DMSP F7 satellite, J* instrument.

The J* instrument was a 4 channel dosimeter sensitive to high energy ions and electrons. The data generated was coarse, but suitable for some cosmic radiation studies and monitoring of

the trapped radiation belts. A program was written to interface with this data base.

## III. DATA ANALYSIS

Emmanuel College provided programming support for and was actively involved in a series of studies of magnetospheric particle precipitation using data from the instruments summarized in section II above as outlined below.

### III.1 Auroral Boundary studies.

The auroral oval is a dynamic phenomena resulting from charged particles precipitating into the ionosphere and its size and location is sensitive to geomagnetic and solar radiation activity. The polar orbiting DMSP satellites cross the boundary into or out of the auroral oval twice per orbit for both the North and South geomagnetic poles. Using the electron data from the F2 satellite, we developed an algorithm for precisely locating this crossing. By accumulating a large sample and sorting it by Geomagnetic Latitude, Magnetic Local Time, and geomagnetic activity as measured by the standard Kp index, we were successful in statistically parametizing its spacial behavior.

The parameterization resulted in a self-consistent set of 24 linear equations, giving Geomagnetic Latitude as a function of Kp for any selected Magnetic Local Time. By inverting the process, each orbit gives four direct observations of geomagnetic activity. Since this information is available in near real

time, it has proved to be of high value to the Air Force.

The entire F2 data set was processed through this algorithm and the results delivered to AFGL. They were subsequently published as an activity index. The original algorithm was later optimized for each instrument in the DMSP series (F2, F4, F6, and F7) to give real time coverage over the span of this contract.

A computer program "AWSAA" written and delivered to AFGL as a product in support of this algorithm. A program maintenance manual was also delivered. This program was also installed on the computer system at AFGWC.

III.2 Auroral Oval Maps

As a generalization of the above concept, we designed a data base structure such that the entire oval could be parameterized. We were successful in sorting the DMSP electron data by geomagnetic activity (as indicated by Kp) over the entire polar region into a large Geomagnetic Latitude, Magnetic Local Time grid. We accumulated each channel of electron data and statistical information for each bin so that the statistically average spectra was effectively developed as a function of spacial position and activity. We wrote programs for graphic summaries of the results and this was the basis for several publications.

A program AWSAB was written and delivered to AFGL along with a program maintenance manual as a finished product in support of this algorithm. This program was also installed on the computer

system at AFGWC.

III.3 Polar Rain Studies

Polar Rain refers to the precipitation occurring inside the Auroral oval. The precipitation levels in this region are orders of magnitude less intense than those occurring within the oval. Since this region is of high interest to the scientific community, the methods developed in III.2 above were applied to the high latitude portions of the polar regions. Because of the low radiation levels to be dealt with, special care was given to eliminating instrument noise and methods had to be developed to prevent contamination from the intense portion of the Auroral oval. This study resulted in several publications.

## HARDWARE

### LABORATORY

The small cryo-pumped thermal vacuum chamber at Emmanuel was used several times to test and diagnose spacecraft hardware including IMPS sub-assemblies and the J4 sensor for the DMSP satellite. The prototype ion source was briefly tested and then removed to deliver to AFGL for further work.

### ELECTRONICS

Work has continued on the IMPS SESA DPU. The prototype processing boards were tested using the Compaq portable computer for the GSE. Software for the processing of the real time data stream was written and tested. The interface for the SPACE particle correlator portion of the experiment was re-worked and the DPU interface requirements were provided to Dr. Paul Gough, our British co-investigator.

The IMPS Interface Control Document (ICD), the Investigation Requirements Document (IRD), and the Policies and Requirements (PAR) documents were revised and updated to reflect the latest IMPS status. Because of the shuttle delays and re-scheduling, as well as other problems with the IMPS carrier definition, this project seems to be slowing down. Because there may be a period of little or no activity on this experiment, the documentation was reviewed, expanded, and archived so that when work is again accelerated, the

documentation will be sufficient to allow prompt recovery of the latest status.

CRESS/LEPA

Integration and environmental testing of the CRESS satellite by Ball Aerospace at their Boulder, Colorado facility has continued during this quarter. The Physics Research Division provided direct support of these tests at BASD. The LEPA experiment was our direct responsibility and the GSE and software for these tests also provided data decommutation for the PROTEL and dosimeter experiments. Several trips to BASD were made to provide the necessary support of the CRESS integration and environmentals.

SNJ4

Delivery of SN11 occurred on January 8, 1987. The unit was delivered to RCA in New Jersey and integrated with the spacecraft.

SN10 was returned to us for refurbishment prior to launch. New channeltrons were installed and the instrument underwent full electrical and environmental tests. A full particle calibration was performed at the AFGL calibration facility. The instrument was then delivered to Vandenberg Air Force Base for final integration on the spacecraft.

SN12, SN13, and SN14 were assembled, electrically tested and delivered to AFGL.

## THEORY

The work of Kahler has dealt primarily with the solar sources of both energetic particles and interplanetary shocks. Observations of coronal mass ejections (CMEs) obtained with the Solwind coronagraph on the P78-1 satellite were used extensively in this analysis. In one study the association between CMEs and type II radio bursts was studied in detail. In two papers the relationship between solar energetic particles and CMEs was investigated. A correlation has been found between peak energetic proton fluxes and the speeds of CMEs. Solar particle events rich in $^3$He were also investigated. They are not associated with CMEs or with type II bursts, in contrast to normal energetic particle events. $^3$He-rich events appear to be produced along with energetic electrons in the corona and to have little to do with underlying H$\alpha$ or X-ray flare events. Another topic of interest has been solar energetic particle events with weak flare signatures. One event, on December 5, 1981, was studied in detail. A particle event and interplanetary shock were produced by the eruption of a quiescent filament well away from any active region. In a follow-up study six cases of energetic particle events and interplanetary shocks arising from quiescent filament eruptions were studied in detail. Work has also been carried out to investigate the properties of shock-associated kilometric radio bursts and the associations of these bursts with energetic particle events. In general, the work described here has been the

result of collaborative programs set up with investigators at the Naval Research Laboratory and Goddard Space Flight Center.

REVIEWS OF GEOPHYSICS, VOL. 25, NO. 3, PAGES 663-675, APRIL 1987
U.S. NATIONAL REPORT TO INTERNATIONAL UNION OF GEODESY AND GEOPHYSICS 1983-1986

# CORONAL MASS EJECTIONS

S. Kahler

Physics Research Division, Emmanuel College, Boston MA 02115

## Introduction

While the first coronal mass ejections (CMEs) were observed with the OSO-7 white light coronagraph (Tousey, 1973), it was the Skylab coronagraph observations that clearly established CMEs as an important component of solar coronal physics. CMEs have been defined by Hundhausen et al.(1984a) as observable changes in coronal structures occurring on time scales of minutes to hours and involving new, discrete bright features in the field of view. Although only a fraction of all observed coronal activity, CMEs are of interest because they involve discrete additions of mass and magnetic fields to the solar wind. These large coherent structures, observed to expand to many times the diameter of the sun as they moved outward into interplanetary space, not only provided a fascinating new phenomenon for study, but were also perceived as the "missing link" between solar flares and geomagnetic storms (Hundhausen et al., 1984b). In addition, they constitute the most energetic phenomena known to occur in the solar system (Gergely, 1986b). The Skylab data base consisted of 77 CMEs observed during 1973-74, about 3 years prior to solar minimum (Munro et al., 1979). A summary of the Skylab results was provided by MacQueen (1980).

Data sets from two orbiting coronagraphs have dominated the studies of CMEs during the past quadrennium. The Solwind coronagraph, provided by the Naval Research Laboratory, was flown on the P78-1 satellite and is described by Sheeley et al.(1980). Solwind observations of more than 1200 CMEs were obtained from March 28, 1979 until the destruction of the spacecraft by the U.S. Air Force in an anti-satellite test on September 13, 1985 (Marshall, 1985). The other coronagraph, the coronagraph-polarimeter (C/P) on the Solar Maximum Mission (SMM) satellite was provided by the High Altitude Observatory and is described by MacQueen et al.(1980). It obtained observations of about 70 CMEs from March 1980 until the instrument failed in September 1980. The C/P was repaired on April 12, 1984 (Maran and Woodgate, 1984) and has continued to function well to the present time on what is now called the SMM-2 satellite.

The C/P views the corona in square azimuthal sectors from 1.6 to about 6 $R_o$, while Solwind observed the entire corona from 2.5-10 $R_o$. Solwind used one broad white-light waveband and two Polaroid rings at 5 and 8 $R_o$ to detect polarization. The C/P, on the other hand, has a number of filters with different bandpasses, but most CMEs have been observed in a single wideband filter. Although the two instruments overlapped in time coverage, fields of view, and wavebands, the two sets of observations are somewhat complementary. The large numbers of Solwind CMEs have proved to be well suited for statistical studies, but detailed studies of individual Solwind CMEs are limited by the relatively coarse spatial resolution of 1.25 arc min. The comparatively fewer C/P CMEs were observed with a superior spatial resolution of 10 arc sec, and many were observed with an Hα filter to isolate cool prominence material. As a result, many of the C/P studies have focussed on details of individual events. Images of C/P and Solwind CMEs are shown in Figures 1 and 2.

The Solwind and C/P observations are complemented by additional CME observations in the inner (< 2 $R_o$) and outer (> 10 $R_o$) corona. The HAO K-coronameter at Mauna Loa, Hawaii, observes in the near infrared at an altitude range of 1.2-2.2 $R_o$, while a prominence monitor simultaneously records disk and limb Hα images (Fisher and Poland, 1981). These observations have been made routinely since before the SMM mission. Observations of CMEs in the interplanetary medium have been made by the zodiacal light photometers on the Helios 2 spacecraft (Jackson and Leinert, 1985). Data from three scanning photometers are converted into low resolution images of CMEs over the north ecliptic hemisphere. CME observations are made at distances of several tenths of an AU from the sun and can even be made from within the CME itself.

The topic of CMEs has been reviewed a number of times over the past quadrennium. Dryer (1982) and Steinolfson (1985) stressed the theories of CME initiation and motion and the relationship of CMEs to shocks. The latter topic was also reviewed by Schwenn (1986). Rust (1983) discussed CMEs as a part of his quadrennial review of solar activity, and Hundhausen et al.(1984b) took a historical approach to CMEs and their interplanetary effects. Reviews of Wagner (1984), Fisher (1984), Low (1986), and Hildner (1986) have discussed the general properties of CMEs, while the CME chapter of the SMM Workshop Proceedings (Hildner et al., 1986) treats event case histories and some recent modelling in detail.

We will review recent work on CMEs by addressing, in rough order, the three fundamental questions about CMEs (Hildner et al., 1986): (1) how are CMEs initiated in the low corona, (2) how are CMEs propelled through the low corona, and (3) what are the manifestations of CMEs in interplanetary space?

## Rates and Associations

Hildner et al.(1976) found a good correlation between Skylab CME production and sunspot number. The additional fact that nearly all the Skylab CMEs lay in the active region latitudes within 45° of the equator (Hildner, 1977) suggested that the stronger and more complex magnetic fields of



Paper number 7R0080.
8755-1209/87/007R-0080$15.00

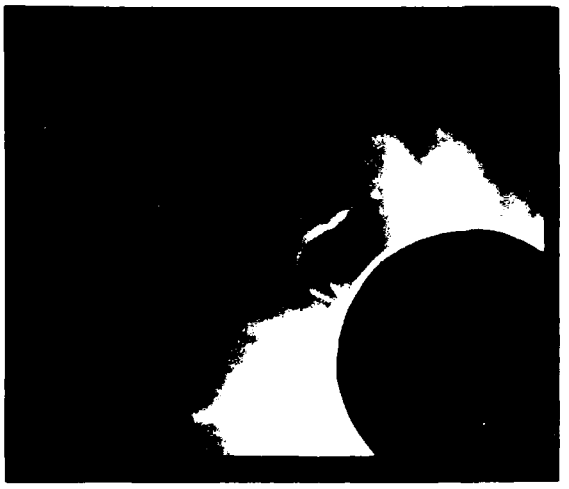

Figure 1. A C/P loop CME centered at a latitude of N87 on the east limb. The sun-centered occulting disk radius is 1.6 $R_o$. The bright inner loop is the eruptive prominence. From Hundhausen et al.(1984a)

active regions were an essential ingredient for CMEs. They speculated that at the maximum of the solar cycle the CME rate would be substantially increased, by about a factor of 4, along with the average sunspot number.

Analysis of the C/P CMEs from SMM-1 showed that they were more uniformly distributed in latitude than were those of Skylab (Hundhausen et al., 1984a; Hundhausen, 1986), as shown in Figure 3, and that high latitude (> 45°) CMEs were not systematically different (Sime, 1986). The observed occurrence rate, corrected for effective observing time, was 0.87 CME/day, only a 20% increase over the recalculated Skylab rate of 0.74 CME/day (Hundhausen et al., 1984a), and contrary to the prediction of Hildner et al. (1976). Howard et al.(1985) compiled statistics on 998 Solwind CMEs observed during 1979-81. They found no obvious relation between CME occurrences and sunspot number on time scales of 7 to 180 days. Their occurrence rate was 1.8 CME/day for all CMEs (double that derived for the C/P data) and 0.9 CME/day for the 56% of the sample they judged as "major" CMEs. Webb (1986) has used the longitude distributions of Hα flares with type II bursts to correct for CMEs near central meridian unobserved by the C/P and Solwind instruments. His corrected rates become 1.5 CME/day for the C/P and 2.1 CME/ day for all the Solwind CMEs.

The availability of 1984-85 Solwind data has enabled the NRL group (Sheeley et al., 1986; Howard et al., 1986) to compare CME occurrence rates near solar maximum with those near solar minimum using only Solwind data. They found not only a substantially lower rate of 0.2-0.4 CME/day during 1984-85, but also a correlation between average annual sunspot number and average annual occurrence rate close to that found by Hildner et al.(1976) and shown in Figure 4. The 1984-85 CMEs had substantially smaller angular widths, speeds, and energies than those of 1979-81 (Figure 5 and Table 1). The class of CMEs called streamer blowouts were found to occur at the same rate during both eras and to be the most numerous type of CME in 1984-85.

The 1984-85 C/P CMEs also show substantially slower speeds and lower occurrence rates in comparison with the restated Skylab and 1980 C/P values (Hundhausen, 1986), as shown in Table 1. Contrary to the NRL group (Howard et al., 1986), Hundhausen finds no simple relationship between sunspot number and CME rate since the Skylab and 1984-85 C/P rates differ by a factor of ~ 4 for similar sunspot numbers. He finds that the 1984-85 C/P CMEs occurred over the belt of coronal helmet streamers. The tilted magnetic dipole defined by this belt evolved slowly in 1984-85 but rapidly during Skylab, suggesting coronal evolution as the crucial factor in the CME occurrence rate. Howard et al.(1986) and Hundhausen (1986) both find that 1984-85 CMEs are confined to low (< 45°) latitudes (Figures 3 and 5), but they seriously disagree on the angular spans. During 1980 both derive an average CME angular span of ~ 40°, but with significantly different distributions. The 1984-85 Solwind angular spans are substantially reduced, but the 1984-85 C/P values remain similar to those of both Skylab and the 1980 C/P values (Table 1). The disagreements between the Solwind and C/P results may arise partly from the different radial fields of view of the instruments or from the different techniques used to produce the CME

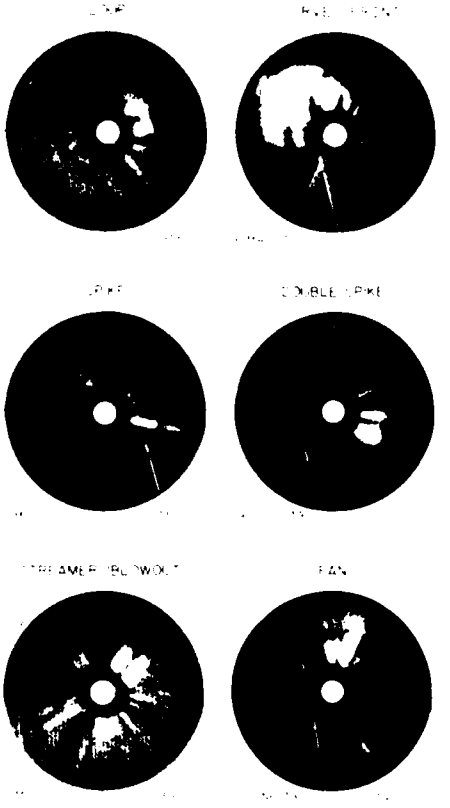

Figure 2. Solwind difference images of 6 of the 10 structural classes of Howard et al.(1985). The field of view extends from 2.5 to 8 $R_o$.

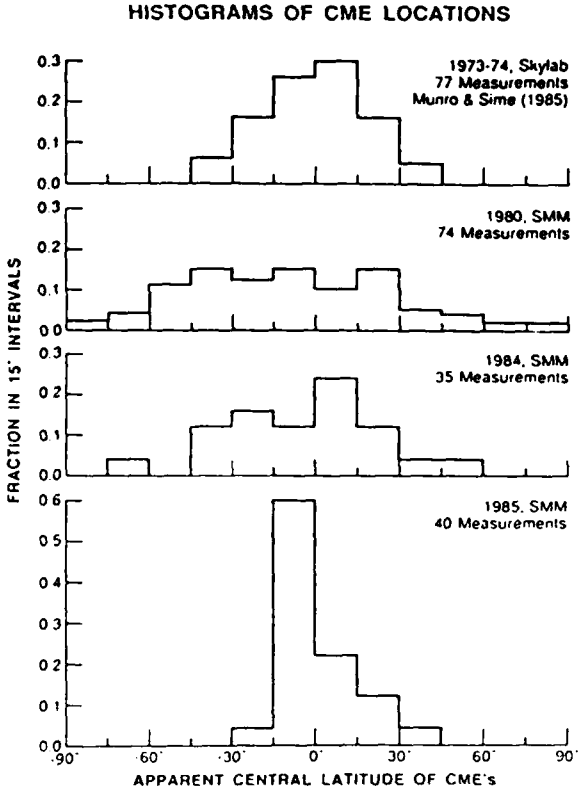


Figure 3. Distributions of the apparent solar latitudes of CMEs measured from Skylab and SMM data. From Hundhausen (1986).

images. Solwind CMEs are evaluated by using subtracted images and the C/P CMEs primarily by direct images. Resolution of these disagreements is recognized as an urgent goal but a nasty problem.

On a shorter time scale, Wagner and Wagner (1984) considered the distribution of time intervals between successive CMEs observed by Skylab and SMM-1. The shortest time bin (0-10 hr) showed a deficit of cases for those CMEs separated by < 60° and a surplus of cases for those CMEs widely separated (120°-180°). They interpreted those results as indicating, respectively, a temporary suppression of subsequent CMEs from a given region and a global coherence to CME occurrence. However, the 0-10 hr time bin consists of only 21 events, so their result is not statistically compelling.

About 66% of the C/P CMEs observed in 1980 could be temporally and spatially associated with some form of solar activity (erupting prominences, Hα flares, X-ray events, and type II and IV radio bursts) (Webb, 1986; Webb and Hundhausen, 1986). This is slightly lower than the 78% of the Skylab CMEs, recalculated from Munro et al.(1976). For both epochs the CME association with erupting prominences (~ 80% of the associated CMEs) was about twice the association with Hα flares. There is also evidence that the CMEs track prominences better than flares in both latitude and occurrence frequency, establishing eruptive prominences as a fundamental element for the origin of CMEs. Wagner (1984) has claimed that a large fraction (> 30%) of CMEs constitute a separate class which leave no detectable near-surface signature. Such CMEs could well be from behind the limb, and some associations may be missed due to accelerations of CMEs (MacQueen, 1985). Since Wagner's claim is not supported in detail, the size of this class of events, if it exists at all, must be considered unknown (see also Webb and Hundhausen, 1986).

## Theoretical Work

The theoretical approach to treating CMEs has been reviewed in detail by Rosner et al.(1986). The basic problem is to explain the properties of CMEs by treating them as a time-dependent magnetohydrodynamic (MHD) process in a $1/r^2$ gravitational field. Since the estimated gravitational potential energy of a CME can sometimes exceed the total kinetic energy, gravity is considered important in the physical treatment. Although the observational uncertainties are often substantial, CMEs above 2-3 $R_o$ tend to approach a constant speed (MacQueen and Fisher, 1983) which, despite the importance of gravity, is sometimes well below that of the gravitational escape speed.

Three main approaches can be identified in CME theory (Rosner et al., 1986). One employs numerical codes to treat the MHD equations with freely prescribed initial and boundary conditions, usually consisting of a potential magnetic field and hydrostatic atmosphere. These models have attempted to use pressure pulses, usually based on associated flare X-ray flux profiles, to drive the ejections (Dryer, 1982). The models are well developed in the sense that numerous comparisons with observed CMEs have been done (e.g., Wu et al., 1983b). However, the credibility of this approach has been challenged for several reasons. In the first place, the magnetic field in these models has acted to retard rather than propel the CME (Rust et al., 1980). A recent parametric study using several multipole potential fields (Hildner et al., 1986)

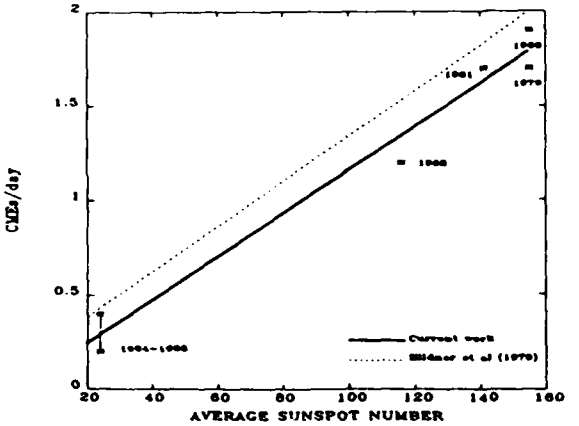


Figure 4. Variation of the Solwind CME occurrence rates with sunspot number. From Howard et al.(1986).

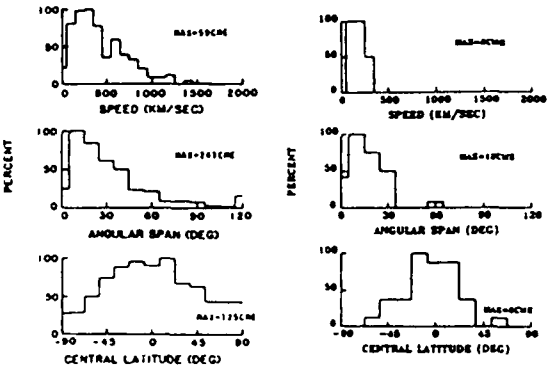


Figure 5. The speeds, angular spans and central latitudes of the 1979-81 Solwind CMEs (left) and 1984-85 Solwind CMEs right. From Howard et al.(1985, 1986).

has shown that reasonable pressure pulses in potential magnetic fields can not result in CMEs. Second, as we discuss later, recent observations have shown that the flare pressure pulses used in the model are not relevant to the CMEs. Third, the models may not be successful in reproducing several fundamental features of CMEs. Sime et al.(1984) attacked the numerical pressure pulse model presented in Dryer et al.(1979) by claiming that the numerical models generally failed to explain three features common to 5 Skylab CMEs: (1) more material at the flanks than the tops of the CMEs; (2) a large region of depleted density below the loops; and (3) a lack of lateral motion in the CME legs late in the events. In the debate on the merits of these claims Dryer and Wu (1985) and Sime et al.(1985) found no common ground.

The second theoretical approach is one in which CMEs are treated as magnetic loops subjected to internal (e.g., Mouschovias and Poland, 1978) or external (e.g., Anzer and Pneuman, 1982) magnetic forces that drive the loops outward. Analytic approximations are made to the MHD equations in these models. However, Yeh (1982) pointed out that the magnetic forces act essentially perpendicular to the loop axis, resulting in a loop volume expansion but not in the translational motion characteristic of CMEs. Thermal pressure gradients are necessary for the proper description of the buoyant driving force of the loop even in a low beta plasma (Rosner et al., 1986). To account for the motion of CMEs Yeh (1985, 1986a,b) has subsequently proposed a theory of hydromagnetic buoyancy force, the major part of which is the diamagnetic force, resulting from the interaction between internal and external currents. The magnetic stress in the peripheral layer of an immersed body is spatially transformed into thermal stress in the interior. The force density associated with that thermal stress overcomes gravity to provide the driving force of a flux rope.

The newest approach in CME theory is that of Low (1984a), who has applied the principle of self-similar MHD to CMEs. Mathematically, the MHD equations become analytically tractible by the introduction of a similarity variable which couples the time and radial distance parameters

TABLE 1. Average Properties of Observed CMEs

| | | Sunspot Number | Daily Rate (events) | Speed km/s | Angular Span |
|---|---|---|---|---|---|
| 1973-74 | Skylab | 33 | 0.55 (77) | 340 | 42° |
| 1980 | C/P | 150 | 0.8 (74) | 340 | 41° |
| 1984-85 | C/P | 25 | 0.15 (75) | 160 | 38° |
| 1979-81 | Solwind | 150 | 1.8 (998) | 472 | 45° |
| 1984-85 | Solwind | 25 | 0.3 (59) | 208 | 24° |

without the need to restrict the treatment to one dimension in space; in fact, a three-dimensional model is feasible. For a certain radial symmetric velocity field function only a single MHD equation needs to be solved. Physically, coronal flows result when bound coronal structures become gravitationally unstable and break away. The natural tendency for plasma to expand in the solar wind can then no longer be resisted by gravity and magnetic tension. Self-similar solutions show that in all cases the flow speeds become asymptotically constant as the Lorentz forces and pressure gradients act to balance gravity. No additional "driving" force is required. Low (1984a) showed that various types of magnetic field configurations in the outflow could generally match commonly observed CME structures. His view is essentially an inversion of the usual approach to CMEs in that he considers the ejection of material from the corona to be the normal situation and the confinement of coronal material by closed magnetic fields as closer to an "event".

Adoption of the self-similar viewpoint suggests that we seek initiation of a CME in

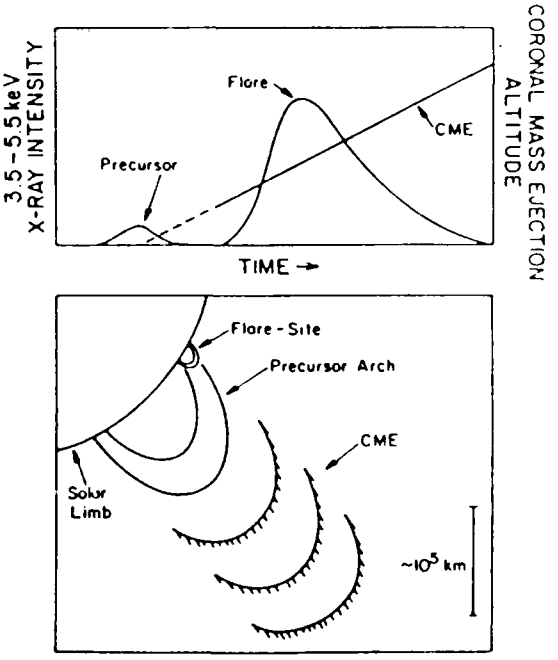


Figure 6. A temporal (above) and spatial (below) schematic of the relationship of the flare-associated CME to the precursor X-ray arch and subsequent flare as derived by Harrison (1986).

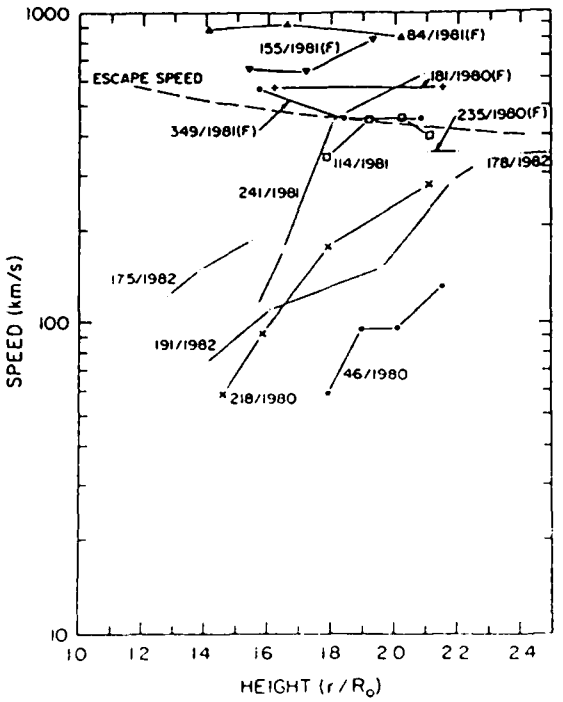


Figure 7. Radial speeds of 12 CMEs as a function of height. The flare-associated events are designated (F); others are prominence-associated. From MacQueen and Fisher (1983).

unstable magnetostatic states of the corona. Low (1984b) has studied the stability of large-scale magnetostatic structures, and Wolfson and Gould (1985) found that magnetostatic equilibria can disappear when the corona is loaded with an excess mass corresponding to that characteristic of CMEs. Pneuman (1984b) has considered a CME initiation mechanism in which a loop structure is constricted at its base by external forces.

## Observations of CME Development

Comparisons between the development of CMEs and that of associated disk prominences or flares can provide clues to the causal agents of CMEs. Only a few C/P CMEs have been compared in detail with Hα and other disk observations. Wagner et al.(1983) found near simultaneity between the eruption of a prominence and the deduced departure time of the associated CME. An early assessment of flare-associated CMEs (Wagner, 1983) indicated that CME departure times preceded flare onsets. Recently, Harrison (1986) has found that CMEs appear to leave the solar surface during weak, soft X-ray bursts preceding subsequent associated flares by tens of minutes (Figure 6). The precursor X-ray brightening has a large spatial scale size of ~ $10^5$ km. The extent, location, and morphology of the CME are consistent with the CME launch occurring during a destabilization of the precursor arch. This result, which applies only to flare-associated CMEs, rather than the more numerous prominence-associated CMEs, is based on three cases for which SMM precursor and flare X-ray burst images and C/P CME observations were obtained. Although additional supporting cases have been claimed (Simnett and Harrison, 1984), there are apparently only 4 more cases with incomplete spatial observations that are consistent with this scenario (Harrison et al., 1985). Harrison (1986) argues against the alternative interpretation that the CME launch occurred during the subsequent X-ray flare. In that case either the acceleration profile would be unrealistic, or the starting altitude would be so high (~ 0.66 $R_o$) that the onset would be observable with the Mauna Loa coronagraph, contrary to experience (Fisher and Munro, 1984). When the CME reaches a height of ~ 0.5 $R_o$, a flare occurs in the primary footpoint of the arch. This suggests that the resulting flare will be positioned near one leg, rather than near the center, of the angle subtended by the CME. A comparison of the position of the Hα flare with the angular extent of the associated CME for 51 flare-associated CMEs revealed a similarly strong tendency for the flare to occur near one leg of the CME (Harrison, 1986; Harrison and Simnett, 1986).

These observations suggest that the flare is triggered by conditions subsequent to the CME launch and is not directly responsible for driving the CME, contrary to the requirements of pressure pulse models (Wu et al., 1983). Cliver et al.(1983) discussed a case of a flare-associated CME which produced a very energetic (E > 500 MeV) particle event but was associated with a faint impulsive microwave burst. In addition, nonflare CMEs associated with no detectible impulsive phase, but with sufficient speeds to result in interplanetary shocks, were discussed by Kahler et al.(1986) and Cane et al. (1986). These events all show a fundamental incompatability with the requirements of the pressure-pulse models.

Harrison's (1986) scenario places the sources of flare-associated CMEs in large X-ray arches connecting different active regions. Since the magnetic fields in these arches may be close to potential and lie roughly perpendicular to the underlying neutral lines, it is not clear how active region prominences, which lie in or adjacent to the active regions in highly sheared fields, can be an integral part of many observed CMEs. It is also unclear why the precursor burst arch structure should again be observable ~ 1 hr after the flare onset if it had earlier erupted to form the CME. McCabe et al.(1986) observed a similar arch structure following an unusual flare in which the active region filament did not erupt. In that case, a flare spray was ejected in a highly nonradial direction from one end of the filament channel, giving rise to a CME. The precursor arch structures also appear similar to the post-flare arches considered by Svestka (1984) to be brightenings of preexisting structures rather than newly formed features. The basic role of the precursor arches in the development of flare-associated CMEs has yet to be defined.

The first appearance of a CME in the low corona is that of a bright arch, followed by a dark depletion region (Fisher, 1984). Occasion-

ally the arch is not well developed until it has reached ~ 1.5 $R_o$, in which case one initially sees a "dark transient", after which the leading arch brightens. Illing and Hundhausen (1985) combined the HAO K-coronameter and C/P observations of a single common looplike CME to deduce its basic structural components. The pre-event structures consisting of the prominence, overlying coronal cavity, and ambient corona first become prominence, depleted mound, and bright outer rim in the K-coronameter images and then bright core, intervening dark shell, and outer loop in the C/P images. Enough mass is observed in the ambient corona above the prominence to account for the loop seen in the C/P, supporting earlier Skylab results (e.g., Hildner et al., 1975).

Bright cores of material, presumed to be the remnants of Hα prominences, have been seen in about one third of all C/P mass ejections (Webb and Hundhausen, 1986) but in only about 1.5% of the Solwind images at the 4.0 $R_o$ polarizer ring position (Howard et al., 1985). This suggests that the Hα material is either ionized or rarefied substantially as it moves outward in the CME. Illing and Athay (1986) analyzed the Hα and continuum C/P observations of 8 CME prominences. The densities of ~ $10^8$ $cm^{-3}$, compared to typical pre-eruptive densities of $10^{11}$ $cm^{-3}$, indicate volume expansions by a factor of $10^3$. The decreased density was the primary factor in the calculated high levels of hydrogen ionization of 90 to 99%. In one event the estimated mass of ~ $1.5 \times 10^{16}$ gm, and increased gravitational potential energy of ~ $3 \times 10^{31}$ erg of the prominence matched or exceeded those of the remaining white light material (Athay and Illing, 1986; Illing and Hundhausen, 1986).

The kinematic properties of 12 inner coronal (1.2-2.4 $R_o$) loop CMEs were examined by MacQueen and Fisher (1983). At first the lateral and radial speeds of CMEs are about equal. When the leading edge reaches ~ 1.5 $R_o$, the lateral extent tends to remain fixed for the event duration. When the radial speeds were plotted as a function of distance from sun center (Figure 7), a clear delineation between flare- and prominence-associated events was found. Flare-associated events show higher speeds with little evidence of acceleration; prominence-associated events are characterized by lower speeds and observable accelerations. MacQueen and Fisher offer the following hypothesis. Flare-associated CMEs are produced in impulsive accelerations acting over small spatial (0.2 $R_o$) and temporal (< 10 min) regimes, while prominence-associated CMEs are subjected to significant accelerations over extended distances and times. A fundamental difference between the two kinds of CMEs is implied in the proffered hypothesis. Because many CMEs are associated with both prominences and flares (Webb and Hundhausen, 1986), there is some ambiguity about the flare and prominence associations of the MacQueen and Fisher study. However, supporting evidence for two classes of CMEs comes from a study by Sime (1986) showing that looplike CMEs are preferentially associated with prominence eruptions and the less ordered non-loop CMEs associated with flares. In his view loop-type CMEs reflect the outward motion of pre-existing structures while flare-associated CMEs result from complications due to energy and mass injection from a compact source.

Anzer and Pneuman (1982) and Cane et al.(1986) have suggested the contrary view of a broad spectrum of CME sources ranging from large flares in complex active regions to eruptions of quiescent prominences well outside active regions. These events would then differ only by degree, rather than by kind, as in the view of MacQueen and Fisher and Sime.

Large, faint regions of enhanced brightness known as "forerunners" were found to border the Skylab CMEs (Jackson and Hildner, 1978). The upper boundaries of forerunners maintained a constant offset of 1-2 $R_o$ from the CME where they blended into the coronal background. They are considered of significance because the volume of corona encompassed by the forerunner is much larger than that of the following CME. Recently, Karpen and Howard (1986) have challenged the view that the forerunner is an entity separate from the CME. In their analysis of the brightness contour maps of 44 Solwind CMEs they found that the apparent presence of the forerunner depended on whether the contour plots were linear, as Jackson and Hildner used, or logarithmic. The Solwind difference images include the forerunners as part of the CME itself, in contrast to the Skylab film images.

The relationship between CMEs and their coronal environment is the subject of several works. Illing (1984) has reported on a CME which pushed aside preexisting streamers, and Illing and Hundhausen (1986) describe a loop CME that completely disrupted a helmet streamer. The streamer increased in brightness for two days before the underlying prominence erupted. Portions of the streamer above the loop showed no change until passed by the loop. The CME loop material appeared to come only from the streamer itself. After CME passage the region of the helmet streamer was depleted. A similar but more complex event was discussed by Low and Hundhausen (1986). These events are probably examples of the CME class Howard et al.(1985) call streamer blowouts. While CMEs clearly perturb local coronal conditions, they appear to be influenced in return by the prevailing coronal magnetic fields and flow conditions. MacQueen et al. (1986) measured an average 2.2° equatorward deflection for Skylab CMEs but no significant deviation from radial motion for C/P CMEs of the SMM-1 epoch. They suggest that near sunspot minimum the dominant large-scale dipolar field directs CMEs toward the solar equator, but the less ordered global fields of solar maximum activity result in little or no equatorward net forces.

MacQueen and Cole (1985) have examined the development of loop breadth and total length for nine looplike CMEs. The total loop length L was well fitted by the relationship $L = aR^{1.3}$ where R is the radial height, and loop breadth h by $h = bR^{0.48}$, but with substantial scatter. MacQueen and Cole found this latter result inconsistent with the requirements of models of magnetically expelled loops (Mouschovias and Poland, 1978), compressive waves (Dryer, 1982), and self-similar flows (Low, 1984a). Although

Illing (1984) found five features of an expanding CME to be consistent with self-similar flows, the velocity field of a complex CME examined by Low and Hundhausen (1986) showed important departures from strictly self-similar flow.

The association between CMEs and X-ray flare events was investigated by Sheeley et al.(1983). They found that the probability of a CME association with an X-ray flare increases with the duration of the X-ray event. Beyond a duration of 6 hrs all X-ray flares are associated with CMEs. An unexpected result of the Sheeley et al. study was that even the shortest duration (< 2 hr) X-ray flares may be associated with CMEs (see also Webb and Hundhausen, 1986). These flares had previously been thought to belong to a distinct class of compact flares with no associated CMEs (Rust et al., 1980).

As part of the statistical analysis of 998 Solwind CMEs observed during 1979-81 Howard et al.(1985) reported on the CME structural classes. They used 10 categories (Figure 2), of which the three "spike" groups - spikes, double spikes, and multiple spikes - comprised ~ 53% of all CMEs. They also rated the importance of each event using size and brightness as subjective criteria. The spike events dominated the lowest importance (N) group but were a small component (~ 18%) of the highest importance (Y) group. Curved fronts and loops were ~ 44% of the Solwind Y events. The distribution of 77 Skylab CME structures was reported by Munro and Sime (1985). Two of their seven morphological categories, loops and filled bottles - the Skylab analogs of the Solwind loops and curved fronts - comprised 36% of the total CMEs, similar to the Solwind Y events. Whether the Solwind spike events are too faint to be easily detected in the Skylab and C/P observations and whether the spike events are really loop structures with very faint loop tops are open questions that complicate studies of CME occurrence rates and morphologies.

Additional results presented in the 1979-81 Solwind CME survey by Howard et al.(1985) are as follows. CMEs occurred over a broad range of latitudes with an average angular span of 45°. The average ejected mass was $4 \times 10^{15}$ gm, and average kinetic energy $3.5 \times 10^{30}$ erg, with a range of about a factor of $10^2$ for both parameters. The curved front, halo and complex CMEs were the most energetic, and single spike, streamer blowout, and diffuse fan CMEs the least energetic. Howard et al. calculate the CME contribution to the equatorial solar wind to be ~ 5%. Their average Solwind CME leading edge speed was 472 km $s^{-1}$, substantially higher than the Skylab and the 1980 C/P values of 340 km $s^{-1}$ (Hundhausen, 1986). CMEs have been observed to move outward as slowly as 14 km $s^{-1}$ (Fisher and Garcia, 1984) and as fast as 1825 km $s^{-1}$ (Sheeley et al., 1985).

The difficulties involved in deducing the basic CME geometry from the available observations were discussed by Fisher (1984). The competing geometrical concepts are the planar loop structure and the three-dimensional bubble. Halo CMEs observed in the Solwind coronagraph (Howard et al., 1982) have provided support for the bubble concept. In addition, the depleted coronal region following a typical CME was modelled by a simple three-dimensional figure with a symmetry axis perpendicular to the limb (Fisher and Munro, 1984). As a result, the bubble geometry is now favored for CMEs (Wagner, 1984).

Metric type IV bursts are sometimes seen in association with CMEs. With several assumptions about the statistics of CMEs and type IV bursts, Gergely (1986a,b) concluded that the mean speed of moving type IV bursts is less than that of associated CMEs and that the burst regions move behind or along with the CME leading edges. It had been thought that the electron densities of the moving type IV source regions were too low for the type IV emission to be explained by plasma emission. In two cases (Stewart et al., 1982; Gergely et al., 1984a) the association of moving type IV bursts with dense blobs of CMEs has allowed the possibility that the emission mechanism could be plasma emission, although gyrosynchrotron emission could not be ruled out. A similar result was drawn for a stationary type IV burst located in the leg of a CME (Gary et al., 1985). The high density (~ 30x background) of one of the moving type IV blobs required a confining magnetic field $B > 0.6$ G at 2.5 $R_\odot$ (Stewart et al., 1982). Bird et al.(1985) used Faraday rotation and spectral broadening measurements of Helios radio signals to deduce the line-of-sight magnetic fields in 5 CMEs. They report values of $10^{-2}$ to $10^{-1}$ G at 2.5 $R_\odot$, lower by a factor of $10-10^2$ than previous estimates using CME radio burst emission. Since these earlier values were based on the questionable gyrosynchrotron interpretations of type IV emission or were representative of the densest parts of CMEs, the lower values of Bird et al. may be better estimates of this parameter, which is fundamental but difficult to measure. A close association between stationary type IV bursts and CMEs was found by Robinson et al.(1986). A CME may be a necessary condition for these type IV bursts, and nearly half of all CMEs with $v > 400$ km $s^{-1}$ were associated with continuum sources located within the CMEs, well away from the leading edge.

MacQueen (1980) noted that for the average CME occurrence rate and an estimated magnetic flux present in each CME, the total flux added to the interplanetary medium would equal the observed background flux in only 100 days. To prevent an indefinite flux buildup he proposed that CME loops magnetically disconnect, leaving a loop that returns to the sun and a closed magnetic structure that continues outward into interplanetary space. An association of the latter structures with magnetic clouds was proposed by Klein and Burlaga (1982). MacQueen suggested that the lack of any observed loops returning to the sun was due to a low loop density rendering it invisible. A candidate for just such an event was reported by Illing and Hundhausen (1983). The feature identified as the lower boundary of the closed loop moved out at ~ 175 km $s^{-1}$, 3 to 4 times faster than the CME leading edge. The fan-shaped region connected to the sun then contracted to form a bright coronal ray. The radial speed of this CME was unusually low (~ 45 km $s^{-1}$) and the event occurred in a previously disrupted streamer (Webb, 1986), so this event may not be characteristic of most CMEs. Illing

and Hundhausen cite factors rendering the observation of this event difficult, but point out that the SMM-1 CME data set contains 7 more candidates for disconnected magnetic structures. Gradual hard X-ray bursts (GHBs) are another phenomenon which may be indicative of the terminal phase of the CME event. These coronal bursts, characterized by flat hard X-ray spectra and relatively high intensity, low frequency microwave bursts, occur in the late phases of major flares. Nine of the 10 events studied by Cliver et al.(1986) were associated with CMEs. The GHB events lasted 10-30 min and occurred when the CME leading edges were at ~ 2-4 $R_o$. Cliver et al. interpreted these events in terms of particle acceleration occurring in the magnetic reconnection regions of the Kopp and Pneuman (1976) model. The possible disconnection event of Illing and Hundhausen would appear to be a much later and less energetic phase of this phenomenon.

## CMEs and Shocks

The super-Alfvenic speeds (> 400 km $s^{-1}$) of the faster CMEs through the corona have made them obvious candidates for initiating coronal and interplanetary shock waves, which are observed as slow drift type II radio bursts. The nearly one-to-one association found between metric type II bursts occurring near the limb and Skylab CMEs with speeds exceeding 400-500 km $s^{-1}$ (Gosling et al., 1976; Munro et al., 1979) appeared to confirm this expectation. However, results of the last quadrennium have left the status of the CME/shock relationship quite confused.

Difficulties arose when Sheeley et al.(1984) and Robinson et al.(1986) compared Solwind CMEs with Culgoora metric type II bursts. Of 64 type II bursts 70% were associated with CMEs but 30% were not. Type II bursts without CMEs were generally simple, had high starting and ending frequencies, and were associated with short duration (~ 0.5 hr) soft X-ray flares. Those type II bursts with CMEs showed a complexity correlated with CME speed, had lower characteristic frequencies, and were associated with long duration (~ 3 hr) soft X-ray flares. When type II bursts were accompanied by CMEs, the speeds of those CMEs ranged upward from 400 km $s^{-1}$, as found for the Skylab CMEs by Gosling et al. (1976). However, many fast CMEs, including 4 CMEs with measured speeds above 1000 km $s^{-1}$, were not associated with metric type II bursts. Sheeley et al.(1984) explained the type II bursts without CMEs as blast wave shocks (as opposed to the "piston-driven" shocks of CMEs). They suggested that coronal regions of unusually high Alfven speeds resulted in fast CMEs without type II bursts.

Kahler et al.(1984a) extended the Solwind study to a larger sample of events and found that about 60% of all type II bursts associated with flares from 31° to 90° in solar longitude were accompanied by observed CMEs. Sawyer (1985), on the other hand, compared Skylab, Solwind, and C/P data to suggest that at least 80% of type II bursts near the limb are associated with CMEs. In their examination of fast (v > 500 km $s^{-1}$) Solwind CMEs Kahler et al.(1985a) reported that although faster CMEs are more likely to be associated with type II bursts, about 33% of all fast frontside CMEs are not associated with such bursts.

These results show that at least some type II bursts may be interpreted as blast waves. Wagner and MacQueen (1983) have suggested that even when a CME is associated with a type II burst, the inferred shock is also produced as a blast wave in the low corona and proceeds to travel through and then ahead of the CME. They based their idea on several observational points (Wagner, 1983): (1) CME trajectories extrapolate back to the inner corona to times earlier than the impulsive phases presumed to generate the flare shocks (Sawyer, 1983; Dulk, 1984; MacQueen, 1985); (2) evidence for type II source regions behind, rather than ahead of, the leading edges of CMEs; and (3) speeds of type II bursts in excess of the CME speeds. Point (1) presents a problem for the earlier shock model of Maxwell and Dryer (1981), in which the CME and resulting piston-driven shock are produced in the flare explosive phase. If the CME begins to erupt well before the flare starts, then the shock, which usually projects back to the impulsive phase (Kahler et al., 1984a), must be a blast wave following the CME. If CMEs and coronal shocks are not cause and effect, we have to ask why shocks are never observed with slow (v < 400 km $s^{-1}$) CMEs. In addition, type II shocks are not well correlated with the fluxes of impulsive 3 cm bursts (Kahler et al., 1984a). Evidence for point (2) is meager because only several CMEs have been accompanied by radioheliographic (positional) observations of type II bursts. The three type II bursts examined by Gary et al.(1984), Stewart et al. (1982), and Gergely et al.(1984a) appear to occur behind the CME leading edges. However, the analysis of a fourth event by Gary et al.(1986) suggests a shock leading the CME. Point (3) is substantiated by Gergely's (1986b) finding that the average speed of type II bursts (1380 km $s^{-1}$) is ~ 1.8 times higher than that of CMEs associated with type II bursts (~ 820 km $s^{-1}$). It should be noted that in Gergely's study the two groups of type II bursts and of CMEs had few events in common. In addition, the derivation of shock speeds depends on the particular coronal density model employed to interpret the type II burst drift rates. In making the case for piston-driven shocks Maxwell (1986) has considered the deduced speeds of type II shocks and emphasizes the lower average speeds (760-930 km $s^{-1}$) reported by Robinson (1985). In particular, Maxwell is critical of the very high speed (4900 km $s^{-1}$) deduced by Gergely et al.(1983) for a type II burst shock associated with a CME. Maxwell et al.(1985) discussed an event in which they concluded that a shock moved at a speed of 1000 km $s^{-1}$, presumably just ahead of the associated CME moving with a speed of 600-800 km $s^{-1}$. They offer this event as one in agreement with the Maxwell and Dryer (1981) piston-driven shock model. Most of the C/P looplike CMEs are preceded by deflections of pre-existing coronal features ahead of the CME flanks, suggesting that waves or shocks are running well ahead of the CME fronts (Sime and Hundhausen, 1986). The two models by Steinolfson (1984) and Wu et al.(1986) represent a new approach to the problem of type II bursts and CMEs and address points (2) and (3)

above. They combined numerical simulations of CME-driven shocks with the Holman and Pesses (1983) shock drift acceleration mechanism for type II burst emission. Although the radio generation mechanisms differ in the two models, the type II sources appear below the CME leading edge in projection, and show high apparent speeds relative to the CME. These models therefore retain the piston-driven shock, but account for the objections cited by Wagner and MacQueen (1983) and Wagner (1984). In summary, the relationships among CMEs, coronal shocks, and flare impulsive phases remain unsettled.

In contrast to coronal shocks, the association between CMEs and interplanetary shocks seems relatively simple. Sheeley et al.(1983a, 1985) looked for Solwind CMEs associated with shocks detected at the Helios 1 spacecraft when it was within 30° of a solar limb. In 49 cases CMEs were found with appropriate timings and positions for confident shock associations, 18 cases were possible, and only 1 doubtful. Associated CMEs were generally major events - relatively large and bright. In the reverse direction Sheeley et al.(1983a) examined 27 major CMEs directed toward Helios but not already associated with shocks. 17 of these were not within 15° of the ecliptic, and 9 of the remaining 10 were associated with some kind of interplanetary disturbance. These results indicate that with very few exceptions interplanetary disturbances are produced by major CMEs and are confined in latitude to within 15° of the angular extents of the CMEs measured at 10 $R_o$ (Michels et al., 1984a). For their 49 confident associations the average CME speed (measured in the plane of the sky) was 749 km $s^{-1}$, the average shock transit speed to Helios was 744 km $s^{-1}$, and the average in situ shock speed at Helios was 656 km $s^{-1}$, indicating some interplanetary deceleration of the shock. Interplanetary deceleration of shocks was also found by Woo et al.(1985) using spacecraft Doppler scintillation measurements. Speeds of the faster shocks near the sun were considerably higher than those of the associated CMEs, leaving unclear whether the shocks were located at the CME front or were moving faster and well ahead of the CME. With the excellent correlation found between Helios shocks and Solwind CMEs, it is not surprising that an initial comparison of interplanetary type II radio bursts with Solwind CMEs also shows a similar association (Cane and Stone, 1984).

While all transient interplanetary shocks appear at least initially to be piston-driven by CMEs, our understanding of the relationship between coronal shocks and interplanetary shocks is as muddled as that between coronal shocks and CMEs. A major problem here is that the lack of observations between 2 and 20 MHz does not allow us to determine whether coronal type II shocks evolve into interplanetary shocks. Sheeley et al.(1984) presented evidence that metric type II shocks without CMEs do not give rise to interplanetary shocks. Cane (1984) has suggested the concept of two independent shocks, a blast-wave coronal shock (Wagner and MacQueen, 1983) and a piston-driven interplanetary shock. She discusses several objections to her model including: (1) most interplanetary type II bursts are preceded by coronal type II bursts; (2) coronal type II bursts associated with interplanetary type II bursts have statistically lower starting frequencies than all coronal type II bursts (Robinson et al., 1984), suggesting a relationship between the two kinds of bursts; and (3) energetic coronal type II bursts are characterized by herringbone emission, presumed due to the escape of energetic electrons along open field lines not supposed to be present in CMEs.

The close association between solar energetic particle (SEP) events and coronal shocks (Lee, 1983) suggests that CMEs may also be linked to SEP events. Kahler et al.(1984b) found that 26 of 27 SEP (E > 4 Mev) events could be associated with CMEs. In addition, the peak proton fluxes were correlated with both CME speeds and CME angular sizes. However, no CME associations could be made for a few events, now thought to be electron-rich particle events (Cane et al., 1986). In addition, no significant CME or type II burst associations were found for $^3$He-rich events (Kahler et al., 1985b).

## Interplanetary Observations and Effects of CMEs

The zodiacal light photometers on board the Helios spacecraft allow low-resolution imaging of CMEs at large distances (~ 15 $R_o$ to 1 AU) from the sun (Jackson et al., 1985). To date 9 CMEs observed by either Solwind or the C/P instruments have been compared to Helios observations (Jackson, 1985a,b; 1986a,b). In general, the gross features deduced for these CMEs at ~ 0.5 AU are quite similar to those deduced from the coronagraph observations. The speeds and angular extents are quite similar, indicating no major changes other than a simple expansion of these 9 events as they travelled through the interplanetary medium. The masses, however, are several times larger than those deduced from coronagraph data. Whether this is due to additional mass flow from the corona or to ambient solar wind plasma compressed ahead of the CME is not known.

It is of obvious interest to make in situ measurements of CMEs at the earth. Coronagraph observations of CMEs are strongly biased toward those events located above the solar limbs, so that in general, Earth-directed CMEs, except for the few halo events (Howard et al., 1982), will not be observed. However, the signature of a major interplanetary disturbance directed at the Earth has long been known: (1) a large solar flare followed 1 to 3 days later by (2) the arrival of an interplanetary shock resulting in a geomagnetic storm sudden commencement and (3) a subsequent storm and Forbush decrease lasting 1 to 10 days, often accompanied by (4) solar wind of enhanced helium abundance. Since we have seen that large flares and interplanetary shocks are well associated with CMEs, we might expect the characterization of CMEs at the earth to be a fairly straightforward task. For several reasons the situation is still regrettably muddled.

Borrini et al.(1982a,b; 1983) have taken an obvious approach to studies of CMEs at the earth. They analyzed the 103 forward shocks and 73 cases of solar wind helium abundance enhancements (He/H > 10% for > 2 hrs) observed during 1971-1978 with the Los Alamos plasma instruments on IMP 6, 7, and 8. Helium enrichments (He/H > 8%) followed

46% of the shocks, and, conversely, shocks were associated with 44% of the helium enhancements. The helium enrichments followed the solar cycle in frequency of occurrence and were often associated with solar type II and IV radio bursts. They preferentially occurred in regions of low proton temperature and high magnetic field behind the strongest shocks. Borrini et al. concluded that virtually all the shocks and helium enhancements of their studies were associated with CMEs. Because the frequency of their shocks and helium abundances at the earth is much lower than the expected incidence of CMEs, they suggested that other CMEs may have weaker or different plasma signatures. Some noncompressive density enhancements may arise from CMEs (Fenimore, 1980).

An examination of the driver gas of 9 shocks (Zwickl et al., 1983) indicated that helium enrichments usually have time scales of minutes and can occur anywhere within the low temperature regions that follow the shell of shocked ambient plasma. From this Zwickl et al. suggest a patchy distribution of the helium enriched material within the cold driver gas. In this model it is possible to observe the shock without detecting driver gas, which is consistent with their finding of a "well defined" driver gas after only 9 of 54 shocks observed in 1978-1979. Another kind of solar wind helium enrichment, that of $He^+$ relative to the normal ion $He^{++}$, also appears promising as a signature of the cool filamentary material known to be ejected in many CMEs (Illing and Hundhausen, 1985). Cane et al.(1986) find that at least 6 of the 15 or so reports of $He^+$ (Bame, 1983) can be associated with solar filament eruptions. Unfortunately, the Los Alamos IMP and ISEE plasma detectors were not designed with a high sensitivity to such an exotic ion (Bame, 1983); otherwise the 1 AU passage of filamentary material might have been routinely detected.

The magnetic loops inferred to exist behind shocks in interplanetary space motivated Klein and Burlaga (1982) to define an interplanetary magnetic structure which they call a magnetic cloud. These are regions with radial dimensions of ~ 0.25 AU at 1 AU in which the magnetic field strengths are high and the field direction changes by the rotation of one component nearly parallel to a plane. This geometry is consistent with a magnetic loop or helix. Klein and Burlaga identified 45 clouds near earth from 1967 to 1978. Each cloud was associated with either a shock, a stream interface or a cold magnetic enhancement (for which they used the ambiguous acronym CME). Because the field and plasma parameters are similar for clouds of each class, they suggest all clouds are the manifestations of a single phenomenon, a CME. The observed masses (~ $2 \times 10^{15}$ g), speeds (400-500 km $s^{-1}$), magnetic field strengths (~ 12 nT), and occurrence rates (0.5 to 1 cloud/month) are all consistent with the identification of coronal clouds as CMEs. The total pressures of magnetic clouds exceeded those of the ambient plasmas, so cloud expansions were inferred. A study of 5 clouds between 2 and 4 AU (Burlaga and Behannon, 1982) showed that the clouds persisted out to those distances with estimated expansion speeds of nearly half the Alfven speed. A good case of an association between a CME observed over the west limb by Solwind and a magnetic cloud observed at 0.54 AU by Helios 1 two days later was presented by Burlaga et al.(1982).

While Klein and Burlaga argued for an association between CMEs and magnetic clouds on statistical grounds, Wilson and Hildner (1984) sought direct CME associations for the post-1970 clouds using proxy solar data for the occurrences of CMEs. They compared four kinds of events (Hα flares, type II and IV radio bursts, gradual-rise-and-fall radio bursts, and soft X-ray events) during appropriate cloud launch windows with similar events during no-cloud control periods. Comparing the four kinds of proxy data for the three classes of magnetic clouds, they found that in one case - type II bursts for the 9 cases of clouds following shocks - a significant signal emerged. This result supports the CME/ magnetic cloud hypothesis only for the clouds following shocks. Wilson and Hildner (1986) compared the magnetic clouds observed between 1967 and mid-1974 with solar filament disappearances during the cloud launch windows. 17 of the 33 cloud windows contained one or more disappearing filaments, compared to only 7 of the 33 control windows. Although less than a one-to-one correlation, this result is further statistically significant evidence for the CME/magnetic cloud hypothesis.

There are several qualifications to the link between CMEs and magnetic clouds. First, the CME loop structure which helped inspire the idea of coronal clouds is observed in less than half the Skylab (Munro and Sime, 1985) and the Solwind (Howard et al., 1985) CMEs. The magnetic structures of cloud, streamer blowout, spike, ray, and fan CMEs are not known. Second, the definition of clouds adopted by Klein and Burlaga (1982) restricts the presumed magnetic loops to those with loop axes (corresponding to the minimum variance direction) close (< 45°) to the ecliptic plane, thus excluding possible loops with axes nearly perpendicular to the ecliptic. In summary, it appears that some of the identified magnetic clouds correspond to CMEs, but many other CMEs drift past the earth eluding detection.

## The Future

While recent studies have advanced our understanding of CMEs, they have been paralleled by vexing inconsistencies and uncertainties. This has been particularly acute in comparing the occurrence rates, angular widths, morphologies, forerunners, and even speeds of the Skylab and C/P observations with those of the Solwind observations. This situation may prove to be fortuitous if it leads the HAO and NRL groups to a deeper understanding of the effects of the differences between their coronagraphs and between the techniques used for measuring the properties of CMEs. We also have to be cautious of some results which are based on small or selected samples of events, often necessarily so restricted. However, we have also been frustrated in cases with large data samples. An egregious example is that of the relationship between metric type II bursts and CMEs, for which no simple or consistent picture has yet emerged.

Future observational work should be particularly fruitful in revealing the origin of CMEs

and their role in coronal evolution. The HAO and NRL groups are now using synoptic observations to investigate the ambient coronal structures from which CMEs arise. This work may help in understanding the currently undefined relationship of the large preflare and postflare coronal X-ray arches to CMEs. It may also help to delineate the differences between prominence- and flare-associated CMEs, perhaps in terms of closed and open magnetic field configurations. The acceleration profiles of CMEs and the nature of the interaction of forerunners with the ambient corona have yet to be examined. We also need to look at the coronal aftermath of CMEs. How long does the corona remain open after a CME, how much total mass escapes, and how does the corona subsequently evolve? All these questions can only be answered with a detailed quantitative analysis of the coronagraph data requiring more effort than the identification and compilation of CME properties characteristic of past studies.

More work can also be expected on the physics of eruptive prominences. They are directly observed to be an important component in many CMEs and their cool ions may be observed in the solar wind and possibly in energetic particle events at 1 AU. Their detailed structures may provide clues to stability criteria and eruptive forces. They also serve as the readily observed disk signatures of CMEs. Finally, there is a strong need to push further efforts in CME theory and modelling. In particular, we need to keep in mind the three-dimensional nature of CMEs and to explore the implications of the third dimension for the disconnection process.

Acknowledgements. I wish to thank D.F. Webb for helpful discussions and B.C. Low and N.R. Sheeley, Jr. for their comments on the manuscript. This work was supported by AFGL contract AF 19628-82-K-0039.

REFERENCES


Anzer, U., and G.W. Pneuman, Magnetic reconnection and coronal transients, Solar Phys., 79, 129, 1982.

Altrock, R.C., and H.L. DeMastus, Coronal transients in FeXIV 5303Å : first two-dimensional photoelectric ground-based observations, in Solar Wind Five, edited by M. Neugebauer, p.63, NASA Conf. Pub. 2280, 1983.

Athay, R.G., and R.M.E. Illing, Analysis of the prominence associated with the coronal mass ejection of August 18, 1980, J. Geophysical Res., 91, 10,961, 1986.

Bame, S.J., Solar wind minor ions - recent observations, in Solar Wind Five, edited by M. Neugebauer, p.577, NASA Conf. Pub. 2280, 1983.

Bird, M.K., H. Volland, R.A. Howard, M.J. Koomen, D.J. Michels, N.R. Sheeley, Jr., J.W. Armstrong, B.L. Seidel, C.T. Stelzried, and R. Woo, Coronal transients observed during solar occultation of the Helios spacecraft in STIP Interval VIII, in STIP Symposium on Solar/Interplanetary Intervals, eds, M.A. Shea, D.F. Smart, and S.M.P. McKenna-Lawlor, Book Crafters, Chelsea, Michigan, 1984.

Bird, M.K., H. Volland, R.A. Howard, M.J. Koomen, D.J. Michels, N.R. Sheeley, Jr., J.W. Armstrong, B.L. Seidel, C.T. Stelzried, and R. Woo, White-light and radio sounding observations of coronal transients, Solar Phys., 98, 341, 1985.

Burrini, G., J.T. Gosling, S.J. Bame, and W.C. Feldman, An analysis of shock wave disturbances observed at 1 AU from 1971 through 1978, J. Geophys. Res., 87, 4365, 1982a.

Borrini, G., J.T. Gosling, S.J. Bame, and W.C. Feldman, Helium abundance enhancements in the solar wind, J. Geophys. Res., 87, 7370, 1982b

Burrini, G., J.T. Gosling, S.J. Bame, and W.C. Feldman, Helium abundance variations in the solar wind, Solar Phys., 83, 367, 1983.

Burlaga, L.F., and K.W. Behannon, Magnetic clouds: Voyager observations between 2 and 4 au, Solar Phys., 81, 181, 1982.

Burlaga, L.F., L. Klein, N.R. Sheeley, Jr., D.J. Michels, R.A. Howard, M.J. Koomen, R. Schwenn, and H. Rosenbauer, A magnetic cloud and a coronal mass ejection, Geophys. Res. Ltrs, 9, 1317, 1982.

Cane, H.V., The relationship between coronal transients, type II bursts and interplanetary shocks, Astron. Astrophys., 140, 205, 1984.

Cane, H.V., and R.G. Stone, Type II solar radio bursts, interplanetary shocks, and energetic particle events, Astrophys. J., 282, 339, 1984.

Cane, H.V., R.E. McGuire, and T.T. von Rosenvinge, Two classes of solar energetic particle events associated with impulsive and long-duration soft X-ray flares, Astrophys. J., 301, 448, 1986a.

Cane, H.V., S.W. Kahler, and N.R. Sheeley, Jr., Interplanetary shocks preceded by solar quiescent prominence eruptions, J. Geophys. Res., in press, 1986b.

Cliver, E.W., S.W. Kahler, H.V. Cane, M.J. Koomen, D.J. Michels, R.A. Howard, and N.R. Sheeley, Jr., The CLE-associated flare of 21 August, 1979, Solar Phys., 89, 181, 1983.

Cliver, E.W., B.R. Dennis, A.L. Kiplinger, S.R. Kane, D.F. Neidig, N.R. Sheeley, Jr., and M.J. Koomen, Solar gradual hard X-ray bursts and associated phenomena, Astrophys. J., 305, 920, 1986.

Dryer, M., Coronal transient phenomena, Space Sci. Rev., 33, 233, 1982.

Dryer, M., S.T. Wu, R.S. Steinolfson, and R.M. Wilson, Magnetohydrodynamic models of coronal transients in the meridional plane. II. simulation of the coronal transient of 1973 August 21, Astrophys. J., 227, 1059, 1979.

Dryer, M., and D.F. Smart, Dynamical models of coronal transients and interplanetary disturbances, Adv. Space Res., 4, 291, 1984.

Dryer, M., and S.T. Wu, Comments on "density distribution in looplike coronal transients: a comparison of observations and a theoretical model" by D.G. Sime, R.M. MacQueen, and A.J. Hundhausen, J. Geophys. Res., 90, 559, 1985.

Dulk, G.A., Radio wave heating in impulsive flares, shock waves, and coronal mass ejections, p.331, in STIP Symposium on Solar/Interplanetary Intervals, edited by M.A. Shea, D.F. Smart and S.M.P. McKenna-Lawlor, p.331, Book Crafters, Chelsea, Michigan, 1984.

Fenimore, E.E., Solar wind flows associated with hot heavy ions, Astrophys. J., 235, 245, 1980.

Fisher, R.R., Coronal mass-ejection events, Adv. Space Res., 4, 161, 1984.

Fisher, R., and C. Garcia, Detection of a slowly moving coronal transient event, Astrophys. J., 282, L35, 1984.

Fisher, R.R., and R.H. Munro, Coronal transient geometry. I. the flare-associated event of 1981 March 25, Astrophys. J., 280, 428, 1984.

Fisher, R.R., and A.I. Poland, Coronal activity below 2 $R_\odot$: 1980 February 15-17, Astrophys. J., 244, 1004, 1981.

Fisher, R.R., L.B. Lacey, R.A. Rock, E.A. Yasukawa, H.R. Sheeley, Jr., D.J. Michels, R.A. Howard, M.J. Koomen, and A. Bagrov, The solar corona on 31 July 1981, Solar Phys., 83, 233, 1983.

Gary, D.E., G.A. Dulk, L. House, R. Illing, C. Sawyer, W.J. Wagner, D.J. McLean, and E. Hildner, Type II bursts, shock waves, and coronal transients: the event of 1980 June 29, 0233 UT, Astron. Astrophys., 134, 222, 1984.

Gary, D.E., G.A. Dulk, L.L. House, R. Illing, W.J. Wagner, and D.J. McLean, The type IV burst of 1980 June 29, 0233 UT: harmonic plasma emission?, Astron. Astrophys., 152, 42, 1985.

Gary, D.E., T.E. Gergely, and N.R. Kundu, Shock waves and coronal transients: the event of 1980 April 17, Adv. Space Res., in press, 1986.

Gergely, T.E., On the relative velocity of coronal transients and type II bursts, in STIP Symposium on Solar/Interplanetary Intervals, edited by M.A. Shea, D.F. Smart, and S.M.P. McKenna-Lawlor, p.347, Book Crafters, Chelsea, Michigan, 1984.

Gergely, T.E., Type IV bursts and coronal mass ejections, Solar Phys., 104, 175, 1986a.

Gergely, T.E., Radio studies of coronal transients, in Solar Terrestrial Physics Proceedings of Second Indo-US Workshop on Solar-Terrestrial Physics, edited by N.R. Kundu, D. Blevins, B.N. Reddy, and S. Ramadurai, p.303, Inadec, New Delhi, 1986b.

Gergely, T.E., N.R. Kundu, and E. Hildner, A coronal transient associated with a high-speed type II burst, Astrophys. J., 268, 403, 1983.

Gergely, T.E., N.R. Kundu, F.T. Erskine, III, C. Sawyer, W.J. Wagner, R. Illing, L.L. House, M.K. McCabe, R.T. Stewart, C.J. Nelson, M.J. Koomen, D. Michels, R. Howard, and N. Sheeley, Radio and visible light observations of a coronal arcade transient, Solar Phys., 90, 161, 1984a.

Gergely, T.E., N.R. Kundu, S.T. Wu, M. Dryer, Z. Smith, and R.T.Stewart, A multiple type-II burst associated with a coronal transient and its MHD simulation, Adv. Space Res., 4, 283, 1984b.

Gosling, J.T., E. Hildner, R.M. MacQueen, R.H. Munro, A.I. Poland, and C.L. Ross, The speeds of coronal mass ejection events, Solar Phys., 48, 389, 1976.

Harrison, R.A., Solar coronal mass ejections and flares, Astron. Astrophys., 162, 283, 1986.

Harrison, R.A., P.W. Waggett, R.D. Bentley, K.J.H. Phillips, M. Bruner, M. Dryer, and C.M. Sianett, The X-ray signature of solar coronal mass ejections, Solar Phys., 97, 367, 1985.

Harrison, R.A., and C.M. Sianett, Soft X-ray bursts associated with coronal mass ejection onsets, in STIP Symposium on Retrospective Analyses, edited by M.A. Shea and D.F. Smart, Book Crafters, Chelsea, Michigan, in press, 1986.

Hildner, E., Mass ejections from the corona into interplanetary space, in Study of Travelling Interplanetary Phenomena, edited by M.A. Shea, D.F. Smart, and S.T. Wu, p.3, D. Reidel, Hingham, Mass., 1977.

Hildner, E., Do we understand coronal mass ejections yet?, Adv. Space Res., in press, 1986.

Hildner, E., J.T. Gosling, R.T. Hansen, and J.D. Bohlin, The sources of material comprising a mass ejection coronal transient, Solar Phys., 45, 363, 1975.

Hildner, E., J.T. Gosling, R.M. MacQueen, R.H. Munro, A.I. Poland, and C.L. Ross, Frequency of coronal transients and solar activity, Solar Phys., 48, 127, 1976.

Hildner, E., et al., Coronal mass ejections and coronal structures, in SMM Workshop Proceedings, edited by B. Woodgate and M. Kundu, in press, 1986.

Holman, G.D., and M.E. Pesses, Solar type II radio emission and the shock drift accleration of electrons, Astrophys. J., 267, 837, 1983.

Howard, R.A., D.J. Michels, N.R. Sheeley, Jr., and M.J. Koomen, The observation of a coronal transient directed at earth, Astrophys. J., 263, L101, 1982.

Howard, R.A., N.R. Sheeley, Jr., M.J. Koomen, and D.J. Michels, The statistical properties of coronal mass ejections during 1979-1981, Adv. Space Res., 4, 307, 1984.

Howard, R.A., N.R. Sheeley, Jr., M.J. Koomen, and D.J. Michels, Coronal mass ejections: 1979-1981, J. Geophys. Res., 90, 8173, 1985.

Howard, R.A., N.R. Sheeley, Jr., D.J. Michels, and M.J. Koomen, The solar cycle dependence of coronal mass ejections, in The Sun and the Heliosphere in Three Dimensions, edited by R.G. Marsden, p.107, D. Reidel, Dordrecht, 1984.

Hundhausen, A.J., Long-term variations in the characteristics of coronal mass ejections, J. Geophys. Res., submitted, 1986.

Hundhausen, A.J., C.B. Sawyer, L. House, R.M.E. Illing, and W.J. Wagner, Coronal mass ejections observed during the solar maximum mission: latitude distribution and rate of occurrence, J. Geophys. Res., 89, 2639, 1984a.

Hundhausen, A.J., et al., Coronal transients and

their interplanetary effects, in Solar Terrestrial Physics: Present and Future, edited by D.M. Butler and K. Papadopoulos, p.8-1, NASA Ref. Pub. 1120, 1984b.
Illing, R.M.E., The complex coronal transient of 1980 March 23, Astrophys. J., 280, 399, 1984.
Illing, R.M.E., and R.G. Athay, Physical conditions in eruptive prominences at several solar radii, Solar Phys., 105, 173, 1986.
Illing, R.M.E., and A.J. Hundhausen, Possible observation of a disconnected magnetic structure in a coronal transient, J. Geophys. Res., 88, 10,210, 1983.
Illing, R.M.E., and A.J. Hundhausen, Observation of a coronal transient from 1.2 to 6 solar radii, J. Geophys. Res., 90, 275, 1985.
Illing, R.M.E., and A.J. Hundhausen, Disruption of a coronal streamer by an eruptive prominence and coronal mass ejection, J. Geophys. Res., 91, 10,951, 1986.
Jackson, B.V., IPS and spacecraft observations of the 14 August 1979 mass ejection transient, in STIP Symposium on Solar/Interplanetary Intervals, edited by M.A. Shea, D.F. Smart, and S.M.P. McKenna-Lawlor, p.169, Book Crafters, Chelsea, Michigan, 1984.
Jackson, B.V., Helios observations of the earthward-directed mass ejection of 27 November, 1979, Solar Phys., 95, 363, 1985a.
Jackson, B.V., Imaging of coronal mass ejections by the Helios spacecraft, Solar Phys., 100, 563, 1985b.
Jackson, B.V., Helios images of coronal mass ejections, in The Sun and the Heliosphere in Three Dimensions, edited by R.G. Marsden, p.111, D. Reidel, Dordrecht, 1986a.
Jackson, B.V., A review of STIP Interval VI (5 April - 15 June 1979), in STIP Symposium on Retrospective Analyses, edited by M.A. Shea and D.F. Smart, Book Crafters, Chelsea, Michigan, in press, 1986b.
Jackson, B.V., Helios photometer measurement of in situ density enhancements, Adv. Space Res., in press, 1986c.
Jackson, B.V., and E. Hildner, Forerunners: outer rims of solar coronal transients, Solar Physics, 60, 155, 1978.
Jackson, B.V., and C. Leinert, Helios images of solar mass ejections, J. Geophys. Res., 90, 10,739, 1985.
Jackson, B.V., R.A. Howard, H.R. Sheeley, Jr., D.J. Michels, M.J. Koomen, and R.M.E. Illing, Helios spacecraft and earth perspective observations of three loop-like solar mass ejection transients, J. Geophys. Res., 90, 5075, 1985.
Kahler, S.W., R.E. McGuire, D.V. Reames, T.T. von Rosenvinge, N.R. Sheeley, Jr., M.J. Koomen, R.A. Howard, and D.J. Michels, The correlation of coronal mass ejections with energetic flare proton events, Proc. 18th Internat. Cosmic Ray Conf. (Bangalore), 4, 8, 1983.
Kahler, S., N.R. Sheeley, Jr., R.A. Howard, M.J. Koomen, and D.J. Michels, Characteristics of flares producing metric type II bursts and coronal mass ejections, Solar Phys., 91, 113, 1984a.
Kahler, S.W., N.R. Sheeley, Jr., R.A. Howard, M.J. Koomen, D.J. Michels, R.E. McGuire, T.T. von Rosenvinge, and D.V. Reames, Associations between coronal mass ejections and solar energetic proton events, J. Geophys. Res., 89, 9683, 1984b.
Kahler, S.W., E.W. Cliver, N.R. Sheeley, Jr., R.A. Howard, M.J. Koomen, and D.J. Michels, Characteristics of coronal mass ejections associated with solar frontside and backside metric type II bursts, J. Geophys. Res., 90, 177, 1985a.
Kahler, S., D.V. Reames, N.R. Sheeley, Jr., R.A. Howard, M.J. Koomen, and D.J. Michels, A comparison of solar $^3$He-rich events with type II bursts and coronal mass ejections, Astrophys. J., 290, 742, 1985b.
Kahler, S.W., E.W. Cliver, N.V. Cane, R.F. McGuire, R.C. Stone, and N.R. Sheeley, Jr., Energetic protons from a disappearing solar filament, Proc. 19th Internat. Cosmic Ray Conf.(La Jolla), 4, 94, 1985c.
Kahler, S.W., E.W. Cliver, N.V. Cane, R.E. McGuire, R.C. Stone, and N.R. Sheeley, Jr., Solar filament eruptions and energetic particle events, Astrophys. J., 302, 504, 1986.
Karpen, J.T., and R.A. Howard, A search for precursor activity associated with coronal mass ejections, J. Geophys. Res., submitted, 1986.
Klein, L.W., and L.F. Burlaga, Interplanetary magnetic clouds at 1 au, J. Geophys. Res., 87, 613, 1982.
Kopp, R.A., and G.W. Pneuman, Magnetic reconnection in the corona and the loop prominence phenomenon, Solar Phys., 50, 85, 1976.
Kreplin, R.W., G.A. Doschek, U. Feldman, N.R. Sheeley, Jr., and J.F. Seely, High resolution X-ray spectra of solar flares. VII. a long-duration X-ray flare associated with a coronal mass ejection, Astrophys. J., 297, 309, 1985.
Lee, M.A., The association of energetic particles and shocks in the heliosphere, Rev. Geophys. Space Physics, 21, 326, 1983.
Low, B.C., Self-similar magnetohydrodynamics. IV. the physics of coronal transients, Astrophys. J., 281, 392, 1984a.
Low, B.C., On the large-scale magnetostatic coronal structures and their stability, Astrophys. J., 286, 772, 1984b.
Low, B.C., Coronal mass ejections, in Highlights of Astronomy, Volume 7, edited by J.-P. Swings, p.743, D. Reidel Publishing Co., Dordrecht, 1986.
Low, B.C., and A.J. Hundhausen, The velocity field of a coronal mass ejection: the event of September 1, 1980, J. Geophys. Res., submitted, 1986.
MacQueen, R.M., Coronal transients: a summary, Phil. Trans. R. Soc. Lond., A297, 605, 1980.
MacQueen, R.M., Coronal mass ejections: acceleration and surface associations, Solar Phys., 93, 359, 1985.
MacQueen, R.M. A. Csoeke-Poeckh, E. Hildner, L. House, R. Reynolds, A. Stanger, H. TePoel, and W. Wagner, The high altitude observatory coronagraph/polarimeter on the solar maximum mission, Solar Phys., 65, 91, 1980.
MacQueen, R.M., and R.R. Fisher, The kinematics of solar inner coronal transients, Solar Phys., 89, 89, 1983.
MacQueen, R.M., and D.M. Cole, Broadening of loop-like solar coronal transients, Astrophys. J., 299, 526, 1985.
MacQueen, R.M., A.J. Hundhausen, and C.W. Conover, The propagation of coronal mass ejection transients, J. Geophys. Res., 91, 31, 1986.
Maran, S.P., and B.L. Woodgate, A second chance for solar use, Sky and Telescope, 67, 499, 1984.
Marshall, J., Working solar monitor shut down by ASAT, Science, 230, 44, 1985.
Marwell, A., Characteristics of flare-generated shocks in the solar corona, in STIP Symposium on Retrospective Analyses, edited by M.A. Shea and D.F. Smart, Book Crafters, Chelsea, Michigan, in press, 1986.
Marwell, A., and M. Dryer, Solar radio bursts of spectral type II, coronal shocks, and optical coronal transients, Solar Phys., 73, 333, 1981.
Marwell, A., M. Dryer, and P. McIntosh, A piston-driven shock in the solar corona, Solar Phys., 91, 401, 1985.
McCabe, M.K., Z.F. Svestka, R.A. Howard, B.V. Jackson, and N.R. Sheeley, Jr., Coronal mass ejection associated with the stationary post-flare arch of 21-22 May 1980, Solar Phys., 70, 399, 1986.
Michels, D.J., R.A. Howard, N.R. Sheeley, Jr., and M.J. Koomen, Evidence for directivity of coronal transients, in STIP Symposium on Solar/Interplanetary Intervals, edited by M.A. Shea, D.F. Smart, and S.M.P. McKenna-Lawlor, p.319, Book Crafters, Chelsea, Michigan, 1984a.
Michels, D.J., N.R. Sheeley, Jr., R.A. Howard, M.J. Koomen, R. Schwenn, K.H. Muhlhauser, and H. Rosenbauer, Synoptic observations of coronal transients and their interplanetary consequences, Adv. Space Res., 4, 311, 1984b.
Michels, D.J., R.A. Howard, N.R. Sheeley, Jr., and M.J. Koomen, Observations of coronal mass ejections, Adv. Space Res., in press, 1986.
Munasheviias, T. Ch., and A.I. Poland, Expansion and broadening of coronal loop transients: a theoretical explanation, Astrophys. J., 220, 675, 1978.
Munro, R.H., J.T. Gosling, E. Hildner, R.M. MacQueen, A.I. Poland, and C.L. Ross, The association of coronal mass ejection transients with other forms of solar activity, Solar Phys., 61, 201, 1979.
Munro, R.H., and B.G. Sime, White-light coronal transients observed from Skylab May 1973 to February 1974: a classification by apparent morphology, Solar Phys., 97, 191, 1985.
Pneuman, G.W., Dimagnetic aspects of the coronal transient phenomenon, Adv. Space Res., 2, 233, 1983.
Pneuman, G.W., Evolution of rising helical prominences in a nonuniform atmosphere, Solar Phys., 96, 299, 1984a.
Pneuman, G.W., The 'melon-seed' mechanism and coronal transients, Solar Phys., 94, 387, 1984b.
Pneuman, G.W., and F.Q. Orrall, Structure, dynamics, and heating of the solar atmosphere, in Physics of the Sun, Volume II: The Solar Atmosphere, edited by P.A. Sturrock, T.E. Holzer, D.M. Mihalas, and R.K. Ulrich, p.71, D. Reidel, Boston, 1986.
Robinson, R.D., Velocities of type II solar radio events, Solar Phys., 95, 343, 1985.
Robinson, R.D., R.T. Stewart, and H.V. Cane, Properties of metre-wavelength solar bursts associated with interplanetary type II emission, Solar Phys., 91, 159, 1984.
Robinson, R.D., R.T. Stewart, H.R. Sheeley, Jr., R.A. Howard, J. Koomen, and D.J. Michels, Properties of metre-wavelength solar bursts associated with coronal mass ejections, Solar Phys., 105, 149, 1986.
Roosen, R., B.C. Low, and T.E. Holzer, Physical processes in the solar corona, in Physics of the Sun Volume II: The Solar Atmosphere, edited by P.A. Sturrock, T.E. Holzer, D.M. Mihalas, and R.K. Ulrich, p.135, D. Reidel, Boston, 1986.
Rust, D.M., Solar Activity, Rev. Geophys. Space Physics, 21, 349, 1983.
Rust, D.M., et al., Mass Ejections, in Solar Flares, edited by P.A. Sturrock, p.273, Colorado Assoc. Univ. Press, Boulder, 1980.
Sawyer, C., Visibility and rate of coronal mass ejections, Solar Phys., 98, 369, 1985.
Sawyer, C., C. Jarnell, P.T. Erskine, III, and T. Gergely, Solar and interplanetary observations of the 1980 April 12 west-limb flare, in STIP Symposium on Solar/Interplanetary Intervals, edited by M.A. Shea, D.F. Smart, and S.M.P. McKenna-Lawlor, p.237, Book Crafters, Chelsea, Michigan, 1984.
Schwenn, R., Relationship of coronal transients to interplanetary shocks: 3d aspects, Space Sci. Rev., 44, 139, 1986.
Sheeley, N.R., Jr., R.A. Howard, D.J. Michels, and M.J. Koomen, Solar observations with a new earth-orbiting coronagraph, in Solar and Interplanetary Dynamics, edited by M. Dryer and E. Tandberg-Hanssen, p.55, D. Reidel, Hingham, Mass., 1980.
Sheeley, N.R., Jr., R.A. Howard, M.J. Koomen, D.J. Michels, R. Schwenn, K.H. Muhlhauser, and H. Rosenbauer, Associations between coronal mass ejections and soft X-ray events, in Solar Wind Five, edited by M. Neugebauer, p.693, NASA Conf. Pub. 2280, 1983a.
Sheeley, N.R., Jr., R.A. Howard, M.J. Koomen, and D.J. Michels, Associations between coronal mass ejections and metric type II bursts, Astrophys. J., 272, 349, 1983b.
Sheeley, N.R., Jr., R.T. Stewart, R.E. Rubinson, R.A. Howard, M.J. Koomen, and D.J. Michels, Associations between coronal mass ejections and metric type II bursts, Astrophys. J., 279, 839, 1984.
Sheeley, N.R., Jr., R.A. Howard, M.J. Koomen, D.J. Michels, R. Schwenn, K.H. Muhlhauser, and H. Rosenbauer, Coronal mass ejections and interplanetary shocks, J. Geophys. Res., 90, 163, 1985.
Sheeley, N.R., Jr., R.A. Howard, M.J. Koomen, and D.J. Michels, Solwind observations of coronal mass ejections during 1979-1985, in Solar Flares and Coronal Physics Using P/OF as a Research Tool, edited by E. Tandberg-Hanssen, R.M. Wilson, and H.S. Hudson, p.241, NASA Conf. Pub. 2421, 1986.
Sime, D.G., Coronal transients at high heliographic latitudes, in The Sun and the Heliosphere in Three Dimensions, edited by R.G. Marsden, p.101, D. Reidel, Dordrecht, 1986.
Sime, D.G., Coronal transient apparent morphology and the associated solar activity, Solar Phys., submitted, 1986.
Sime, D.G., and A.J. Hundhausen, The coronal mass ejection of July 6, 1980: a candidate for interpretation as a coronal shock wave, J. Geophys. Res., submitted, 1986.
Sime, D.G., R.M. MacQueen, and A.J. Hundhausen, Density distribution in loop-like coronal transients: a comparison of observations and a theoretical model, J. Geophys. Res., 89, 2113, 1984.
Sime, D.G., R.M. MacQueen, and A.J. Hundhausen, Reply, J. Geophys. Res., 90, 563, 1985.
Sionett, C.M., and R.A. Harrison, The relationship between coronal mass ejections and solar flares, Adv. Space Res., 4, 229, 1984.
Steinolfson, R.S., Modeling of transient disturbances in coronal-streamer configurations, in Solar Wind Five, edited by M. Neugebauer, p.447, NASA Conf. Pub. 2280, 1983.
Steinolfson, R.S., Type II radio emission in coronal transients, Solar Phys., 94, 193, 1984.
Steinolfson, R.S., Theories of shock formation in the solar atmosphere, in Collisionless Shocks in the Heliosphere: Reviews of Current Research, edited by B.T. Tsurutani and R.G. Stone, p.1, American Geophysical Union, Washington, 1985.
Stewart, R.T., G.A. Dulk, R.V. Sheridan, L.L. House, W.J. Wagner, C. Sawyer, and R. Illing, Visible light observations of a dense plasmoid associated with a moving type IV solar radio burst, Astron. Astrophys., 116, 217, 1982.
Suess, S.T., and R.L. Moore, Wave speeds in the corona and the dynamics of mass ejections, in Solar Flares and Coronal Physics Using P/OF as a Research Tool, edited by E. Tandberg-Hanssen, R.M. Wilson, and H.S. Hudson, p.262, NASA Conf. Pub. 2421, 1986.
Svestka, Z., Revivals of a coronal arch, Solar Phys., 94, 171, 1984.
Tousey, R., The solar corona, in Space Research XIII, edited by M.J. Rycroft and S.K. Runcorn, p.713, Akademie-Verlag, Berlin, 1973.
Wagner, W.J., SERF studies of mass motions arising in flares, Adv. Space Res., 2, 203, 1983.

Wagner, W.J., Coronal mass ejections, Ann. Rev. Astron. Astrophys., 22, 267, 1984.

Wagner, W.J., R.M.E. Illing, C.B. Sawyer, L.L. House, N.R. Sheeley, Jr., R.A. Howard, M.J. Koomen, D.J. Michels, R.M. Smartt, and M. Dryer, A white-light/Fe X/Hα coronal transient observation to 10 solar radii, Solar Phys., 83, 153, 1983.

Wagner, W.J., and B.M. MacQueen, The excitation of type II radio bursts in the corona, Astron. Astrophys., 120, 136, 1983.

Wagner, W.J., and J.J. Wagner, Coronal mass ejection recurrence studies indicating global activity and local suppression, Astron. Astrophys., 133, 288, 1984.

Webb, D.F., The origin and kinematics of coronal mass ejections, in Solar Terrestrial Physics Proceedings of Second Indo-US Workshop on Solar-Terrestrial Physics, edited by M.R. Kundu, B. Biswas, B.M. Reddy, and S. Ramadurai, p.283, Inadec, New Delhi, 1986.

Webb, D.F., and A.J. Hundhausen, Activity associated with the solar origin of coronal mass ejections, Solar Phys., submitted, 1986.

Wilson, R.M., and E. Hildner, Are interplanetary magnetic clouds manifestations of coronal transients at 1 au?, Solar Phys., 91, 169, 1984.

Wilson, R.M., and E. Hildner, On the association of magnetic clouds with disappearing filaments, J. Geophys. Res., 91, 5867, 1986.

Wolfson, R., and S.A. Gould, The onset of coronal mass ejections, Astrophys. J., 296, 287, 1985.

Woo, R., J.W. Armstrong, N.R. Sheeley, Jr., R.A. Howard, M.J. Koomen, D.J. Michels, and R. Schwenn, Doppler scintillation observations of interplanetary shocks within 0.3 AU, J. Geophys. Res., 90, 154, 1985.

Wu, C.S., R.S. Steinolfson, and G.C. Zhou, The synchrotron-maser theory of type II solar radio emission processes: the physical model and generation mechanism, Astrophys. J., 309, 392, 1986.

Wu, S.T., Propagation of solar disturbances: theories and models, Space Sci. Rev., 34, 73, 1983).

Wu, S.T., M. Dryer, and S.M. Han, Non-planar MHD model for solar flare-generated disturbances in the heliospheric equatorial plane, Solar Phys., 84, 395, 1983a.

Wu, S.T., S. Wang, M. Dryer, A.I. Poland, D.C. Sime, C.J. Wolfson, L.E. Orwig, and A. Maxwell, Magnetohydrodynamic simulation of the coronal transient associated with the solar limb flare of 1980, June 29, 18:21 UT, Solar Phys., 85, 351, 1983b.

Yeh, T., A magnetohydrodynamic theory of coronal loop transients, Solar Phys., 78, 287, 1982.

Yeh, T., Hydromagnetic buoyancy force in the solar atmosphere, Solar Phys., 95, 83, 1985.

Yeh, T., Magnetic structure of a flux rope, Astrophys. J., 305, 864, 1986a.

Yeh, T., Dynamics of magnetic flux ropes in the solar atmosphere, in STIP Symposium on Retrospective Analyses, edited by M.A. Shea and D.F. Smart, Book Crafters, Chelsea, Michigan, in press, 1986b.

Zirker, J.B., Progress in coronal physics, Solar Phys., 100, 281, 1985.

Zwickl, R.D., J.R. Asbridge, S.J. Bame, W.C. Feldman, J.T. Gosling, and E.J. Smith, Plasma properties of driver gas following interplanetary shocks observed by ISEE-3, in Solar Wind Five, edited by M. Neugebauer, p.711, NASA Conf. Pub. 2280, 1983).

(Received October 7, 1985,
revised January 16, 1987,
accepted January 16, 1987.)

# CHARACTERISTICS OF SOLAR CORONAL SOURCE REGIONS PRODUCING $^3$He-RICH PARTICLE EVENTS

S. W. KAHLER

*Emmanuel College, U.S.A.*

R. P. LIN

*Space Sciences Laboratory, University of California at Berkeley, U.S.A.*

D. V. REAMES

*Laboratory for High Energy Astrophysics, Goddard Space Flight Center, U.S.A.*

R. G. STONE

*Laboratory for Extraterrestrial Physics, Goddard Space Fight Center, U.S.A.*

and

M. LIGGETT

*Big Bear Solar Observatory, California Institute of Technology, U.S.A.*

(Received 13 May, in revised form 12 November, 1986)

**Abstract.** We use Hα, X-ray, and kilometric radio data to examine the solar coronal activity associated with energetic (~1 MeV/nucl$^{-1}$) $^3$He-rich particle events observed near Earth. The basis of the study is the 12 $^3$He-rich events observed in association with impulsive 2 to 100 keV electron events reported by Reames *et al.* (1985). We find that when Hα and X-ray brightenings can be associated with $^3$He/electron events, they have onsets coinciding to within 1 min of that of the associated metric type III bursts. In three or four events we found no associated Hα or X-ray flares, and in two events even the metric type III bursts were weak or absent. The measured low-energy (2 keV) electron spectra for these events show no evidence of a flattening due to Coulomb collisional losses. These results and several other recent findings are consistent with the idea that the $^3$He/electron events are due to particle acceleration in the corona well above the associated Hα and X-ray flares.

## 1. Introduction

It is now clear that $^3$He-rich solar energetic particle (SEP) events are a distinct class, distinguished from the SEP events of greater fluxes and energies not only by their anomalous He isotopic composition, but also by their lack of association with metric type II bursts and coronal mass ejections (Kahler *et al.*, 1985). A detailed study of twelve observed $^3$He-rich events suggests that > 1.3 MeV $^3$He ions are impulsively accelerated and injected into interplanetary space along with impulsive 2 to 100 keV electrons (Reames *et al.*, 1985; hereafter referred to as RvL). In that study energetic electrons were observed with each of the $^3$He-rich events and the times of onset and maximum for the $^3$He and electron increases were closely related by velocity dispersion. More recently, Reames and Lin (1985) have examined the inverse relationship by asking how many solar electron events are accompanied by $^3$He particles. They found $^3$He present in over half the 2 keV electron events and in two thirds of the 19 keV electron events, suggesting

*Solar Physics* **107** (1987) 385–394.

that with greater collecting efficiency $^3$He particles would be found in all electron events. We will refer to these events as $^3$He/electron events to indicate the common origin of the two particle species. The low fluxes and slow speeds of the $E \sim 1$ MeV nucl$^{-1}$ $^3$He ions render the solar injection times uncertain, but the close associations of the electron events with fast drift type III radio bursts provide the relatively precise timings needed to make the associations of the particle events with solar phenomena.

In this paper we examine the characteristics of the solar Hα and X-ray flares and the metric and kilometric type III bursts associated with the 12 $^3$He/electron events studied by RvL. The flare associations are based on the timings of the Hα and X-ray flares and on the positional information derived from the kilometric type III bursts. We use the results of these associations and the shapes of the interplanetary electron spectra to infer the coronal heights of the acceleration regions.

## 2. Hα Flare Associations

The times of the 12 events, taken from RvL, are given in Table I. Several of these events occurred on the same day and in these cases are associated with Hα flares in the same

TABLE I

$^3$He electron events

| Date | Metric type III | | Approx. location | Hα onset UT | McMath region | Total 18 hr km type III | Total with reported Hα flares |
|---|---|---|---|---|---|---|---|
| | Start UT | Class | | | | | |
| 8 Nov., 1978 | 17 : 51[f] | 3GG | N18 E12 | 17 : 51 | 643 | 2 | 2 |
| 27 Nov., 1978 | 20 : 56 | 3GG | N26 W47[a] | 20 : 55 | 672 | 6 | 0 |
| | | | | | (673) | | (3) |
| 26 Dec., 1978 | (13 : 19)[g,f] | – | S21 W41[d] | – | 721 | 4 | 0 |
| 26 Dec., 1978 | 21 : 22[f] | WNG[c] | S21 W45[a] | 21 : 04 | 721 | | |
| 10 Feb., 1979 | 18 : 18 | 3GG | N13 W23[b] | < 18 : 00 | 807 | 6 | 2 |
| | | | | | (808) | | (1) |
| 17 May, 1979 | 05 : 58[f] | 2G | S35 W78[b] | 05 : 51 | 996 | 12 | 3 |
| | | | | | (010) | | (0) |
| 14 Aug., 1979 | 17 : 28 | 3GG | S18 W45 | 17 : 28 | 205 | 4 | 2 |
| 14 Aug., 1979 | 20 : 48 | 3GG | S17 W48 | 20 : 48 | 205 | | |
| 6 Sept., 1979 | 09 : 06[f] | 2GG | N20 W62 | 09 : 06 | 252 | 10 | 5 |
| 6 Sept., 1979 | 11 : 38[f] | 3GG | N17 W65[a,e] | 11 : 39 | 252 | | |
| | 11 : 48[f] | 3G | N18 W67[e] | 11 : 48 | 252 | | |
| 6 Sept., 1979 | 13 : 32[f] | 3GG | N16 W63 | 13 : 32 | 252 | | |
| 6 Sept., 1979 | 18 : 51[f] | 2GG | N16 W65[a] | 18 : 50 | 252 | | |

[a] Flare not listed in SGD, but found in visual inspection of Hα patrol films.

[b] Flare not listed in SGD; observed flaring activity probably not associated with type III burst.

[c] Weak intermittent group lasting more than 1 hr; the start time of the 1980 kHz burst was 21 : 24 UT.

[d] No event found in inspection of Hα patrol films (P. Simon, private communication).

[e] Both flares probably contributed to the $^3$He/electron event since each was associated with an intense kilometric type III burst.

[f] $^3$He and electron flux profiles for these events are illustrated in RvL.

[g] Start time of 1980 kHz burst.

active region. In each case we give the time of the onset and the maximum reported burst size of the associated metric type III radio burst. The approximate flare sites and McMath region numbers, based on both reported Hα flares (*Solar-Geophysical Data*, 1978–1980) and inspection of Hα patrol films, are also listed. All Hα events were subflares except for the 8 November event, which was a 1B flare.

Each $^3$He/electron event was associated with a prominent kilometric type III burst observed with the solar radio experiment on ISEE-3. The experiment has been described briefly by Cane *et al.* (1982) and the techniques of calculating antenna temperatures and solar elongation angles by Bougeret *et al.* (1984). By measuring the elongation angles to the centroids of the radio emission regions and using a model of the interplanetary plasma density (Bougeret *et al.*, 1984) to relate emission frequency to radial distance, the trajectory of the electron population can be plotted as it moves from the Sun to the Earth. We show the trajectory of the 17 May, 1979 event in Figure 1. In this case we

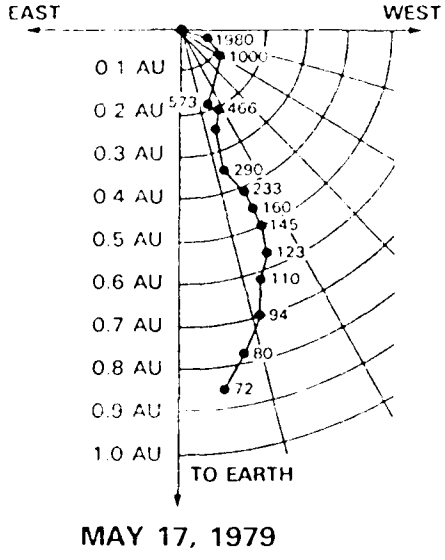


Fig. 1. The type III burst trajectory of the 17 May, 1979 event of Table I. The frequencies in kilohertz are shown at points along the trajectory, which is projected onto the ecliptic plane. The 1980 kHz point lies at a longitude of W 74°, in good agreement with the solar source region at W 78°.

see a good match between the angle subtended by the 1980 kHz burst position and the solar flare longitude. In general, the kilometric type III burst defines the source of the associated $^3$He/electron event with good timing and a solar longitudinal position to within about ± 25°.

We find, however, that making an Hα flare association with the kilometric type III burst is often difficult. In some cases there may be several candidate Hα flares or brightenings and in other cases no such candidates exist. A solution to this problem lies

in the fact that each type III burst of Table I is one of a family of such bursts, all of which occur over a period of ~1 day and show nearly identical solar elongation angles as a function of radio frequency. This suggests that a particular solar region is the source of each of these bursts in which the energetic electrons producing the bursts traverse similar paths through the outer corona. Figure 2 shows an example of such bursts during a 6 hr interval on 14 August, 1979.

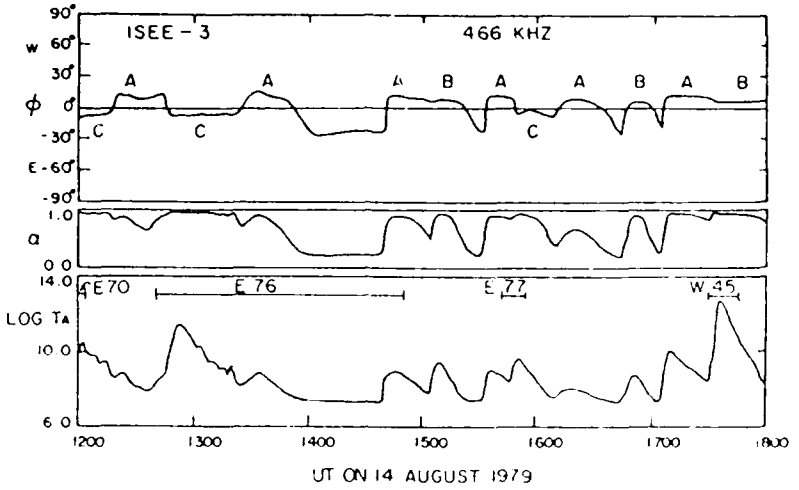


Fig. 2. 466 kHz data from the ISEE-3 radio experiment on 14 August, 1979. Top panel shows the burst solar elongation angle, $\phi$. Three families of bursts labeled $A$, $B$, and $C$ were present during the 6 hr interval. $B$ events were associated with McMath 205. The $B$ event beginning at 17:30 UT was associated with a $^3$He/electron event. $C$ events were probably associated with McMath 224 in the eastern hemisphere. The $\alpha$ parameter of the middle panel is a measure of the apparent size of the source region, with unity indicating a point source. The bottom panel is a plot of antenna temperature $T_A$ for the averaged rotating (despun) antenna. The start and end times and longitudes of the reported H$\alpha$ flares are also shown.

By associating reported H$\alpha$ flares with each family of bursts, we can expect to gain confidence in making the correct H$\alpha$ flare association for the particular burst with the $^3$He/electron event. We have listed in Table I the number of prominent kilometric type III bursts in each family during an 18 hr period around the time of the $^3$He/electron burst. The last column gives the number of bursts possibly associated on the basis of the timings with reported H$\alpha$ flares in the active region presumed to be the source of the $^3$He/electron event. Numbers in parentheses are the numbers of bursts possibly associated with reported H$\alpha$ flares in alternative candidate McMath regions for the three dates for which the active region is in some doubt. The fact that 3 of the 4 events of 6 September and both 14 August events were associated with reported H$\alpha$ flares in the same regions provides a measure of confidence in this technique. In two of the three events with questionable active region associations we see that the H$\alpha$ flare associations of the alternative regions are worse than for the preferred active regions, although the

statistics are limited. Two of the three 27 November H$\alpha$ flares in McMath 673, the alternative region given in Table I, peaked well before the onsets of the metric type III bursts and for that reason were probably not correctly associated with the kilometric events of Table I.

Using only the kilometric and reported H$\alpha$ flare data, we could have selected the preferred region for all the $^3$He/electron events except for the 27 November event and the two on 26 December. In the latter case no choice could be made. On the other hand, by ignoring the kilometric data and looking only for reported H$\alpha$ flares at well connected longitudes, we would have found no associated flares for 4 or 5 of the $^3$He/electron events and would have misidentified the source regions in two or three other cases. The 8 November event would have been associated with a reported subflare at W61 in McMath 635 and the 10 February event with a reported subflare at W21 in McMath 808. An examination of the H$\alpha$ films from Big Bear Solar Observatory shows that in neither of these cases could a significant brightening be observed in the region at the time of the reported subflare. The reported H$\alpha$ flare in McMath 673 on 27 November was short in duration, ending at 20 : 55 UT, 1 min before the type III burst onset. Whether this flare association would have been made depends on the timing criteria used. The result is that the use of only reported H$\alpha$ flares and timings of the metric type III bursts would have yielded correct flare source regions for only 5 of the 12 events of Table I.

### 3. H$\alpha$ and X-Ray Flare Timings

It is of interest to examine the timing relationship between the metric type III bursts and the associated H$\alpha$ flares of the last column of Table I. For the six events of 8 November, 14 August, and 6 September with reported H$\alpha$ flares, the onsets of the metric type III bursts and the associated H$\alpha$ flares were within 1 min of each other. This was also the case for the small unreported H$\alpha$ flares we observed in the Big Bear Solar Observatory films for the $^3$He/electron events of 27 November and 11 : 39 UT and 18 : 50 UT on 6 September. The weak, extended intermittent type III activity of the 21 : 22 UT 26 December event was apparently accompanied by motions of a small clumpy filament with very weak associated brightenings in McMath 721 beginning at 21 : 04 UT. The filament began showing large morphological changes about 21 : 25 UT, within 1 min of the onset of the 1980 kHz type III burst. On the other hand, the onsets of the 2 H$\alpha$ flares reported on 10 February in McMath 807 occurred 10 min or more before the associated type III bursts, and the suspected 17 May H$\alpha$ flare brightening associated with the $^3$He/electron event was observed to begin 7 min prior to the type III burst onset (C. Wright, private communication).

In view of the excellent agreement between the type III and H$\alpha$ onsets for most of the events of Table I, we may ask why the agreement is so poor for the $^3$He/electron events of 10 February and 17 May. Although H$\alpha$ brightenings in the appropriate regions were found, it seems more likely that in those cases no obvious chromospheric activity occurred in true association with the type III activity. All the events of Table I appear

consistent with the hypothesis that some of the kilometric type III bursts are unaccompanied by Hα brightenings, but when an Hα brightening does occur, the brightening onset closely coincides within 1 min of the type III onset. The 5 to 15 keV X-ray data from the UC Berkeley detector on ISEE-3 (Anderson *et al.*, 1978) support this conclusion for the $^3$He/electron events. Data for the 26 December, 10 February, and 17 May $^3$He/electron events show no obvious low-energy X-ray events near the times of the type III burst onsets. For all other $^3$He/electron events the X-ray onsets appeared within 1 min of the type III onsets. Both the Hα and the X-ray observations suggest that clear flare signatures were present in the eight $^3$He/electron events of 8 and 27 November, 14 August, and 6 September, but were absent in the 3 events of 13 : 19 UT 26 December, 10 February, and 17 May. The signature of 21 : 04 UT 26 December is unclear.

## 4. The Interplanetary Electron Spectra

We have examined the event-averaged electron energy spectra for all the $^3$He/electron events of Table I. In each case the spectral slopes show no evidence of flattening down to the lowest measured energy of 2 keV. If we assume that a power-law spectrum, as measured for the 17 May, 1979 event (see Figure 10 of RvL), characterizes the electron acceleration process, then the observed low-energy end of the spectrum can be interpreted in terms of an upper limit to the amount of material traversed by the accelerated electrons. By assuming an appropriate coronal density model, the minimum height of the acceleration region can be calculated. Using the procedure of Lin (1974) and the average corona characteristic of solar minimum (Fainberg and Stone, 1974), we calculate a minimum height of 0.2 $R_0$ ($\geq 1.4 \times 10^5$ km above the photosphere) for the acceleration region.

## 5. $^3$He/Electron Event Flare Characteristics

We looked for evidence of an energetic impulsive phase in each of the $^3$He/electron events. Only the three events of 8 November and 14 August were associated with reported microwave bursts. These three were also the only events with impulsive bursts in the 12 to 20 keV energy range of the ISEE-3 X-ray detector.

An examination of the Hα flare sites of the $^3$He/electron events shows that the flares of the 8 November, 14 August, and 6 September (see Figure 3) events all occurred close to sunspots. The 27 November flare occurred in an old spotless region, and the 26 December source region was rather similar. The 10 February and 17 May source plage regions were bright and with spots, but, as discussed above, no flares could be associated with the $^3$He/electron events. The 21 : 04 UT 26 December, and 09 : 06 UT and 11 : 48 UT events of 6 September definitely had filament eruptions. With the possible exception of the 8 November event, the other flares did not. Other than their small sizes, there is no obvious common characteristic of the Hα flares.

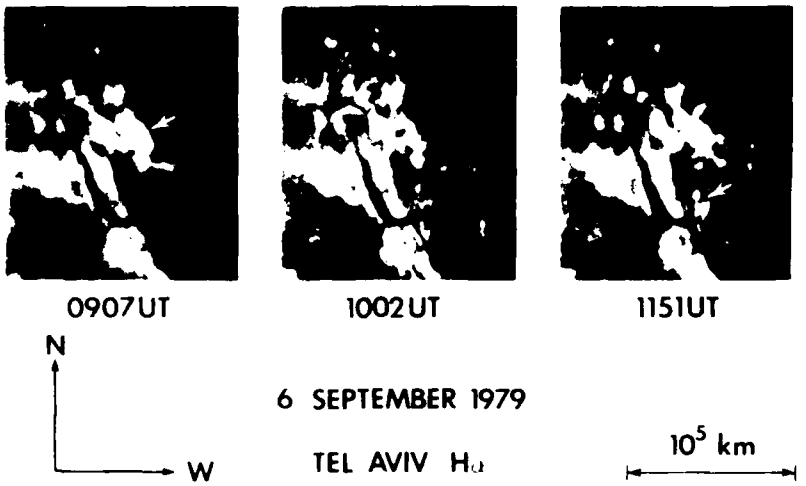


Fig. 3. Two of the four 6 September Hα flares in McMath 252 associated with $^3$He/electron events. The flare shown at 09 : 07 UT was north of the sunspot (arrow) and was associated with a filament eruption. The 10 : 02 UT image shows the nonflaring active region for comparison. At 11 : 39 UT a flare began in the region west of the sunspot (arrow) and was followed at 11 : 48 UT by a second flare at the same location as that of the earlier 09 : 06 UT flare. Both the 11 : 39 UT and 11 : 48 UT flares are shown in the 11 : 51 UT image. Later flares beginning at 13 : 32 UT and 18 : 55 UT also occurred at the flare site west of the sunspot. The 11 : 39 UT and 18 : 55 UT flares were not listed in *Solar-Geophysical Data*.

## 6. Discussion

Past efforts to associate reported Hα flares with $^3$He-rich events were often unsuccessful, partially because of large uncertainties in the timings of injection of the particles into the interplanetary medium (Ramaty *et al.*, 1980; Kocharov and Kocharov, 1984). In Section 2 we found that even when the injection times are known quite precisely, the Hα flare reports in SGD were a poor guide to the source flares of the $^3$He/electron events. The use of the Hα flare patrol films and the families of kilometric type III bursts has enabled us to make Hα flare associations in the 7 of 12 cases where the association would otherwise have been ambiguous or erroneous. As shown in Table I, the 3 kilometric burst families of 8 November, 14 August, and 6 September are well associated with reported Hα flares while the other four families are not. Considering the five $^3$He/electron events of the latter group, only the 27 November event appears convincingly associated with an Hα flare.

The lack of any observed associated Hα and X-ray activity for at least three of the twelve $^3$He/electron events suggests a coronal origin for the energetic $^3$He ions and electrons. The very close coincidence we found between the onsets of the metric type III bursts and the onsets of the associated Hα and X-ray flares is also compatible with the view that the initial activity of the $^3$He/electron events begins in the high corona. Hα activity may have little to do with the acceleration of the $^3$He ions and electrons other

than to reflect indirectly the presence of the overlying event, presumably as a result of the precipitation of some fraction of the energized particles. This idea has been suggested by Kane *et al.* (1974). They argued from the lack of observed hard X-ray bursts in association with some metric type III bursts that the density of the acceleration region, $n_i \leq 4 \times 10^9$ cm$^{-3}$. The lack of flattening at the 2 keV ends of the low-energy electron spectra provides another reason for invoking a high-coronal acceleration region. The height of the $^3$He/electron acceleration region inferred from those data is $\geq 0.2\ R_0$, i.e., $\geq 1.4 \times 10^5$ km above the photosphere.

If we take the lack of a reported type III burst at $\sim 20$ MHz, as in the case of the 13 : 19 UT 26 December event, as indicating that the acceleration did not occur in or below that region, then the acceleration region may be characterized by $n_i < 4 \times 10^6$ cm$^{-3}$, a height of $\sim 2\ R_0$. We must remember, however, that observations of type III emission from interplanetary electron beams are complicated by a number of factors involving the generation (Lin *et al.*, 1981) and propagation (Steinberg *et al.*, 1984) of the bursts, so the true situation may prove to be more complex.

As with past studies of the Hα manifestations of metric type III bursts (Švestka, 1976), we do not find a consistent morphology or characteristic of either the Hα flares or the active regions associated with the $^3$He/electron events. Filaments appear important in some observed Hα flares but not in others. In addition, some source active regions were weak and spotless; others were large and dominated by spots. Only seven $^3$He/electron event flares occurred close to sunspots, and small impulsive hard X-ray and microwave bursts were observed with only the three events of 8 November and 14 August. The lack of a consistent pattern in either the Hα flares or the active regions is also consistent with a high coronal origin for the associated $^3$He/electron events.

Another recent study provides further evidence of a high-coronal origin of the $^3$He/electron events. Reames and Stone (1986) have examined the kilometric type III burst associations for the largest of the $^3$He-rich events detected from 1978 to 1982. By measuring the time over which $^3$He-rich events from a given active region can be seen at 1 AU, they deduce a narrow longitudinal angular width of 5 to 10° for the particle injection profile. From the timings and pitch angle distributions of the $^3$He event onsets Reames and Stone found no evidence of any delays due to coronal diffusion or scattering. The relative ease with which the $^3$He particles leave the acceleration region again suggests a high coronal origin rather than a lower, flare-initiated origin.

We cannot rule out the possibility that in some $^3$He/electron events, particularly those of 14 August (Table I) and others associated with larger Hα flares (Kocharov and Kocharov, 1984), the particle acceleration takes place in a low altitude impulsive phase accompanied by obvious Hα and X-ray flare signatures. Švestka (1976) has suggested two classes of type III events, one of this type, and one appearing only at high levels in the corona with no flare association. For the latter class he mentioned type III storms, but we are suggesting this possibility for large, well developed groups of type III bursts, clearly distinguished from type III storms in the kilometric radio data.

$^3$He-rich events characteristically show an enrichment of heavy ions relative to the

normal composition in large SEP events (Mason *et al.*, 1986). The ionization states of energetic Si and Fe ions observed in $^3$He-rich events have been found by Luhn *et al.* (1985) to be characteristic of a temperature of $\sim 10^7$ K, significantly higher than the temperatures of $\sim 3 \times 10^6$ K characteristic of the Fe and Si ions from normal-abundance SEP events and also characteristic of the quiescent corona. We might expect such high temperatures to occur only in X-ray flares located in the lower corona immediately over the associated H$\alpha$ flares. However, the fact that we often find no associated observed X-ray flare with the $^3$He/electron events and the other reasons discussed earlier for a high coronal source region suggest that the heating occurs in a region of the corona where the emission measure $n_e^2 V$, where $n_e$ is the electron density and $V$ the volume, of the heated region is so small that X-ray fluxes can not be detected. For a large coronal region this scenario implies small electron densities and a high coronal source region.

The high ionization temperatures and high altitudes deduced for the sources of the $^3$He/electron events are also incompatible with the $^3$He-rich solar flare model proposed by Kocharov and Kocharov (1984). To allow for particle acceleration by ion acoustic turbulence, they required a low temperature ($T = 8 \times 10^4$ K) and high density ($n_e = 10^{11}$ cm$^{-3}$), conditions contrary to our findings for the source region. Their model further requires substantial fluxes of suprathermal electrons which should produce clear flare signatures such as impulsive hard X-ray and microwave bursts. The observational results discussed above indicate that the $^3$He acceleration source region is not compatible with the proposed flare model.

## 7. *Conclusions*

The H$\alpha$ activity associated with the twelve $^3$He/electron events of Table I was at most minor and sometimes undetectable on H$\alpha$ flare patrol films. Using only the SGD H$\alpha$ flare reports and the precise timings of the associated type III bursts, we would have correctly identified the source regions for only five of the twelve events. By using the kilometric type III burst data, we have identified the source regions for all twelve bursts with a high degree of confidence.

The following results of this study suggest a high coronal source region for the $^3$He/electron events:

(1) when an associated H$\alpha$ or X-ray brightening does occur, it begins within 1 min of the onset of the type III burst;

(2) in three or four of the twelve events no associated H$\alpha$ or X-ray activity was detected;

(3) the lack of any flattening of the electron energy spectra at 2 keV implies a source height of $> 1.4 \times 10^5$ km above the photosphere;

(4) no consistent flare or active region morphology can be associated with the $^3$He/electron event sources; and

(5) for two events the reported metric type III bursts were weak or absent.

The narrow coronal injection profiles (5 to 10° in longitude) and prompt arrival at

earth of the $^3$He particles (Reames and Stone, 1986) and lack of detection of the heated coronal source regions (Luhn *et al.*, 1985) are also consistent with a high coronal source for these events.

## Acknowledgements

This work was supported at Emmanuel College by AFGL Contract AF 19628-82-K-0039, at GSFC/University of Maryland by NASA grant NGR 21-002316, and at the University of California, Berkeley in part by NASA grant NAG 5-376. We thank Clint Wright for his comments on the Culgoora observations of the 17 May event and acknowledge the helpful comments of H. Cane and E. Cliver.

## References

Anderson, K. A., Kane, S. R., Primbsch, J. H., Weitzmann, R. H., Evans, W. D., Klebesadel, R. W., and Aiello, W. P.: 1978, *IEEE Trans. Geosci. Elec.* **GE-16**, 157.
Bougeret, J.-L., Fainberg, J., and Stone, R. G.: 1984, *Astron. Astrophys.* **141**, 17.
Bougeret, J.-L., King, J. H., and Schwenn, R.: 1984, *Solar Phys.* **90**, 401.
Cane, H. V., Stone, R. G., Fainberg, J., Steinberg, J. L., and Hoang, S.: 1982, *Solar Phys.* **78**, 187.
Fainberg, J. and Stone, R. G.: 1974, *Space Sci. Rev.* **16**, 145.
Kahler, S., Reames, D. V., Sheeley, N. R., Jr., Howard, R. A., Koomen, M. J., and Michels, D. J.: 1985, *Astrophys. J.* **290**, 742.
Kane, S. R., Kreplin, R. W., Martres, M.-J., Pick, M., and Soru-Escaut, I.: 1974, *Solar Phys.* **38**, 483.
Kocharov, L. G. and Kocha[illegible] E.: 1984, *Space Sci. Rev.* **38**, 89.
Lin, R. P.: 1974, *Space Sci. R[illegible]* **16**, 189.
Lin, R. P., Potter, D. W., [illegible]nett, D. A., and Scarf, F. L.: 1981, *Astrophys. J.* **251**, 364.
Luhn, A., Klecker, B., Hovestadt, D., and Mobius, E.: 1985, *Proc. 19th Internat. Cosmic Ray Conf. (La Jolla)* **4**, 285.
Mason, G. M., Reames, D. V., Klecker, B., Hovestadt, D., and von Rosenvinge, T. T.: 1986, *Astrophys. J.* **303**, 849.
Ramaty, R. *et al.*: 1980, in P. A. Sturrock (ed.), *Solar Flares*, Boulder, Colorado Associated University Press, p. [illegible].
Reames, D. V. and Lin, R. P.: 1985, *Proc. 19th Internat. Cosmic Ray Conf. (La Jolla)* **4**, 273.
Reames, D. V. and Stone, R. G.: 1986, *Astrophys. J.* **308**, 902.
Reames, D. V., von Rosenvinge, T. T., and Lin, R. P.: 1985, *Astrophys. J.* **292**, 716.
*Solar-Geophysical Data*: 1978–1980, Boulder: National Oceanic and Atmospheric Administration.
Steinberg, J. L., Dulk, G. A., Hoang, S., Lecacheux, A., and Aubier, M. G.: 1984, *Astron. Astrophys.* **140**, 39.
Švestka, Z.: 1976, *Solar Flares*, D. Reidel Publ. Co., Dordrecht, Holland, p. 205.

THE ASTROPHYSICAL JOURNAL, 302:504–510, 1986 March 1


# SOLAR FILAMENT ERUPTIONS AND ENERGETIC PARTICLE EVENTS

S. W. KAHLER
*Emmanuel College*
E. W. CLIVER
Air Force Geophysics Laboratory
H. V. CANE[1] AND R. E. MCGUIRE[1]
Laboratory for High Energy Astrophysics, Goddard Space Flight Center
R. G. STONE
Laboratory for Extraterrestrial Physics, Goddard Space Flight Center
AND
N. R. SHEELEY, Jr.
E. O. Hulburt Center for Space Research, Naval Research Laboratory
*Received 1985 March 22; accepted 1985 July 29*

## ABSTRACT

We discuss the 1981 December 5 solar filament eruption that we associate with an energetic ($E > 50$ MeV) particle event observed at 1 AU. The eruption was photographed in Hα, and was observed by the Solwind whitelight coronagraph on *P78-1*. It occurred well away from any solar active region and was not associated with an impulsive microwave burst, indicating that magnetic complexity and a detectable impulsive phase are *not* required for the production of a solar energetic particle (SEP) event. No metric type II or IV emission was observed, but an associated interplanetary type II burst was detected by the low-frequency radio experiment on *ISEE 3*. The December 5 and two other SEP events lacking evidence for low coronal shocks had unusually steep energy spectra ($\gamma > 3.5$). In terms of shock acceleration, this suggests that shocks formed relatively high in the corona may produce steeper energy spectra than those formed at lower altitudes. We note that the filament itself may be one source of the ions accelerated to high energies, since it is the only plausible coronal source of the $He^+$ ions observed in SEP events.

*Subject headings:* particle acceleration — Sun: corona — Sun: flares

## I. INTRODUCTION

Solar particle acceleration to tens of MeV is often presumed to occur only during flares in active regions (see Švestka 1981 for a general review). In many flares impulsive hard X-ray and microwave bursts indicate a rapid acceleration of electrons to energies of tens of keV. The γ-ray observations from the *Solar Maximum Mission* satellite (*SMM*) have shown that MeV ion production can also occur during the impulsive phase (Forrest and Chupp 1983). Acceleration of ions to tens of MeV then sometimes occurs in a subsequent "second phase" characterized by metric type II and type IV radio bursts and long-enduring soft X-ray and microwave events. The active regions producing these energetic flares are characterized by strong and complex magnetic fields, and the flares themselves are usually double ribbon structures as observed in Hα (Švestka 1981). While even relatively large solar energetic ($E > 1$ MeV) particle (SEP) events can be observed in interplanetary space in the absence of such a suitably defined candidate parent flare, it is often assumed that these events are due to unobservable flares on the invisible hemisphere (Smart *et al.* 1976).

Exceptions to this conventional picture are known to exist. In 1970 Dodson and Hedeman described a class of major (importance ≥ 2) Hα flares that occurred in active regions with only small or no sunspots. These flares were generally deficient in impulsive phase bursts but not in gradual microwave and soft X-ray emission nor in type II bursts. A few of these flares were associated with SEPs. More recently, Cliver, Kahler, and McIntosh (1983) and Cliver *et al.* (1983) have shown that even the largest SEPs may be associated with flares having weak impulsive phase bursts. While most SEPs originate in complex active regions and have strong impulsive bursts, these phenomena are clearly not essential to the particle acceleration process.

More compelling associations for SEP events have been found with phenomena characteristic of the upper ($h > 2 \times 10^5$ km) corona. Lin (1970) and Švestka and Fritzova-Švestkova (1974) found good associations of SEP events with metric type II bursts, while Kahler *et al.* (1978, 1984) and Cane and Stone (1984) also found good associations of SEP events with coronal mass ejections (CMEs) and kilometric type II bursts, respectively. A consistent picture relating the metric type II shocks, the interplanetary kilometric type II shocks, and CMEs has yet to be achieved (Cane 1984), but the close association of these phenomena to each other and to SEP events suggests that the upper corona is the source of most interplanetary energetic particles.

In a study of the *Skylab* CME events, Munro *et al.* (1979) found that 70% of the CMEs that could be associated with near-surface activity were associated with eruptive prominences or disappearing filaments. They concluded that essentially all eruptive prominences observed at heights beyond $0.2R_\odot$ above the limb are associated with CMEs. CMEs associated with eruptive events generally are slower than those considered predominantly flare associated (Hildner 1977; MacQueen and Fisher 1983) and are less likely to be associated with metric type II bursts (Gosling *et al.* 1976). Although the

[1] Also, Department of Physics and Astronomy, University of Maryland.

eruptive-associated CMEs tend to be less energetic than their flare-associated counterparts, we might still expect that a few eruptive-associated CMEs would result in SEP events. The discovery of such an event, in which the roles of active region and flare are minor at most, would extend the statistical studies discussed above that indicated the importance of the upper corona for SEP production.

There have been a few previous reports of possible associations between prompt SEP events and filament eruptions. The first such association of which we are aware was made by Hyder (1967), who suggested that the filament eruption event of 1959 September 1 led to a polar cap absorption (PCA) event on the following day (Švestka and Simon 1975, p. 160). The filament in that event lay between two plage regions (Dodson and Hedeman 1970), and its eruption was accompanied by a 2+ flare. In a second reported association, Domingo, Hynds, and Stevens (1979) associated a geomagnetic storm sudden commencement (SSC) observed at 0247 UT on 1978 August 27 with a filament disappearance near the center of the disk at ~0120 UT on August 23 (see Joselyn and Bryson 1980). Protons of ~1 MeV energy were observed beginning on August 25, both ahead of and at the interplanetary shock. The authors, however, were uncertain about the origin of the protons and did not attribute them to the filament disappearance. Most recently, Sanahuja *et al.* (1983) attributed a $1 \leq E < 15$ MeV proton event to the disappearance early on 1979 April 23 of a large filament at least partially located in McMath 15956, a relatively small and weak active region in its third of four rotations. A pair of double ribbon 1F flares, one in McMath region 15956, accompanied the filament disappearance. However, Sanahuja *et al.* concluded that the filament eruption, rather than the flares, triggered the interplanetary shock which gave rise to the related SEP event. To our knowledge, this is the most convincing published example of a non-flare source for a prompt SEP event.

In this paper we discuss the SEP event of 1981 December 5, which is associated with an erupting filament located well away from any active region. In § II we present the Hα, coronagraph, and kilometric radio data that allow us to associate the SEP event with the erupting filament. In § III we discuss the implications of this event for SEP production. We also examine the role of the cool filaments as sources of the energetic particles.

## II. DATA ANALYSIS

### *a) The SEP Event*

The SEP event of 1981 December 5 was observed with the Goddard Space Flight Center (GSFC) medium energy cosmic-ray experiment on the *ISEE 3* spacecraft at the Sun-Earth libration point. The experiment has been described by von Rosenvinge *et al.* (1978). In Figure 1 we show profiles of particle fluxes of several energy ranges observed with the high-energy telescope of that experiment. The MeV electron onset was between 1415 and 1430 UT, followed by the proton onset between 1500 and 1530 UT. The velocity dispersion and rapid rise to maximum are evidence of an impulsive injection of particles from a well-connected solar longitude. The decay phase of the event continued until late on December 9 when a second SEP event occurred.

At the time of the event the *Helios 1* spacecraft was ~13° behind the west limb at a distance of 0.44 AU from the Sun. We have no data from the GSFC particle experiment on that spacecraft until 0800 UT on December 6, but at that time the decaying 11–22 MeV proton flux was $2 \times 10^{-2} p$ (cm$^2$ s sr MeV)$^{-1}$, a factor of 10 lower than that measured simultaneously for the same energy range by the GSFC experiment on *IMP 8* at the Earth. This result is consistent with our association of the SEP event with the disappearance of the disk filament, rather than with a source from behind the limb.

We have used proton fluxes measured by the GSFC particle experiments on both *ISEE 3* and *IMP 8* to derive the spectrum at the times of peak fluxes in the 3–80 MeV energy range. If we assume a differential power-law spectrum in energy, the best fit to the *IMP 8* data yields $\gamma = 4.3 \pm 0.1$, where $\gamma$ is the power-law exponent. This spectrum is quite steep in comparison with the spectra of a large sample of 4–19 MeV and 20–80 MeV SEPs obtained by van Hollebeke *et al.* (1975).

### *b) The Hα Filament Disappearance and History*

We obtained the Haute Provence photographic observations for December 5, courtesy of P. Simon, who noted that the Hα patrol on this date was affected by instrumental difficulties and adverse weather. Several of the Haute Provence Hα filtergrams, depicting key times in the filament eruption event, are reproduced in Figure 2 (Plate 15). They show that the large filament, located at ~W35-45, N15-30, became active and began to erupt at ~1215 UT. The smaller filament to the northeast in Figure 2 also began to disappear at ~1315 UT. Hα brightenings were first observed at 1315 UT, forming a classic double-ribbon pattern along the filament channel. The length of the longer eastern ribbon at 1457 UT was $\sim 2.9 \times 10^5$ km. Although fainter, the ribbons were still visible on an Hα filtergram obtained at Big Bear Solar Observatory at 1743 UT (F. Tang, private communication). A comparison of that image with the 1457 UT image shows that the ribbons separated with an average speed of ~2.2 km s$^{-1}$, consistent with the range observed for the late stages of bright double-ribbon flare events (Švestka 1976).

The filament was not at the location of a former active region, and it lay at least 25 heliographic degrees from the nearest plage region. It was situated along a line dividing negative magnetic polarity in the west from positive polarity in the east. This was opposite to the sense of polarity inversion for northern hemisphere active regions (P. McIntosh, private communication) and so was an inversion line lying between, rather than within, active regions.

### *c) The Coronal Mass Ejection*

Figure 3 (Plate 16) shows the ejected filament and coronal material as they were observed by the NRL white-light coronagraph (Solwind) on the *P78 1* satellite (see Michels *et al.* 1982). The first of these difference images shows that the coronal disturbance was not yet visible at 0658 UT, but was in progress during the next available image at 1447 UT. At this time the leading edge of the coronal material was already located at $6.2R_0$ in the northwest quadrant. During the subsequent images the ejected coronal material left the $2.5$–$10.0R_0$ field of view.

At 1622 UT a bright moving feature appears superposed against the background of the coronagraph's inner polarizing ring (which is designed to block radiation that is azimuthally polarized). This indicates that the feature is relatively unpolarized prominence Hα radiation in the 4000–7000 Å spectral

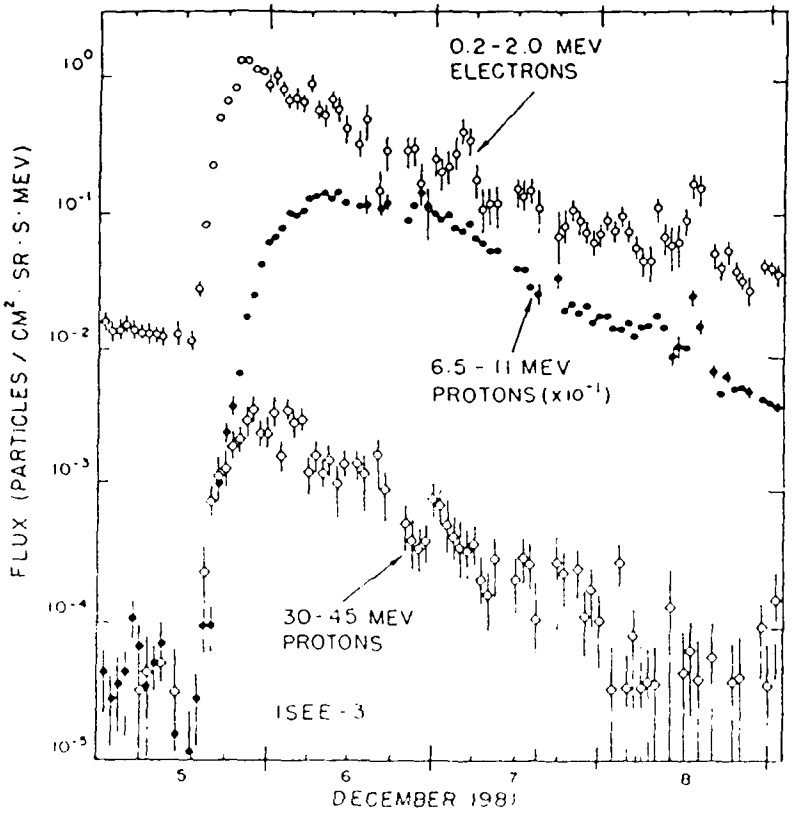


FIG. 1.—Flux-time plots of several particle energy ranges for the 1981 December 5 SEP. The precise calibration of the electron fluxes is uncertain. Data are from the GSFC experiment on *ISEE 3*.

bandpass rather than azimuthally polarized Thomson-scattered radiation from coronal electrons. The prominence first entered the field of view near the occulting disk at ~1447 UT. It then moved uniformly outward in the plane of the sky. (Its position at 1521 UT is indicated by an arrow in Fig. 3.) In the final difference image, the darker-than-average region indicates the depletion of the ejected coronal material between 1447 UT and 1622 UT, and the brighter-than-average feature indicates the position of the prominence at 1622 UT. Its apparent latitude 30° north of west is consistent with the original location of the filament at N15-30, W35-45 on the disk.

From these observations, we found that the prominence was moving with a speed of 305 ± 20 km $s^{-1}$ in the plane of the sky. Extrapolated back to the $0.65R_0$ location of the disk filament, this speed gives a starting time of 1329 ± 0010 UT, or ~1 hr after the disk filament began to disappear. This 1 hr time delay suggests that the erupting filament accelerated during the first hour after its initial disappearance from the Hα spectral bandpass as one usually observes for erupting prominences (see Martin and Ramsey 1972). Assuming that the coronal mass ejection also began at 1329 UT, we derived a speed of 840 km $s^{-1}$ for the leading edge of the coronal material. The resulting pattern in which the coronal material precedes the more slowly moving prominence is characteristic of most prominence-associated coronal mass ejections (see MacQueen 1980; House *et al.* 1981; Sheeley *et al.* 1981).

*d) The Soft X-Ray Event*

Soft X-ray events associated with major (i.e., large or bright) CMEs similar to that of December 5 are usually long duration X-ray events (LDEs) (Sheeley *et al.* 1983). In addition, Webb, Krieger, and Rust (1976) used *Skylab* data to associate filament disappearances outside active regions with faint soft X-ray enhancements unobservable in full Sun detectors. We have examined the *GOES* full-Sun X-ray plots of December 5 for evidence of an associated X-ray event. A faint and very gradual 1–8 Å enhancement began shortly after 1300 UT, arising from a C2.5 background to a peak level of only C3.5 at 1430–1450 UT. Taking a peak 0.5–4 Å signal of (3 ± 1) × $10^{-8}$ W $m^{-2}$ during this event, we calculate a temperature of (5 ± 1) × $10^6$ K and an emission measure of (7 ± 3) × $10^{48}$ $cm^{-3}$ from the plots of Thomas, Starr, and Crannell (1985).

*e) Radio Observations*

We have examined the reports of the microwave and metric burst events (*Solar Geophysical Data* 1982) and data from the Meudon-GSFC kilometric radio astronomy experiment on *ISEE 3* (Cane *et al.* 1982) during the time of the filament eruption. The only reported microwave burst was a short (~2 minute duration) event of ~20 sfu with a peak at 1317 UT. In the metric range a group of intense type III/V bursts was observed from 1316 to 1318 UT at Weissenau Observatory. These bursts were also seen on the 1980 kHz band of the *ISEE*

*3* detector as a single event from 1317 to 1321 UT, as shown in Figure 4 (Plate 17). Another group of metric type III bursts with weak continuum was observed from 1320–1326 UT, probably appearing as the 1980 kHz event from 1324 to 1329 UT. These events were not due to the filament activity, because the deduced position of both 1980 kHz bursts was east of central meridian, the first probably occurring in association with a reported Hα subflare at E59° with a maximum at 1318 UT. A hard X-ray burst was also observed at 1317 UT by the University of California–Berkeley detector on *ISEE 3*, but no further bursts were observed until after 1400 UT (S. Kane, private communication).

An apparent shock-accelerated (SA) event (Cane *et al.* 1981) was observed at 1980 kHz in the *ISEE 3* radio data from the end of the type III emission at ~1328 UT until 1352 UT. The SA event could be tracked out to ~0.7 AU, and the centroid of the emission could be determined for each frequency. From this technique we estimate that the source longitude for this event was in the range W10°–W40°, indicating a spatial as well as temporal association with the filament disappearance and CME. The SA event was followed by an interplanetary type II burst which could barely be discerned above an unusually quiet background (Cane 1985).

The Algonquin Observatory at Ottawa reported a weak (8 sfu maximum) gradual-rise-and-fall burst beginning at 1430 UT. An examination of their records provided by M. Beli shows that the event began early in their observing day while the flux level was still increasing, so the true onset may have been earlier. An examination of the 4995 MHz record of the Sagamore Hill Observatory shows a gradual rise-and-fall event beginning at ~1300 UT with a peak flux of 21 ± 3 sfu at ~1400 UT. Using the X-ray values for the temperature and emission measure given in § II*d* and formulae from the Appendix of Webb and Kundu (1978), we derive a thermal microwave flux density of 12 ± 6 sfu, in reasonable agreement with the measured 4995 MHz flux density. We find no other events in either the microwave or metric ranges that may have been associated with the filament activity.

## III. DISCUSSION

### *a) Energetics of the Eruptive Event*

The $E \geq 50$ MeV SEP event of 1981 December 5 has been associated with a filament eruption and Hα brightening well removed from any active region. The solar Hα emission event is properly termed a "flare-like brightening" rather than a flare (P. Simon and H. Dodson-Prince, private communication). According to Smith and Smith (1963), "These events are distinguished from true flares by their considerably longer lifetimes (average three hours), their slower rise times (30 to 100 minutes) and their occurrence well away from spot groups . . . The eruption precedes the chromospheric brightening by about half an hour; hence it is probable that both phenomena result from the same unknown cause." In addition, Švestka (1976) points out that one use of the term "disparition brusque" (DB) is for the "disappearance of a quiescent dark filament far away from any active region giving rise to slight brightenings along the filament channel. Such brightenings usually are not classified as a flare."

The motion of the filament observed in the second and third images of Figure 2 and the direct observation of the filament in the coronagraph images of Figure 3 show that it it was a true eruptive (hence, a DB) rather than a quasi-eruptive disappearance (Martin 1973) which does not lead to the expulsion of matter from the corona. Švestka, Martin, and Kopp (1980) speculated that DBs might be associated with the occurrence of long-lived low-energy particle events in space. Subsequently, as discussed in § I, Sanahuja *et al.* (1983) associated the low-energy SEP on 1979 April 23 with a DB at least partially located in a weak active region. In comparison with that event, the 1981 December 5 SEP event was somewhat more energetic, and the DB lay clearly outside any active region. In addition, we found no evidence of any impulsive phase microwave or hard X-ray emission from this event. This indicates that neither active regions nor obvious impulsive phase phenomena are *necessary* for energetic particle production. The good association of SEPs with Hα flares and flare impulsive phase bursts is most likely not a direct cause-and-effect relationship but rather the result of the "big flare syndrome" (Kahler 1982) that states that, statistically, energetic flare phenomena are more intense in larger flares, regardless of the detailed physics.

Besides the filament disappearance and the Hα double ribbon emission shown in Figure 2, the solar signatures of the December 5 event were the accompanying weak gradual thermal soft X-ray and microwave events which were similar to those of the active region DB of 1974 January 18 studied by Sheeley *et al.* (1975). The Hα ribbons appear to be the footpoints of cool loop arcades overlain by hotter soft X-ray loops (see Bruzek 1964; Kahler 1977; MacCombie and Rust 1979). The rate of separation of the ribbons ~2–4 hr after initial brightening (~2 km $s^{-1}$) was the same as that of the well-observed *Skylab* X-ray flare of 1973 July 29 (Švestka *et al.* 1982). The coronal response to an eruptive filament may be illustrated by the DB of 1973 September 1. *Skylab* soft X-ray and Hα images of this event were shown by Rust (1976) and reproduced by Švestka (1976, 1981). It occurred in an old spotless region in the absence of a reported flare and resulted in a large X-ray cloud which was unobservable with full-Sun X-ray detectors. Webb, Krieger, and Rust (1976) have discussed similar filament disappearances outside active regions. Those events were characterized by relatively faint thermal X-ray and microwave emission and usually by no observable Hα emission.

The total energy of a DB event with no or weak Hα emission may, however, be substantial, if it consists primarily of convected magnetic field energy (Webb *et al.* 1980; Dulk 1980, 1984). Anzer and Pneuman (1982) have concluded that the occurrence of a flare in association with a CME is not an important question for the nature of an eruptive event. A common process occurs in all CME events with the flares being the most energetic. The energy is derived from the magnetic field, and weak fields will not result in chromospheric flares. In this view the Hα filament in the DB event is a signature of a magnetically dominated eruption occurring over a much larger coronal volume. Low, Munro, and Fisher (1982), for example, suggested that the CME of 1980 August 5 was initiated in the low corona by magnetic buoyancy. Although that CME was slower ($v = 210$ km $s^{-1}$ at $2.2R_0$) than the December 5 CME, both events were characterized by a lack of any signature of an impulsive process. Yeh (1982) has also concluded that the driving force of a CME is the magneto-hydrodynamic buoyancy force, and he finds that magnetic unwinding is the dynamical cause of the ejection of a loop. The December 5 event shows that energetic eruptive events can be accompanied by only minimal impulsive phase and thermal flare signatures.

Other SEP events similar to that of December 5 undoubtedly exist. The association of a SEP event with a filament disappearance outside an active region is generally difficult to make, however, since filament disappearances are not routinely reported despite their potential importance for geophysical effects (Joselyn and McIntosh 1981). The December 5 event was particularly well observed. In addition to definitive Hα photographs of this event, white light coronagraph images and low-frequency radio observations were available. The observed CME, SA event, and interplanetary type II burst in this event revealed the subsequent high coronal position and effects of the filament disappearance.

### *b) Metric Shocks and SEP Energy Spectra*

To see whether the apparent late onset of shock formation in the December 5 event, as indicated by the absence of any observed metric type II emission and the presence of an SA event and interplanetary type II burst, might somehow be related to the unusually steep ($\gamma = 4.3$) SEP event spectrum, we looked for other examples of this behavior. The eight large SEP events in the list compiled by Cliver, Kahler, and McIntosh were similar to the December 5 SEP in that the parent flares were weak impulsive phase events that originated, in several cases, in magnetically simple active regions. Six of the eight parent flares were located on the western hemisphere.

Like the December 5 proton flare, two of these six well-connected events, 1969 September 25 and 1970 May 30, were not associated with metric type II bursts and had SEP power-law spectral exponents of 3.5 and 4.0, respectively, in the $10 \leq E \leq 100$ MeV range. Moreover, the September 25 and May 30 flares also apparently resulted in interplanetary shocks (Cliver, Kahler, and McIntosh 1983). The four remaining well-connected proton flares of the Cliver, Kahler, and McIntosh (1983) study were accompanied by metric type II bursts, and the associated SEP events had relatively hard spectra ($\gamma \leq 2.6$) in the $10 \leq E \leq 100$ MeV range. Thus, although a more comprehensive statistical study is required, there exists preliminary evidence that steep energy spectra in apparently well connected SEP events might result from a larger than usual coronal height of shock formation.

The energetic particle spectrum resulting from first-order Fermi acceleration by diffusive particle motion in a planar shock is known theoretically to be a power law in momentum (e.g., Blandford and Ostriker 1978; Axford 1981; Lee and Fisk 1982). Transforming to a differential power law in kinetic energy for nonrelativistic ions, a strong shock yields a spectral index $\gamma \geq 2$, roughly the range of values for the SEP events with metric type II bursts considered above. Weaker shocks yield softer spectra. In this simplified context, the association of hard SEP spectra with metric type II bursts implies that shocks formed in the lower corona are stronger than those formed at greater heights. However, this interpretation neglects several important aspects of shock acceleration, such as energy-dependent escape of the particles from the shock region, second-order Fermi acceleration, energy losses, and shock-drift acceleration (Decker, Pesses, and Armstrong 1981). In addition, it is not theoretically obvious that coronal height of shock formation should be related to shock strength. We thus regard the suggestion that SEP spectral slopes may be correlated with the height of shock formation as tentative, at best.

### *c) The Role of Cool Filamentary Material in SEPs*

CMEs observed with *Skylab* and *SMM* are better associated with erupting prominences than with any other solar phenomena, including flares (Munro *et al.* 1979; Webb 1984). However, cool prominence material is rarely observed at great solar distances in CMEs. Hα material appears in many CMEs observed by the *SMM* coronagraph (House *et al.* 1981), which has an inner field of view of only $1.5R_0$, but Howard *et al.* (1985) found Hα material at $4R_0$ in only 1.5% of ~1000 Solwind CMEs in their survey. In the 1980 April 16 CME, Hα emission was observed out to $3R_0$ with the *SMM* coronagraph but not at $4R_0$ with the Solwind coronagraph (Wagner *et al.* 1983). This may be the result of ionization of the prominence material as it rises through the corona, as indicated by Hα and He II λ304 emission in the well-studied *Skylab* case of 1973 August 21 (Poland and Munro 1976). Absorption of solar Lyman continuum radiation should be the dominant ionizing mechanism, although Poland and Munro (1976) have suggested conductive heating from the corona or wave heating as additional possibilities. Another reason for the paucity of observed Hα features beyond $\sim 4R_0$ might be that the cool material has achieved a sufficient outward velocity (> 150 km $s^{-1}$) such that it is Doppler shifted out of the Lyβ waveband of radiation needed to excite the hydrogen atoms (Poland and Munro 1976). However, several Solwind CME events have been observed in which Hα prominence material has reached speeds of ~1000 km $s^{-1}$ near $10R_0$. In sum, the relationship of Hα brightness to the degree of ionization in the prominence material is not well understood at present.

The relative positions of the prominence and the ejected coronal material are only beginning to be understood, at least for the frequently observed loop CMEs. Illing and Hundhausen (1985) studied the "depletion" CME of 1980 August 5 and concluded that the outer loop, intervening dark shell, and bright core of the CME were due to the overlying coronal material, the void in coronal material known as the filament cavity, and the filament, respectively. *Skylab* observations had previously suggested (Hildner *et al.* 1975) that the bulk of the ejected material comes from the low corona above the filament and that the total CME is far larger than would be inferred from filament observations alone.

Most SEP events are associated with fast ($V \gtrsim 500$ km $s^{-1}$) CMEs (Kahler *et al.* 1984). One explanation of this association (e.g., Kahler *et al.* 1984) is that shocks generated by, and moving ahead of, the CME white light fronts (MacQueen 1980; Maxwell and Dryer 1981) produce the energetic particles. The origin of the shock–CME association has been questioned by Wagner and MacQueen (1983), who suggest that the shock is generated *after* the CME onset and then proceeds to move through and overtake the CME. Attempts to distinguish observationally between the two models have been unsuccessful (Cane 1984; Kahler *et al.* 1985*a*).

The recent measurements of ionic charge states in SEPs have provided powerful clues for identifying SEP source regions (see Fan, Gloeckler, and Hovestadt 1984 for a recent review). The highest ionization stages are generally consistent with a coronal source temperature of $\sim 2 \times 10^6$ K. However, observations of $He^+$ abundances in 10 SEP events over a 1 yr period showed that $He^+$ was present in all events with an average $He^+/He^{++}$ ratio of ~0.1. Measurement of the daily $He^+/He^{++}$ ratios in the energy range 0.4–0.62 MeV per nucleon for 216 days in 1978–1979 by Hovestadt *et al.* (1984) yielded a median value of $He^+/He^{++} = 0.11$. Since this ratio is $\sim 10^{-5}$ for ionization equilibrium in the corona (Ahmad 1977), cool source material ($< 10^5$ K) has also been invoked as part of the SEP source region. As we have seen in the December 5 and similar events, only the filament itself,

where $He^+/He^{++} > 1$ for $T < 50{,}000$ K (Tandberg-Hanssen 1974, p. 72), can be a solar source of such cool material. No cool Hα material has been observed in the leading portions of CMEs (House *et al.* 1981). In the few cases when $He^+$ enhancements have been observed in the solar wind, they have been part of the driver gas following interplanetary shocks and were usually temporally associated with eruptive filaments (Schwenn, Rosenbauer, and Muhlhauser 1980; Gosling *et al.* 1980; Bame 1983). These events show that at least in some cases cool filament material remains unheated to 1 AU.

The coronagraph, SEP ionization stage, and solar wind ion observations are all consistent with the conclusion that a significant fraction of the SEPs are accelerated from the cool filament itself. The filament will form the bright core of a loop CME, and, if it remains cool at great heights, may be observed in a coronagraph in the Hα line. This conclusion, however, seems incompatible with the concept favored by Kahler *et al.* (1984) that most SEPs are produced by shocks moving ahead of the front of the CME. If shock acceleration is assumed, then it appears that the shock must move through the underlying filament, perhaps as part of the scenario suggested by Wagner and MacQueen (1983). When SEPs are produced in the filament, it is not at all clear whether they can readily escape to interplanetary space, since the filament is surrounded by large-scale looplike magnetic fields defining the CME. However, restructuring subsequent to the ejection may radically change the geometry of the fields (e.g., Illing and Hundhausen 1983).

Alternatively, to retain the model in which particle acceleration occurs in shocks, well ahead of the cooler filamentary material, we would need a source other than a directly associated filament eruption for the $He^+$ ions in a SEP event. The persistently high values of $He^+/He^{++}$ measured by Hovestadt *et al.* (1984) does suggest that some stable $He^+$ source population may exist at the Sun or in interplanetary space (D. Hovestadt, private communication). An interplanetary population of $He^+$ ions, formed from interstellar neutral atoms that are singly ionized by UV fluxes after entering the heliosphere, has been theoretically proposed by Fisk, Kozlovsky, and Ramaty (1974) as a source for the anomalous component of cosmic rays. However, attempts to measure the charge states of the anomalous He component (at tens of MeV per nucleon) and thereby test this theory have not been definitive (see the review of Jones 1983). Whether any stable $He^+$ population has sufficient number density to contribute significantly to SEP fluxes is also not obvious. Nonetheless, at this time we believe the source of the $He^+$ ions in SEPs remains an open question.

### *d) Comment on $^3$He SEPs*

Kahler *et al.* (1985*b*) and Reames, von Rosenvinge, and Lin (1985) have shown that $^3$He-rich SEPs are well associated with impulsive phase rather than second phase flare events. Although mixed first and second phase events would be expected, the "pure" $^3$He impulsive phase acceleration mechanism does not appear to involve coronal shocks or CMEs, or, by implication, filament eruptions. The lack of any measurable $He^+$ fluxes in $^3$He-rich events found by Klecker *et al.* (1984) appears consistent with this view.

## IV. CONCLUSIONS

We have used the 1981 December 5 SEP and filament eruption ev t to draw several conclusions.

1. A solar active region is not necessary for the occurrence of a SEP. The essential ingredient for most observed SEPs seems to be a magnetically dominated mass ejection.

2. The occurrence of a detectable impulsive phase event is also not necessary for a SEP. A similar conclusion has been drawn by Cliver, Kahler, and McIntosh (1983).

3. The unusually steep spectrum ($\gamma \approx 4$) of the December 5 SEP may be related to the apparent late onset of shock formation in this event, as indicated by the absence of a metric type II burst and the presence of an SA event and interplanetary type II burst.

4. If the corona is the source of all SEPs, then a significant fraction of the SEPs must be drawn from the ejected filamentary material. This is the only coronal material cool enough ($T < 5 \times 10^4$ K) to contain $He^+$ ions found in SEPs (Fan, Gloeckler, and Hovestadt 1984).

This work was supported at Emmanuel College by AFGL contract AF 19628-82-K-0039, at NRL by NASA DPR W 14,429, and at GSFC/University of Maryland by NASA grant NGR 21-002316. The Air Force Space Test Program provided integration, launch, and operational support for the *P78-1* spacecraft. D. Roberts, F. Harlow, and W. Funk of NRL assisted in the coronagraph data reduction. The Hα photographs were generously supplied by P. Simon, the Weissenau radio data by H. Urbarz, and the Ottawa 2800 MHz data by M. Bell. We are indebted to J. Browne of the AFGL Photo Lab for his valuable assistance with the Hα images. R. Howard, M. Koomen, and D. Michels are gratefully acknowledged for their help with the analysis of the coronagraph data.

## REFERENCES

Ahmad, I. A. 1977, *Solar Phys.*, 53, 409.
Anzer, U., and Pneuman, G. W. 1982, *Solar Phys.*, 79, 129.
Axford, W. I. 1981, *Proc. 17th Internat. Cosmic Ray Conf.* (Paris), 12, 155.
Bame, S. J. 1983, in *Solar Wind Five*, ed. M. Neugebauer (NASA Conf. Pub. No. 2280), p. 573.
Blandford, R. D., and Ostriker, J. P. 1978, *Ap. J. (Letters)*, 221, L29.
Bruzek, A. 1964, *Ap. J.*, 140, 746.
Cane, H. V. 1984, *Astr. Ap.*, 140, 205.
———. 1985, *J. Geophys. Res.*, 90, 191.
Cane, H. V., and Stone, R. G. 1984, *Ap. J.*, 282, 339.
Cane, H. V., Stone, R. G., Fainberg, J., Steinberg, J. L., and Hoang, S. 1982, *Solar Phys.*, 78, 187.
Cane, H. V., Stone, R. G., Fainberg, J., Stewart, R. T., Steinberg, J. L., and Hoang, S. 1981, *Geophys. Res. Letters*, 8, 1285.
Cliver, E. W., Kahler, S. W., Cane, H. V., Koomen, M. J., Michels, D. J., Howard, R. A., and Sheeley, N. R., Jr. 1983, *Solar Phys.*, 89, 191.
Cliver, E. W., Kahler, S. W., and McIntosh, P. S. 1983, *Ap. J.*, 264, 699.
Decker, R. B., Pesses, M. E., and Armstrong, T. P. 1981, *Proc. 17th Internat. Cosmic Ray Conf.* (Paris), 3, 406.
Dodson, H. W., and Hedeman, E. R. 1970, *Solar Phys.*, 13, 401.
Domingo, V., Hynds, R. J., and Sievens, G. 1979, *Proc. 16th Internat. Cosmic Ray Conf.* (Kyoto), 5, 192.
Dulk, G. A. 1980, in *Radio Physics of the Sun*, ed. M. R. Kundu and T. E. Gergely (Boston: Reidel), p. 419.
———. 1984, in *STIP Symposium on Solar/Interplanetary Intervals*, ed. M. A. Shea, D. F., Smart, and S. M. P. McKenna-Lawlor (Chelsea, MI: Book Crafters), p. 331.
Fan, C. Y., Gloeckler, G., and Hovestadt, D. 1984, *Space Sci. Rev.*, 38, 143.
Fisk, L. A., Kozlovsky, B., and Ramaty, R. 1974, *Ap. J. (Letters)*, 190, L35.
Forrest, D. J., and Chupp, E. L. 1983, *Nature*, 305, 291.
Gloeckler, G., *et al.* 1981, *Proc. 17th Internat. Cosmic Ray Conf.* (Paris), 3, 136.
Gosling, J. T., Asbridge, J. R., Bame, S. J., Feldman, W. C., and Zwickl, R. D. 1980, *J. Geophys. Res.*, 85, 3431.
Gosling, J. T., Hildner, E., MacQueen, R. M., Munro, R. H., Poland, A. I., and Ross, C. L. 1976, *Solar Phys.*, 48, 389.
Hildner, E. 1977, in *Study of Traveling Interplanetary Phenomena*, ed. M. A. Shea, D. F. Smart, and S. T. Wu (Hingham, Mass.: Reidel), p. 3.

Hildner, E., Gosling, J. T., Hansen, R. T., and Bohlin, J. D. 1975, *Solar Phys.*, 45, 363.
House, L. L., Wagner, W. J., Hildner, E., Sawyer, C., and Schmidt, H. U. 1981, *Ap. J. (Letters)*, 244, L117.
Hovestadt, D., Klecker, B., Gloeckler, G., Ipavich, F. M., and Scholer, M. 1984, *Ap. J. (Letters)*, 282, L39.
Howard, R. A., Sheeley, N. R., Jr., Koomen, M. J., and Michels, D. J. 1985, *J. Geophys. Res.*, 90, 8173.
Hyder, C. L. 1967, *Solar Phys.*, 2, 49.
Illing, R. M. E., and Hundhausen, A. J. 1983, *J. Geophys. Res.*, 88, 10, 210.
———. 1985, *J. Geophys. Res.*, 90, 275.
Jones, F. C. 1983, *Rev. Geophys. Space Phys.*, 21, 318.
Joselyn, J. A., and Bryson, J. F., Jr. 1980, in *Solar and Interplanetary Dynamics*, ed. M. Dryer and E. Tandberg-Hanssen (Boston: Reidel), p. 413.
Joselyn, J. A., and McIntosh, P. S. 1981, *J. Geophys. Res.*, 86, 4555.
Kahler, S. 1977, *Ap. J.*, 214, 891.
———. 1982, *J. Geophys. Res.*, 87, 3439.
Kahler, S. W., Cliver, E. W., Sheeley, N. R., Jr., Howard, R. A., Koomen, M. J., and Michels, D. J. 1985*a*, *J. Geophys. Res.*, 90, 177.
Kahler, S. W., Hildner, E., and van Hollebeke, M. A. I. 1978, *Solar Phys.*, 57, 429.
Kahler, S. W., Reames, D. V., Sheeley, N. R., Jr., Howard, R. A., Koomen, M. J., and Michels, D. J. 1985*b*, *Ap. J.*, 290, 742.
Kahler, S. W., Sheeley, N. R., Jr., Howard, R. A., Koomen, M. J., Michels, D. J., McGuire, R. E., von Rosenvinge, T. T., and Reames, D. V. 1984, *J. Geophys. Res.*, 89, 9683.
Klecker, B., Hovestadt, D., Gloeckler, G., Ipavich, F. M., Scholer, M., Fan, C. Y., and Fisk, L. A. 1984, *Ap. J.*, 281, 458.
Lee, M. A., and Fisk, L. A. 1982, *Space Sci. Rev.*, 32, 205.
Lin, R. P. 1970, *Solar Phys.*, 12, 266.
Low, B. C., Munro, R. H., and Fisher, R. R. 1982, *Ap. J.*, 254, 335.
MacCombie, W. J., and Rust, D. M. 1979, *Solar Phys.*, 61, 69.
MacQueen, R. M. 1980, *Phil. Trans. Roy. Soc. London, A*, 297, 605.
MacQueen, R. M., and Fisher, R. R. 1983, *Solar Phys.*, 89, 89.
Martin, S. F. 1973, *Solar Phys.*, 31, 3.
Martin, S. F., and Ramsey, H. E. 1972, in *Solar Activity Observations and Predictions*, ed. P. S. McIntosh and M. Dryer (Cambridge: MIT Press), p. 371.
Maxwell, A., and Dryer, M. 1981, *Solar Phys.*, 73, 313.
Michels, D. J., Sheeley, N. R., Jr., Howard, R. A., and Koomen, M. J. 1982, *Science*, 215, 1097.
Munro, R. H., Gosling, J. T., Hildner, E., MacQueen, R. M., Poland, A. I., and Ross, C. L. 1979, *Solar Phys.*, 61, 201.
Poland, A. I., and Munro, R. H. 1976, *Ap. J.*, 209, 927.
Reames, D. V., von Rosenvinge, T. T., and Lin, R. P. 1985, *Ap. J.*, 292, 716.
Rust, D. M. 1976, *Solar Phys.*, 47, 21.
Sanahuja, B., Domingo, V., Wenzel, K.-P., Joselyn, J. A., and Keppler, E. 1983, *Solar Phys.*, 84, 321.
Schwenn, R., Rosenbauer, H., and Muhlhauser, K.-H. 1980, *Geophys. Res. Letters*, 7, 201.
Sheeley, N. R., Jr., *et al.* 1975, *Solar Phys.*, 45, 377.
Sheeley, N. R., Jr., Howard, R. A., Koomen, M. J., and Michels, D. J. 1983, *Ap. J.*, 272, 349.
Sheeley, N. R., Jr., Michels, D. J., Howard, R. A., and Koomen, M. J. 1981, *EOS*, 62, 153.
Smart, D. F., Shea, M. A., Dodson, H. W., and Hedeman, E. R. 1976, in *Space Research XVI*, ed. M. J. Rycroft (Berlin: Akademie Verlag), p. 797.
Smith, H. J., and Smith, E. v. P. 1963, *Solar Flares* (New York: MacMillan).
*Solar-Geophysical Data.* 1982–1984, No. 449–484 (Boulder: NOAA Environmental Data and Information Service).
Švestka, Z. 1976, *Solar Flares* (Dordrecht: Reidel).
———. 1981, in *Solar Flare Magnetohydrodynamics*, ed. E. R. Priest (New York: Gordon & Breach), p. 47.
Švestka, Z., and Fritzova-Švestkova, L. 1974, *Solar Phys.*, 36, 417.
Švestka, Z., and Simon, P., eds. 1975, *Catalog of Solar Particle Events 1955–1969* (Boston: Reidel).
Švestka, Z., Martin, S. F., and Kopp, R. A. 1980, in *IAU Symposium 91, Solar and Interplanetary Dynamics*, ed. M. Dryer and E. Tandberg-Hanssen (Dordrecht: Reidel), p. 217.
Švestka, Z., Dodson-Prince, H. W., Martin, S. F., Mohler, O. C., Moore, R. L., Nolte, J. T., and Petrasso, R. D. 1982, *Solar Phys.*, 78, 271.
Tandberg-Hanssen, E. 1974, *Solar Prominences* (Dordrecht: Reidel).
Thomas, R. J., Starr, R., and Crannell, C. J. 1985, *Solar Phys.*, 95, 323.
van Hollebeke, M. A. I., MaSung, L. S., and McDonald, F. B. 1975, *Solar Phys.*, 41, 189.
von Rosenvinge, T. T., McDonald, F. B., Trainor, J. H., van Hollebeke, M. A. I., and Fisk, L. A. 1978, *IEEE Trans. Geosci. Electronics*, GE-16, 208.
Wagner, W. J., *et al.* 1983, *Solar Phys.*, 83, 153.
Wagner, W. J., and MacQueen, R. M. 1983, *Astr. Ap.*, 120, 136.
Webb, D. F. 1984, in *Proc. 2d Indo-US Workshop on Solar Terrestrial Physics*, in press.
Webb, D. F., Cheng, C.-C., Dulk, G. A., Edberg, S. J., Martin, S. F., McKenna-Lawlor, S., and McLean, D. J. 1980, in *Solar Flares*, ed. P. A. Sturrock (Boulder: Colorado Associated University Press), p. 471.
Webb, D. F., Krieger, A. S., and Rust, D. M. 1976, *Solar Phys.*, 48, 159.
Webb, D. F., and Kundu, M. R. 1978, *Solar Phys.*, 57, 155.
Yeh, T. 1982, *Solar Phys.*, 78, 287.

H. V. CANE and R. E. MCGUIRE: Code 661, Goddard Space Flight Center, Greenbelt, MD 20771

E. W. CLIVER and S. W. KAHLER: AFGL/PHP, Hanscom AFB, MA 01731

N. R. SHEELEY, JR.: Code 4172, Naval Research Laboratory, Washington, DC 20375

R. G. STONE: Code 690, Goddard Space Flight Center, Greenbelt, MD 20771

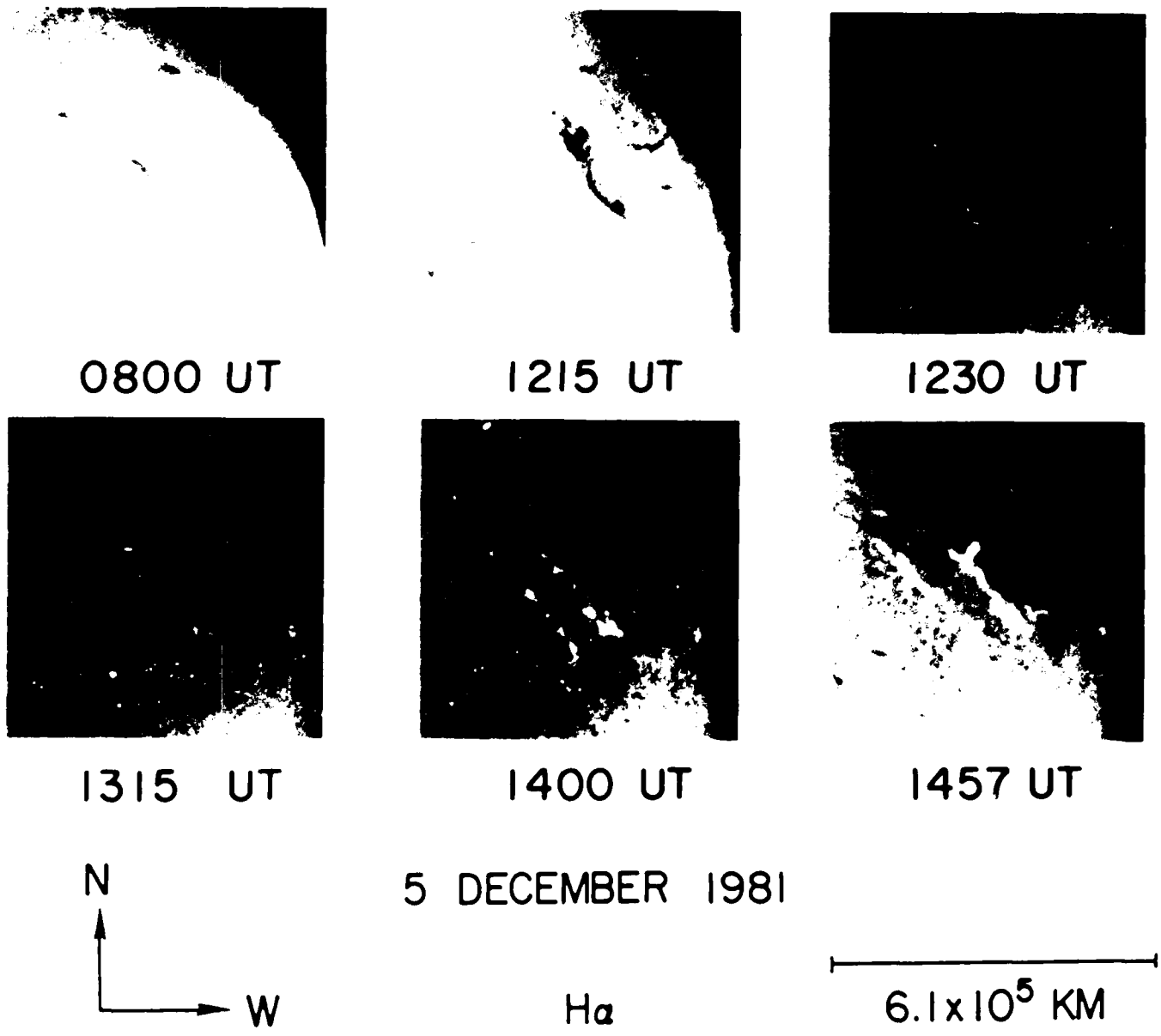


FIG. 2.—Hα images from the Haute Provence Observatory showing the filament disappearance (*top*) and subsequent two-ribbon brightening (*bottom*) on 1981 December 5. Comparison of the top three images shows a clear outward motion of the northernmost part of the filament.

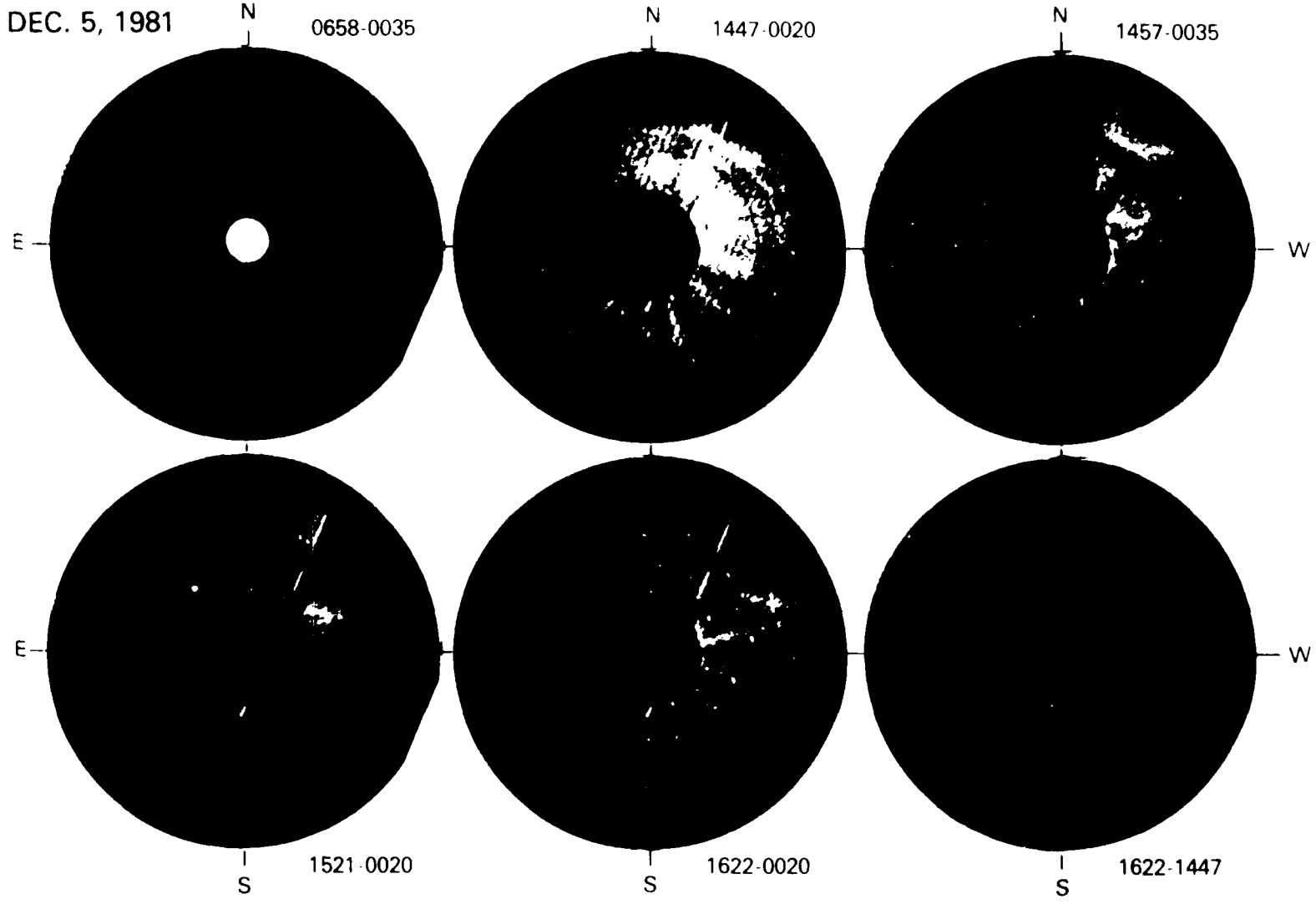


FIG. 3.—Subtracted images from the NRL Solwind coronagraph showing the CME of December 5. The Hα filament can be seen as the small bright structure at the inner core of the CME. Its position in the 1521 UT image is indicated with a black arrow.

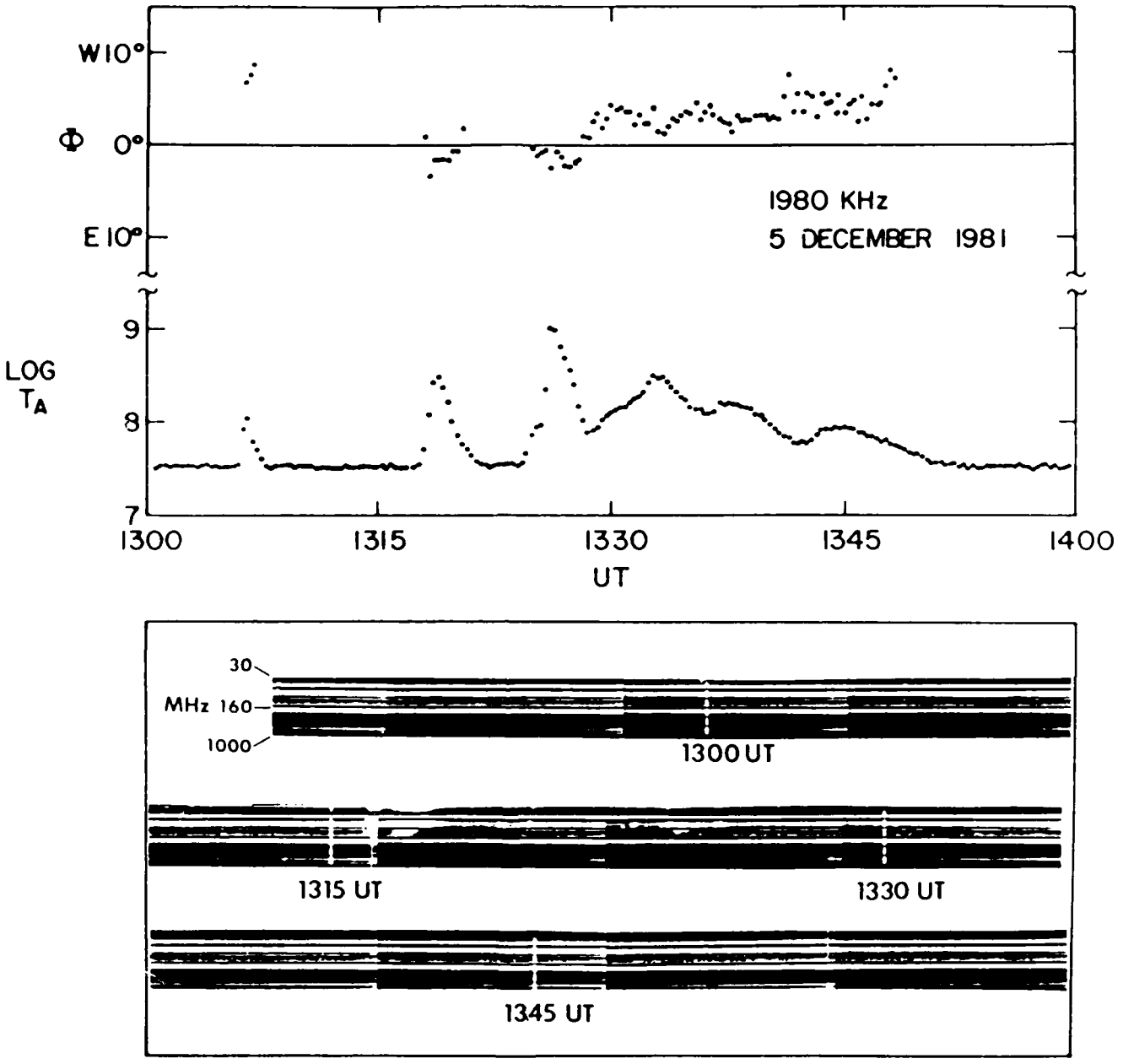


FIG. 4.—*Top:* plots of the log of the antenna temperature $T_A$ and the solar elongation angle Φ at 1980 kHz on 1981 December 5. Values of Φ are shown only when the standard deviation of the computed angle is less than 1°.5. *Below:* the Weissenau dynamic spectrum from 1248 to 1359 UT. The gaps in the six white vertical bars at the 15 minute time marks correspond to the frequency channel boundaries at 30, 46, 86, 160, 290, 546, and 1000 MHz, from top to bottom. The type III GG (group of more than 10 bursts) events from 1316 to 1318 UT and from 1320 to 1326 UT observed in the Weissenau spectrum are also observed in the *ISEE 3* 1980 kHz profile. The solar elongation angles for those bursts are east of the Sun, indicating that the bursts were not associated with the December 5 erupting filament which lay in the western hemisphere. The SA event observed from 1328 to 1352 UT at 1980 kHz had no observed counterpart in the Weissenau spectrum but clearly came from the western hemisphere.

KAHLER *et al.* (*see* page 507)

JOURNAL OF GEOPHYSICAL RESEARCH, VOL. 91, NO. A12, PAGES 13,321-13,329, DECEMBER 1, 1986

# Interplanetary Shocks Preceded by Solar Filament Eruptions

H. V. CANE[1]

*Laboratory for High Energy Astrophysics, Goddard Space Flight Center, Greenbelt, Maryland*

S. W. KAHLER

*Emmanuel College, Boston, Massachusetts*

N. R. SHEELEY, JR.

*E. O. Hulburt Center for Space Research, Naval Research Laboratory, Washington, D. C.*

We discuss the solar and interplanetary characteristics of six interplanetary shock and energetic particle events associated with the eruptions of solar filaments lying outside active regions. The events are characterized by the familiar double-ribbon Hα brightenings observed with large flares, but only very weak soft X ray and microwave bursts. Both impulsive phases and metric type II bursts are absent in all six events. The energetic particles observed near the earth appear to be accelerated predominantly in the interplanetary shocks. The interplanetary shock speeds are lower and the longitudinal extents considerably less than those of flare-associated shocks. Three of the events were associated with unusual enhancements of singly ionized helium in the solar wind following the shocks. These enhancements appear to be direct detections of the cool filament material expelled from the corona. We suggest that these events are part of a spectrum of solar eruptive events which include both weaker events and large flares. Despite their unimpressive and unreported solar signatures, the quiescent filament eruptions can result in substantial space and geophysical disturbances.

## 1. INTRODUCTION

It is well established [*Hundhausen*, 1972; *Chao and Lepping*, 1974] that the most disturbed geomagnetic conditions, resulting from an energetic interplanetary shock, occur about 1.5 to 2 days after big solar flares which are easily observed as large brightenings in Hα. Such flares are typically accompanied by solar energetic particle (SEP) events, meter wavelength type II and type IV bursts, and long duration soft X ray events [*Cane and Stone*, 1984; *Cane*, 1985].

Since these major flares are usually accompanied by prominence eruptions [*Martin*, 1973], *Anzer and Pneuman* [1982] have suggested that a large flare event differs from an eruptive prominence event without a flare only in being more energetic. They interpreted non-flare-related mass ejections as being those that "are produced by magnetic fields that are too weak to produce chromospheric brightenings." In their view the kind of event that results is merely a matter of magnetic field strength.

Eruptive prominences are now recognized as playing important roles in most, if not all, coronal mass ejections (CMEs). *Munro et al.* [1979] found that more than 70% of all Skylab CMEs were associated with eruptive prominence or filament disappearances. More recently, *Illing and Hundhausen* [1985] studied the three-part structure of a CME similar to many large CMEs observed with the Solar Maximum Mission (SMM) coronagraph instrument. One component, a bright core, was identified as the erupting prominence, showing that in these CME events the prominence itself plays an important role.

CMEs have recently been shown to be closely associated with interplanetary shocks. *Sheeley et al.* [1985] found that about 70% of all interplanetary shocks observed at Helios 1 could be confidently associated with CMEs. Only 2% of the shocks clearly lacked associated CMEs. If we then assume that CMEs are the drivers of interplanetary shocks and that most or all CMEs are associated with erupting prominences, we might expect a good association between erupting prominences and interplanetary shocks. Eruptive prominences have in fact long been suspected of being linked to geomagnetic storms, as *Joselyn and McIntosh* [1981] have documented. *Wright and McNamara* [1983] have established a statistical relationship between disappearing filaments and geomagnetic activity using data from 1974 to 1980. They found that geomagnetic disturbances followed filament disappearances by typically 3-6 days. The magnitude of the disturbance increased with the size of the disappearing filament.

In this paper we examine the solar and interplanetary signatures of six interplanetary shocks associated with disappearing filaments outside active regions to compare the eruptive events as a class with flare events. Each shock has been the subject of individual publications in which only one or two aspects of the event were discussed. In section 2 we summarize the results of these papers, presenting all the data on each event separately. In section 3 we include new data to summarize the observational characteristics of all the events. The significance of these events for forecasting space disturbances and learning about particle acceleration is discussed in section 5 by comparing them with the more familiar flare-associated events.

## 2. REPORTS AND ASSOCIATIONS OF THE SHOCK EVENTS

Summaries of the reports of the shock events and the associations with filament disappearances follow. The dates refer

[1]Also at Department of Physics and Astronomy, University of Maryland, College Park.



Paper number 6A8590.
0148-0227/86/006A-8590$05.00

to the times of occurrence of the phenomena of principal concern to the initial reports.

### 2.1. *January 29, 1977*

*Schwenn et al.* [1980] detected singly ionized helium in the driver gas plasma following an interplanetary shock detected by Helios 1 at 0103 UT on this date. They proposed that this ion must have come from cold chromospheric material which had been ejected in an eruptive prominence as part of a CME. They did not report whether a filament had disappeared; however, it is clear from the Hα photographs in Solar-Geophysical Data (SGD) that a large quiescent filament was present at about 40°S, 50°E on January 25 and was gone on January 26. K. Harvey (private communication, 1985) has determined the disappearance interval to be from 2249 UT on January 25 to 0853 UT on January 26.

### 2.2. *July 29, 1977*

Like the January 29 event, the shock detected by IMP 8 at 0031 UT on July 29 was followed by large fluxes of singly ionized helium [*Gosling et al.*, 1980]. Because of the lack of any obvious reported flare candidates or type II or IV bursts during the 7 days prior to July 29, Gosling et al. suggested an association of the shock with the disappearance of a quiescent filament at 50°N, 50°W. According to *Harvey and Sheeley* [1979], the disappearance occurred between 2006 UT on July 25 and 1713 UT on July 26. Further examination of Hα images (F. Tang, private communication, 1985) shows that the event occurred before 2345 UT on July 25.

### 2.3. *August 27, 1978*

A major geomagnetic storm with a sudden commencement (SC) at 0247 UT was attributed by *Joselyn and Bryson* [1980] to the disappearance at about 0130 UT on August 23 of a filament located at 15°N, 15°E. However, Hα observations at 0748 UT at Tel Aviv showed that the filament had re-formed by that time. In subsequent observations, in which the filament was just outside the field of view, an Hα ribbon appeared parallel to the filament location at about 1200 UT (F. Tang, private communication, 1985). The Boulder full disk image at 1436 UT showed that the filament had again disappeared [*Joselyn and Bryson*, 1980]. Since the first filament disappearance was short-lived (≤6 hours) and no subsequent filament reappearance followed the 1200 UT disappearance, we assume that the interplanetary shock was associated with the 1200 UT disappearance. *Domingo et al.* [1979] reported that the interplanetary shock was accompanied by an energetic storm particle (ESP) event and that this event was preceded by a low-energy SEP event. Protons in the 0.6- to 1-MeV energy range were first detected at ISEE 3 at about 1200 UT on August 25 (i.e., 2 days after the second filament disappearance). Using interplanetary scintillation observations, *Tappin et al.* [1983] detected the disturbance east of central meridian, consistent with the position of the filament identified by *Joselyn and Bryson* [1980]. From their model of the observations, Tappin et al. derived a speed of 430 km/s near 1 AU for the disturbance.

### 2.4. *April 23, 1979*

An interplanetary type II event [*Cane et al.*, 1982] was observed to commence at about 1200 UT on April 23. The associated shock passed ISEE 3 at 2328 UT on April 24 and produced an SC at the earth at 2357 UT. Because no large flares were reported during the early part of April 23, Cane et al. associated a shock-accelerated (SA) event [*Cane et al.*, 1981] at 0150 UT with the shock. The SA event was associated with possible weak type II and type IV bursts reported by the Culgoora Observatory. The elongation angle of the SA event clearly indicated a west limb source, and Cane et al. suggested that an active region behind the limb was the source of the event. However, a study of the associated low-energy proton event by *Sanahuja et al.* [1983] showed that this association was very unlikely because the Venera 11 spacecraft, which was well connected to the west limb, did not detect a particle event. Low-energy ($E \sim 100$ keV) protons were first observed at Helios 2, magnetically connected to the sun at about 20°W, between 0100 and 0200 UT on April 23. Sanahuja et al. suggested that the solar source of the shock and particle event was the eruption of a large quiescent filament extending from 10°S, 00°E to 30°S, 20°E. This eruption resulted in a parallel ribbon brightening [*Tang*, 1985] in Hα beginning at 2215 UT on April 22, the continuation of which was reported as two class 1F flares by the Culgoora Observatory. In her survey of the properties of interplanetary shocks, *Cane* [1985], noting the lack of observed strong shocks from west limb flares and acknowledging the suggestion of Sanahuja et al. about the source of the event, tentatively agreed with their source position but retained the 0150 UT April 23 SA association. A reexamination of the 1980-kHz data from the ISEE 3 radio experiment shows a possible SA event from 2210 UT to 2300 UT on April 22 with a source position near central meridian, consistent with that of the erupting filament. We now associate this earlier 1980-kHz burst with the shock and particle event. It occurred at approximately the right time to account for the onset of the 100-keV protons at Helios 2 and resulted in an average sun-earth transit speed of 840 km/s compared with the previous higher value of 900 km/s reported by *Cane* [1985].

### 2.5. *November 27, 1979*

*Howard et al.* [1982] reported the observation of a "head-on" CME which they associated with the sudden disappearance of a large quiescent filament at 5°N, 3°W. The disappearing filament may have been associated with a reported 1N flare at 18°N, 5°E in a nearby active region. The CME was presumed to be the driver of an interplanetary shock which

TABLE 1. The Events and the Associated Phenomena

| Date and Time of Filament Disappearance | H Alpha Ribbons | Soft X Rays, >C1 | Gradual 10-cm Burst | CME | He* |
|---|---|---|---|---|---|
| January 25, 1977, 2300 UT, to January 26, 1977, 0900 UT | ... | no | no | ... | yes |
| July 25, 1977, 2000–2330 UT | ... | no | no | ... | yes |
| August 23, 1978, 1200 UT | probably | no | yes | ... | ... |
| April 22, 1979, 2230 UT | yes | yes | yes | ... | ... |
| November 27, 1979, 0600 UT | ... | no | no | yes | ... |
| December 5, 1981, 1330 UT | yes | yes | yes | yes | yes |

Three dots correspond to cases in which we have no information.

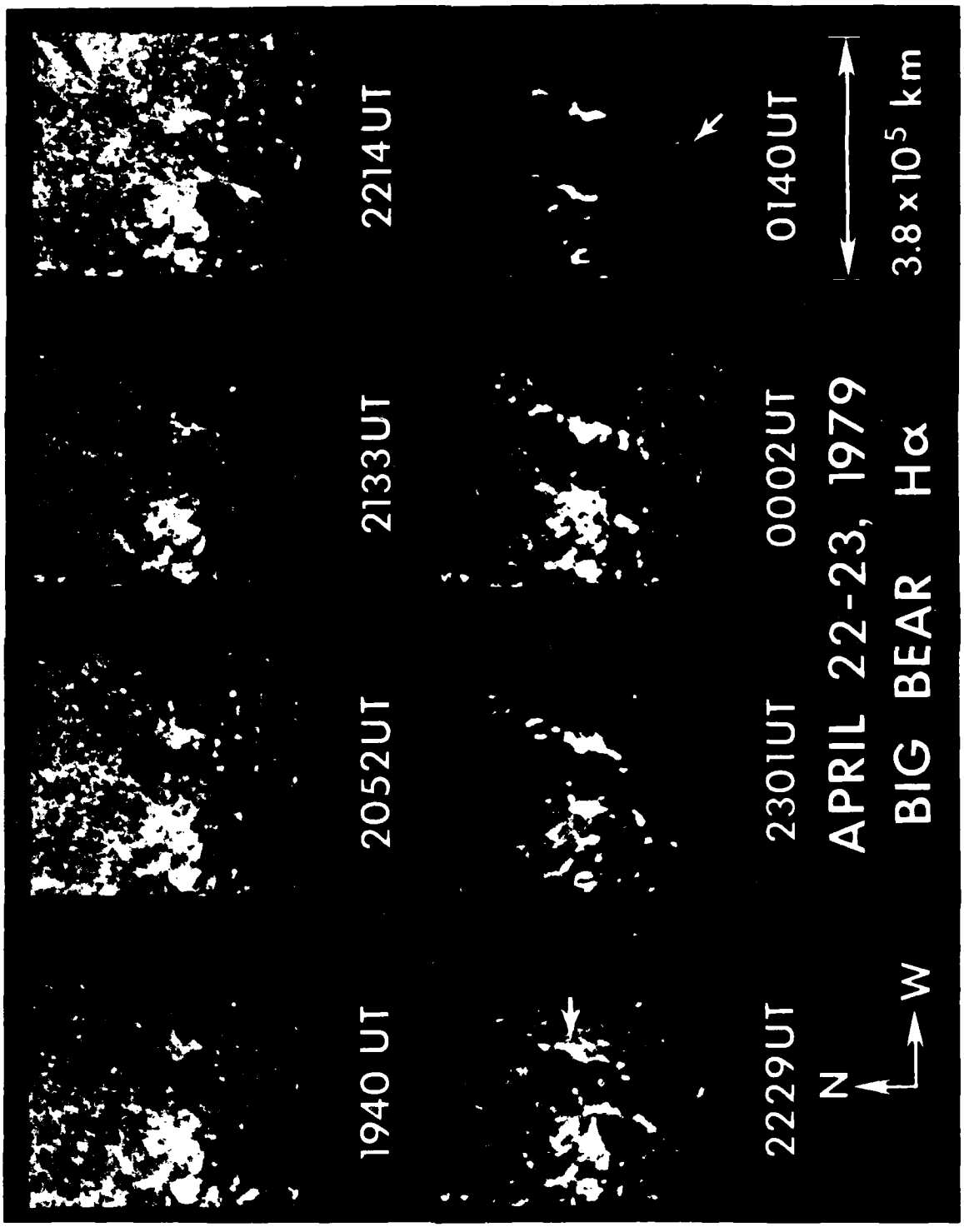


Fig. 1. The disappearance of the Hα filament on April 22–23, 1979. The double-ribbon brightenings associated with the filament disappearances are indicated by arrows at 2229 UT and 0140 UT.

TABLE 2. Speed Characteristics of the Shocks

| Date of Filament Disappearance | Solar Longitude | Speed, km/s | Distance, AU | Reference |
|---|---|---|---|---|
| January 26, 1977 | 50°E | 460 ± 20 | 0.5 | transit to earth |
| | | 570 ± 40 | 0.5 | transit to Helios 1 (0.95 AU) |
| July 25, 1977 | 50°W | 560 ± 10 | 0.5 | transit to earth (SC) |
| | | 450 | 1.0 | *King et al.* [1982] |
| August 23, 1978 | 15°E | 480 | 0.5 | transit to earth (SC) |
| | | 430 | 1.0 | *Tappin et al.* [1983] |
| | | 510 | 1.0 | *Ogilvie et al.* [1982] |
| April 22, 1979 | 10°E | 980 | 0.2 | transit to Helios 2 [*Sanahuja et al.* [1983] |
| | | 840 | 0.5 | transit to earth (SC) |
| | | 760 | 0.7 | Helios 2 to earth |
| November 27, 1979 | 3°W | 1160 | | CME [*Howard et al.*, 1982] |
| | | 800 | 0.2 | CME [*Jackson*, 1985] |
| | | 570 | 0.5 | transit to earth (SC) |
| | | 372 | 1.0 | *Ogilvie et al.* [1982] |
| December 5, 1981 | 40°W | 840 | | CME [*Kahler et al.*, 1986] |
| | | 570 | 0.5 | transit to earth (ISEE 3) |

reached ISEE 3 at 0649 UT on November 30 and produced an SC at the earth at 0738 UT. The CME was also detected by *Jackson* [1985] using zodiacal light photometers on the Helios spacecraft. An average speed of 800 km/s for the CME was implied from the transit time between the sun and Helios 2. Jackson noted that the mass ejection was well collimated along the sun-earth line.

### 2.6. *December 5, 1981*

*Cane and Stone* [1984] reported the observation on December 5 of kilometric radio emission which had the characteristics of an interplanetary type II event but for which there were no reported related solar phenomena at the time of the preceding SA event, apart from a SEP event. Recently, *Kahler et al.* [1986] showed that the SA and interplanetary type II burst were well associated with an erupting filament at 20°N, 40°W and with a CME observed by the Solwind coronagraph. The interplanetary shock in this event did not cause an SC, but a well-defined disturbance was detected by the plasma instrument on ISEE 3 (W. C. Feldman, private communication, 1985) at 1400 UT on December 8. Following this disturbance an enhancement of singly ionized helium was detected at ISEE 3 [*Bochsler*, 1983]. The comprehensive observations of this event by both solar and interplanetary instruments have provided an unambiguous association of energetic interplanetary phenomena with an erupting prominence well outside any active region.

## 3. SUMMARY OF OBSERVATIONAL DATA ON THE SIX EVENTS

Having outlined previous work on each of the six events, we now discuss additional observations derived primarily from reports in Solar-Geophysical Data (SGD). In addition, we examine the unpublished energetic particle data obtained from Goddard Space Flight Center detectors on Helios 1 and 2, IMP 8, and ISEE 3. The results are summarized in the various observational areas. For clarification the information is summarized in Table 1.

### 3.1. *Hα*

We have no data showing the filament disappearances of January 25 and July 25, 1977. *Joselyn and Bryson* [1980] and *Howard et al.* [1982] have reported only the timings of the filament disappearances of August 1978 and November 1979, respectively, but give no further details. The Hα observaitons of the April 1979 event were discussed by *Sanahuja et al.* [1983] (see also *Tang* [1985]), and those of the December 1981 event were shown by *Kahler et al.* [1986]. We have obtained Hα images of the April 1979 event from Big Bear Solar Observatory (M. Liggett, private communication, 1985). The sequence of images showing the filament disappearance followed by double-ribbon brightenings is presented in Figure 1. Two separate filament disappearance events occurred, each associated with Hα ribbon brightenings.

For the two events where we have observations, the filament eruptions were accompanied by Hα double-ribbon brightenings which, since they lay outside active regions, are properly termed "flarelike brightenings" rather than flares [*Kahler et al.*, 1986]. It is probable that the 1200 UT August 23, 1978, filament disappearance also was accompanied by a double-ribbon brightening.

An examination of the full disk Hα images of each of the six filaments shows that they all lay outside active regions. Such filaments are called quiescent filaments rather than active region filaments, but of course in our cases the quiescent filaments were also active in the sense of erupting.

### 3.2. *1- to 8-Å Soft X Rays*

The soft X ray signature of the December 1981 event was the most prominent of the six events, consisting of a 3-hour long decay event (LDE) with a peak X ray flux of C3.5 [*Kahler et al.*, 1986]. A C1.5 LDE with a 6-hour duration began at about 2220 UT on April 22, 1979, at about the time of the reported Hα brightening associated with that filament disappearance [*Sanahuja et al.*, 1983].

Soft X ray events associated with the remaining four events were weak, at most. A C1 LDE occurred on November 27, 1979, from about 0630 UT to 1200 UT, but this event may be the soft X ray signature of the flare reported in the active region near the disappearing filament [*Howard et al.*, 1982]. Because the timings of the January 1977 and July 1977 filament disappearances are uncertain on time scales of hours, we can find possible LDE associations for both events, but the peak fluxes of these events are less than C0.2. No soft X ray event could be associated with the August 1978 event at about

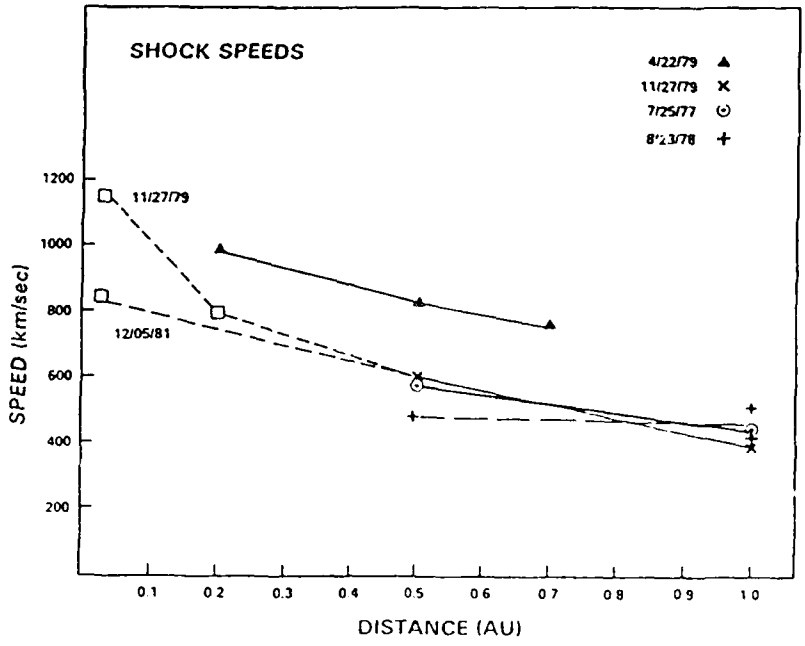


Fig. 2. Speeds as a function of heliocentric distance for five eruptive filament-associated shocks. The squares denote CME speeds. See Table 1 for details.

0130 UT, at which time the background flux was C0.2. A C0.3 LDE accompanied the presumed filament disappearance at 1200 UT. The X ray fluxes of these four events must therefore be well below the C1 level.

### 3.3. *Radio*

Three gradual 10-cm bursts could be associated with the six events. Bursts of 4 and 8 solar flux units at 2800 MHz were observed at Ottawa on August 23, 1978, and December 5, 1981, respectively. A burst of 14 solar flux units at 2695 MHz was observed at Penticton on April 22 and 23, 1979. No gradual microwave bursts were reported for any of the other three events. However, for those events, only one (July 1977) occurred during the Ottawa and Penticton observing windows. It is these stations which usually report weak ( < 10 solar flux units) bursts.

None of the six events was associated with any reported metric type II or type IV burst. We also examined 1980-kHz data from the ISEE 3 radio astronomy experiment for any associated events in the kilometric range. Data coverage exists for only the last four of the six events, and of those, only two, the April 1979 (see section 2.4) and December 1981 [*Kahler et al.*, 1986] events, showed SA events. Both these events were also associated with interplanetary type II bursts [*Cane*, 1985]. Emission at 1980 kHz did occur at about the times of the August 1978 and November 1979 events but did not appear to be related.

### 3.4. *Coronal Mass Ejections*

Solwind coronagraph observations were available for the three events of April 22, 1979, November 27, 1979, and December 5, 1981. For the November 1979 and December 1981 events, associated CMEs were observed with estimated speeds in the plane of the sky of 600 km/s [*Howard et al.*, 1982] and 840 km/s [*Kahler et al.*, 1986], respectively. By making assumptions about the shape of the December 1981 CME, *Howard et al.* [1982] estimate a frontal speed of 1160 km/s. No CME was found for the April 1979 event, but the first observation after the filament disappearance was 5 hours later. Observations of CME events originating near disk center show that such CMEs are not detectable more than 3 hours after their initiation.

### 3.5. *Interplanetary Shock Speeds and Sizes*

The calculated or measured speeds of the six interplanetary shocks are listed in Table 2 and plotted in Figure 2. Filament disappearance times were used for shock initiations at the sun. The speed uncertainties for the January and July 1977 events reflect the use of earliest and latest times of filament disappearances. Spacecraft shock observations or the sudden commencements (SC) of geomagnetic storms were used for the shock arrival times at earth. The transit speeds are assumed to give estimates of the speeds midway between two observation points. SCs were associated with four of the events; in another case (December 1981) a disturbance was observed at a spacecraft located near 1 AU.

The January 1977 event was detected at Helios 1, which was situated 13°W of the normal to the filament site. It appears that the shock did not reach the earth or Helios 2. We do not believe that a minor shock observed at Helios 2 was related to the shock. Our reasons are as follows: a minor shock was observed at Helios 2 [*Schwenn et al.*, 1980], situated 28° west of Helios 1 at 0.98 AU, at 2103 UT on January 28 and was preceded by an SC at 1840 UT which was probably due to the same shock. This minor shock preceded by 4 hours the prominent shock at Helios 1, although Helios 1 was closer in longitude to the filament eruption.

A weak SC reported by two stations on January 30 may have been caused by a disturbance related to the filament disappearance. For the purpose of comparison, we use this SC

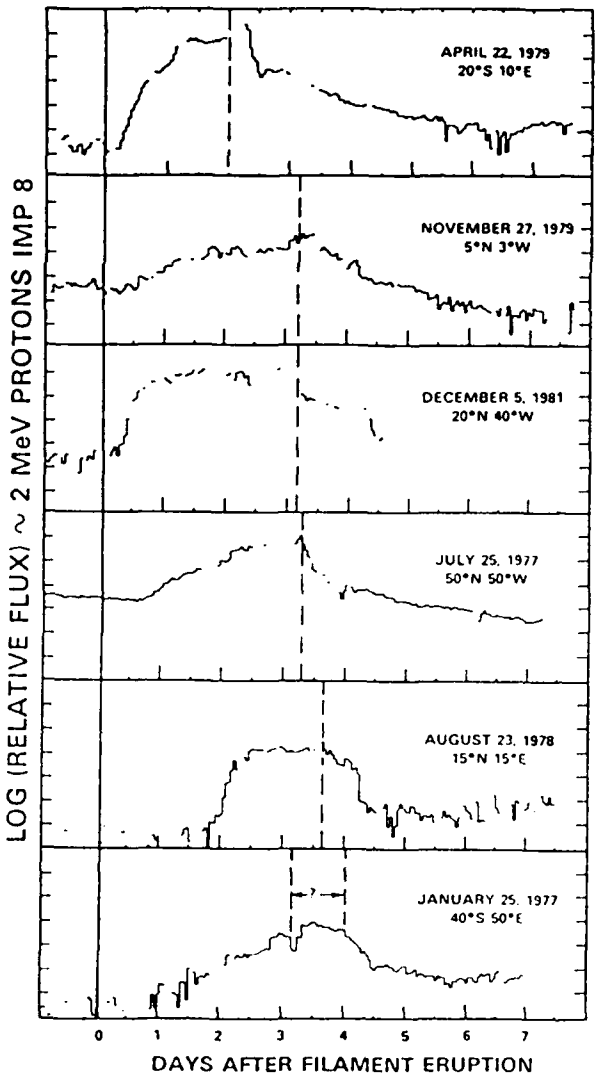


Fig. 3. Time profiles of 2-MeV proton fluxes as observed at IMP 8. The events are organized such that shock speed decreases down the figure. In each event the shock passage is indicated by a dashed line. The positions of the filaments are noted.

time to estimate the speed of the disturbance to the earth. The deduced transit speed is about 80% of the transit speed to Helios 1 situated at about the same distance but closer to the radial from the shock origin.

Other shock speed measurements and the source references are also given in Table 2. In addition, we include the speeds of the two observed associated CMEs. Because the relationship between the CME leading edges and the associated shock fronts is not known, the CME speeds are joined to shock speeds by dashed lines in Figure 2.

The shocks of Table 2 are rather narrow in longitudinal extent. We see that two (January 1977 and December 1981) of the three shocks originating from longitudes located more than 30° from central meridian did not produce SCs at the earth. The December 1981 event resulted in a disturbance at ISEE 3 which was not clearly a shock. In the November 1979 event a small disturbance, but not a shock, was seen at Helios 2 on November 28 when Helios 2 was only 30° east of the erupting filament. The CME itself also appeared to be rather highly collimated when observed from Helios 2 [*Jackson*, 1985]. In the April 1979 event a plasma disturbance, but not a shock, was seen at Helios 1 when that spacecraft was only 45° east of the erupting filament. From these observations we estimate the angular half-widths of the shocks to be at most 50°.

### 3.6. *Energetic Particles*

Each of the six events was accompanied by energetic particles. The August 1978, April 1979, and December 1981 SEP events have been mentioned in section 2. We find that SEP events were also associated with the other three filament disappearances. The July 1977 and December 1981 events were well connected to the earth, and particles with energies up to about 40 and 80 MeV, respectively, were detected in those events. The November 1979 event was well connected to Helios 2, which detected particles of up to 20 MeV. For the three eastern hemisphere events the maximum observed particle energy was less than 15 MeV.

Figure 3 shows time profiles of IMP 8 proton fluxes at about 2 MeV for the six events, ordered as a function of decreasing shock speed. It can be seen that the time profiles of the particle fluxes are roughly centered at the times of shock passages. For the slowest shock, of August 1978, there was a delay of 2 days between the filament eruption and the particle onset.

### 3.7. *Singly Ionized Helium Enhancements in the Solar Wind*

Enhancements of singly ionized helium in the solar wind following the arrival of the interplanetary shocks were reported for the January 1977, July 1977, and December 1981 events, as discussed in section 2. We are not aware of any reports of singly ionized helium observed with the other three events of our study.

## 4. SEARCH FOR ADDITIONAL EVENTS

We have looked for other events with properties similar to those discussed above. We examined data from the Goddard Space Flight Center (GSFC) energetic particle experiment on IMP 8 and ISEE 3 for SEP events lacking the usual velocity dispersion characteristic of flare-associated events. We also used the times of filament disappearances to search for associated SEP events. However, we could not find additional particle events during 1978 to 1984 which could be associated as confidently with erupting filaments as the six events discussed here. A less confident candidate for another example of this class of event is the SEP event beginning on May 25, 1979, and the subsequent SC at 1850 UT on May 29. If we associate this event with a filament disappearance at about 28°N, 22°W between 1520 UT on May 25 and 0550 UT on May 26 (K. Harvey, private communication, 1985), the average shock transit speed to the earth would be 420 to 490 km/s, a relatively slow event compared to the events of our study. No interplanetary type II burst was observed for this shock, as expected from its low speed [*Cane*, 1985].

## 5. DISCUSSION

Our results show clearly that solar disturbances occurring outside active regions and showing few, if any, of the signatures characteristic of "large" flares can result in interplanetary

shocks and SEP events. *Joselyn and McIntosh* [1981] have emphasized the importance of disappearing filaments as a useful tool in forecasting geomagnetic storms. We find that the disappearing filaments can also give rise to SEP events of modest (~10 MeV) energy. We emphasize the importance of these events for understanding the physics of shock propagation and particle acceleration in interplanetary space.

### 5.1. *Solar Origins of the Events*

The solar signatures of the six events of this study are similar. All the disappearing filaments lay outside active regions, and they may all have produced double-ribbon Hα events, such as the example in Figure 1. If any soft X ray or microwave events occurred, they were weak and had time scales of hours. The events also lacked evidence of impulsive phases or of coronal shocks.

The common links of these events and large flares are the filament eruptions and double-ribbon brightenings. On this basis, *Anzer and Pneuman* [1982] concluded that a common process occurs in both large flares and filament eruption events with the flares being the most energetic events. The Skylab X ray events [cf. *Webb et al.*, 1976] lie at the other end of the energy spectrum. These events were weak, long duration soft X ray enhancements originating outside active regions and associated with disappearing filaments or filament channels. In contrast to the six events of our study, some of the Skylab X ray events were not accompanied by detectable filaments and had only faint patches of Hα brightenings. While the spectrum of filament eruption event sizes has previously been appreciated, the fact that apparently innocuous events, such as those of this study, can result in both interplanetary shocks and SEP events has not generally been understood.

### 5.2. *SEP Events Sources*

*Evenson et al.* [1982] have compared the $E > 30$ MeV proton profiles for two kinds of flare SEP events, those with associated interplanetary shocks and those without. They concluded that large particle events can have two components. The first component consists of particles which escape directly from the corona and are easily observed from regions well connected to the particle source region. The second component has a time scale of days and results from the acceleration of particles by interplanetary shocks. *Lee* [1983] has summarized the properties of such shock-associated ESP events.

The two-component model is also an appropriate description for the SEP events of our study, but here the second component seems to be dominant, consistent with the lack of the usual flare signatures of impulsive phenomena and metric radio bursts. We illustrated the SEP profiles in Figure 3 and showed the gradual rises with maxima near the arrival times of the associated shocks. Metric type II bursts are the well-known signatures of coronal shocks which have a good association with >10-MeV proton events [*Svestka and Fritzova-Svestkova*, 1974] and are presumed to be the sources of the first particle component. Although there are no type II bursts associated with the six SEP events in our study, the presence of SA activity in at least two events can be taken as evidence of a coronal shock. However, the coronal shock responsible for the acceleration of the particles comprising the first component did not form or did not radiate until high in the corona (i.e., below the ground-based observing frequency range).

Two events (July 25, 1977, and December 5, 1981) were well connected to the earth and showed clear evidence of velocity dispersion in the MeV range, which is characteristic of flare-associated SEP events. At energies above 10 MeV these events had the usual profiles associated with flare events, i.e., a rapid onset and a slower decay. This characteristic shape was also seen for the November 1979 event observed from Helios 1, which had a connection longitude of 37°W.

Within our limited statistics it seems that the first particle component is more restricted in the filament eruption events than in flare events. The rapid onset and gradual decay profiles can be seen in flare events which originate near central meridian, yet only the disappearing filament events connected near 50°W have this shape. Assuming that prompt particles are injected only onto field lines directly connected to a coronal shock, we suggest that in the filament eruption events the coronal shock extends over a limited range in heliolongitude. The lack of metric type II activity is an indication that the coronal shocks in these events are probably rather weak.

### 5.3. *Shock Characteristics*

We find that the six shocks of our study originated within 50° of central meridian and that only four of the shocks were responsible for SCs at the earth. This fact and the other observations discussed in section 3.5 suggest that the shocks associated with disappearing filaments extend at most to 50° in heliographic longitude from the source normal. In contrast, flare-associated shocks can extend to 90° [*Cane*, 1985].

In recent years a number of observations concerning interplanetary shock speeds as a function of heliocentric distance have become available. The first kind of observation is the direct in situ measurements of the solar wind from the Helios 1 spacecraft. The positions of the Helios spacecraft ranged from 0.3 to 1.0 AU, so one can use the Helios observations to learn how, in a statistical sense, shocks evolve. Figure 4 shows in situ shock speeds as a function of heliocentric distance for the shocks associated with CMEs presented by *Sheeley et al.* [1985]. Only the well-determined shock speeds were used. The figure shows that whereas at 0.5 AU, shock speeds range from about 400 to 1300 km/s, the range at 1 AU is much smaller, approximately 450 to 650 km/s. This means that most shocks decelerate en route to 1 AU, an interpretation supported by the *Sheeley et al.* [1985] comparison of Solwind CME and Helios 1 shock observations. They found that the average shock transit speeds were generally higher than the in situ shock speeds, indicating that the shocks must undergo a deceleration between the sun and Helios 1.

Speed profiles for individual shocks within 0.3 AU of the sun have been presented by *Woo et al.* [1985]. Their analysis combined spacecraft Doppler scintillation observations with coronagraph and in situ plasma measurements. Their derived speed profiles for a number of shocks are shown by the curves in Figure 4. The heavy curves correspond to shocks which are well associated with flares; all these shocks generated interplanetary type II radio emission [*Cane*, 1985]. The light curves correspond to the slow shocks of their study, which suggest acceleration or at least constant speed out to quite large distances. *Woo et al.* [1985] did not associate these shocks with flares. By comparing Figures 2 and 4, it can be seen that all the shocks of our study except that of April 1979 are relatively low speed shocks. We suggest a continuum of speed profiles ranging from strong flare-associated shocks, which are fast and decelerate rapidly, to the eruptive filament-

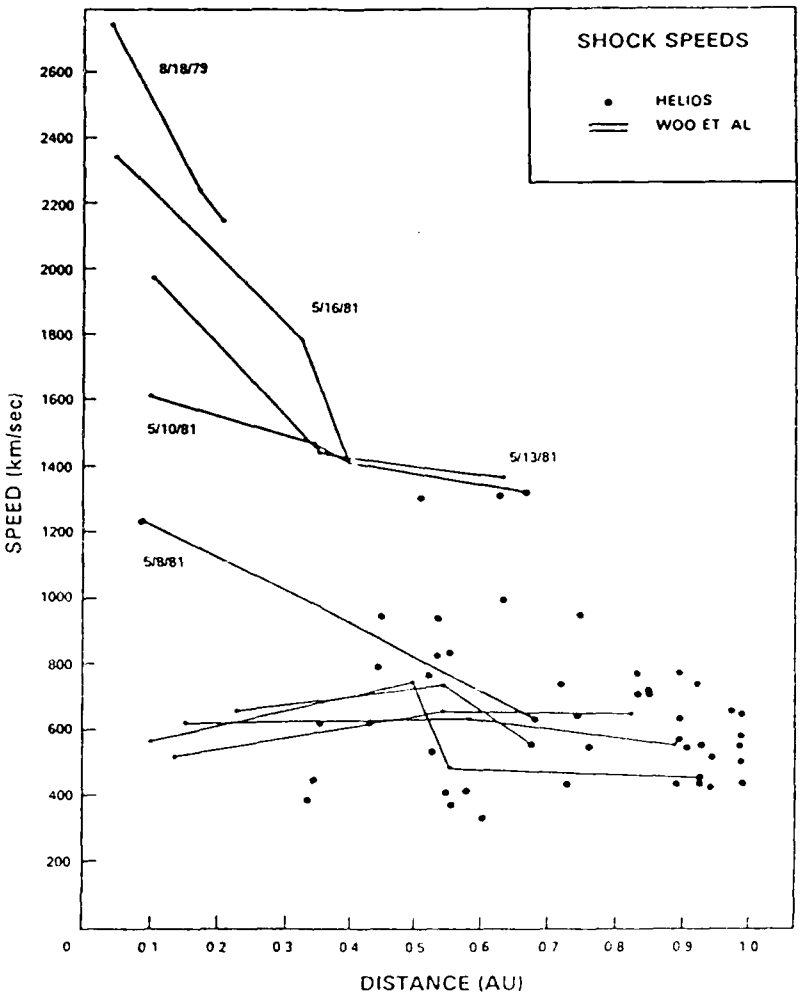


Fig. 4. Shock speeds measured in situ at a number of heliocentric distances [*Sheeley et al.*, 1985]; each circle represents a single shock. Also shown are speed profiles for a number of shocks [*Woo et al.*, 1985]. The heavy curves identify the strong flare-associated events. The scale of this figure is the same as that of Figure 2, and it can be seen that apart from the April 1979 event the eruptive events of our study are relatively slow.

associated events which are low-speed shocks and may not decelerate at all.

### 5.4. *Singly Ionized Helium Enhancements*

The first report of a substantial enhancement in abundance of singly ionized helium in the solar wind was reported by *Schwenn et al.* [1980], who attributed its origin to eruptive prominence material. Because solar wind plasma analyzers have not been designed to look for this ion, which was expected to have a very low abundance, the number of reported singly ionized helium enhancements is only about 15 (see the review of *Bame* [1983]). The fact that three of those events are also included in the events of our study supports the view that the enhancements are due to eruptive prominence material. Several other singly ionized helium enhancements not mentioned in this paper also appear to be associated with eruptive prominences. *Schwenn* [1983] associated an enhancement observed at Helios 1 following a shock on May 9, 1979, with an observed eruptive prominence on the west limb. *Zwickl et al.* [1982] found two additional enhancements in a search of plasma data from 1972 to 1980. One of those events, following an SC at 2000 UT on December 1, 1977, may have been due to a quiescent filament disappearance in the northeast quadrant of the sun between 1500 UT on November 28 and 1500 UT on November 29. As in the cases of our six events, no metric type II bursts were associated with the May 1979 and November 1977 filament disappearances.

One of the singly ionized helium enhancements is of interest because of its flare association. The enhancement observed on January 13, 1967 [*Bame*, 1983], following the SC at 1203 UT was associated with a 3B flare in McMath region 8632 on January 11. A very large filament was present before the flare and absent on the following day. A metric type II burst at 0223 UT was associated with the flare, but the only associated microwave burst was a gradual rise and fall event of 15 solar flux units. We suggest that the January 1967 event is intermediate between the filament eruption events discussed in this

study and the well-known large active region flares characterized by prominent impulsive phases.

## 6. CONCLUSIONS

We have examined the solar and interplanetary characteristics of six interplanetary shock and SEP events resulting from erupting filaments. The common features of these events were (1) the disappearance of a quiescent filament; (2) the appearance of a double-ribbon Hα brightening and a weak soft X ray and microwave burst, all with time scales of hours; (3) the absence of a metric type II burst or an impulsive phase; (4) an interplanetary shock with a lower speed and smaller angular size than those associated with large flares; (5) a SEP event of low energy ($E < 50$ MeV) with fluxes strongly influenced by the shock; and (6) an enhancement of singly ionized helium in the solar wind.

We suggest that interplanetary shocks and SEP events are due to a broad spectrum of solar eruptive disturbances. At one end of the spectrum are the very energetic active region flares accompanied by strong impulsive phases and coronal shocks, prompt acceleration of SEPs, and fast and broad interplanetary shocks which undergo substantial interplanetary deceleration. These events command considerable attention because of their easy detectability in nearly every observing waveband. At the other end of the spectrum are the unreported and relatively unfamiliar events characterized by the eruption and ejection of cool filamentary material from coronal quiescent regions. Other than the Hα, soft X ray, and microwave enhancements, often too faint to be observed, their chief manifestations are interplanetary shocks of relatively low speeds, which may decelerate or move uniformly through the interplanetary medium. If the mass of the cool ($\sim 10^4$ K) ejected material is substantial and the observing solar wind plasma spectrometer sufficiently sensitive, these events may be detected as enhancements of singly ionized helium.

*Acknowledgments.* This work was supported at GSFC/University of Maryland by NASA grant NGR 21-002316, at Emmanuel College by AFGL contract AF 19623-82-K-0039, and at NRL by NASA DPR W 14, 429. We thank M. Liggett for the Big Bear Solar Observatory images of the April 1979 disappearing filament event, F. Tang for information on the August 1978 events, K. Harvey for several times of disappearing filaments, and R. McGuire for assistance with the IMP 8 plots.

The Editor thanks V. Domingo and R. M. E. Illing for their assistance in evaluating this paper.

## REFERENCES

Anzer, U., and G. W. Pneuman, Magnetic reconnection and coronal transients, *Sol. Phys.*, *79*, 129, 1982.

Bame, S. J., Solar wind minor ions—Recent observations, Solar Wind Five, *NASA Conf. Publ., CP-2280*, 573, 1983.

Bochsler, P., Mixed solar wind originating from coronal regions of different temperatures, Solar Wind Five, *NASA Conf. Publ. CP-2280*, 613, 1983.

Cane, H. V., The evolution of interplanetary shocks, *J. Geophys. Res.*, *90*, 191, 1985.

Cane, H. V., and R. G. Stone, Type II radio bursts, interplanetary shocks, and energetic particle events, *Astrophys. J.*, *282*, 339, 1984.

Cane, H. V., R. G. Stone, J. Fainberg, R. T. Stewart, J. L. Steinberg, and S. Hoang, Radio evidence for shock acceleration of electrons in the solar corona, *Geophys. Res. Lett.*, *8*, 1285, 1981.

Cane, H. V., R. G. Stone, J. Fainberg, J. L. Steinberg, and S. Hoang, Type II radio events observed in the interplanetary medium, 1, General characteristics, *Sol. Phys.*, *78*, 187, 1982.

Chao, J. K., and R. P. Lepping, A correlative study of SSC's, interplanetary shocks and solar activity, *J. Geophys. Res.*, *79*, 1799, 1974.

Domingo, V., R. J. Hynds, and G. Stevens, A solar proton event of possible non-flare origin, *Conf. Pap. Int. Cosmic Ray Conf. 17th*, *5*, 192, 1979.

Evenson, P., P. Meyer, and S. Yanagita, Solar flare shocks in interplanetary space and solar flare particle events, *J. Geophys. Res.*, *87*, 625, 1982.

Gosling, J. T., J. R. Asbridge, S. J. Bame, W. C. Feldman, and R. D. Zwickl, Observations of large fluxes of $He^+$ in the solar wind following an interplanetary shock, *J. Geophys. Res.*, *85*, 3431, 1980.

Harvey, J. W., and N. R. Sheeley, Jr., Coronal holes and solar magnetic fields, *Space Sci. Rev.*, *23*, 139, 1979.

Howard, R. A., D. J. Michels, N. R. Sheeley, Jr., and M. J. Koomen, The observation of a coronal transient directed at earth, *Astrophys. J.*, *263*, L101, 1982.

Hundhausen, A. J., *Coronal Expansion and Solar Wind*, Springer-Verlag, New York, 1972.

Illing, R. M. E., and A. J. Hundhausen, Observation of a coronal transient from 1.2 to 6 solar radii, *J. Geophys. Res.*, *90*, 275, 1985.

Jackson, B. V., Helios observations of the earthward-directed mass ejection of 27 November, 1979, *Sol. Phys.*, *95*, 363, 1985.

Joselyn, J. A., and J. F. Bryson, Jr., Magalert: August 27, 1978, *Symp. Int. Astron. Union*, *91*, 413, 1980.

Joselyn, J. A., and P. S. McIntosh, Disappearing filaments: A useful predictor of geomagnetic activity, *J. Geophys. Res.*, *86*, 4555, 1981.

Kahler, S. W., E. W. Cliver, H. V. Cane, R. E. McGuire, R. G. Stone, and N. R. Sheeley, Jr., Solar filament eruptions and energetic particle events, *Astrophys. J.*, *302*, 504, 1986.

King, J. H., R. F. Lepping, and J. D. Sullivan, On the complex state of the interplanetary medium of July 28–29, 1977, *J. Geophys. Res.*, *87*, 5881, 1982.

Lee, M. A., The association of energetic particles and shocks in the heliosphere, *Rev. Geophys.*, *21*, 324, 1983.

Martin, S., The evolution of prominences and their relation to active centers, *Sol. Phys.*, *31*, 3, 1973.

Munro, R. H., J. T. Gosling, E. Hildner, R. A. MacQueen, A. I. Poland, and C. L. Ross, The association of coronal mass ejection transients with other forms of solar activity, *Sol. Phys.*, *61*, 201, 1979.

Ogilvie, K. W., M. A. Coplan, and R. D. Zwickl, Helium, hydrogen and oxygen velocities observed on ISEE 3, *J. Geophys. Res.*, *87*, 7363, 1982.

Sanahuja, B., V. Domingo, K.-P. Wenzel, J. A. Joselyn, and E. Keppler, A large proton event associated with solar filament activity, *Sol. Phys.*, *84*, 321, 1983.

Schwenn, R., Direct correlations between coronal transients and interplanetary disturbances, *Space. Sci. Rev.*, *34*, 85, 1983.

Schwenn, R., H. Rosenbauer, and K.-H. Mühlhäuser, Singly-ionized helium in the driver gas of an interplanetary shock wave, *Geophys. Res. Lett.*, *7*, 201, 1980.

Sheeley, N. R., Jr., R. A. Howard, M. J. Koomen, D. J. Michels, R. Schwenn, K.-H. Mühlhauser, and H. Rosenbauer, Coronal mass ejections and interplanetary shocks, *J. Geophys. Res.*, *90*, 163, 1985.

Svestka, Z., and L. Fritzova-Svestkova, Type II radio bursts and particle acceleration, *Sol. Phys.*, *36*, 417, 1974.

Tang, F., The filament eruption and flare that caused the interplanetary shocks and large proton events of April 1979, *Eos Trans AGU*, *66*, 330, 1985.

Tappin, S. J., A. Hewish, and G. R. Gapper, Tracking a major interplanetary disturbance, *Planet. Space Sci.*, *31*, 1171, 1983.

Webb, D. F., A. S. Krieger, and D. M. Rust, Coronal X-ray enhancements associated with Hα filament disappearances, *Sol. Phys.*, *48*, 159, 1976.

Woo, R., J. W. Armstrong, N. R. Sheeley, Jr., R. A. Howard, M. J. Koomen, D. J. Michels, and R. Schwenn, Doppler scintillation observations of interplanetary shocks within 0.3 AU, *J. Geophys. Res.*, *90*, 154, 1985.

Wright, C. S., and L. F. McNamara, The relationship between disappearing solar filaments, coronal mass ejections, and geomagnetic activity, *Sol. Phys.*, *87*, 401, 1983.

Zwickl, R. D., J. R. Asbridge, S. J. Bame, W. C. Feldman, and J. T. Gosling, $He^+$ and other unusual ions in the solar wind: A systematic search covering 1972–1980, *J. Geophys. Res.*, *87*, 7379, 1982.

H. V. Cane, Goddard Space Flight Center, Code 661, Greenbelt, MD 20771.

S. W. Kahler, Emmanuel College, Boston, MA 01731.

N. R. Sheeley, Jr., E. O. Hulbert Center for Space Research, Naval Research Laboratory, Washington, DC 20375.

(Received June 12, 1986;
revised August 8, 1986;
accepted August 27, 1986.)

THE ASTROPHYSICAL JOURNAL, 290:742–747, 1985 March 15


# A COMPARISON OF SOLAR $^3$HELIUM-RICH EVENTS WITH TYPE II BURSTS AND CORONAL MASS EJECTIONS

S. KAHLER
Emmanuel College, Boston; and American Science and Engineering, Inc., Cambridge, Massachusetts
D. V. REAMES
Laboratory for High Energy Astrophysics, Goddard Space Flight Center, Greenbelt, Maryland
AND
N. R. SHEELEY, JR., R. A. HOWARD, M. J. KOOMEN,[1] AND D. J. MICHELS
E. O. Hulburt Center for Space Research, Naval Research Laboratory, Washington, DC
*Received 1984 July 9; accepted 1984 September 27*

## ABSTRACT

It is generally presumed that $E \geq 1$ MeV per nucleon solar particle events of enhanced abundances, referred to as "$^3$He-rich" or "$Z$-rich" events, are due to a two-step acceleration process. The first step selectively heats $^3$He and certain heavy ions such as Fe to a threshold energy for the second step, which then provides the bulk of the particle energization. If the second phase involves the same process that operates to produce energetic particle events of normal abundances, $^3$He-rich events should be significantly associated with both metric type II bursts and coronal mass ejections, as are solar energetic particle events of normal abundances. Using 66 $^3$He-rich periods observed on *ISEE 3* from 1979 to 1982, we find that these associations are due only to random chance unless the $^3$He-rich event is accompanied by an energetic proton event. This and other recent evidence indicates that enhanced abundance events may be produced only in the impulsive phases of flares, while normal abundance events are produced in subsequent flare shock waves.

*Subject headings:* Sun: corona — Sun: flares — Sun: radio radiation

## I. INTRODUCTION

The physical origin of energetic ($\sim$10 MeV) particles produced in the solar corona and detected in interplanetary space remains unclear. However, two observational signatures now appear well associated with energetic proton events. Švestka and Fritzova-Švestkova (1974) concluded that 50%–75% of all proton events observed over a 30 month period were preceded by metric type II radio bursts. More recently, Kahler *et al.* (1984) found that nearly all flare proton events are associated with coronal mass ejections (CMEs). These observations suggest an important role for coronal shocks in proton acceleration.

Elemental and isotopic abundances found in large solar energetic particle events of $E \sim 1$–10 MeV per nucleon (hereafter MeV n$^{-1}$) generally match accepted solar coronal, but not photospheric, abundances (Cook, Stone, and Vogt 1984). This is often not true for smaller events, however, where substantial enhancements of $^3$He/$^4$He and $(Z > 6)$/H over solar abundances are seen (Anglin, Dietrich, and Simpson 1977; Zwickl *et al.* 1978; Mason *et al.* 1980). Of particular interest are the "$^3$He-rich" events, characterized by $^3$He/$^4$He $\geq 0.2$, nearly three orders of magnitude larger than the solar wind or solar prominence values of $4 \times 10^{-4}$ (Coplan *et al.* 1983; Hall 1975). The properties of these events were reviewed by Ramaty *et al.* (1980), who tabulated all $^3$He-rich events observed through 1976. This list was updated to 1980 in the recent review article by Kocharov and Kocharov (1984).

Several explanations have been advanced to account for these events with enhanced abundances. They generally invoke a two-step process consisting of $^3$He or high-$Z$ enrichment through nonthermal heating, followed by the second process, which provides most of the energization. As a first process Fisk (1978) proposed selective heating by a resonant interaction with ion cyclotron waves. Varvoglis and Papadopoulos (1983) considered the nonlinear physics of particle energization by ion cyclotron waves and found the dominant process to be nonresonant. This eliminated the requirement for exciting $^4$He$^{++}$ cyclotron waves in Fisk's model. Alternative proposals by Ibragimov and Kocharov (1977) and Kocharov and Orishchenko (1983) invoked Langmuir waves and ion sound waves, respectively, for the initial heating process. However, Weatherall (1984) has shown that the velocity diffusion coefficient used by Ibragimov and Kocharov (1977) and by Kocharov and Orishchenko (1983) is not proportional to $Z^4/A^2$, where $Z$ is the charge and $A$ the mass of the ion, but rather to $Z^2/A^2$. Their mechanisms therefore do not have the required sensitivity to ion charge needed to account for the enhanced particle abundances. Melrose (1983) has argued that preacceleration mechanisms which draw a small fraction of the ions out of the tail of a Maxwellian distribution will lead to unacceptably low abundances for accelerated ions due to the slower speeds of the heavier ions. This conclusion holds for both events of normal and enhanced compositions.

An important question is whether the enhanced event ions are energized, after the presumed first-step heating, in the same way as ions in the larger cosmic-ray events of normal abundances. Studies of associated flares could be helpful in this regard, but, in contrast to the larger events, it is usually difficult to determine flare associations for the enhanced events. Probable H$\alpha$ source flares appear to be small subflares at well-connected longitudes (Zwickl *et al.* 1978), but the low particle fluxes and energies generally result in injection times too

[1] Sachs/Freeman Associates, Inc., Bowie, Maryland.

poorly determined to make specific flare associations (Anglin, Dietrich, and Simpson 1977). However, Kocharov and Kocharov (1984) identified parent solar flares for 18 cases in which short-duration $^3$He-rich events were associated with energetic proton events. They found that type II bursts were associated with 40%–50% of those flares, a result reported earlier by Kocharov (1979). This suggests a common second step acceleration mechanism for normal and enhanced abundance events.

Statistical comparisons have also been used to suggest that the flare acceleration mechanism is the same for the two kinds of events. An observed similarity in their energy spectra led Zwickl *et al.* (1978) to suggest a common acceleration mechanism. Mason *et al.* (1980) pointed out that the variation of abundance ratios increases smoothly with decreasing size, giving no evidence that the small events represent a separate compositional class. They suggested that enhanced abundances may occur only over small regions and that if particles from only such a region are accelerated, an enhanced abundance event results. In the intense flux events, on the other hand, these particles are mixed with those from larger regions of normal abundances, and the result appears as an event of normal solar abundances. Implicit in the Mason *et al.* (1980) view is that both populations of particles are accelerated in the same mechanism.

In this paper we ask whether the energetic particles of $^3$He-rich events are accelerated in the same process as that resulting in particles of normal-abundance events. We first present in § II a list of 66 $^3$He-rich events observed with the Goddard Space Flight Center (GSFC) particle detector on *ISEE 3*. We then show that these events are not statistically associated with either of the two common signatures of normal-abundance events, metric type II bursts and coronal mass ejections. The implications of this result are discussed in § III.

## II. DATA ANALYSIS

The 66 $^3$He-rich events in the 1.3–1.6 MeV n$^{-1}$ energy range were obtained from a survey of data from the *ISEE 3* very low-energy telescope (VLET). The detector was described by von Rosenvinge *et al.* (1978) and its elemental and isotopic resolution by von Rosenvinge and Reames (1979). The survey and the criteria for selecting the $^3$He-rich periods were discussed in detail by Reames and von Rosenvinge (1983). The $^3$He and $^4$He fluxes were averaged in 6 hr intervals from 1978 August 15 to 1982 July 10. A $^3$He-rich interval had to meet the following criteria: (1) the uncertainty in the $^3$He flux was less than 50%; and (2) the $^3$He/$^4$He ratio was $\geq$0.20. Candidate $^3$He-rich events, consisting of two or more successive $^3$He-rich intervals, were observed with higher time resolution to identify obvious multiple events and define the onset times. The 66 events are listed in Table 1. The $^3$He/$^4$He ratios of Table 1 are averaged over the event durations and are not corrected for ambient background levels. Only in about half the events (35) were distinct associated increases in the $^4$He flux observed. These events are plotted in Figure 1. In the remaining 31 events, no accompanying increase in the $^4$He flux was observed, so the resulting $^3$He/$^4$He ratios are lower limits only. These events are noted in Table 1.

Only 15 of the 66 $^3$He-rich events were accompanied by obvious $E \geq 1$ MeV proton events. These events are indicated in the last column of Table 1. Twelve of the 15 proton events are also associated with $^4$He flux increases and shown in Figure 1. The median $^3$He/$^4$He ratio for the 12 proton events is

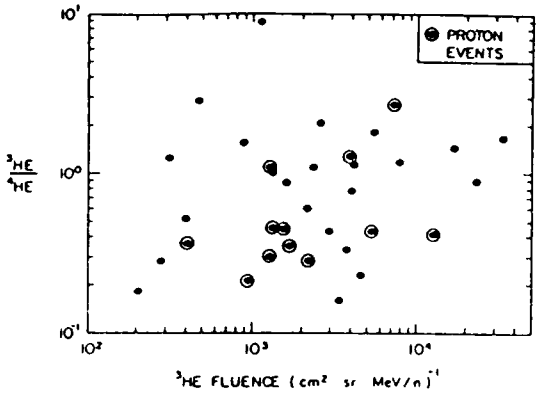


FIG. 1.—Average $^3$He/$^4$He values vs. $^3$He fluences for the events of Table 1 with observed $^4$He flux increases. Events with accompanying proton events are indicated with circles. The median $^3$He/$^4$He value for the proton event is 0.42, for all 35 events it is 0.76. The median $^3$He fluence for the proton events is $1.6 \times 10^3$ (cm$^2$ sr MeV n$^{-1}$)$^{-1}$; for all 35 events it is $2.2 \times 10^3$ (cm$^2$ sr MeV n$^{-1}$)$^{-1}$.

0.42, compared to a higher value of 0.76 for all 35 events. The proton events are also associated with a smaller median $^3$He fluence, $1.6 \times 10^3$ (cm$^2$ sr MeV n$^{-1}$)$^{-1}$, compared to $2.2 \times 10^3$ (cm$^2$ sr MeV n$^{-1}$)$^{-1}$ for all 35 events.

Multiple injections well associated with low-energy electron events (Reames, von Rosenvinge, and Lin 1984) characterize most $^3$He-rich events. The electron associations, the occurrence of spike events, and, for larger events, the velocity dispersion and magnetic field–aligned arrival from the solar direction all suggest nearly scatter-free propagation from well-connected sources. In this study we use only the event onset times in our search for the solar signatures of $^3$He-rich events. The approximate Sun–Earth propagation time for a 1.3 MeV n$^{-1}$ particle is 3 hr. Allowing several hours for the uncertainty in the determination of event onset times and an additional several hours for possible coronal and interplanetary propagation, we select the time interval 0–10 hr prior to the event onset as the period to search for solar signatures of the $^3$He-rich events.

### *a) Metric Type II Burst Associations*

For each of the 66 events of Table 1 we looked for metric type II burst listings in *Solar-Geophysical Data* (1978–1982) during the 10 hr period preceding the event onset. We found type II bursts during 16 of these 66 periods. As control samples we also examined the same 10 hr time periods 1 day earlier and 1 day later for each event. As shown in Table 2, there were 12 type II bursts for the 66 10 hr periods 1 day earlier and another 12 bursts for the 66 periods 1 day later. The periods immediately preceding the $^3$He-rich events therefore have only a few more type II bursts than the earlier and later control periods.

When we consider the proton-associated events separately, a different picture emerges. Six of the 15 events with protons were associated with type II bursts in the preceding 10 hr period, compared with only two for the preceding day and none for the following day. In addition, the event of 1980 March 25 1500 UT was probably associated with a type II burst at 0424 UT on that date, 10.6 hr prior to the $^3$He event onset. Counting this event as associated, we get a total of seven of 15 proton events with type II bursts. This result is similar to

TABLE 1

*ISEE 3* $^3$He EVENT LIST

| $^3$He Onset Time (UT) | Duration (hr) | $^3$He Fluence $(cm^2\ sr\ MeV\ n^{-1})^{-1}$ | Average $^3$He/$^4$He | | Proton Events |
|---|---|---|---|---|---|
| 1978 Oct 23 1600 | 24 | 1293. | 1.10 ± | 0.19 | yes |
| 1978 Nov 3 0800 | 28 | 3884. | 1.29 | 0.14 | yes |
| 1978 Nov 8 2200 | 24 | 411. | 0.36 | 0.10 | yes |
| 1978 Nov 27 2000 | 24 | 766. | 26. | +36. − 10.* | no |
| 1978 Dec 26 1600 | 20 | 2589. | 2.07 | 0.30 | no |
| 1979 Feb 6 0200 | 72 | 1314. | 1.00 | 0.17 | no |
| 1979 Feb 10 0500 | 48 | 4127. | 1.11 | 0.11 | no |
| 1979 Mar 24 < 1530 | 16 | 646. | 5.6 | +5.6 − 1.9* | no |
| 1979 May 17 0900 | 30 | 5118. | 5.94 | 0.93* | no |
| 1979 Jun 11 2000 | 36 | 3776. | 0.15 | 0.02* | no |
| 1979 Aug 15 0800 | 14 | 1892. | 0.26 | 0.04* | no |
| 1979 Sep 6 1400 | 44 | 2924. | 0.43 | 0.05 | no |
| 1979 Oct 3 1600 | 40 | 2155. | 0.60 | 0.08 | no |
| 1979 Oct 5 1800 | 16 | 406. | 0.28 | 0.08* | no |
| 1979 Oct 22 0000 | 72 | 879. | 1.54 | 0.33 | no |
| 1979 Nov 3 2200 | 12 | 332. | 0.34 | 0.11* | no |
| 1979 Dec 14 1200 | 36 | 33460. | 1.67 | 0.07 | no |
| 1979 Dec 19 0400 | 12 | 476. | 2.80 | 1.15 | no |
| 1979 Dec 20 2000 | 12 | 217. | 0.32 | 0.11* | yes |
| 1979 Dec 23 1100 | 48 | 7259. | 2.67 | 0.33 | yes |
| 1980 Jan 13 2400 | 32 | 5433. | 1.80 | 0.18 | no |
| 1980 Feb 4 2300 | 16 | 3972. | 0.96 | 0.10* | no |
| 1980 Feb 11 0400 | 36 | 1524. | 0.60 | 0.09* | no |
| 1980 Feb 13 2000 | 12 | 2329. | 1.09 | 0.14 | no |
| 1980 Mar 1 0800 | 36 | 1136. | 8.80 | 3.12 | no |
| 1980 Mar 16 1000 | 32 | 317. | 1.27 | 0.45 | no |
| 1980 Mar 25 1500 | 24 | 1515. | 0.44 | 0.09 | yes |
| 1980 Mar 27 0200 | 36 | 761. | 0.36 | 0.08* | no |
| 1980 Mar 29 0000 | 32 | 780. | 1.25 | 0.30* | yes |
| 1980 Mar 30 1400 | 16 | 3916. | 0.76 | 0.07 | no |
| 1980 Apr 2 2200 | 16 | 2945. | 0.37 | 0.05* | no |
| 1980 Apr 12 1400 | 12 | 382. | 0.38 | 0.11* | no |
| 1980 Apr 13 1300 | 8 | 206. | 0.18 | 0.08 | no |
| 1980 Apr 15 0800 | 48 | 850. | 0.45 | 0.09* | yes |
| 1980 Jun 23 0600 | 18 | 5394. | 0.43 | 0.04 | yes |
| 1980 Jun 28 0200 | 28 | 951. | 0.21 | 0.04 | yes |
| 1980 Jun 29 1600 | 18 | 1723. | 0.35 | 0.05 | yes |
| 1980 Jul 9 0200 | 12 | 1288. | 0.30 | 0.05 | yes |
| 1980 Nov 9 1700 | 20 | 16738. | 1.43 | 0.08 | no |
| 1980 Nov 15 1300 | 8 | 4050. | 1.27 | 0.14* | no |
| 1980 Dec 16 1900 | 16 | 1340. | 0.45 | 0.08 | yes |
| 1980 Dec 20 1300 | 12 | 757. | 1.25 | 0.29* | no |
| 1980 Dec 21 0400 | 44 | 1270. | 0.77 | 0.13* | no |
| 1980 Dec 24 2000 | 36 | 612. | 2.69 | 0.85* | no |
| 1981 Feb 5 1400 | 12 | 352. | 1.49 | 0.57* | no |
| 1981 Mar 13 1800 | 18 | 575. | 1.76 | 0.51* | no |
| 1981 Mar 23 0800 | 36 | 2211. | 0.28 | 0.04 | yes |
| 1981 Jun 15 .800 | 18 | 979. | 1.04 | 0.20* | no |
| 1981 Jun 18 0200 | 14 | 280. | 0.28 | 0.09 | no |
| 1981 Jul 17 1200 | 20 | 390. | 0.51 | 0.14 | no |
| 1981 Jul 20 0800 | 6 | 411. | 32. | +∞ − 16.* | no |
| 1981 Jul 31 >0400 | 24 | 3727. | 0.33 | 0.03 | no |
| 1981 Sep 2 1200 | 24 | 956. | 0.39 | 0.08* | no |
| 1981 Sep 11 1600 | 12 | 816. | 0.46 | 0.10* | no |
| 1981 Sep 13 0000 | 24 | 403. | 0.64 | 0.18* | no |
| 1981 Sep 15 2200 | 36 | 7825. | 1.17 | 0.10 | no |
| 1981 Nov 20 1330 | 36 | 3407. | 0.16 | 0.02 | no |
| 1981 Dec 5 0600 | 12 | 396. | 0.87 | 0.29* | no |
| 1982 Feb 12 0600 | 30 | 9602. | 0.54 | 0.03* | no |
| 1982 Mar 5 <0600 | 24 | 374. | 4.0 | +9.5 − 1.6* | no |
| 1982 Mar 10 1600 | 28 | 22718. | 0.88 | 0.04 | no |
| 1982 Mar 18 2000 | 24 | 1333. | 0.39 | 0.06* | no |
| 1982 Apr 3 1100 | 18 | 1397. | 0.56 | 0.10* | no |
| 1982 Jun 25 0800 | 12 | 4533. | 0.23 | 0.03 | no |
| 1982 Jun 25 2300 | 12 | 12787. | 0.41 | 0.04 | yes |
| 1982 Jun 30 1300 | 12 | 1600. | 0.88 | 0.14 | no |

* No observed associated $^4$He flux increases. The ratio is based on the ambient $^4$He fluence.

TABLE 2

TYPE II BURST ASSOCIATIONS FOR THE $^3$He EVENTS

| Time Period Examined | All Events (66) | Events with MeV Protons (15) | Events with No MeV Protons (51) |
|---|---|---|---|
| 0–10 hr prior to event onset | 16 | 7* | 10 |
| Same interval, 1 day earlier | 12 | 2 | 10 |
| Same interval, 1 day later | 12 | 0 | 12 |

* Includes the type II burst of 1980 Mar 25 0424 UT, which began 10.6 hr before the $^3$He onset, but is considered associated with the parent flare of the particle event.

the 40%–50% figure for type II burst associations reported by Kocharov and Kocharov (1984) for proton-associated events, and is significantly above the random type II burst occurrence rate.

The expected type II association for proton events can be inferred from data in Švestka and Simon (1975). Using only their $E > 10$ MeV confirmed proton events for which the flare association is certain and for which dynamic spectra in the metric wavelength range are available, we find that 84 of 112 events, or 75%, were associated with reported type II bursts. Three of the 15 proton events of Table 1 could not be associated with either H$\alpha$ flares or type II bursts, so for the probable flare associations we get seven type II bursts for 12 proton flares, a rate lower than, but not inconsistent with, the Švestka and Simon association rate.

Type II burst associations for the 51 remaining events of Table 1 with no accompanying energetic protons are shown in the last column of Table 2. It is obvious that for the "pure" $^3$He events there is no significant association with type II bursts.

### b) *Coronal Mass Ejection Associations*

The Solwind coronagraph has been described by Sheeley *et al.* (1980). Since 1979 March it has provided images of the solar white light corona from 2.5 to 10 $R_\odot$ with an angular resolution of 1.25 per pixel. CMEs are easily detected in differenced images obtained by subtracting a base image taken at the beginning or middle of each day from those taken in subsequent orbits. The data coverage is not uniform and numerous gaps exist, so it is necessary to assume the period of time prior to a subtracted image during which any CME could be detected in the image. In our case we take a relatively conservative time period of 3.0 hr.

A CME with a nominal speed of $\sim 400$ km s$^{-1}$ travels about 2 $R_\odot$ hr$^{-1}$, so to observe a CME in the Solwind coronagraph field of view, we must allow 1 hr from the time the CME leaves the Sun. To look for any CMEs leaving the solar disk in the period 0–10 hr prior to a $^3$He-rich event onset, we look at the Solwind data during the period from 9 hr before to 1 hr after the event onset. Assuming that any CME will be observed in a Solwind subtracted image obtained up to 3 hr later, we found that some Solwind data coverage existed for 45 of the 66 events of Table 1. Nine of the 45 events were also proton events.

In each 10 hr time interval we looked for west limb CMEs on the assumption that the $^3$He-rich event sources are well connected to the Earth. We first looked only for fast CMEs with speeds of $V \geq 400$ km s$^{-1}$, those found to be associated with proton events (Kahler *et al.* 1984). Definite fast CMEs were found for only two events, those of 1979 November 3 and 1981 March 23. In addition, possible CMEs of undetermined speeds were found in the 10 hr periods preceding four other events. Thus, only two to six of the 45 $^3$He-rich events could be associated with fast west limb CMEs. This is far fewer than the 26 out of 27 cases for proton events with likely flare associations and 39 out of 50 cases for all proton events in the Kahler *et al.* (1984) study.

We also examined the occurrence rate of all west limb CMEs, regardless of speed, during the 10 hr periods preceding the 45 $^3$He-rich events. CMEs were found for three of the nine proton events (with an average data coverage of 6.1 hr per event) and nine of the 36 nonproton events (with an average coverage of 7.5 hr per event). A total of 14 CMEs was observed in 324.2 hr, resulting in a rate of $1.04 \pm 0.28$ per day, closely matching the rate of 1.1 per day calculated for the 1979–1982 period, assuming, as we have, a 3 hr time coverage for each Solwind image (Howard *et al.* 1984). There is therefore no evidence of any enhanced rate of CME occurrence during the 10 hr periods preceding the $^3$He-rich event onsets.

## III. DISCUSSION

If $^3$He particles were accelerated in the same kinds of events that produce normal-abundance energetic particle events, we should expect to see good correlations between the $^3$He events and metric type II bursts and CMEs. The correlation of type II bursts and CMEs with energetic proton events is $\sim 75\%$ and $\geq 90\%$, respectively. However, the correlation we find for the $^3$He event onsets yields only 24% and 4%–13% for the type II bursts and CMEs respectively, despite our use of very broad 10 hr time windows.

One might suppose that, because the particle fluxes of $^3$He-rich events are generally smaller than those of normal abundance events, any associated type II bursts and CMEs may also be fainter and hence less likely to be observed. Several observational results argue against this interpretation. First, about 40% of all flares associated with type II bursts are subflares, and another 40% are class 1 events (Wright 1980). This suggests that even the very small flares producing $^3$He events should be capable of generating observable type II bursts if the primary acceleration mechanism involves coronal shocks. Second, although CMEs too faint or small to be detected may in principle exist, those associated with proton events are nearly always the larger halo, loop, fan, or quadrant filler structures. Only one of the 25 CMEs associated with the likely proton flares of Kahler *et al.*'s (1984) study was a "spike" event, although the various kinds of spike structures constituted over 50% of the observable Solwind CMEs (Howard *et al.* 1984). Third, we found in Figure 1 that the proton events were statistically associated with smaller, not larger, $^3$He fluences. This is not what we would expect if $^3$He production takes place in association with normal proton flares of relatively small size. Finally, we might expect that a reasonable brightness range for the fainter type II bursts and CMEs

should still yield a significant enhancement above background for the type II burst and CME associations. This possibility is precluded by the fact that these associations are consistent with random-chance occurrences. The $^3$He events, therefore, appear not to be produced in the same way as events of normal abundances.

Another definitive result concerning the injection of $^3$He particles has been presented by Reames, von Rosenvinge, and Lin (1984). For 11 event onsets they find interplanetary injection times for the $^3$He particles and 2–100 keV electrons detected at *ISEE 3* to be simultaneous to within ~20 minutes. This suggests that $^3$He particles could be accelerated along with electrons in short bursts characterized by metric or dekametric type III solar radio bursts (Lin 1974). Type III bursts are sometimes closely temporally associated with impulsive ($\tau \approx 10$–100 s) hard X-ray bursts due to 10–100 keV electrons (Kane 1981). It is now clear from $\gamma$-ray observations that both ions and electrons are produced in these phases (Forrest and Chupp 1983). Only a small fraction of the impulsive phase ions inferred from the $\gamma$-ray measurements are thought to escape to the interplanetary medium (von Rosenvinge, Ramaty, and Reames 1981), and acceleration in coronal shocks which follow the impulsive phase appears more likely for nearly all $E \approx 10$ MeV interplanetary particle events (Kahler *et al.* 1984). Acceleration of $^3$He particles takes place in solar events far less energetic than those characterized by $\gamma$-rays or coronal shocks, but it seems reasonable that ions impulsively accelerated along with the 2–100 keV electrons escaping the corona along magnetically open field lines would also be expected to escape the corona. This appears a likely explanation for the results of Reames, von Rosenvinge, and Lin (1984).

Klecker *et al.* (1984) have recently studied the ionic charge composition of $^3$He, $^4$He, and Fe in five $^3$He- and Fe-rich events. They found that essentially all the helium was doubly ionized, but the mean charge state of Fe was $19 \pm 2$, a value significantly higher than that in events of normal abundances. Their result and the apparent close association of $^3$He-rich events with the 2–100 keV electrons found by Reames, von Rosenvinge, and Lin (1984) suggest an origin for the $^3$He- and Fe-rich events different from that of normal abundance events.

The results we have obtained provide further evidence for this view. Our result yields no insight into the detailed acceleration mechanisms for enhanced or normal abundance events, but it indicates that enhanced-event particles are not accelerated along with normal abundance particles. Our data further suggest the possibility that a large flare may give rise to both kinds of abundances, with the enhanced abundances produced in the early impulsive phase and the normal abundances in a subsequent coronal shock wave. We found that the $^3$He-rich events with observable proton events were well associated with type II bursts, as were proton events of normal abundances. On the other hand, when no proton event was observed, the type II association was due only to random chance. If we have both "pure" and "mixed" $^3$He-rich events, we should expect that the occurrence of an observable proton event is not dependent on the $^3$He fluence since the two are produced in separate processes. We should also expect that when a proton event occurs, the $^3$He/$^4$He ratio should tend to be smaller due to the mixing of particles of enhanced and normal abundances. As we saw in Figure 1 and reported in § II, both these expected results were found.

As a possible example of a mixed event, the temporal behavior of the large $^3$He-rich event on 1974 May 9 was treated by Möbius *et al.* (1980) as due to a short time injection ($\tau \leq 15$ minutes) for the $Z$-rich population and a longer time injection ($\tau \approx 6$ hr) for the population of normal abundance. These different injection time scales do not preclude the possibility that both populations of particles were accelerated by the same basic process, but it would seem unlikely that they were accelerated together in a common event. If low intensities of enhanced abundances are produced along with intensities of normal abundances varying widely from event to event, we would expect to see the smooth increase in the variation of abundance ratios with decreasing event sizes as Mason *et al.* (1980) found.

Let us now consider the relevance of these results for $Z$-rich events. The relationship between $^3$He-rich and $Z$-rich (usually meaning Fe-rich) events has generally been treated cautiously in the literature. Anglin, Dietrich, and Simpson (1977) plotted Fe/$^4$He ratios against $^3$He/$^4$He ratios for a large number of events and concluded that while $^3$He-rich events are always Fe-rich, some Fe-rich events are not $^3$He-rich. This conclusion has been widely accepted (Zwickl *et al.* 1978; Ramaty *et al.* 1980; McGuire 1983). Zwickl *et al.* (1978) also claimed to confirm that all identified $^3$He-rich events are rich in $Z \geq 20$ nuclei. Based on this apparent asymmetry in the relationship of $^3$He-rich and Fe-rich events, they proposed a subclass of Fe-rich events in addition to a subclass of $^3$He-rich events.

A reexamination of the plot in Figure 5 of Anglin, Dietrich, and Simpson (1977) suggests that their conclusion that all $^3$He-rich events are also Fe-rich is unjustified. Six of their Fe/$^4$He ratios were only upper limits, and they did not define a numerical threshold for Fe-richness. In addition, the confirmation claimed by Zwickl *et al.* (1978) was based on only five events. Finally, Mason *et al.* (1980) have pointed out that the $^3$He-rich event of 1974 October 5 appears without any measurable increase in heavy-nucleus fluxes. Contrary to the general consensus, we conclude that there are $^3$He-rich events which are not Fe-rich and vice versa. A more appropriate description of the situation is that there is a correlation between $^3$He-richness and Fe-richness, but it is not very strong, as Anglin, Dietrich, and Simpson (1977) and Reames and von Rosenvinge (1981) found. The symmetry of the correlation suggests, however, that $^3$He-rich and Fe-rich events can be treated as a single class of events rather than as separate classes as Zwickl *et al.* (1978) suggested. This implies that the results we have discussed above for the $^3$He-rich events can also be applied to the Fe-rich events as well.

This work was supported at AS&E by NSF grant ATM-8116126 and NASA grant NAS5-27223, at Emmanuel College by Air Force Geophysical Laboratory (AFGL) contract AF19628-82-K-0039, at NRL by NASA DPR W 14,429, and at GSFC/University of Maryland by NASA grant NGR 21-002316. The Air Force Space Test Program provided integration, launch, and operational support for the *P78-1* spacecraft. D. Roberts, F. Harlow, and W. Funk of NRL assisted in the coronagraph data reduction. S. K. was a NASA *ISEE* Guest Investigator and thanks M. A. Shea of AFGL and D. Peacock of NSF for their support.

## REFERENCES


Anglin, J. D., Dietrich, W. F., and Simpson, J. A. 1977, *Proc. 15th Internat. Cosmic Ray Conf.* (Plovdiv), 5, 43.
Cook, W. R., Stone, E. C., and Vogt, R. E. 1984, *Ap. J.*, 279, 827.
Coplan, M. A., Ogilvie, K. W., Bochsler, P., and Geiss, J. 1983, in *Solar Wind Five*, ed. M. Neugebauer (NASA Conf. Pub. 2280), p. 591.
Fisk, L. A. 1978, *Ap. J.*, 224, 1048.
Forrest, D. J., and Chupp, E. L. 1983, *Nature*, 305, 291.
Hall, D. N. B. 1975, *Ap. J.*, 197, 509.
Howard, R. A., Sheeley, N. R., Jr., Koomen, M. J., and Michels, D. J. 1984, *J. Geophys. Res.*, 89, 9683.
Ibragimov, I. A., and Kocharov, G. E. 1977, *Proc. 15th Internat. Cosmic Ray Conf.* (Plovdiv), 11, 340.
Kahler, S. W., Sheeley, N. R., Jr., Howard, R. A., Koomen, M. J., Michels, D. J., McGuire, R. E., von Rosenvinge, T. T., and Reames, D. V. 1984, *J. Geophys. Res.*, in press.
Kane, S. R. 1981, *Ap. J.*, 247, 1113.
Klecker, B., Hovestadt, D., Gloeckler, G., Ipavich, F. M., Scholer, M., Fan, C. Y., and Fisk, L. A. 1984, *Ap. J.*, 281, 458.
Kocharov, L. G. 1979, *Proc. 16th Internat. Cosmic Ray Conf.* (Kyoto), 2, 277.
Kocharov, L. G., and Kocharov, G. E. 1984, *Space Sci. Rev.*, 38, 89.
Kocharov, L. G., and Orishchenko, A. V. 1983, *Proc. 18th Internat. Cosmic Ray Conf.* (Bangalore), 4, 37.
Lin, R. P. 1974, *Space Sci. Rev.*, 16, 189.
Mason, G. M., Fisk, L. A., Hovestadt, D., and Gloeckler, G. 1980, *Ap. J.*, 239, 1070.
McGuire, R. E. 1983, *Rev. Geophys. Space Phys.*, 21, 305.
Melrose, D. B. 1983, *Solar Phys.*, 89, 149.
Möbius, E., Hovestadt, D., Klecker, B., and Gloeckler, G. 1980, *Ap. J.*, 238, 768.
Ramaty, R., *et al.* 1980, in *Solar Flares*, ed. P. A. Sturrock (Boulder: Colorado Associated University Press), p. 117.
Reames, D. V., and von Rosenvinge, T. T. 1981, *Proc. 17th Internat. Cosmic Ray Conf.* (Paris), 3, 162.
———. 1983, *Proc. 18th Internat. Cosmic Ray Conf.* (Bangalore), 4, 48.
Reames, D. V., von Rosenvinge, T. T., and Lin, R. P. 1984, *Ap. J.*, submitted.
Sheeley, N. R., Jr., Michels, D. J., Howard, R. A., and Koomen, M. J. 1980, *Ap. J. (Letters)*, 237, L99.
*Solar-Geophysical Data*. 1978–1982 (Boulder: National Oceanic and Atmospheric Administration).
Švestka, Z., and Fritzova-Švestkova, L. 1974, *Solar Phys.*, 36, 417.
Švestka, Z., and Simon, P., eds. 1975, *Catalog of Solar Particle Events, 1955–1969* (Dordrecht: Reidel).
Varvoglis, H., and Papadopoulos, K. 1983, *Ap. J. (Letters)*, 270, L95.
von Rosenvinge, T. T., McDonald, F. B., Trainor, J. H., van Hollebeke, M. A. I., and Fisk, L. A. 1978, *IEEE Trans.*, GE-16, 208.
von Rosenvinge, T. T., Ramaty, R., and Reames, D. V. 1981, *Proc. 17th Internat. Cosmic Ray Conf.* (Paris), 3, 28.
von Rosenvinge, T. T., and Reames, D. V. 1979, *Proc. 16th Internat. Cosmic Ray Conf.* (Kyoto), 5, 68.
Weatherall, J. 1984, *Ap. J.*, 281, 468.
Wright, C. S. 1980, *Proc. Astr. Soc. Australia*, 4, 59.
Zwickl, R. D., Roelof, E. C., Gold, R. E., Krimigis, S. M., and Armstrong, T. P. 1978, *Ap. J.*, 225, 281.



R. A. HOWARD: Code 4173H, Naval Research Laboratory, Washington, DC 20375

S. KAHLER: AFGL/PHP, Hanscom AFB, MA 01731

M. J. KOOMEN: Code 7171, Naval Research Laboratory, Washington, DC 20375

D. J. MICHELS: Code 4173, Naval Research Laboratory, Washington, DC 20375

D. V. REAMES: Code 661, Laboratory for High Energy Astrophysics, Goddard Space Flight Center, Greenbelt, MD 20771

N. R. SHEELEY, JR.: Code 4172, Naval Research Laboratory, Washington, DC 20375

JOURNAL OF GEOPHYSICAL RESEARCH, VOL. 90, NO. A1, PAGES 177–182, JANUARY 1, 1985

# Characteristics of Coronal Mass Ejections Associated With Solar Frontside and Backside Metric Type II Bursts

S. W. KAHLER

*Emmanuel College, Boston, Massachusetts*

E. W. CLIVER

*Space Physics Division, Air Force Geophysics Laboratory, Hanscom Air Force Base, Massachusetts*

N. R. SHEELEY, JR., R. A. HOWARD, M. J. KOOMEN,[1] AND D. J. MICHELS

*E. O. Hulburt Center for Space Research, Naval Research Laboratory, Washington, D. C.*

We compare fast ($v \geq 500$ km s$^{-1}$) coronal mass ejections (CME's) with reported metric type II bursts to study the properties of CME's associated with coronal shocks. We confirm an earlier report of fast frontside CME's with no associated metric type II bursts and calculate that $33 \pm 15\%$ of all fast frontside CME's are not associated with such bursts. Faster CME's are more likely to be associated with type II bursts, as expected from the hypothesis of piston-driven shocks. However, CME brightness and associated peak 3-cm burst intensity are also important factors, as might be inferred from the Wagner and MacQueen (1983) view of type II shocks decoupled from associated CME's. We use the equal visibility of solar frontside and backside CME's to deduce the observability of backside type II bursts. We calculate that $23 \pm 7\%$ of all backside type II bursts associated with fast CME's can be observed at the earth and that $13 \pm 4\%$ of all type II bursts originate in backside flares. CME speed again is the most important factor in the observability of backside type II bursts.

## 1. INTRODUCTION

Prior to the launch of the Solar Maximum Mission (SMM) spacecraft in 1980 it was generally assumed that metric type II bursts occurred at or ahead of the fronts of coronal mass ejections (CME's) viewed by orbiting coronagraphs (see *MacQueen* [1980] for a review). The few observations relating the type II burst source to the CME front were consistent with this point of view, but the strongest evidence came from the statistical studies using Skylab data. *Gosling et al.* [1976] found that only two of 13 CME's with speeds exceeding 500 km s$^{-1}$ were not associated with type II or IV radio bursts and that such bursts were associated only with CME's moving faster than 400 km s$^{-1}$. Furthermore, *Munro et al.* [1979] reported that 21 of 23 type II or IV bursts occurring within 45° of a limb during the Skylab period were associated with CME's. These results were consistent with models of piston-driven coronal MHD shocks (reviewed by *Maxwell and Dryer* [1982]).

More recent results from the SMM and Solwind coronagraphs have presented serious difficulties for this simple model. First, some associated CME/type II source timings and positions are inconsistent with the model [*Wagner and MacQueen*, 1983]. Second, the close statistical association between CME's and type II bursts found in the Skylab results has not been confirmed by the Solwind results. *Sheeley et al.* [1984] and *Kahler et al.* [1984] found that about a third of all metric type II bursts are not associated with CME's. In addition, *Sheeley et al.* [1984] found 17 fast ($v \geq 450$ km s$^{-1}$) CME's with no obvious metric type II bursts. In five cases these CME's were associated with Hα and 1- to 8-Å X ray flares and hence were clearly frontside solar events from which type II emission, if present, should have been readily observed.

In this paper, in an effort to further our understanding of the relationship between CME's and coronal shock waves, we examine data from the Solwind coronagraph [*Sheeley et al.*, 1980] to look for additional examples of fast ($v \geq 500$ km s$^{-1}$) frontside CME's that lacked metric type II emission. We want to determine what fraction of all fast CME's do not have type II association and to see what CME properties (speed, angular extent, brightness) are significant for the formation of coronal shocks. While *Sheeley et al.* [1984] considered only those CME's occurring during Culgoora observing hours to establish the existence of a class of fast CME's without obvious type II association, we are interested in determining the statistical properties of such events. Thus, to obtain sufficient events, we considered all fast CME's for which either the Culgoora, Weissenau, or Harvard observations reported in Solar-Geophysical Data (SGD) were available.

As an additional point for study, we note that fast CME's without type II bursts might well be expected in the view of *Wagner and MacQueen* [1983] (see also *Cane* [1984]), who suggest that the CME and type II shock are separate, decoupled entities in which the shock is initiated in the flare impulsive phase and then catches up with and moves through the preceding CME. Their view might also imply that the strength of the flare impulsive phase is a more important factor in the generation of the type II shock than is any characteristic of the CME with which the shock is associated. We thus attempt to assess the significance of the flare impulsive phase energy release relative to the importance (speed, angular extent, brightness) of the CME in determining whether a type II burst occurs with a fast CME.

[1] Permanently at Sachs/Freeman Associates, Inc., Bowie, Maryland.



Paper number 4A8130.
0148-0227/85/004A-8130$05.00

Finally, once we have determined the statistical association between fast CME's and type II bursts for events on the visible disk, we can use this knowledge to infer the observability of backside type II bursts. Many individual cases of type II bursts observed from flares tens of degrees beyond the limb have been reported (i.e., March 30, 1969 [*Smerd*, 1970]; September 1, 1971 [*Gergely and Kundu*, 1976]; July 22, 1972 [*Hudson et al.*, 1982]; and March 20, 1976 [*Nelson and McLean*, 1977]), but the frequency of such events is unknown. Studies of associations between Hα flares and type II bursts have not dealt directly with this problem. In the two most comprehensive studies to date, *Dodge* [1975] unambiguously associated 459 of 580 reported type II bursts with confirmed flares, and *Wright* [1980] 416 of the 673 type II bursts of his study. These studies suggest that backside type II bursts may constitute up to 20–40% of all observed type II bursts, but gaps in flare patrols and the diminishing observability near the limb of the subflares that constitute ~40% of the type II burst parent flares [*Wright*, 1980] can also play important roles in the statistics. As an alternative to using Hα observations, we infer the observability of backside type II bursts by using CME's, which are assumed to be equally observable from the solar frontside and backside.

Studies of the solar associations of CME's by *Munro et al.* [1979] showed that more than 70% of all CME's are associated with eruptive prominences or filament disappearances, but only about 40% with Hα flares. There are, however, several difficulties in determining these solar associations. About half the associated Hα flares should occur beyond the limb and not be observed. The flares associated with CME's also usually show some kind of Hα mass ejection [*Gosling et al.*, 1976]. In addition, some CME's considered eruptive-associated are also associated with flares (e.g., the event of August 29, 1981, in the work by *MacQueen and Fisher* [1983]). Despite these problems, we note that *Gosling et al.* [1976] found an average speed of 775 km $s^{-1}$ for flare-associated CME's and a much lower average speed of 330 km $s^{-1}$ for eruptive-associated events. More recent results by *MacQueen and Fisher* [1983] show that in the inner corona (1.2–2.4 $R_S$), flare-associated CME speeds are fairly constant and exceed those of eruptive-associated CME's. In our study, we initially assume that a fast CME observed at 2.5–10 $R_S$ will nearly always be associated with an Hα flare brightening even though the flare itself may not be energetically important for the CME. We examine the consequences of this assumption in section 2, where we describe our analysis. The results of the study are discussed in section 3.

## 2. DATA ANALYSIS

We began with a listing of all Solwind CME's for which the measured speeds of the fastest moving regions were at least 500 km $s^{-1}$. The data period covered extended from launch in March 1979 to December 1982. In each case the inferred speed and times of observations were used to derive the time of injection of the CME at 1 $R_S$. In the majority of cases, several points on a height-time diagram were used to deduce the velocity. In these cases the resulting injection times are estimated to have an uncertainty of ±15 min. In other cases where only one subtracted image of a transient can be compared to a preevent image, the injection times are uncertain by at least ±30 min. Each event was further described by its angular width projected in the plane of the sky, angular position on the solar limb, and morphology. Surface brightness had been subjectively estimated as faint, average, or bright for most events at the time of the analysis.

We sought an associated metric type II burst and Hα flare (Solar-Geophysical Data, 1979–1983) consistent with both the timing and the limb position of each CME. The comprehensive Hα flare listings from the SGD books were used through June 1981 and a National Oceanic and Atmospheric Administration (NOAA) prepublication listing for the subsequent months (J. McKinnon, personal communication, 1983). Events for which there were no Hα flare patrol or metric observations by the Harvard, Culgoora, or Weissenau observatories during the CME injection times were eliminated from the study. If CME accelerations were present [*MacQueen and Fisher*, 1983], the limb times, extrapolated from the Solwind data assuming constant velocity, would be systematically delayed. Nevertheless, we found most flare onsets to be within the 15- to 30-min uncertainties of the extrapolated limb times. We also compared the CME list to the interplanetary type II shock event list of *Cane* [this issue]. We found one event on December 5, 1981, for which the inferred solar origin was ~10°–30°W but no Hα flare was reported. This CME contained Hα ejecta and was considered to be a frontside event.

As discussed in section 1, we assume in this study that all fast CME's are associated with Hα flares, some of which will be on the solar backside and hence unobservable. If no associated Hα flare was reported, the CME was presumed to originate on the solar backside. This assumption is not always correct, as we found for the CME of December 5, 1981. In general, however, this assumption appears to be justified by the resulting statistics showing a rather even split between events with and without flares: CME's with Hα flares (81 events) and CME's with no Hα flare (87 events). We considered an additional 28 events to be possibly associated with Hα flares.

### 2.1. *CME's With Possible Flare Associations*

In some cases an Hα flare association with a CME was considered possible but unlikely. In general, these were short-lived subflares that occurred during the appropriate time windows and on the appropriate hemisphere to qualify for a CME association, but because they were unimpressive in size and duration in the Hα and 1- to 8-Å wavebands, the association was considered questionable. Several cases of sizable Hα and 1- to 8-Å events in the appropriate hemisphere, but just outside the appropriate time window, were also included in this category of 28 events.

Only one of these events was associated with a type II burst. This is due, at least partially, to a selection effect in the flare associations, since the onset time of a type II burst associated with a given CME provides additional confidence in making the association of a candidate small flare with that CME.

### 2.2. *CME's With Associated Hα Flares*

Fifty-four of the 81 events in this category were associated with metric type II or "possible" type II bursts reported by the Harvard, Culgoora, or Weissenau observatories. For the 27 events with no reported type II bursts, we examined the metric reports further for any kind of emission which might be indicative of a type II burst. This included the terms "continuum," "IV," and "unclassified." We found nine such events and considered them questionable examples of CME's with no type II bursts. Three additional events were also considered doubtful because of small data gaps in the coverage by the three observatories near but not at the times of the CME

TABLE 1. CME's Associated With Hα Flares but Without Associated Metric Type II Bursts

| | CME | | | Hα/X ray | | | |
|---|---|---|---|---|---|---|---|
| Date | Limb Time, UT | Speed,* km s$^{-1}$ | Location (Size) | Hα Onset, UT | Location | Size | 1–8 Å |
| June 6, 1979 | 2049 | 725 P | S20°E(40°) | 2105 | 17°N, 71°E | 1B | M3 |
| Dec. 3, 1979 | 1425 | 600 P | S50°E(90°) | <1514 | 24°S, 54°E | 2B | M1 |
| April 11, 1980 | 0734 | 700 F | N20°W(80°) | 0642 | 15°N, 22°W | SN | C6 |
| Aug. 15, 1980 | 0727 | 535 F | S80°E(20°) | 0730 | 24°S, 20°E | 1F | C2 |
| Dec. 9, 1980 | 0622 | 575 P | S15°E(20°) | 0621 | 18°S, 51°E | SN | C4 |
| Dec. 9, 1980 | 0712 | 870 F | S30°W(160°) | 0658 | 19°S, 40°W | 2N | C8 |
| Feb. 25, 1981 | 0159 | 715 G | N30°E(20°) | 0205 | 16°S, 76°E | 1N | C7 |
| March 15, 1981 | 0505 | 700 E | W(40°) | 0520 | 12°S, 90°W | 1N | M1 |
| April 18, 1981 | 0113 | 950 F | S40°E(360°) | 0118 | 10°N, 35°W | 1B | M5 |
| June 22, 1981 | 1448 | 750 P | N50°E(30°) | 1441 | 15°N, 41°E | SB | M1 |
| Oct. 8, 1981 | 0807 | 600 F | S27°W(60°) | 0820 | 16°S, 61°W | 1N | C8 |
| Oct. 16, 1981 | 2222 | 812 F | S17°E(10°) | 2212 | 09°S, 52°E | 1B | M1 |
| Oct. 31, 1981 | 0529 | 730 F | N25°E(130°) | 0439(?) | 15°N, 34°E | 1N | C6 |
| Dec. 5, 1981 | 1328 | 890 | N50°W(160°) | ... | 10°–30°W† | ... | C3 |
| Nov. 21, 1982 | 0600 | 735 P | S17°W(70°) | 0605 | 11°S, 79°W | SN | M1 |

*E is estimated; G is good; F is fair; P is poor.
†No Hα flare report; position estimated from associated kilometric type II burst [*Cane*, this issue, also personal communication, 1984].

ejections. The remaining 15 good examples of fast CME's with Hα flares but without metric type II bursts are listed in Table 1. The list includes the event of December 5, 1981, for which, as discussed above, no Hα flare is reported. Radio activity reported during these events consisted only of type III/V bursts or type I noise storms (possibly with underlying continuum), neither of which should be confused with the slow-drift type II bursts.

The speed distributions of the CME's with and without type II bursts are compared in Figure 1. The events of Table 1 are shown by the shading, and it is obvious that there are several events with high ($\gtrsim$800 km s$^{-1}$) speeds which failed to produce reported possible type II bursts.

Projected angular size does not appear to be a factor in the association of these events with type II bursts. For events in the speed range 500 to 799 km s$^{-1}$ the 60° median size of CME's with type II bursts exceeds the 45° median of those without. However, for fast events with speeds of at least 800 km s$^{-1}$ the median angular size of 90° for the events without type II bursts exceeds that of 70° for those with type II bursts. These differences appear insignificant in view of the large range of angular sizes (10°–360°) for both groups.

The available surface brightnesses for the CME's with Hα flares are given in Table 2. We see that most average and bright CME's are associated with type II bursts, but only about half the faint CME's are similarly associated. Since the two groups of CME's with and without type II bursts have very similar Hα flare longitude distributions and relatively small differences in angular sizes, this implies that more massive CME's are more likely to be associated with type II bursts.

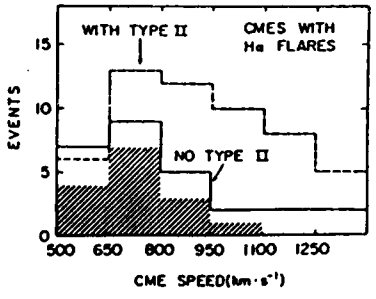


Fig. 1. Speed distribution of flare-associated fast CME's with and without metric type II bursts. Events shown in shading are the 15 best examples of the 26 events with no reported type II bursts and are listed in Table 1.

To test the importance of the flare impulsive phase in the generation of the type II burst shock, we obtained the peak 3-cm impulsive phase flux density for each CME flare (Solar-Geophysical Data, 1979–1983). The importance of the peak 3-cm flux densities versus that of the CME speeds for the generation of type II burst shocks is shown in Table 3. Both the 3-cm flux densities and the speeds are divided into three bins. The type II burst associations increase substantially from the lowest to the highest CME speed bin. The same is true, however, with very similar numbers, for the peak 3-cm burst distribution. Thus we cannot distinguish between CME speed and impulsive phase burst intensity as the more important factor in the generation of the type II shock.

We can estimate the fraction of fast frontside CME's with no type II bursts by considering the CME's with Hα flares shown in Figure 1. As noted above, 27 of 81, or 33%, of all flare-associated fast CME's lacked associated type II bursts. However, we must also consider the role of the 28 possible flare-associated events, 27 of which were not associated with type II bursts. Because backside CME's should be as easily observed as frontside CME's, we expect the number of CME's without flares to match the number of those with flares. Assuming that 17 of the 28 possible flare-associated events are frontside events would result in matching totals of 98 frontside events and 98 backside events. Then, if 16 of those 17 events have no type II bursts, 43 of the total 98 (44%) frontside CME's would be associated with no type II burst, a figure we take as an upper limit.

For a lower limit we take only the 15 confirmed cases of Table 1 and assume the CME's with possible flare associations are all backside events. The result is that at least 15 of 81 (19%) fast CME's failed to be associated with type II bursts. A reasonable estimate for the percentage of fast, frontside CME's associated with no type II burst appears to be $\sim 33 \pm 15\%$.

TABLE 2. CME Surface Brightnesses

| Brightness | With Hα Flare | | No Hα Flare | | Possible Hα Flare A'i Events |
|---|---|---|---|---|---|
| | With Type II | No Type II | With Type II | No Type II | |
| Faint | 8 | 9 | 3 | 18 | 7 |
| Average | 23 | 8 | 1 | 25 | 12 |
| Bright | 19 | 9 | 5 | 27 | 3 |

### 2.3. *CME's With No Associated Hα Flares*

Only 10 of the 87 CME's with no associated Hα flares, presumed to be backside CME's, were associated with metric type II bursts reported by one of the three radio observatories. These events are listed in Table 4, where we show for eight of the 10 events a likely source region behind the solar limb. The regions were selected on the basis of information given in the NOAA preliminary reports on solar-geophysical activity. In four cases the region lay at least 30° over the limb.

As shown in Figure 2, these 10 events are characterized by speeds substantially higher than those characterizing the bulk of the events with no type II bursts. The only event with a type II burst in the 500–650 km $s^{-1}$ bin is that of June 29, 1980, which was associated with an M3 1- to 8-Å X ray burst and is attributed to an active region at 90°W. In addition, the event of November 19, 1981, which had a speed of 800 km $s^{-1}$, involved a C8 X ray burst and is attributed to a region only about 5° over the west limb. Since the purpose of treating CME's with no associated Hα flares is to isolate those events originating on the backside of the sun, we see that these events only marginally qualify for this category. The other eight events with reported type II bursts have speeds of at least 870 km $s^{-1}$, which is their most striking characteristic. Angular size seems unimportant as a factor for backside CME's with type II bursts, since the median angular size for CME's with no type II bursts and speeds of at least 800 km $s^{-1}$ is 70° while that of those with type II bursts is 65°, slightly smaller. The brightness distributions of CME's with no associated Hα flares are shown in Table 2. No significant difference between the events with type II bursts and those without type II bursts is obvious, although the statistics of the former are too small for a meaningful comparison.

To estimate the observability of backside type II bursts, we first start wtih the association of type II bursts and frontside fast CME's discussed in the previous section. There we saw that 67 ± 15% of all fast frontside CME's were associated with metric type II bursts. However, only 10 of 87 fast CME's with no associated Hα flares were associated with type II bursts. Assuming that 67% of these CME's were associated with type II bursts suggests that only 17 ± 5% (10/(0.67 × 87)) of the backside type II bursts associated with CME's were observable.

TABLE 3. Comparison of Speeds and Associated Peak 3-cm Bursts for CME's With Hα Flares

| | Speed, km $s^{-1}$ | | | 3-cm Flux Density, s.f.u. | | |
|---|---|---|---|---|---|---|
| | 500–749 | 750–999 | ≥1000 | <50 | 50–500 | >500 |
| With type II | 16 | 18 | 20 | 14 | 12 | 28 |
| No type II | 15 | 7 | 5 | 17 | 6 | 4 |

Here s.f.u. is solar flux units.

A difficulty with this comparison is that the speed distributions for the frontside and assumed backside events are dissimilar, as a comparison of Figures 1 and 2 shows. Only 35 of the 81 CME (43%) speeds of the frontside events are under 800 km $s^{-1}$, but 57 of 87 CME speeds (66%) of the backside events are under that speed. We consider two plausible explanations for this disparity. First, many of the slower CME's with flares may have been categorized as possible flare associations, leaving a low speed deficit in Figure 1. The speed distribution of the possible association group is peaked at the lowest speed bin, in accordance with this explanation. By adding 17 of the 28 possible flare events to the lowest two speed bins of Figure 1, and nine to the higher ($v \geq 800$ km $s^{-1}$) and two to the lower ($v < 800$ km $s^{-1}$) speed bins of Figure 2, we can obtain rather similar frontside and backside speed distributions with 98 events in each group. This results in 11 of 98 backside events associated with type II bursts as compared with 54 of 98 on the frontside, indicating a 20% (11/54) observability of backside type II bursts associated with fast CME's.

An alternative explanation for the dissimilarity of the speed distributions of Figures 1 and 2 is that some of the lower-speed CME's with no Hα flares of Figure 2 may in fact be frontside events but not associated with Hα flares, contrary to our assumption. In this case, we can compensate by subtracting enough events from the first two bins of Figure 2 so that the ratio of low-speed ($v < 800$ km $s^{-1}$) to high-speed ($v \geq 800$ km $s^{-1}$) events matches that of Figure 1. This requires that we subtract 34 events (and the one type II burst) from the first two speed bins of Figure 2, with the result of nine type II bursts for 53 backside events. Again assuming that 67% of the fast CME's are associated with type II shocks, we get a 25% (9/(0.67 × 53)) observability for backside type II bursts. We see that compensating separately for each explanation of the speed distribution differences between Figures 1 and 2 leads to similar results, about a 23 ± 7% observability for backside type II bursts.

It should be noted that we have dealt only with backside type II bursts associated with CME's. *Sheeley et al.* [1984] and *Kahler et al.* [1984] found that 30–40% of all type II bursts are not accompanied by CME's. Sheeley et al. found that 1- to 8-Å X ray events were associated with at least 18 of their sample of 19 type II bursts with no CME's, suggesting that essentially none of these events originated with a backside flare. If we take 0.23 as the ratio of backside to frontside observable type II bursts with CME's and assume that one third of all frontside type II bursts are not associated with CME's, we conclude that ~13 ± 4% (0.23/(0.23 + 1.0 + 0.5)) of all observed type II bursts originate in backside events.

This result does not include the effect of type II bursts due to slow ($v < 500$ km $s^{-1}$) CME's. *Sheeley et al.* [1984] found only five of their 40 type II bursts with CME's were due to slow CME's, and one of these five appeared due to a backside

TABLE 4. CME's Without Associated Hα Flares but With Associated Type II Bursts

| | CME | | | Type II Burst | | Source Region | | | |
|---|---|---|---|---|---|---|---|---|---|
| Date | Limb Time, UT | Speed,* km s$^{-1}$ | Location (Size) | Duration, UT | Intensity | NOAA | Latitude | Longitude Over Limb | 1–8 Å |
| May 4, 1979 | 0217 | 870 | N45°E(115°) | 0222–0255 | 3 | | ? | | <C1 |
| Nov. 2, 1979 | 2233 | 1000 E | N35°E(100°) | 2258–2306 | 1 | 2110? | 32°N | ≥30° | <C1 |
| Nov. 4, 1979 | 0456 | 1000 E | N50°E(100°) | 0511–0547 | 2 | 2110? | 32°N | ≥15° | C8 |
| June 29, 1980 | 0224 | 560 F | S17°W(25°) | 0241–0301 | 3 | 2522 | 28°S | ~0° | M3 |
| July 30, 1980 | 1251 | 1000 F | N30°W(20°) | 1312–1316 | 1 | | ? | | >C2 |
| Sept. 1, 1980 | 0534 | 960 E | N15°W(90°) | 0554–0600 | 1 | 2629 | 19°N | ≥55° | <C1 |
| Nov. 19, 1981 | 0216 | 800 | N32°W(65°) | 0230–0246 | 2 | 3451 | 18°N | ~5° | C8 |
| June 3, 1982 | 0244 | 1490 F | N70°W(40°) | 0233–0302 | 3 | 3739 | 15°N | ≥60° | <C1 |
| July 1, 1982 | 1606 | 1000 P | S10°E(40°) | 1606–1625 | 3 | 3801 | 15°S | ≥15° | <C1 |
| Dec. 7, 1982 | 0904 | 1600 F | E(60°) | 0914–0933 | 3 | 4026 | 11°S | ≥35° | <C1 |

*E is estimated; F is fair; P is poor.

event. Assuming that all observed type II bursts associated with slow CME's are frontside events reduces the calculated fraction of backside type II bursts only slightly, to 12 ± 4% (0.23/(0.23 + 1.14 + 0.57)). With an assumed 20% backside origin for slow CME's, the figure of 13% is unchanged. Thus the percentage of backside events derived above is not significantly changed by consideration of the slow CME's.

## 3. Discussion

We explore two basic questions in this paper. First, we discuss the statistics and characteristics of fast CME's from the visible disk which fail to produce type II bursts. We then consider the observability of backside type II bursts.

### 3.1. *Frontside CME's With No Associated Type II Bursts*

The 15 events of Table 1 confirm the conclusion of *Sheeley et al.* [1984] that a class of fast frontside CME's with no associated metric type II bursts exists. Twelve of the events of the table were not used in their study. The approach taken in this study has been complementary to that of Sheeley et al. They examined metric burst records of Culgoora in detail to find cases of fast CME's with no type II bursts. We have relied on SGD reports but have used a much larger data sample taken from three observatories which provide nearly full-time solar observations. In addition to confirming the Sheeley et al. finding of fast CME's with no type II bursts, we estimate the percentage of fast, frontside CME's associated with no type II burst to be ~33 ± 15%.

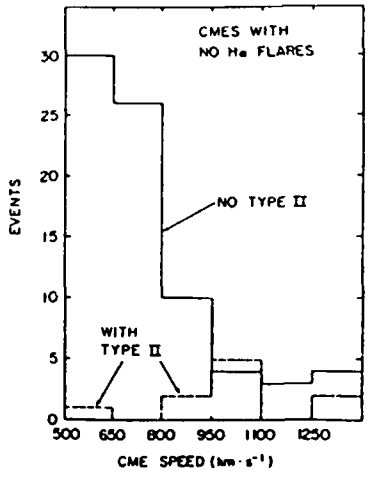


Fig. 2. Speed distribution of fast CME's for which no Hα flare association could be found. Although a few exceptions undoubtedly exist, these events are presumed to arise from flares on the solar backside. The 10 events associated with reported type II bursts are listed in Table 4.

What can the statistical properties of fast CME's with and without type II bursts tell us about the source of the type II shock? In section 1 we discussed the competing concepts of the piston-driven shock and the decoupled shock originating in the flare impulsive phase. The increasing probability of a type II burst association with increasing CME speed, shown in Figure 1 and Table 3, argues for the piston-driven model of type II shocks, as does the finding of *Sheeley et al.* [1984] that type II bursts are not associated with CME's with speeds less than 400 km s$^{-1}$. Sheeley et al. suggested that variations in the ambient Alfvén speed from event to event could explain why even some of the fastest CME's fail to produce detectable shocks in the lower ($R \sim 1.5\ R_S$) corona. Variations of a factor of 3 from the average coronal magnetic fields are inferred from the various field measurement techniques reviewed by *Dulk and McLean* [1978]. Since the Alfvén speed scales with the field strength, the explanation of *Sheeley et al.* [1984] seems quite reasonable, since nearly all fast CME's can be associated with interplanetary shocks detected in situ [*Sheeley et al.*, 1983].

On the other hand, with the piston-driven model we might also expect that CME's of larger angular width would traverse a larger area of the corona, encounter a wider range of Alfvén speeds, and be more likely to produce type II shocks than would narrower CME's. As discussed in section 2, we found no such effect. We might further suppose that the brightnesses of CME's are not relevant for producing type II shocks in the context of the piston-driven model because the CME's are low-$\beta$ plasmas in which the mass serves primarily as a tracer and because the shock should occur in front of the CME. Nevertheless, the data of Table 2 do show a correlation between type II burst association and CME brightness. Finally, the data of Table 3 show that the size of the peak 3-cm burst is equally as important as the CME speed in determining the type II burst association.

None of these three factors in type II burst association (independence of CME angular width, and dependence on both CME brightness and peak 3-cm flux) are an obvious prediction from the piston-driven shock model. All three do, how-

ever, appear to be consistent with the Wagner-MacQueen hypothesis of decoupling between CME and shock origins. The enhanced CME brightness in that case may be indicative of higher particle densities and lower Alfvén speeds for the shock traversing the CME. Alternatively, the enhanced density regions of CME's may be particularly favorable regions from which radio emission at the plasma frequency can escape the corona. In the decoupled view, the shock is generated in the impulsive phase, the strength of which may be indicated by the peak flux density of the 3-cm burst. The importance of CME speed for type II burst association might then be a result of the big flare syndrome [*Kahler*, 1982], in which more energetic CME's tend to be associated with more energetic impulsive bursts, but not through a direct cause-and-effect relationship.

One can make the argument in the opposite direction, of course, by asserting in the context of piston-driven shocks that the CME speed is the determining factor and that it is the observed dependence on impulsive 3-cm burst intensity and CME brightness that follows from the big flare syndrome. Thus we feel that the data do not clearly favor either the piston-driven or the decoupled shock model.

### 3.2. *Observability of Backside Type II Bursts*

We found in section 2.3 that 23 ± 7% of the backside type II bursts associated with fast CME's can be observed at the earth. The difference in speed distributions between the frontside and backside events obvious in Figures 1 and 2 was taken into account in the calculation. Using the *Sheeley et al.* [1984] result suggesting that essentially all type II bursts with no associated CME's are frontside events, we concluded that 13 ± 4% of all type II bursts originate in backside events. This result of ~13% for backside type II bursts is below the upper limit of 20–40% of all type II bursts deduced for backside events in the Hα flare association studies discussed in section 1.

The most striking characteristic of the backside CME's with associated type II bursts is their high speed. Excluding the two events within 5° of the limb, we find that the lowest measured speed of the backside group is 870 km $s^{-1}$. As in the case of the frontside CME's, it is difficult to understand in the context of the decoupled CME/type II hypothesis why the CME speed is so important for the generation of an observable type II burst. The fast speeds of these events favor the piston-driven origin for the type II shocks.

*Acknowledgments.* This work was supported at Emmanuel College by AFGL contract AF19628-82-K-0039, and at NRL by NASA DPR W 14,429. The Department of Defense Space Test Program provided integration, launch, and operational support for the P78-1 spacecraft. D. Roberts, F. Harlow, and W. Funk of NRL assisted in the coronagraph data reduction. We thank J. McKinnon for providing unpublished Hα flare listings.

The Editor thanks R. M. MacQueen and M. R. Kundu for their assistance in evaluating this paper.

## REFERENCES

Cane, H. V., The relationship between coronal transients, type II bursts, and interplanetary shocks, *Astron. Astrophys.*, in press, 1984.

Cane, H. V., The evolution of interplanetary shocks, *J. Geophys. Res.*, this issue.

Dodge, J. C., Source regions for type II radio bursts, *Solar Phys.*, *42*, 445, 1975.

Dulk, G. A., and D. J. McLean, Coronal magnetic fields, *Solar Phys.*, *57*, 279, 1978.

Gergely, T. E., and M. R. Kundu, A decameter type II burst associated with a behind-the-limb flare, *Solar Phys.*, *48*, 357, 1976.

Gosling, J. T., E. Hildner, R. M. MacQueen, R. H. Munro, A. I. Poland, and C. L. Ross, The speeds of coronal mass ejection events, *Solar Phys.*, *48*, 389, 1976.

Hudson, H. S., R. P. Lin, and R. T. Stewart, Second-stage acceleration in a limb-occulted flare, *Solar Phys.*, *75*, 245, 1982.

Kahler, S. W., The role of the big flare syndrome in correlations of solar energetic proton fluxes and associated microwave burst parameters, *J. Geophys. Res.*, *87*, 3439, 1982.

Kahler, S., N. R. Sheeley, Jr., R. A. Howard, M. J. Koomen, and D. J. Michels, Characteristics of flares producing metric type II bursts and coronal mass ejections, *Solar Phys.*, in press, 1984.

MacQueen, R. M., Coronal transients: A summary, *Philos. Trans. R. Soc. London, Ser. A*, *297*, 605, 1980.

MacQueen, R. M., and R. R. Fisher, The kinematics of solar inner coronal transients, *Solar Phys.*, *89*, 89, 1983.

Maxwell, A., and M. Dryer, Characteristics of shocks in the solar corona, as inferred from radio, optical, and theoretical investigations, *Space Sci. Rev.*, *32*, 11, 1982.

Munro, R. H., J. T. Gosling, E. Hildner, R. M. MacQueen, A. I. Poland, and C. L. Ross, The association of coronal mass ejection transients with other forms of solar activity, *Solar Phys.*, *61*, 201, 1979.

Nelson, G. J., and D. J. McLean, Type II radio bursts originating from well behind the solar limb, in *Contributed Papers to the Study of Travelling Interplanetary Phenomena*, edited by M. A. Shea, D. F. Smart, and S. T. Wu, p. 287, Air Force Geophysics Laboratory, Hanscom Air Force Base, Mass., 1977.

Sheeley, N. R., Jr., D. J. Michels, R. A. Howard, and M. J. Koomen, Initial observations with the Solwind coronagraph, *Astrophys. J.*, *237*, L99, 1980.

Sheeley, N. R., Jr., R. A. Howard, M. J. Koomen, D. J. Michels, R. Schwenn, K. H. Muhlhauser, and H. Rosenbauer, Associations between coronal mass ejections and interplanetary shocks, Solar Wind Five, *NASA Conf. Publ.*, *2280*, 693, 1983.

Sheeley, N. R., Jr., R. T. Stewart, R. D. Robinson, R. A. Howard, M. J. Koomen, and D. J. Michels, Associations between coronal mass ejections and metric type II bursts, *Astrophys. J.*, *279*, 839, 1984.

Smerd, S. F., Radio evidence for the propagation of magnetohydrodynamic waves along curved paths in the solar corona, *Proc. Astron. Soc. Aust.*, *1*, 305, 1970.

Wagner, W. J., and R. M. MacQueen, The excitation of type II radio bursts in the corona, *Astron. Astrophys.*, *120*, 136, 1983.

Wright, C. S., On the longitude distribution of solar type II bursts, *Proc. Astron. Soc. Aust.*, *4*, 59, 1980.

E. W. Cliver and S. W. Kahler, Air Force Geophysics Laboratory/PHP, Hanscom Air Force Base, MA 01731.

R. A. Howard, M. J. Koomen, D. J. Michels, and N. R. Sheeley, Jr., E. O. Hulburt Center for Space Research, Naval Research Laboratory, Washington, DC 20375.

(Received May 1, 1984;
revised July 30, 1984;
accepted August 27, 1984.)

# GRADUAL HARD X-RAY EVENTS AND SECOND PHASE PARTICLE ACCELERATION

S. W. KAHLER

*Physics Research Division, Emmanuel College, Boston MA 02115, U.S.A.*

(Received 1 March; in revised form 29 September, 1983)

**Abstract.** In the second phase acceleration process the close time coincidence between the gradual hard X-ray burst and the type II shock wave is presumed due to shock acceleration of the electrons producing the gradual phase burst. We point out that recent studies of gradual hard X-ray bursts place the source heights well below the heights of $2-10 \times 10^5$ km traversed by the shock. Gradual phase energetic electrons therefore cannot be accelerated in the shock but must be produced elsewhere. We propose the loop systems of long decay X-ray events (LDEs) as the sites of the gradual phase electron production.

## 1. Introduction

The current view of particle acceleration in solar flares is that it occurs in two phases (Švestka, 1976). In the first, electrons are accelerated to energies of tens of kilovolts, producing an impulsive hard X-ray and microwave burst. This phase occurs in most, if not all, flares and frequently consists of several individual burst components (Kane *et al.*, 1980). SMM gamma-ray observations have shown (Chupp, 1982) that MeV electrons and tens of MeV protons are also sometimes produced in the first phase.

In the second phase, usually observed in the most energetic flares, MeV electrons and tens of MeV protons are produced through some mechanism associated with the passage of shock waves through the corona. The two-phase picture was first proposed by de Jager (1969) on the basis of the close association of type IV radio bursts, presumed due to the radiation of energetic electrons, with interplanetary MeV proton events. Strong evidence for this picture was provided by Frost and Dennis (1971), who argued that the flatter spectrum and more gradual time variations of the hard X-ray fluxes observed after the impulsive phase of the 30 March, 1969 event must be due to an acceleration mechanism different from that operating in the impulsive phase. The nearly simultaneous onset of the gradual hard X-ray phase and the metric type II burst in that event provided convincing evidence that the energetic electrons producing the X-ray bremsstrahlung must have been accelerated in association with the type II shock. Hudson (1978) discussed a gradual hard X-ray event observed on 14 December, 1971 which occurred at least 20° behind the limb and showed no soft X-ray burst or impulsive hard X-ray component. This event was similar to that of 30 March, 1969 in that it was attributed to a flare behind the limb and was closely associated in time with a type II burst. While the height of the X-ray source region had to exceed the occultation altitude of $6.6 \times 10^4$ km, Hudson was unable to distinguish among the type II shock, the observed white light transient, the moving type IV burst, or the stationary type IV burst as candidate locations for the X-ray source region. The greater source heights of the first

*Solar Physics* 90 (1984) 133–138. 0038–0938/84/0901–0133$00.90.

three possibilities imply lower ambient electron densities and larger numbers of energetic electrons than does the height ($\sim 1.1\ R_0$) of stationary type IV events. A third limb occulted gradual hard X-ray event, observed on 22 July, 1972, was analyzed by Hudson *et al.* (1982). They concluded that a single acceleration mechanism gave rise to both the electrons producing the gradual hard X-ray bremsstrahlung and the electrons escaping into interplanetary space. The type II shock wave was suggested as the accelerating agent, with the acceleration occurring continuously throughout the event over a wide spatial region. The ambient electron density of $n_e \sim 10^8\ \mathrm{cm}^{-3}$ inferred for the hard X-ray region was consistent with that of the type II burst source region. This recent result appears to confirm the earlier conclusions of Hudson (1979) and Ramaty *et al.* (1980) that the electrons of the gradual hard X-ray bursts are produced in the second phase acceleration process along with the MeV protons and relativistic electrons which escape to interplanetary space.

In the preceding discussion it is clear that a requirement of the second phase acceleration model is that the gradual hard X-ray source region be spatially, as well as temporally, associated with the type II shock wave. This means that the source heights must be in the range $2\text{–}10 \times 10^5$ km for metric type II bursts in an atmosphere characterized by $10\times$ Baumbach–Allen densities (Maxwell and Thompson, 1962). In the following sections we discuss recent gradual phase hard X-ray observations from the International Sun Earth Explorer 3 (ISEE-3) and Hinotori spacecraft which yield information about these source heights. These observations suggest a source height $h < 10^5$ km, well below the height of the type II shock wave, and a size scale $l \leq 5 \times 10^4$ km, much smaller than the huge coronal volumes traversed by the shocks. These results imply that, contrary to current belief, the energetic electrons producing the gradual hard X-ray events are not produced in the associated shock waves, but probably arise in the lower altitude post-flare loop systems.

## 2. Recent Observations

In some gradual phase events energy-dependent time delays can be observed in temporal features. One such event was observed with the ISEE-3 X-ray spectrometer on 14 August, 1979. In their analysis of this event Vilmer *et al.* (1982) proposed that the electrons were efficiently trapped in a coronal loop. The ambient electron density derived from their four-parameter fit was $n_e = 6 \times 10^{10}\ \mathrm{cm}^{-3}$, suggesting a relatively low coronal source height. A similar analysis of the 4 and 7 August, 1972 X-ray flares by Bai and Ramaty (1979) also yielded a similar density, $n_e \sim 3 \times 10^{10}\ \mathrm{cm}^{-3}$, but they did not distinguish the gradual phases from the impulsive phases in their analysis.

In a different approach to deduce source region heights Kane *et al.* (1982) and Kane (1983) compared ISEE-3 and Pioneer Venus Orbiter (PVO) observations of gradual hard ($\sim 150$ keV) X-ray events partially occulted at one of the two spacecraft. They found that $\sim 70\%$ of the total X-ray emission originated at altitudes of $\leq 2500$ km for one event and $\sim 87\%$ at less than 30 000 km for the other, again suggesting relatively high coronal electron densities for the gradual event.

Images of a gradual phase hard X-ray event of 13 May, 1981 were obtained with the SXT telescope on the Hinotori and discussed by Tsuneta (1983) and Tsuneta *et al.* (1984). The optical flare of importance 3B at N10 E65 began at 03 : 36 UT and is described by Loughhead *et al.* (1983). No type II burst was reported, but an examination of the Culgoora radio records indicates a possible metric type II burst from 04 : 00 to 04 : 06 UT (Stewart, 1982). Hard X-ray spectral fits over the range 40 to ~ 200 keV were obtained from 04 : 02 to 04 : 28 UT with the Hinotori hard X-ray spectrometer. The photon spectrum throughout that time was well fitted by a single power law with a spectral index which systematically hardened in time from about 4.5–5 to about 3. Hard

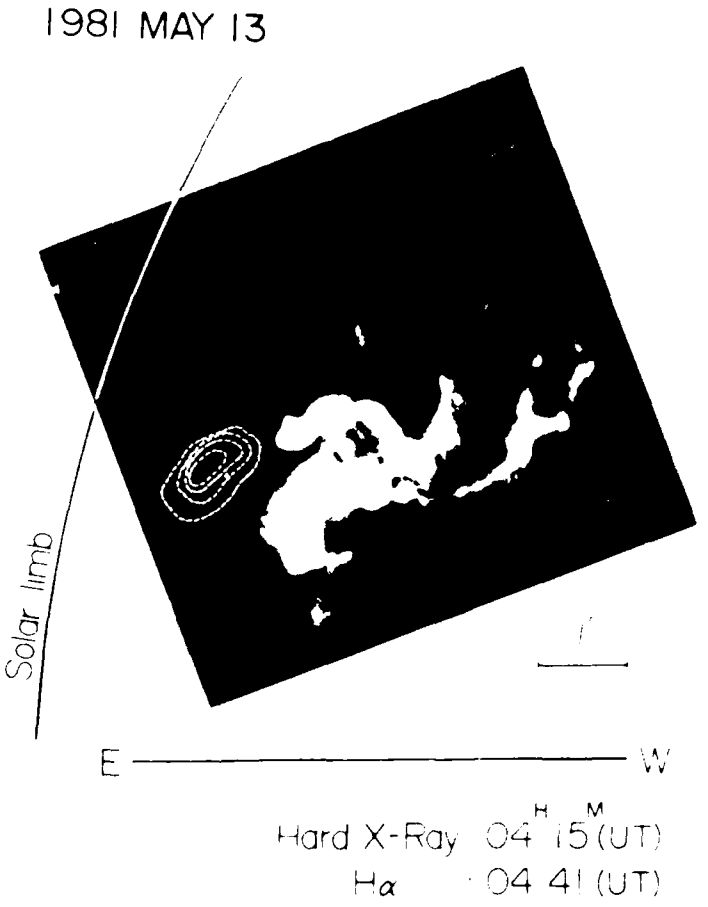


Fig. 1. Superposition of the 20% hard X-ray contours on the Hα image of the 13 May 1981 two-ribbon flare. The Hinotori observations were obtained near the peak of the gradual hard X-ray event and show the hard X-ray source lying just over the tops of the post-flare loop system. Figure from Tsuneta *et al.* (1984).

X-ray (16–38 keV) images were obtained with the SXT between 04 : 02 and 04 : 14 UT, and soft X-ray (5–10 keV) images between 04 : 14 and 04 : 18 UT, allowing a direct comparison between the two imaged wavebands. The hard X-ray source nearly coincided in size and position with the soft X-ray source, lying just over the tops of the Hα coronal loops at a height of ~40 000 km above the photosphere as shown in Figure 1. About 40% of the hard X-ray counts in the SXT were due to the power-law spectrum, the rest probably due to thermal plasmas of $T \geq 20 \times 10^6$ K (Lin *et al.*, 1981). Tsuneta *et al.* (1984) argue that the spatial coincidence of the 35 GHz gyrosynchrotron emission source and the gradual hard X-ray source supports the view that a population of nonthermal electrons were generated around the coronal loop structure.

These observations show that when gradual hard X-ray events occur in association with type II bursts, the required high ambient electron densities and low altitudes are incompatible with the usual presumed association of those events with type II shock waves of the upper corona in a second phase acceleration process. In addition, the $5 \times 10^4$ km by $2 \times 10^4$ km gradual hard X-ray source size of the 13 May event argues that the electron acceleration region is far more localized than that of the type II shock waves. However, Kai *et al.* (1983) observed gradual enhancements simultaneously in the hard X-ray, microwave, and metric bands 20–50 min after the impulsive phase of the 6 November, 1980 flare which suggest that energetic electrons can reach altitudes of $10^5$ km above the lower-lying microwave and hard X-ray sources. They suggest a columnar structure, probably a magnetic loop, for the gradual source structure.

The 5 to 10 keV source region imaged in the 13 May event may be presumed to be a post-flare loop or soft X-ray long decay event (LDE) as observed in Skylab images (Sheeley *et al.*, 1975; Kahler, 1977). Besides the gradual hard X-ray burst, the 13 May event displayed energetic phenomena characteristically associated with large LDE flares – an X1.5 soft X-ray event lasting ~12 hr, a metric type IV radio burst, and a fast (~1500 km s$^{-1}$) coronal mass ejection which produced an interplanetary shock (Sheeley *et al.*, 1983). The growth of soft X-ray LDE loop systems requires a continued energy input for periods of hours (MacCombie and Rust, 1979). LDE events have been associated with metric emission, apparently from stationary type IV bursts in one case (Švestka *et al.*, 1982), and from a type I noise storm in another (Lantos *et al.*, 1981). The stationary type IV bursts have also recently been associated with simultaneous centimetric bursts (Cliver, 1983). These radio observations strongly suggest that the X-ray loop systems supply not only thermal energy observed in the heated loops but also electrons energetic enough to emit centimeter emission in weak coronal fields. We suggest that the energetic gradual phase electrons are produced in or above the systems of LDEs and not in the type II shock wave as commonly believed.

## 3. Discussion

The close temporal association observed between gradual hard X-ray bursts and metric type II bursts has been presumed to indicate that the energetic electrons producing the gradual burst are accelerated in the type II shock wave at heights of $2–10 \times 10^5$ km. The

earliest observations of gradual events were from limb-occulted flares and provided lower limits to the heights of the gradual events which were consistent with that hypothesis. However, recent observations by the ISEE-3 and Hinotori hard X-ray detectors of gradual events in disk flares provide no evidence for these required heights, but rather indicate emission regions well below $10^5$ km. The value of the 13 May, 1981 gradual phase event is that it indicates a close association of that phase with the soft X-ray loops of the LDE and clearly shows that the gradual phase size scale is much smaller than would be expected of an energetic coronal shock wave traversing a large area of the corona. In view of the radio observations discussed in Section 2, there now appears little question that energetic electrons are produced in the large loop systems observed after filament-eruption flares. We have argued that it is these loop systems, not the simultaneous but spatially separated shock waves, in which the energetic electrons of the gradual phase are produced. This implies that the impulsive phase in a large flare is followed by two independent acceleration processes. In the shock wave energetic electrons and protons which are generally observed in the interplanetary medium are produced. The second acceleration process occurs in the LDE loop systems. There, energetic electron production continues, even though the gradual hard (and soft) X-ray flux profiles are declining in time or are no longer observable in full Sun detectors.

## Acknowledgements

This research was supported by AFGL contract F19628-82-K-0039. I wish to acknowledge helpful discussions with E. Cliver, H. Hudson, R. Lin, and S. Kane. I thank S. Tsuneta for providing the figure from their paper.

## References

Bai, T. and Ramaty, R.: 1979, *Astrophys. J.* **227**, 1072.
Chupp, E. L.: 1982, in R. E. Lingenfelter, H. S. Hudson, and D. M. Worrall (eds.), *Gamma Ray Transients and Related Astrophysical Phenomena*, American Institute of Physics, New York, p. 363.
Cliver, E. W.: 1983, *Solar Phys.* **84**, 347.
de Jager, C.: 1969, in C. de Jager and Z. Švestka (eds.), *Solar Flares and Space Research*, North-Holland Publ. Co., Amsterdam, p. 1.
Frost, K. J. and Dennis, B. R.: 1971, *Astrophys. J.* **165**, 655.
Hudson, H. S.: 1978, *Astrophys. J.* **224**, 235.
Hudson, H. S.: 1979, in J. Arons, C. McKee, and C. Max (eds.), *Particle Acceleration Mechanisms in Astrophysics*, American Institute of Physics, New York, p. 115.
Hudson, H. S., Lin, R. P., and Stewart, R. T.: 1982, *Solar Phys.* **75**, 245.
Kahler, S.: 1977, *Astrophys. J.* **214**, 891.
Kai, K., Nakajima, H., Kosugi, T., and Kane, S. R.: 1983, *Solar Phys.* **86**, 231.
Kane, S. R.: 1983, *Solar Phys.* **86**, 355.
Kane, S. R. and 10 co-authors: 1980, in P. A. Sturrock (ed.), *Solar Flares*, Colorado Assoc. Univ. Press, Boulder, p. 187.
Kane, S. R., Fenimore, E. E., Klebesadel, R. W., and Laros, J. G.: 1982, *Astrophys. J.* **254**, L53.
Lantos, P., Kerdraon, A., Rapley, C. G., and Bentley, R. D.: 1981, *Astron. Astrophys.* **101**, 33.
Lin, R. P., Schwartz, R. A., Pelling, R. M., and Hurley, K. C.: 1981, *Astrophys. J.* **251**, L109.

Loughhead, R. E., Jia-Long, W., and Duncan, R. A.: 1983, *Solar Phys.* **83**, 257.
MacCombie, W. J. and Rust, D. M.: 1979, *Solar Phys.* **61**, 69.
Maxwell, A. and Thompson, A. R.: 1962, *Astrophys. J.* **135**, 138
Ramaty, R., and 11 co-authors: 1980, in P. A. Sturrock (ed.), *Solar Flares*, Colorado Assoc. Univ. Press, Boulder, p. 117.
Sheeley, N. R., Jr., Bohlin, J. D., Brueckner, G. E., Purcell, J. D., Scherrer, V. E., Tousey, R., Smith, J. B., Speich, D. M., Tandberg-Hanssen, E., Wilson, R. M., DeLoach, A. C., Hoover, R. B., and McGuire, J. P.: 1975, *Solar Phys.* **45**, 377.
Sheeley, N. R., Jr., Howard, R. A., Koomen, M. J., Michels, D. J., Schwenn, R., Muhlhauser, K. H., and Rosenbauer, H.: 1983, in M. Neugebauer and A. Lazarus (eds.), *Proc. Solar Wind 5*, in press.
Stewart, R. T.: 1982, private communication.
Švestka, Z.: 1976, *Solar Flares*, D. Reidel Publ. Co., Dordrecht, Holland
Švestka, Z., Stewart, R. T., Hoyng, P., van Tend, W., Acton, L. W., Gabriel, A. H., Rapley, C. G., and 8 co-authors: 1982, *Solar Phys.* **75**, 305
Tsuneta, S.: 1983, Ph.D. Thesis, University of Tokyo
Tsuneta, S., Takakura, T., Nitta, N., Ohki, K., Tanaka, K., Makishima, K., Murakami, T., Oda, M., Ogawara, Y., and Kondo, I.: 1984, *Astrophys. J.*, in press
Vilmer, N., Kane, S. R., and Trottet, G.: 1982, *Astron. Astrophys.* **108**, 306

## MODELS AND DATA

An extensive study re-examined the relationship between "U-shaped" peak flux density spectra of large solar radio bursts and solar proton events. Approximately 200 large (Sp($\geq$ 200 GHz) $\geq$ 800 solar flux units) microwave bursts occurring during the years 1965 to 1979 were classified and their associations with Type II and/or Type IV meter wavelength bursts and > 10-MeV proton events were studied.

Using the trajectory-tracing technique and the 1980.0 geomagnetic field model, vertical cutoff rigidities have been calculated every $5^{o}$ in latitude and $5^{o}$ in longitude from $75^{o}$N to $75^{o}$S. Location of the cosmic ray equator has also been calculated using the trajectory-tracing technique. Studies have been done on the use of the McIlwain L-parameter to approximate cutoff rigidity values at specific locations providing a reasonable estimate of cutoff rigidities without the extensive computer calculations required for cosmic ray trajectory tracing. Studies have also been done correlating changes between asymptotic directions of cosmic ray particles and cutoff rigidities in the evolving geomagnetic field.

Work has continued on the project to assemble a data base of Ground Level Event Data for the thirty-nine events which have occurred during the past forty years, and convert the data into a standard format. The suggested standard format includes corrected, uncorrected, and barometric pressure values for both hourly and small time intervals during a 48 to 72-hour time period surrounding each event.

Each file also contains a nine line header with pertinent station information to aid in data analysis. Four of the more recent events received particular attention: Event #31 on 7 May 1978, Event #36 on 12 October 1981, Event #38 on 7 December 1982, and Event #39 on 16 February 1984.

# A REVISED STANDARD FORMAT FOR COSMIC RAY GROUND-LEVEL EVENT DATA

M. A. Shea and D. F. Smart
Air Force Geophysics Laboratory, Hanscom AFB, Bedford, MA 01731, U.S.A.

J. E. Humble
Physics Department, University of Tasmania, Hobart, Tasmania, Australia 7001

E. O. Flückiger
Physikalisches Institut, Universität Bern
Sidlerstrasse 5, CH-3012 Bern, Switzerland

L. C. Gentile and M. R. Nichol
Emmanuel College, 400 The Fenway, Boston, MA 02115, U.S.A.

## ABSTRACT

A revision to the suggested standard format for the exchange and archiving of cosmic ray ground-level event data is presented.

1. Introduction. A standard format for cosmic ray ground-level event data was suggested at the 19th International Cosmic Ray Conference /1/. In utilizing this format for compilation of data for both recent and historical events we encountered several problems. Although only slight changes have been made in the basic format, provision has been made to include a header containing station information, a data code indicating the type of cosmic ray data in each line, and a time code indicating the timing accuracy. The format has also been expanded to accommodate time intervals accurate to the nearest second.

2. Revised Format. An example of the revised format for the exchange of ground-level cosmic ray data is shown in Table 1. The format includes a nine-line header followed by the data for the event.

3. Header Information. The header information was added to provide as much station information as possible for the user, and to aid in future data analysis. The header information should be provided in the exact format shown in Table 1 as detailed in the following list:

Line 1:
- Columns 1-10: Station Name (abbreviate if necessary).
- Columns 12-19: The word "LATITUDE".
- Columns 22-27: Station latitude (F6.2). Indicate southern latitudes by a minus sign in Column 22.
- Columns 32-40: The word "LONGITUDE".
- Columns 44-49: Station longitude (F6.2) in degrees east of Greenwich; all positive numbers.
- Columns 54-61: The word "ALTITUDE".
- Columns 64-67: Station altitude (I4) in meters above sea level.
- Column 69: The letter "M" to designate meters.

Line 2:
- Columns 1-10 : Station Name (abbreviate if necessary).
- Columns 12-21: The word "INSTRUMENT".
- Columns 24-31: Start of instrument description as follows: for an NM-64 the designation is XX-NM-64 where XX is the number of tubes (columns 24-25). For an IGY monitor, IGY appears in columns 26-28; leave the remaining columns blank. For other instrumentation leave columns 24-31 blank.
- Columns 34-75: The type of detector (e.g. neutron monitor). If the detector is an ionization chamber, a muon telescope, or a specialized instrument such as a bare counter or multiplicity counter, identify it here and leave columns 24-31 blank.

Line 3:
- Columns 1-10: Station Name (abbreviate if necessary).
- Columns 12-28: The words "STANDARD PRESSURE".

Table 1. An example of ground-level event data in the standard format for the 7 May 1978 event. Only a partial data set for the Kiel neutron monitor is shown. Five-minute data continue until 0700 UT and hourly data until 2400 UT for this event. The time interval of 0200-0300 UT was selected as the pre-increase baseline time interval.

KIEL LATITUDE 54.33 LONGITUDE 10.13 ALTITUDE 54 M
KIEL INSTRUMENT 18-NM-64 NEUTRON MONITOR
KIEL STANDARD PRESSURE 755. MMHG COEFFICIENT -0.961 % / MMHG
KIEL PRE-INCREASE BASELINE TIME INTERVAL 780507 020000-030000 UT
KIEL PRE-INCREASE AVERAGE COUNTING RATE 159.90 COUNTS PER SECOND
KIEL TIME INTERVALS 3600 300
KIEL SCALE FACTORS 10. 1.

| STATION | YYMMDD | SEC | TIME (UT) INTERVAL | CODE TD | UNCORR. C/S | PRESS. (MMHG) | CORR. C/S | INC. |
|---|---|---|---|---|---|---|---|---|
| KIEL | 780506 | 3600 | 000000-010000 | 00 | 157.66 | 755.2 | 157.97 | -1.2 |
| KIEL | 780506 | 3600 | 010000-020000 | 00 | 158.23 | 754.9 | 158.07 | -1.1 |
| KIEL | 780506 | 3600 | 020000-030000 | 00 | 158.67 | 754.5 | 157.91 | -1.2 |
| KIEL | 780506 | 3600 | 030000-040000 | 00 | 159.67 | 754.2 | 158.45 | -.9 |
| KIEL | 780506 | 3600 | 040000-050000 | 00 | 160.05 | 754.1 | 158.68 | -.8 |
| KIEL | 780506 | 3600 | 050000-060000 | 00 | 159.42 | 754.0 | 157.90 | -1.3 |
| KIEL | 780506 | 3600 | 060000-070000 | 00 | 159.55 | 754.0 | 158.03 | -1.2 |
| KIEL | 780506 | 3600 | 070000-080000 | 00 | 160.27 | 753.9 | 158.58 | -.6 |
| KIEL | 780506 | 3600 | 080000-090000 | 00 | 161.25 | 753.7 | 159.25 | -.4 |
| KIEL | 780506 | 3600 | 090000-100000 | 00 | 161.87 | 753.4 | 159.40 | -.3 |
| KIEL | 780506 | 3600 | 100000-110000 | 00 | 161.40 | 753.0 | 158.33 | -1.0 |
| KIEL | 780506 | 3600 | 110000-120000 | 00 | 162.27 | 752.6 | 158.57 | -.8 |
| KIEL | 780506 | 3600 | 120000-130000 | 00 | 163.17 | 752.3 | 158.99 | -.6 |
| KIEL | 780506 | 3600 | 130000-140000 | 00 | 163.17 | 752.2 | 158.84 | -.7 |
| KIEL | 780506 | 3600 | 140000-150000 | 00 | 163.32 | 752.1 | 158.83 | -.7 |
| KIEL | 780506 | 3600 | 150000-160000 | 00 | 163.49 | 752.0 | 158.85 | -.7 |
| KIEL | 780506 | 3600 | 160000-170000 | 00 | 162.93 | 752.1 | 158.45 | -.9 |
| KIEL | 780506 | 3600 | 170000-180000 | 00 | 163.75 | 752.0 | 159.10 | -.5 |
| KIEL | 780506 | 3600 | 180000-190000 | 00 | 164.01 | 752.1 | 159.50 | -.2 |
| KIEL | 780506 | 3600 | 190000-200000 | 00 | 163.82 | 752.3 | 159.63 | -.2 |
| KIEL | 780506 | 3600 | 200000-210000 | 00 | 164.09 | 752.3 | 159.89 | .0 |
| KIEL | 780506 | 3600 | 210000-220000 | 00 | 164.26 | 752.2 | 159.91 | .0 |
| KIEL | 780506 | 3600 | 220000-230000 | 00 | 164.58 | 752.2 | 160.22 | .2 |
| KIEL | 780506 | 3600 | 230000-240000 | 00 | 164.99 | 752.1 | 160.46 | .4 |
| KIEL | 780507 | 3600 | 000000-010000 | 00 | 165.44 | 752.0 | 160.74 | .5 |
| KIEL | 780507 | 3600 | 010000-020000 | 00 | 165.25 | 751.9 | 160.40 | .3 |
| KIEL | 780507 | 300 | 020000-020500 | 00 | 163.60 | 751.8 | 158.64 | -.8 |
| KIEL | 780507 | 300 | 020500-021000 | 00 | 164.93 | 751.8 | 159.94 | .0 |
| KIEL | 780507 | 300 | 021000-021500 | 00 | 166.12 | 751.8 | 161.09 | .7 |
| KIEL | 780507 | 300 | 021500-022000 | 00 | 166.31 | 751.9 | 161.43 | 1.0 |
| KIEL | 780507 | 300 | 022000-022500 | 00 | 164.19 | 751.8 | 159.22 | -.4 |
| KIEL | 780507 | 300 | 022500-023000 | 00 | 164.06 | 751.9 | 159.25 | -.4 |
| KIEL | 780507 | 300 | 023000-023500 | 00 | 164.36 | 751.9 | 159.54 | -.2 |
| KIEL | 780507 | 300 | 023500-024000 | 00 | 165.93 | 751.8 | 160.90 | .6 |
| KIEL | 780507 | 300 | 024000-024500 | 00 | 163.85 | 751.8 | 158.89 | -.6 |
| KIEL | 780507 | 300 | 024500-025000 | 00 | 165.13 | 751.8 | 160.13 | .1 |
| KIEL | 780507 | 300 | 025000-025500 | 00 | 163.38 | 751.8 | 158.44 | -.9 |
| KIEL | 780507 | 300 | 025500-030000 | 00 | 166.52 | 751.7 | 161.32 | .9 |
| KIEL | 780507 | 300 | 030000-030500 | 00 | 165.11 | 751.7 | 159.96 | .0 |
| KIEL | 780507 | 300 | 030500-031000 | 00 | 165.57 | 751.8 | 160.56 | .4 |
| KIEL | 780507 | 300 | 031000-031500 | 00 | 164.78 | 751.9 | 159.94 | .0 |
| KIEL | 780507 | 300 | 031500-032000 | 00 | 164.28 | 752.0 | 159.61 | -.2 |
| KIEL | 780507 | 300 | 032000-032500 | 00 | 162.94 | 752.0 | 158.31 | -1.0 |
| KIEL | 780507 | 300 | 032500-033000 | 00 | 166.43 | 752.0 | 161.70 | 1.1 |
| KIEL | 780507 | 300 | 033000-033500 | 00 | 164.33 | 752.0 | 159.67 | -.1 |
| KIEL | 780507 | 300 | 033500-034000 | 00 | 268.88 | 751.9 | 260.99 | 63.2 |
| KIEL | 780507 | 300 | 034000-034500 | 00 | 313.37 | 751.7 | 304.17 | 90.2 |
| KIEL | 780507 | 300 | 034500-035000 | 00 | 266.19 | 752.0 | 258.63 | 61.7 |
| KIEL | 780507 | 300 | 035000-035500 | 00 | 232.49 | 752.0 | 225.89 | 41.3 |
| KIEL | 780507 | 300 | 035500-040000 | 00 | 211.88 | 752.1 | 206.06 | 28.9 |
| KIEL | 780507 | 300 | 040000-040500 | 00 | 195.22 | 752.2 | 190.04 | 18.8 |
| KIEL | 780507 | 300 | 040500-041000 | 00 | 190.16 | 752.2 | 185.12 | 15.8 |
| KIEL | 780507 | 300 | 041000-041500 | 00 | 180.79 | 752.2 | 175.99 | 10.1 |
| KIEL | 780507 | 300 | 041500-042000 | 00 | 177.55 | 752.2 | 172.84 | 8.1 |
| KIEL | 780507 | 300 | 042000-042500 | 00 | 176.12 | 752.2 | 171.45 | 7.2 |
| KIEL | 780507 | 300 | 042500-043000 | 00 | 172.24 | 752.2 | 167.67 | 4.9 |
| KIEL | 780507 | 300 | 043000-043500 | 00 | 171.17 | 752.2 | 166.62 | 4.2 |
| KIEL | 780507 | 300 | 043500-044000 | 00 | 171.29 | 752.1 | 166.59 | 4.2 |
| KIEL | 780507 | 300 | 044000-044500 | 00 | 168.17 | 752.1 | 163.55 | 2.3 |
| KIEL | 780507 | 300 | 044500-045000 | 00 | 169.69 | 752.1 | 165.03 | 3.2 |
| KIEL | 780507 | 300 | 045000-045500 | 00 | 168.28 | 752.1 | 163.66 | 2.4 |
| KIEL | 780507 | 300 | 045500-050000 | 00 | 169.75 | 752.2 | 165.24 | 3.3 |

3 Columns 31-37: The standard pressure (F7.2). If the standard pressure is in centimeters or inches use (F7.2); if in millimeters or millibars, use (F6.1,1X).
Columns 41-44: The unit of pressure: "MMHG", "CMHG" or "INHG" as appropriate. If "MB" is used, the letters go in columns 42 and 43 with columns 41 and 44 blank.
Columns 47-57: The word "COEFFICIENT".
Columns 60-66: The value of the barometric pressure coefficient in percent per unit pressure (F7.4).
Column 68: The percent sign (i.e. %).
Column 70: The slash sign (i.e. /).
Columns 72-75: The unit of pressure: "MMHG", "CMHG", or "INHG" as appropriate. If "MB" is used, the letters go in columns 73 and 74 with columns 72 and 75 blank.

Line 4: Columns 1-10: Station Name (abbreviate if necessary).
Columns 12-46: The words "PRE-INCREASE BASELINE TIME INTERVAL".
Columns 50-55: The year, month and day of the pre-increase baseline time interval (312).
Columns 59-64: The hour, minutes and seconds of the start of the baseline time interval (312).
Column 65: The hyphen (i.e. -).
Columns 66-71: The hour, minutes and seconds of the end of the baseline time interval (312).
Columns 74-77: The letters "UT".

The baseline time interval is the interval from which the percentage increase is calculated. The complete hour (in UT) before the onset of the particle increase at the earth would be the commonly used time interval. The earliest onset for the increase for the event on 7 May 1978 was between 0335 and 0338 UT; thus percentage increases would be determined using the average counting rate for the hourly interval 0200-0300 UT.

Line 5: Columns 1-10: Station Name (abbreviate if necessary).
Columns 12-45: The words "PRE-INCREASE AVERAGE COUNTING RATE".
Columns 50-56: The value of the pre-increase average counting rate in counts per second (F7.2).
Columns 59-75: The words "COUNTS PER SECOND".

Line 6: Columns 1-10: Station Name (abbreviate if necessary).
Columns 12-25: The words "TIME INTERVALS".
Columns 29-32: The number of seconds (I4) in the largest time interval of data in this data set (e.g. 3600 for hourly data).
Columns 33-72: The number of seconds in the various time intervals used in the data set in a 5(4X,I4) format. (For example if both 5 minute and 1 minute data are included, use bbbbb300bbbbbb60 where b indicates blanks.) Five time intervals can be given in addition to the first interval, for a total of six.

Line 7: Columns 1-10: Station Name (abbreviate if necessary).
Columns 12-24: The words "SCALE FACTORS".
Columns 30-35: Scale factor used in the largest time interval (F6.2) (e.g. a scale factor of 128, is given as 128.00.)
Columns 36-75: The scale factors used for each of the various time intervals given in Columns 33-72 of Line 6 in the same order as given on that line. The format is 5(2X,F6.2).

Lines 8 and 9 are column headings for the data that follow.

Line 8: Columns 1-10: Station Name (abbreviate if necessary).
Columns 12-17: The letters "YYMMDD" indicating year, month and day.
Columns 20-22: The letters "SEC" indicating number of seconds in the time interval.
Columns 26-34: The words "TIME (UT)".
Columns 37-40: The word "CODE".
Columns 44-50: The letters "UNCORR." indicating values not corrected for barometric pressure.
Columns 52-57: The letters "PRESS." indicating barometric pressure.

4 Columns 63-67: The letters "CORR." indicating values corrected for barometric pressure.
Columns 70-75: The identification "% INC." indicating percentage increase (i.e. above baseline).

Line 9: Columns 26-33: The word "INTERVAL".
Column 38: The letter "T" for the Time code (see below).
Column 39: The letter "D" for the Data code (see below).
Columns 46-48: The designation "C/S" indicating counts per second..
Columns 52-57: The units of pressure, within parentheses, as follows: "(MMHG)", "(CMHG)", "(INHG)", or "( MB )".
Columns 64-66: The designation "C/S" indicating counts per second.

4. Cosmic Radiation Data Information. The remaining lines contain cosmic radiation data in the following format:

Columns 1 - 10: Station identification (alphanumeric; abbreviate if necessary). Use the same identification as in header lines.
Columns 12 - 17: Year, month and day (3I2).
Columns 19 - 22: Number of seconds in this time interval (I4).
Columns 24 - 36: The hour, minutes, and seconds of the beginning and end of this time interval (3I2, 1H-, 3I2).
Column 38: Time code as follows:
0 - Time accurate to the nearest minute.
1 - Time accurate to the nearest second.
2 - Time accurate to the nearest 10 seconds.
3 - Time accurate to the nearest 30 seconds.
7 - Time uncertainty greater than 1 minute and less than five minutes.
8 - Time uncertainty greater than or equal to 5 minutes.
9 - Probable time error of undetermined amount in source data; approximate time adjustment has been made.
Column 39: Data code as follows:
0 - Uncorrected, pressure (measured) and corrected cosmic ray data.
1 - Uncorrected, pressure (interpolated) and corrected cosmic ray data.
2 - Corrected cosmic ray data only.
3 - Uncorrected cosmic ray data only.
4 - Corrected and uncorrected cosmic ray data only. (No pressure given for observation period; insufficient information for pressure interpolation.)
5 - Percent increase only. (Baseline time interval used may be different from standard.)
6 - Cosmic ray data do not exist (e.g. due to calibration, equipment failure, etc.).
9 - Existence of cosmic ray data unknown.
Columns 42 - 50: Uncorrected counting rate; counts per second (F9.2).
Columns 52 - 58: Barometric pressure. (F7.2 if pressure is in centimeters or inches; F6.1,1X if pressure is in millimeters or millibars.)
Columns 60 - 68: Corrected counting rate; counts per second (F9.2).
Columns 70 - 75: Percentage increase (F6.1) above the pre-increase average counting rate determined from the baseline time interval.

We hope that all cosmic ray data for ground-level events will now be reported to the World Data Centers in this standard format.

5. Acknowledgments. The research at the Universität Bern was sponsored by Swiss National Science Foundation grants 2.632-0.85 and 2.089-0.86. The research at Emmanuel College was supported by the AF Geophysics Laboratory.

Reference

1. Shea, M.A., D.F. Smart, H. Wada, and A. Inoue, 19th International Cosmic Ray Conference, Conference Papers, 5, 510, 1985.

Reprint from 19th International Cosmic Ray Conference,
Conference Papers, 5, 336-339, 1985.

# ESTIMATING THE CHANGE IN ASYMPTOTIC DIRECTION DUE TO SECULAR CHANGES IN THE GEOMAGNETIC FIELD

E. O. Fluckiger
Physikalisches Institut, Universitat Bern, Sidlerstrasse 5,
CH-3012 Bern, Switzerland

D. F. Smart and M. A. Shea
Air Force Geophysics Laboratory, Hanscom Air Force Base,
Bedford, Massachusetts 01731, U.S.A.

L. C. Gentile and A. A. Bathurst
Emmanuel College, 400 The Fenway, Boston, MA, 02115, U.S.A.

ABSTRACT

The concept of geomagnetic optics, as described by the asymptotic directions of approach, is extremely useful in the analysis of cosmic radiation data. However, when changes in cutoff occur as a result of evolution in the geomagnetic field, there are corresponding changes in the asymptotic cones of acceptance. We introduce here a method of estimating the change in the asymptotic direction of approach for vertically incident cosmic ray particles from a reference set of directions at a specific epoch by considering the change in the geomagnetic cutoff.

1. Introduction. Cosmic ray particles must travel along specific allowed trajectories through the geomagnetic field to reach a location on or near the earth. In order to relate cosmic ray intensity variations observed at different cosmic ray stations to the cosmic ray flux in space the concept of asymptotic directions of approach was developed (see McCracken et al., 1968, for a review). By application of the asymptotic directions of approach the user need not be concerned about the specific details of the allowed cosmic ray trajectories and can relate any specific cosmic ray particle with a unique direction in space. For a cosmic ray particle with rigidity R, arriving at a specific location (characterized by the geographic latitude $\Lambda$ and the geographic longitude $\Phi$) from a direction of incidence (described by the zenith angle $\theta$ and the azimuthal angle $\phi$) the asymptotic direction of approach is given by the unit vector $\underline{A}(R,\Lambda,\Phi,\theta,\phi)$ pointing in the reverse direction to the particle's velocity vector prior to the particle's entry into the geomagnetic field. For the purposes of this paper and for a specific location the vector $\underline{A}$ is specified for vertical incidence in terms of the geocentric coordinate system as asymptotic latitude, $\lambda(R) = \lambda(R,R_1(\Lambda,\Phi), \theta = 0°)$ and asymptotic longitude, $\psi(R) = \psi(R,R_1(\Lambda,\Phi), \theta = 0°)$ where $R_1$ is the rigidity corresponding to the first discontinuity in asymptotic longitude as defined below.

The allowed rigidity spectrum of cosmic ray particles arriving from a specific direction at any location in the geomagnetic field contains distinct fiducial marks: $R_1$, the rigidity associated with the first discontinuity in asymptotic longitude occurring as the trajectory calculations are progressing down through the rigidity spectrum, and $R_U$, the rigidity at and above which the trajectory calculations yield allowed

orbits. The rigidity value $R_l$ is always greater than or equal to $R_U$ if both are determined by employing the same uniform discrete (usually 0.01 GV) rigidity intervals in the trajectory calculations. $R_l$ is, in general, a value extremely close to the main cone cutoff rigidity as defined by Lemaitre and Vallarta (1936). A change in the geomagnetic field has an almost equivalent effect on both the rigidity corresponding to the first discontinuity and the vertical upper cutoff, and results in a similar effect on the vertical effective cutoff rigidity (Fluckiger et al., 1983a, 1983b).

Fluckiger et al., (1983b) have shown that geomagnetic disturbances reduce the cutoff rigidity in a predictable manner dependent on the strength and longitudinal structure of the magnetic perturbation and the longitudinal difference between the magnetic perturbation and the observing location. Furthermore, the change in asymptotic longitude (down to the first discontinuity) also behaves in a similarly predictable manner. Therefore the asymptotic directions of approach during perturbed geomagnetic conditions can be deduced with considerable accuracy from the asymptotic directions computed using the quiescent geomagnetic field if the associated change in cutoff rigidity is known. In this paper we extend these concepts to include the time evolution of the geomagnetic field on the asymptotic direction of approach for cosmic ray particles arriving at a particular location.

2. Method. We will define the terms $\delta\lambda^*(R)$ and $\delta\psi^*(R)$ as $\delta\lambda^*(R) = \lambda'(R) - \lambda(R-\delta R_l)$, and $\delta\psi^*(R) = \psi'(R) - \psi(R-\delta R_l)$, where $\delta R_l = R_l' - R_l$, and the primed values indicate the evolved geomagnetic field and the unprimed values indicate the reference geomagnetic field. When these values are plotted as a function of rigidity, it has been found that there are practically no changes for $\delta\lambda^*$ down to the rigidity value of $R_l'$. Therefore, we may set $\delta\lambda^* = 0°$ (Fluckiger et al., 1983b). For $\delta\psi^*$ only small residual changes on the order of several degrees are found down to rigidities approaching the value of $R_l$. For any particular location and for rigidities up to several GV above the main cutoff the following expressions can be used to describe the correlation between the asymptotic directions in an evolved geomagnetic field and the asymptotic directions in a reference geomagnetic field:

$$\lambda'(R) = \lambda(R - \delta R_l), \text{ and } \psi'(R) = \psi(R - \delta R_l) + C \cdot \delta R_l,$$

where C is a measure of the residual change $\delta\psi^*$. This procedure is valid only for rigidities larger than $R_l$ or $R_l'$, respectively.

At rigidities below $R_l$ no similar relation has been found, although coherent clusters of trajectories may be distorted uniformly by magnetic changes. It has been shown that the main features of allowed and forbidden regions in the penumbra are conserved to a certain extent in a perturbed geomagnetic field (Fluckiger et al., 1979, 1982). However, the asymptotic longitudes of the allowed trajectories of the fine detailed structure in the cosmic ray penumbra continue to be quasi-random.

3. Application. We have applied this procedure by comparing the asymptotic directions calculated for the International Geomagnetic Reference Field Epoch 1965.0 with those calculated for epoch 1980.0 for cosmic ray stations and world grid locations. To illustrate this application, we

considered the 1965 epoch as the reference values and the 1980 epoch as the evolved values. We would expect a close comparison between the asymptotic directions above the first discontinuity ($R_1$) such that $\psi(R_1^* + \Delta R) = \psi'(R_1'^* + \Delta R)$ where $\Delta R$ represents an arbitrary rigidity value above $R_1^*$ and $R_1'^*$. Here $\psi$ denotes the asymptotic longitude in the reference field, and $\psi'$ the asymptotic longitude in the evolved field. $R_1^*$ and $R_1'^*$ are approximations to the rigidity value of the first discontinuity obtained by examining the gradient in the change of the asymptotic direction with rigidity as the first discontinuity is approached from rigidity values above the main cutoff. The values selected to approximate the first discontinuity in asymptotic direction, $R_1^*$ and $R_1'^*$ were the rigidity values where the gradient in asymptotic direction was greater than 1000° per GV and increased by more than 1.5 times in the next 0.01 GV increment. Examination of these results and comparison with other calculations have shown that this approximation is close to and slightly greater than the rigidity of the first discontinuity calculated using very small rigidity intervals.

For the examples given in the following tables, the increment of rigidity added to the approximation of the first discontinuity value was the change in rigidity of the first discontinuity between the reference field and the evolved field. This value was used because it was sure to be in the set of continuous asymptotic directions above the main cutoff in both data sets. In Table 1 we illustrate the results for cosmic ray stations at locations where the geomagnetic cutoff is decreasing with time. In Table 2 we show results for cosmic ray stations at locations where the cosmic ray cutoff is increasing with time. An inspection of the asymptotic longitudes given in the second and third columns from the right in these tables indicates that the asymptotic longitudes for the specified rigidity values are quite similar.

4. Conclusions. We have illustrated that the asymptotic directions for an evolved geomagnetic field for rigidity values above the $R_1$ value (the first discontinuity in asymptotic direction progressing down through the rigidity scale) can be obtained from a "known" reference set of asymptotic directions if the change in cutoff is known.

5. Acknowledgments. A. A. Bathurst and L. C. Gentile acknowledge support from the U. S. Air Force Geophysics Laboratory under Contract No. F19628-82-K-0039.

References.

Fluckiger, E., H. Debrunner, D.F. Smart, and M.A. Shea, 16th International Cosmic Ray Conference, Conference Papers, 4, 273, 1979.

Fluckiger, E., AFGL-TR-82-0177, 1982, ADA126328.

Fluckiger, E.O., D.F. Smart, and M.A. Shea, J. Geophys. Res., 88, 6961, 1983a.

Fluckiger, E.O., D.F. Smart, and M.A. Shea, 18th International Cosmic Ray Conference, Conference Papers, 3, 431, 1983b.

Lemaitre, G., and M.S. Vallarta, Phys. Rev., 50, 493, 1936.

McCracken, K.G., U.R. Rao, B.C. Fowler, M.A. Shea, and D.F. Smart, Cosmic Rays, Annals of the IQSY, Vol. 1, Edited by C.M. Minnis, Chapter 14, 198, The MIT Press, Cambridge, Massachusetts, 1968.

TABLE 1.
Changes of Asymptotic Longitude for Cosmic Ray Stations Where the Cutoff is Decreasing.

$\psi$ for 1980 at $R_1^{*'} + |\Delta R|$ = $\psi$ for 1965 at $R_1^{*} + |\Delta R|$, where $\Delta R = (R_1^{*'}$ for 1980) - ($R_1^{*}$ for 1965)

| STATION NAME | GEOGRAPHIC LAT | GEOGRAPHIC LONG | EPOCH 1965 $R_U$ | EPOCH 1965 $R_1^*$ | EPOCH 1965 $\psi$ | EPOCH 1980 $R_U'$ | EPOCH 1980 $R_1^{*'}$ | EPOCH 1980 $\psi'$ | $\Delta R_1^*$ | 1965 RIG | 1965 $\psi$ | 1980 $\psi'$ | 1980 RIG |
|---|---|---|---|---|---|---|---|---|---|---|---|---|---|
| Ahmedabad | 23.01 | 72.61 | 15.90 | 15.92 | 46 | 15.77 | 15.79 | 51 | -0.13 | 16.05 | 329 | 327 | 15.92 |
| Alma Ata | 43.20 | 76.94 | 6.92 | 6.93 | 36 | 6.87 | 6.90 | 30 | -0.03 | 6.96 | 358 | 355 | 6.93 |
| Brisbane | -27.50 | 153.01 | 7.39 | 7.42 | 121 | 7.22 | 7.26 | 116 | -0.16 | 7.58 | 31 | 30 | 7.42 |
| Buenos Aires | -34.58 | 301.50 | 10.59 | 10.61 | 266 | 10.12 | 10.15 | 246 | -0.46 | 11.07 | 130 | 124 | 10.61 |
| Chacaltaya | -16.31 | 291.85 | 12.85 | 12.87 | 257 | 12.53 | 12.54 | 263 | -0.33 | 13.20 | 144 | 144 | 12.87 |
| Climax | 39.37 | 253.82 | 3.14 | 3.24 | 146 | 3.12 | 3.22 | 153 | -0.02 | 3.26 | 124 | 128 | 3.24 |
| Gulmarg | 34.07 | 74.42 | 12.33 | 12.35 | 44 | 12.24 | 12.26 | 45 | -0.09 | 12.44 | 336 | 337 | 12.35 |
| Hermanus | -34.42 | 19.22 | 5.02 | 5.06 | 307 | 4.83 | 4.86 | 311 | -0.20 | 5.26 | 215 | 214 | 5.06 |
| Hobart | -42.90 | 147.33 | 2.10 | 2.12 | 44 | 2.06 | 2.08 | 43 | -0.04 | 2.16 | 13 | 11 | 2.12 |
| Huancayo | -12.05 | 284.67 | 13.24 | 13.25 | 266 | 12.91 | 12.93 | 253 | -0.32 | 13.57 | 142 | 140 | 13.25 |
| Mexico City | 19.33 | 260.82 | 9.57 | 10.24 | 257 | 9.27 | 9.94 | 250 | -0.30 | 10.54 | 121 | 123 | 10.24 |
| Mildura | -34.23 | 142.22 | 4.56 | 4.59 | 97 | 4.43 | 4.46 | 87 | -0.13 | 4.72 | 11 | 11 | 4.59 |
| Mt. Wellington | -42.92 | 147.24 | 2.03 | 2.11 | 49 | 1.99 | 2.07 | 49 | -0.04 | 2.15 | 14 | 12 | 2.11 |
| Palestine | 31.75 | 264.35 | 4.74 | 4.90 | 185 | 4.69 | 4.86 | 194 | -0.04 | 4.94 | 145 | 147 | 4.90 |
| Potchefstroom | -26.70 | 27.10 | 7.68 | 7.72 | 346 | 7.49 | 7.53 | 337 | -0.19 | 7.91 | 247 | 245 | 7.72 |
| Sydney | -33.60 | 151.10 | 5.16 | 5.19 | 86 | 5.06 | 5.09 | 84 | -0.10 | 5.29 | 21 | 21 | 5.19 |
| Tbilisi | 41.72 | 44.80 | 6.96 | 7.00 | 357 | 6.95 | 6.97 | 14 | -0.03 | 7.03 | 322 | 321 | 7.00 |

TABLE 2.
Changes of Asymptotic Longitude for Cosmic Ray Stations Where the Cutoff is Increasing.

$\psi$ for 1980 at $R_1^{*'} + |\Delta R|$ = $\psi$ for 1965 at $R_1^{*} + |\Delta R|$, where $\Delta R = (R_1^{*'}$ for 1980) - ($R_1^{*}$ for 1965)

| STATION NAME | GEOGRAPHIC LAT | GEOGRAPHIC LONG | EPOCH 1965 $R_U$ | EPOCH 1965 $R_1^*$ | EPOCH 1965 $\psi$ | EPOCH 1980 $R_U'$ | EPOCH 1980 $R_1^{*'}$ | EPOCH 1980 $\psi'$ | $\Delta R_1^*$ | 1965 RIG | 1965 $\psi$ | 1980 $\psi'$ | 1980 RIG |
|---|---|---|---|---|---|---|---|---|---|---|---|---|---|
| Athens | 37.97 | 23.72 | 8.98 | 8.99 | 355 | 9.06 | 9.08 | 340 | 0.09 | 9.08 | 280 | 275 | 9.17 |
| Bologna | 44.50 | 11.33 | 5.41 | 5.44 | 297 | 5.52 | 5.55 | 295 | 0.11 | 5.55 | 231 | 231 | 5.66 |
| Budapest | 47.50 | 18.90 | 4.74 | 4.77 | 309 | 4.82 | 4.83 | 309 | 0.06 | 4.83 | 254 | 253 | 4.89 |
| Calgary | 51.08 | 245.91 | 1.16 | 1.22 | 123 | 1.17 | 1.24 | 125 | 0.02 | 1.24 | 95 | 94 | 1.26 |
| Deep River | 46.10 | 282.50 | 1.13 | 1.19 | 170 | 1.25 | 1.32 | 150 | 0.13 | 1.32 | 80 | 85 | 1.45 |
| Dourbes | 50.10 | 4.60 | 3.42 | 3.44 | 298 | 3.57 | 3.60 | 294 | 0.16 | 3.60 | 208 | 215 | 3.76 |
| Durham | 43.10 | 289.16 | 1.67 | 1.69 | 197 | 1.84 | 1.86 | 179 | 0.17 | 1.86 | 93 | 103 | 2.03 |
| Fukushima | 37.75 | 140.48 | 11.36 | 11.38 | 104 | 11.45 | 11.47 | 100 | 0.09 | 11.47 | 40 | 38 | 11.56 |
| Irkutsk | 52.47 | 104.03 | 3.92 | 3.95 | 34 | 3.95 | 3.98 | 42 | 0.03 | 3.98 | 359 | 4 | 4.01 |
| Jungfraujoch | 46.55 | 7.98 | 4.81 | 4.82 | 300 | 4.91 | 4.94 | 289 | 0.12 | 4.94 | 222 | 220 | 5.06 |
| Kerguelen Is. | -49.35 | 70.22 | 1.24 | 1.31 | 299 | 1.15 | 1.31 | 315 | 0.00 | 1.31 | 299 | 315 | 1.31 |
| Kiel | 54.33 | 10.13 | 2.39 | 2.50 | 298 | 2.59 | 2.61 | 307 | 0.11 | 2.61 | 224 | 226 | 2.72 |
| Kiev | 50.72 | 30.30 | 3.74 | 3.77 | 335 | 3.79 | 3.80 | 332 | 0.03 | 3.80 | 290 | 289 | 3.83 |
| Leeds | 53.82 | 358.45 | 2.26 | 2.35 | 265 | 2.41 | 2.48 | 267 | 0.13 | 2.48 | 191 | 204 | 2.61 |
| Lomnicky Stit | 49.20 | 20.22 | 4.21 | 4.24 | 314 | 4.28 | 4.31 | 329 | 0.07 | 4.31 | 256 | 257 | 4.38 |
| Magadan | 60.11 | 151.01 | 2.22 | 2.33 | 52 | 2.34 | 2.36 | 45 | 0.03 | 2.36 | 9 | 6 | 2.39 |
| Morioka | 39.70 | 141.13 | 10.47 | 10.51 | 122 | 10.61 | 10.63 | 109 | 0.12 | 10.63 | 35 | 32 | 10.75 |
| Moscow | 55.47 | 37.32 | 2.60 | 2.61 | 320 | 2.50 | 2.62 | 313 | 0.01 | 2.62 | 302 | 297 | 2.63 |
| Mt. Norikura | 36.12 | 137.56 | 12.02 | 12.04 | 09 | 12.09 | 12.11 | 107 | 0.07 | 12.11 | 45 | 46 | 12.18 |
| Mt. Washington | 44.30 | 288.70 | 1.41 | 1.50 | 165 | 1.55 | 1.66 | 214 | 0.16 | 1.66 | 89 | 96 | 1.82 |
| Mussala | 42.18 | 25.58 | 6.50 | 6.51 | 346 | 6.56 | 6.57 | 343 | 0.06 | 6.57 | 281 | 280 | 6.63 |
| Pic du Midi | 42.93 | 0.25 | 5.58 | 5.61 | 294 | 5.80 | 5.81 | 306 | 0.20 | 5.81 | 204 | 209 | 6.01 |
| Predigtstuhl | 47.70 | 12.88 | 4.59 | 4.60 | 309 | 4.68 | 4.70 | 299 | 0.10 | 4.70 | 235 | 232 | 4.80 |
| Rome | 41.90 | 12.52 | 6.35 | 6.37 | 318 | 6.50 | 6.54 | 324 | 0.17 | 6.54 | 235 | 236 | 6.71 |
| Tokyo-Itabashi | 35.75 | 139.72 | 12.12 | 12.13 | 115 | 12.19 | 12.21 | 99 | 0.08 | 12.21 | 45 | 41 | 12.29 |
| Yakutsk | 62.02 | 129.72 | 1.74 | 1.85 | 22 | 1.78 | 1.87 | 32 | 0.02 | 1.87 | 352 | 356 | 1.89 |
| Zugspitze | 47.42 | 10.98 | 4.62 | 4.64 | 314 | 4.72 | 4.75 | 298 | 0.11 | 4.75 | 230 | 227 | 4.86 |

Reprint from 19th International Cosmic Ray Conference, Conference Papers, 5, 332-335, 1985.

# THE USE OF THE McILWAIN L-PARAMETER TO ESTIMATE COSMIC RAY VERTICAL CUTOFF RIGIDITIES FOR DIFFERENT EPOCHS OF THE GEOMAGNETIC FIELD

M.A. Shea and D.F. Smart
Air Force Geophysics Laboratory
Hanscom AFB, Bedford, Massachusetts 01731, U.S.A.

L.C. Gentile
Physics Research Division, Emmanuel College
400 The Fenway, Boston, Massachusetts 02115, U.S.A.

## ABSTRACT

A useful relationship employing the McIlwain L-parameter to estimate vertical cutoff rigidities has been derived for the twenty-five year period 1955-1980.

1. Introduction. It is intuitively pleasing to utilize the dipolar geometry inherent in the McIlwain L-parameter to order cosmic ray cutoff rigidities. However, in some areas of the world, secular changes in the geomagnetic field between 1955 and 1980 have been large enough to produce significant differences in both the vertical cutoff rigidities and in the L-value for a specified position. In this paper we show that these changes are complimentary, and it is possible to derive a relationship between the L-value and vertical cutoff rigidity that can be used for the twenty-five year period, 1955-1980.

2. Background. The trajectory-tracing process is generally recognized as the most accurate method for calculating cosmic ray cutoff rigidities. Since cutoff rigidities are a function of latitude, longitude, altitude, zenith angle, azimuthal angle, and field model, using the trajectory-tracing method for a large number of positions and directions is impractical. For this reason, cosmic radiation data from many experiments are often ordered by the cutoff rigidity values in the vertical direction.

One method of estimating vertical cutoff rigitities was suggested by Smart and Shea (1967) who derived three equations for the relationship between the McIlwain L-parameter (McIlwain, 1961) and (1) the upper calculated cutoff, (2) the lower calculated cutoff and (3) the effective cutoff rigidities.* These three equations were derived using cutoff rigidities calculated for the Finch and Leaton (1957) field for Epoch 1955.0 and the Jensen and Cain (1962) field for Epoch 1960. The equations thus derived for the upper calculated cutoff, the lower calculated cutoff and the effective cutoff rigidities were essentially the same for both field models.

At the time of this original work, cosmic ray physicists did not recognize that the secular changes in the geomagnetic field were sufficiently large over a relatively small time period (on the order of 25 years) to significantly affect the detection, at the surface of the earth, of galactic cosmic radiation above 1 GV. It was not until Shea (1971) suggested

* In the paper of Smart and Shea (1967), these rigidity values were called main cone cutoff, Stormer cone cutoff and effective cutoff, respectively. Since new terminology for cosmic ray cutoffs has been agreed upon by scientists working in this area (Cooke et al., 1985) we will use these newer terms throughout this paper.

that the decrease in vertical cutoff rigidity at Huancayo over a 20-year period might possibly be observed as an increase in the background radiation measured by a stable neutron monitor at this location (since verified by Cooper and Simpson, 1979), that it became apparent that the secular changes in the geomagnetic field might be sufficiently large in some areas of the world that changes in cutoff rigidities, and consequently measured changes in cosmic radiation, would occur.

In view of the changes in the main geomagnetic field and the related changes in the calculated cutoff rigidities, we feel it is necessary to re-examine the use of the McIlwain L-parameter to estimate cosmic ray vertical cutoff rigidities for the 25-year period 1955-1980.

3. Method. The world grid of vertical cutoff rigidities calculated each 5° in latitude and 15° in longitude for Epochs 1955, 1965 and 1980 (Shea et al., 1968; Shea and Smart, 1975, 1983) and the McIlwain L-values (McIlwain, 1961) calculated for these same locations comprised the basic data sets used for this analysis. All calculations were made for an altitude of 20 km above the surface of the earth as defined by the international reference ellipsoid. Both the vertical cutoff rigidities and the McIlwain L-values were calculated using the geomagnetic field coefficients for the appropriate Epoch (i.e., 1955, 1965 and 1980).

Expressing the cosmic ray cutoffs by an equation of the form $R=KL^{\gamma}$ where R is the cutoff rigidity, L is the McIlwain L-value, K is a constant and $\gamma$ is an exponent, K and $\gamma$ were evaluated by a least-squares fit of the (1) upper calculated cutoff rigidity, (2) effective cutoff rigidity and (3) lower calculated cutoff rigidity. Each of the equations derived for each Epoch, together with the RMS error for each set of calculations, is given in Table 1. It is important to note that vertical cutoff rigidities < 0.20 GV were omitted from these calculations. Since the cosmic ray equator and the equator defined by the minimum L-value do not coincide, all grid points within a band ±5 degrees of either equator (or between the two equators) were also omitted. Figure 1 illustrates the locations of each of these equators for Epoch 1980.

Table 1. Equations to estimate cutoff rigidities for various Epochs

| Epoch | $R_U$ = | $R_C$ = | $R_L$ = |
|---|---|---|---|
| 1955 | $16.727\ L^{-2.0054}$<br>RMS = 6.28 % | $16.192\ L^{-2.0177}$<br>RMS = 5.48 % | $14.992\ L^{-1.9986}$<br>RMS = 6.61 % |
| 1965 | $16.722\ L^{-2.0212}$<br>RMS = 6.70 % | $16.222\ L^{-2.0418}$<br>RMS = 5.52 % | $14.942\ L^{-2.0296}$<br>RMS = 6.98 % |
| 1980 | $16.717\ L^{-2.0206}$<br>RMS = 7.06 % | $16.222\ L^{-2.0441}$<br>RMS = 5.74 % | $14.823\ L^{-2.0311}$<br>RMS = 7.27 % |
| Composite 1955-1980 | $16.762\ L^{-2.0174}$<br>RMS = 6.67 % | $16.237\ L^{-2.0353}$<br>RMS = 5.64 % | $14.912\ L^{-2.0185}$<br>RMS = 7.19 % |

4. Discussion. From an inspection of the equations in Table 1 it is evident that the constants K and $\gamma$ for each of the three vertical cutoff rigidities are essentially independent of Epoch. The root mean square values are also similar, with the slightly larger RMS values for 1980 attributed to the evolution of the magnetic field and an increasing divergence between the cosmic ray equator and the minimum L equator. The area between these two equators has increased approximately 10 percent between 1955 and 1980.

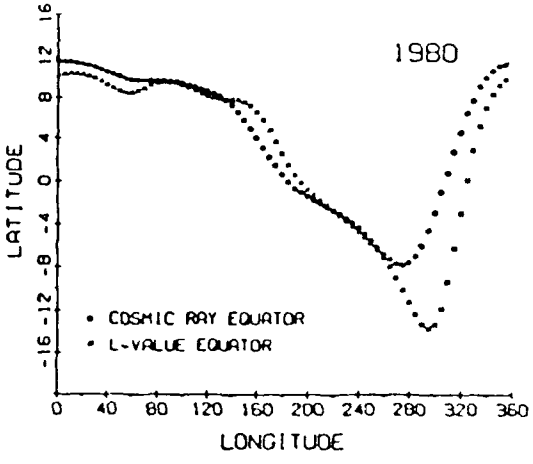


Figure 1. Geographic location of the cosmic ray equator and the minimum L equator for 1980.

Since these equations were almost identical we combined the data for all three Epochs in an effort to determine a suitable equation for the upper calculated cutoff, the effective cutoff and the lower calculated cutoff for the entire 25-year period from 1955 to 1980. Again all locations with cutoffs less than 0.20 GV were omitted from the analysis. Since the location of the cosmic ray equator changed between 1955 and 1980 (Shea et al., 1983), and different equatorial grid locations had been removed for each Epoch, we removed all locations within ±5° of any of the three equators (i.e., if a particular location had been removed for the analysis for one Epoch, it was removed from all three data sets for the composite analysis). Again the constants K and $\gamma$ were determined by the method of least squares. The results for this composite set of over 1875 data

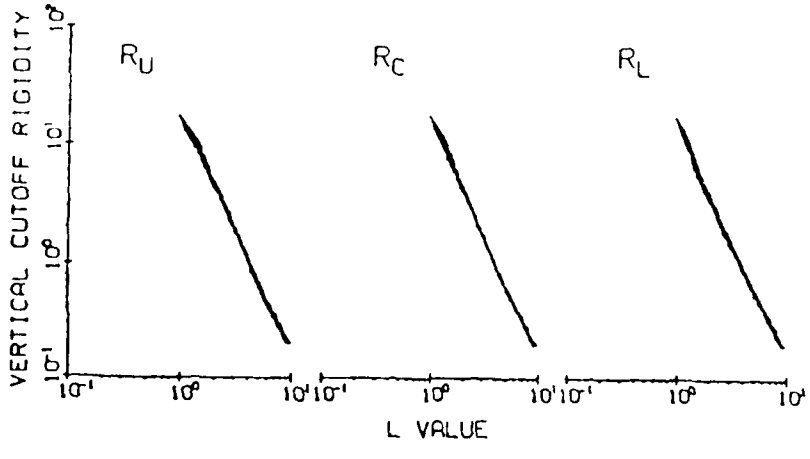


Figure 2. The upper calculated vertical cutoff rigidity ($R_U$), effective vertical cutoff rigidity ($R_C$), and lower calculated vertical cutoff rigidity ($R_L$), plotted as a function of the McIlwain L-value. The data set is a composite of the world grid locations for 1955, 1965 and 1980.

points are graphically illustrated in Figure 2; the equations are given in the bottom line of Table 1. From these results we feel that it is possible to use these three equations to estimate the upper, effective and lower cutoff rigidities for the entire period 1955 to 1980 provided the L-values are calculated using the field model for the same time period that the cutoffs are needed.

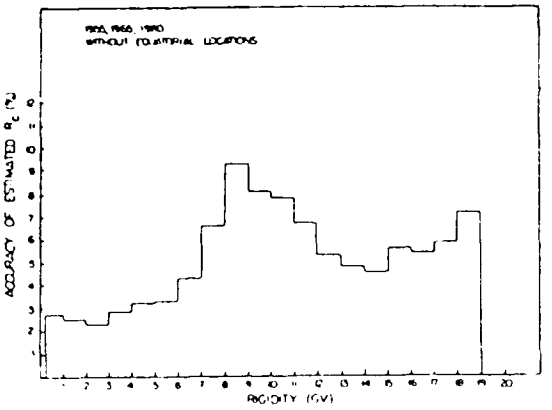

Figure 3: Accuracy of estimated vertical cutoff rigidity.

Figure 3 illustrates the accuracy that can be expected for an estimate of the effective vertical cutoff rigidity as a function of rigidity. These data were obtained by calculating for each location the percentage difference (in rigidity) between the cutoff rigidity value determined by the trajectory-tracing procedure and the value estimated by using the L-value approximation equation. These individual percentages were then averaged as a function of intervals of estimated cutoff rigidity.

5. Conclusion. From this analysis we conclude that the McIlwain L-parameter can be used to estimate upper calculated, effective, and lower calculated vertical cutoff rigidities for the period 1955 to 1980.

Acknowledgments. We gratefully acknowledge the computational assistance of A.A. Bathurst. LCG acknowledges support from the U.S. Air Force Geophysics Laboratory under contract No. F19628-82-K-0039.

References

Cooke, D.J., J.E. Humble, M.A. Shea, D.F. Smart, N. Lund, I.L. Rasmussen, B. Byrnak, P. Goret, and N. Petrou, Paper No. SH 6.1-11, 19th International Cosmic Ray Conference, these proceedings, 1985.

Cooper, J.F., and J.A. Simpson, 16th International Cosmic Ray Conference, Conference Papers, 12, 176, 1979.

Finch, H.P., and B.R. Leaton, Monthly Notices Roy. Astron. Soc., Geophys. Suppl., 7, 314, 1957.

Jensen, D.C., and J.C. Cain, J Geophys. Res., 67, 3568, 1962.

McIlwain, C.E., J. Geophys. Res., 66, 3681, 1961.

Shea, M.A., 12th International Conference on Cosmic Rays, Hobart, Conference Papers (University of Tasmania), 3, 859, 1971.

Shea, M.A., and D.F. Smart, 14th International Cosmic Ray Conference, Conference Papers, 4, 1298, 1975.

Shea, M.A., and D.F. Smart, 18th International Cosmic Ray Conference, Conference Papers, 3, 415, 1983.

Shea, M.A., D.F. Smart, and John R. McCall, Can. J. Phys., 46, S1098, 1968.

Shea, M.A., D.F. Smart and L.C. Gentile, 18th International Cosmic Ray Conference, Conference Papers, 3, 423, 1983.

Smart, D.F., and M.A. Shea, J. Geophys. Res., 72, 3447, 1967.

Papers, 3, 423-426, 1983.



# THE COSMIC RAY EQUATOR DETERMINED USING THE INTERNATIONAL GEOMAGNETIC REFERENCE FIELD FOR 1980.0

M. A. Shea and D. F. Smart
Air Force Geophysics Laboratory, Hanscom AFB, Bedford, MA 01731, U.S.A.

L. C. Gentile
Emmanuel College, 400 The Fenway, Boston, MA 02115, U.S.A.

## ABSTRACT

The location of the cosmic ray equator has been determined by the trajectory-tracing technique using the new International Geomagnetic Reference Field for 1980.0. Vertical cutoff rigidities were calculated for an altitude of 20 km at intervals of one degree in latitude and 5 degrees in longitude in the equatorial region. The location of the cosmic ray equator was determined by a least squares fit to the calculated vertical cutoff rigidities. In comparing these results with the cosmic ray equators calculated using geomagnetic field models for 1955 and 1965 we find a steady and consistent northerly shift in latitude of the cosmic ray equator between longitudes 265° E and 10° E with a maximum change of ~4° in latitude for geographic longitudes between 310° E and 325° E. Vertical cutoff rigidities along the cosmic ray equator have decreased between 1955 and 1980 for longitudes between 45° E and 325° E with a maximum decrease of ~0.5 GV between 260° E and 285° E. Slight increases (< 0.07 GV) occurred elsewhere.

## 1. Background

The location of the cosmic ray equator has been experimentally determined at a number of different longitudes and by a variety of experiments since 1936. The usual procedure was to measure the cosmic ray intensity as a function of latitude while the equipment was transported, usually on board ship or aircraft, from one hemisphere to the other. The latitude of the minimum in cosmic ray intensity determined the location of the cosmic ray equator at whatever longitude the crossing was made.

When it became practical to calculate vertical cutoff rigidities by the trajectory-tracing technique (Shea et al., 1965), it also became feasible to locate the maximum in the vertical cutoff rigidity as a function of longitude thereby determining the location of the cosmic ray equator by theoretical methods. A comparison of the theoretically determined equator with the experimentally measured cosmic ray equator was first made by Shea et al. (1964) when the theoretical equator at 190°E longitude was compared with a large number of experimental measurements made in that region of the world. Later Shea (1969) compared the location of the theoretical equator with experiments made at 32 longitudes over a period of 30 years. These comparisons were made using theoretically

determined cosmic ray equators for Epoch 1955.0 and Epoch 1960.0. At that time it was concluded that although differences were found between the equators determined for the two epochs, the calculated effects of the secular variation were too small to satisfactorily explain the deviations of the experimentally determined cosmic ray equator from the theoretically derived equator.

Using latitude survey data acquired by a shipboard neutron monitor along the 346° meridian in 1956-59 and 1964, Sporre and Pomerantz (1969) found that the location of the cosmic ray equator had shifted ~ 1.5° northward between the time periods of the two sets of measurements. Shea and Smart (1975) determined the theoretical cosmic ray equator for Epochs 1965.0 and 1975.0 and, in comparing these results with the equator location calculated using the Epoch 1955.0 geomagnetic field coefficients, concluded that the location of the cosmic ray equator had indeed shifted northward in the longitude range 280° to 350°E and compared favorably with the experimental results of Sporre and Pomerantz. In this paper we determine the location of the cosmic ray equator using the IGRF Epoch 1980.0 geomagnetic field coefficients (Peddie, 1982) to ascertain if this northward shift in the location of the cosmic ray equator is still present.

## 2. Method

Using the trajectory-tracing technique and the method described by Shea et al. (1965) vertical cutoff rigidities were calculated at intervals of 1° in latitude and 5° in longitude in the region of the cosmic ray equator. These calculations were made for approximately 10 discrete latitudes at each longitude centered around the location of the equator determined for 1975.0. Since these calculations were in the equatorial region it was not necessary to correct for the cosmic ray penumbra. The location of the cosmic ray equator was determined by a least squares fit to the vertical cutoff rigidities along each longitudinal meridian.

## 3. Results and Discussion

The latitude of the cosmic ray equator for each 5° longitudinal meridian is given in Table 1. The latitude is given to the nearest 0.1 degree as determined from a least squares fit to the data. The corresponding vertical cutoff rigidity for this latitude was also determined from the least squares fit.

This location of the cosmic ray equator for Epoch 1980.0 was then compared with the location of the cosmic ray equator determined for Epoch 1955.0. For this comparison, the latitude of the cosmic ray equator for Epoch 1955.0 was determined in exactly the same manner using the vertical cutoff rigidity calculations as given by Shea et al. (1974) for approximately 10 discrete latitudes roughly centered about the equator. The location of each of these cosmic ray equators is shown in Figure 1.

As can be seen from Figure 1, the location of the cosmic ray equator for Epoch 1980.0 has shifted northward by a significant amount (i.e. more

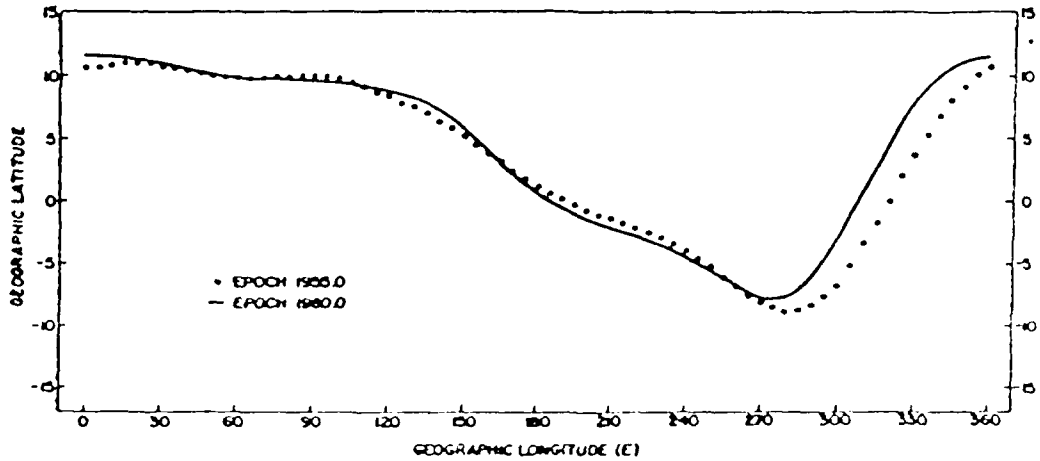


Figure 1. The location of the cosmic ray equator as calculated for Epoch 1955.0 (dots) and Epoch 1980.0 (solid line).

Table 1.
The Geographic Latitude of the Location of the
Cosmic Ray Equator each 5° in Longitude as Calculated for Epoch 1980.0

| GEOG. LON | GEOG. LAT | $R_C$ (GV) | GEOG. LON | GEOG. LAT | $R_C$ (GV) | GEOG. LON | GEOG. LAT | $R_C$ (GV) | GEOG. LON | GEOG. LAT | $R_C$ (GV) |
|---|---|---|---|---|---|---|---|---|---|---|---|
| 0 | 11.6 | 14.71 | 90 | 9.6 | 17.57 | 180 | .7 | 15.53 | 270 | -7.7 | 13.39 |
| 5 | 11.6 | 14.88 | 95 | 9.6 | 17.59 | 185 | -.0 | 15.44 | 275 | -7.9 | 13.24 |
| 10 | 11.5 | 15.04 | 100 | 9.4 | 17.56 | 190 | -.6 | 15.35 | 280 | -7.6 | 13.10 |
| 15 | 11.4 | 15.20 | 105 | 9.3 | 17.51 | 195 | -1.0 | 15.25 | 285 | -7.0 | 13.01 |
| 20 | 11.3 | 15.36 | 110 | 9.1 | 17.42 | 200 | -1.4 | 15.15 | 290 | -6.0 | 12.95 |
| 25 | 11.2 | 15.52 | 115 | 8.9 | 17.30 | 205 | -1.8 | 15.06 | 295 | -4.5 | 12.95 |
| 30 | 11.0 | 15.67 | 120 | 8.8 | 17.16 | 210 | -2.0 | 14.96 | 300 | -2.9 | 13.00 |
| 35 | 10.8 | 15.83 | 125 | 8.5 | 17.00 | 215 | -2.4 | 14.85 | 305 | -1.0 | 13.09 |
| 40 | 10.6 | 15.99 | 130 | 8.2 | 16.83 | 220 | -2.7 | 14.75 | 310 | .9 | 13.21 |
| 45 | 10.3 | 16.17 | 135 | 7.8 | 16.65 | 225 | -3.0 | 14.64 | 315 | 2.8 | 13.35 |
| 50 | 10.1 | 16.36 | 140 | 7.3 | 16.48 | 230 | -3.4 | 14.52 | 320 | 4.7 | 13.50 |
| 55 | 9.9 | 16.55 | 145 | 6.6 | 16.31 | 235 | -3.8 | 14.41 | 325 | 6.6 | 13.65 |
| 60 | 9.8 | 16.75 | 150 | 5.8 | 16.15 | 240 | -4.3 | 14.28 | 330 | 7.8 | 13.80 |
| 65 | 9.7 | 16.95 | 155 | 5.0 | 16.01 | 245 | -4.8 | 14.15 | 335 | 9.2 | 13.95 |
| 70 | 9.8 | 17.13 | 160 | 4.1 | 15.89 | 250 | -5.5 | 14.02 | 340 | 10.0 | 14.10 |
| 75 | 9.8 | 17.29 | 165 | 3.2 | 15.79 | 255 | -6.1 | 13.87 | 345 | 10.7 | 14.25 |
| 80 | 9.7 | 17.42 | 170 | 2.3 | 15.70 | 260 | -6.7 | 13.71 | 350 | 11.2 | 14.40 |
| 85 | 9.7 | 17.52 | 175 | 1.5 | 15.61 | 265 | -7.3 | 13.55 | 355 | 11.4 | 14.56 |

than 1° in latitude) between longitudes 280°E to 360°E. The maximum shift of slightly more than 4° in latitude is found between longitudes 310°E and 325°E. This northward shift is consistent with the equatorial positions calculated using Epoch 1965.0 and 1975.0 and represents a maximum shift of approximately 0.16° per year - clearly measurable by latitude surveys conducted over an interval of several years. All other differences in the location of the cosmic ray equator are less than 1° in latitude, and would not likely be measurable by latitude surveys.

In addition to changes in the location of the cosmic ray equator, the vertical cutoff rigidity along the equator has also changed. Minor increases, less than 0.07 GV, were calculated between longitudes 330°E and 35°E. Significant decreases in the vertical cutoff rigidity (i.e. changes more than 0.2 GV) were calculated between longitudes 160°E and 305°E with a maximum decrease of 0.51 GV at 275°E. These decreases are consistent with the decreases noted in the world grid of vertical cutoff rigidities for Epoch 1980.0 (Shea and Smart, 1983).

## 4. Conclusions

The location of the cosmic ray equator, as determined by the trajectory-tracing method, has consistently shifted in a northerly direction for the past 25 years between longitudes 280°E to 360°E, with a maximum shift of ~ 0.16° per year. This change in equatorial location should be measurable by latitude surveys conducted in this longitudinal region.

## References

Peddie, N.W., (1982), PAGEOPH, 120, p. 197.
Shea, M.A., (1969), J. Geophys. Res., 74, p. 2407.
Shea, M.A., and D.F. Smart, (1975), 14th ICRC, Conference Papers, 4, p. 1294.
Shea, M.A., and D.F. Smart, (1983), Paper MG10-3, this conference.
Shea, M.A., D.F. Smart, and J.F. Kenney, (1964), J. Geophys. Res., 69, p. 4162.
Shea, M.A., D.F. Smart, and K.G. McCracken, (1965), J. Geophys. Res., 70, p. 4117.
Shea, M.A., D.F. Smart, J.R. McCall, and B.S. Gumm, (1974), AFCRL-TR-74-0550, ADA006677.
Sporre, B., and M. Pomerantz, (1969), Proc. 11th Int. Conf. on Cosmic Rays, Budapest, Acta Physica Academiae Scientiarum Hungaricae, 29, Suppl. 2, p. 545.

Reprint from 18th International Cosmic Ray Conference, Conference Papers, 3, 411-414, 1983.



# VERTICAL CUTOFF RIGIDITIES FOR SELECTED COSMIC RAY STATIONS FOR EPOCH 1980.0

M.A. Shea and D.F. Smart
Air Force Geophysics Laboratory, Hanscom AFB, Bedford, MA 01731, U.S.A.

L. C. Gentile
Emmanuel College, 400 The Fenway, Boston, MA 02115, U.S.A.

ABSTRACT

Using the trajectory-tracing technique and the new 1980.0 geomagnetic field model, vertical cutoff rigidities have been calculated for 98 cosmic ray stations and these values are compared with those calculated using earlier Epochs of the geomagnetic field. In general there are significant decreases in vertical cutoff rigidities in the Mexico, Central American and South American areas; significant increases are noted in Japan. Some of these changes are of such magnitude as to be measurable over a period of several years.

## 1. Introduction

Using the trajectory-tracing method and the International Geomagnetic Reference Field model for Epoch 1980.0 (Peddie, 1982), vertical cutoff rigidities for 98 locations have been calculated. These locations, indicated by dots in Figure 1, include all cosmic ray stations believed to be presently operating as well as some locations from which cosmic ray balloon experiments are launched. In addition some locations where cosmic ray equipment previously operated are included.

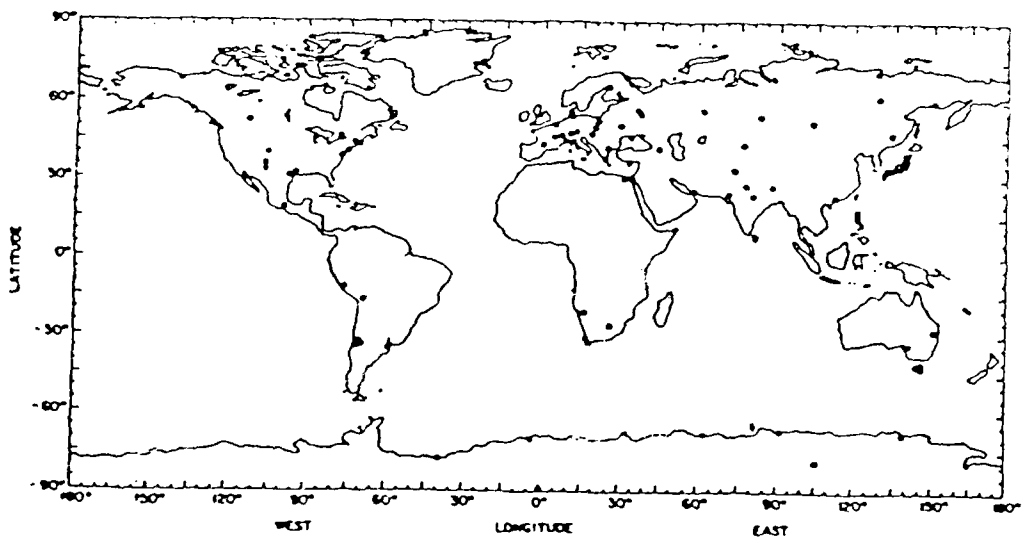


Figure 1. World map illustrating cosmic ray station locations (dots) for which vertical cutoff rigidities have been calculated using the IGRF 1980.0 geomagnetic field coefficients.

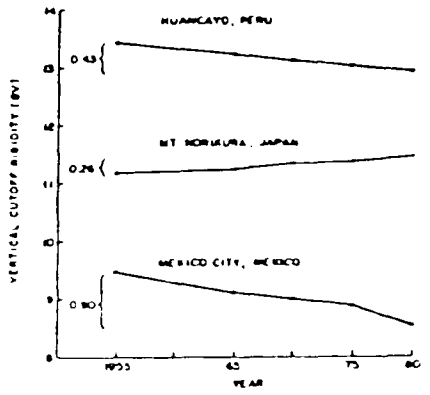


Fig. 2. Vertical cutoff rigidities for three locations for various Epochs. The change in cutoff rigidity (in GV) is indicated by the brackets.

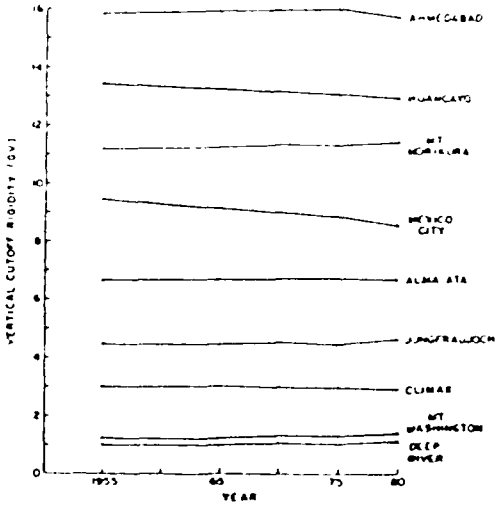


Fig. 3. Vertical cutoff rigidities for selected locations for various Epochs.

## 2. Method

The trajectory-tracing technique was used to calculate the effective vertical cutoff rigidity for each of these locations. All calculations were made for an altitude of 20 km; the technique and procedure for determining the effective vertical cutoff rigidity are summarized by Shea and Smart (1983). The only significant difference between the method used for these calculations and the method used for previous calculations is that we have specified the "vertical" direction as a geodetic vertical rather than along a geocentric radial direction. This results in a maximum difference of ~0.2 degrees between the geodetic vertical direction and a geocentric radial direction, with the maximum at mid-latitude locations.

## 3. Results

The effective vertical cutoff rigidity values calculated for the 98 cosmic ray station locations are given in Table 1. In comparing these results with those calculated for previous Epochs (Shea et al , 1976) we find that in general the vertical cutoff rigidities are decreasing in Latin and South America, in Southern Africa and in India; increases are noted in Europe and Japan.

## 4. Discussion

The major changes over the past 25 years are attributed to changes in the geomagnetic field itself. Some of the major changes over this time period are illustrated in Figure 2 showing decreasing vertical cutoff rigidity at Huancayo and Mexico City and increasing vertical cutoff rigidity at Mt. Norikura. To put these changes in their proper perspective, Figure 3 illustrates the vertical cutoff rigidity changes at these three stations as well as at selected locations in other parts of the world.

TABLE 1. VERTICAL CUTOFF RIGIDITIES FOR SELECTED COSMIC RAY STATIONS (EPOCH 1980.0)

| STATION NAME | GEOGRAPHIC LAT | GEOGRAPHIC LON | $R_C$ (GV) | STATION NAME | GEOGRAPHIC LAT | GEOGRAPHIC LON | $R_C$ (GV) |
|---|---|---|---|---|---|---|---|
| Ahmedabad | 23.01 | 72.61 | 15.77 | Matsumoto | 36.23 | 138.00 | 11.38 |
| Alert | 82.50 | 297.67 | 0.00 | Mawson | -67.60 | 62.88 | 0.20 |
| Aligarh | 27.91 | 78.07 | 14.65 | McMurdo | -77.85 | 166.72 | 0.00 |
| Alma Ata | 43.20 | 76.94 | 6.72 | Mexico City | 19.33 | 260.82 | 8.56 |
| Apatity | 67.55 | 33.33 | 0.61 | Mildura | -34.23 | 142.22 | 4.11 |
| Athens | 37.97 | 23.72 | 8.65 | Mirny | -66.55 | 93.00 | 0.03 |
| Belsk | 51.83 | 20.80 | 3.13 | Misato | 36.20 | 137.83 | 11.40 |
| Bologna | 44.50 | 11.33 | 5.28 | Mont Blanc | 45.80 | 4.52 | 4.66 |
| Brisbane | -27.50 | 153.01 | 7.02 | Morikura | 39.70 | 141.13 | 10.23 |
| Budapest | 47.50 | 18.90 | 4.43 | Moscow | 55.47 | 37.32 | 2.41 |
| Buenos Aires | -34.58 | 301.50 | 9.71 | Moscow University | 55.73 | 37.63 | 2.30 |
| Cairo | 30.03 | 31.15 | 12.10 | Mt. Morikura | 36.12 | 137.56 | 11.44 |
| Calgary | 51.08 | 245.91 | 1.09 | Mt. Washington | 44.30 | 288.70 | 1.43 |
| Cambridge Tunnel | -42.85 | 147.42 | 1.88 | Mt. Wellington | -42.92 | 147.24 | 1.80 |
| Cape Town | -33.93 | 18.47 | 4.65 | Murmansk | 68.97 | 33.08 | 0.48 |
| Chacaltaya | -16.31 | 291.85 | 12.53 | Mussala | 42.18 | 25.58 | 6.33 |
| Climax | 39.37 | 253.82 | 2.95 | Nagoya | 35.01 | 136.90 | 12.14 |
| College Station | 30.63 | 263.65 | 4.62 | Newark | 39.68 | 284.25 | 2.10 |
| Darjeeling | 27.03 | 88.33 | 15.12 | Norilsk | 69.26 | 88.05 | 0.59 |
| Darwin | -12.42 | 130.87 | 14.09 | Novosibirsk | 54.80 | 83.00 | 2.84 |
| Deep River | 46.10 | 282.50 | 1.15 | Oulu | 65.00 | 25.42 | 0.78 |
| Dourbes | 50.10 | 4.60 | 3.34 | Palestine | 31.75 | 264.35 | 4.43 |
| Dumont Durville | -66.67 | 140.02 | 0.00 | Pic du Midi | 42.93 | 0.25 | 5.64 |
| Durham | 43.10 | 289.16 | 1.61 | Poatina | -41.62 | 146.88 | 2.08 |
| El Infiernillo | -33.17 | 289.72 | 10.61 | Potchefstroom | -26.70 | 27.10 | 6.94 |
| Embudo | 35.20 | 253.59 | 4.25 | Predigtstuhl | 47.70 | 12.88 | 4.37 |
| Fredericksburg | 38.30 | 282.50 | 2.31 | Rewa | 24.32 | 81.24 | 15.71 |
| Fukushima | 37.75 | 140.48 | 10.59 | Rome | 41.90 | 12.52 | 6.31 |
| Goose Bay | 53.33 | 299.58 | 0.61 | Sakashita | 35.58 | 137.53 | 11.77 |
| Grand Canyon Caverns | 35.53 | 246.58 | 4.61 | Sanae | -70.30 | 357.65 | 0.86 |
| Gulmarg | 34.07 | 74.42 | 11.59 | San Jose dos Campos | -23.23 | 314.15 | 10.90 |
| Hermanus | -34.42 | 19.22 | 4.55 | Sapporo | 43.08 | 141.35 | 8.28 |
| Hobart | -42.90 | 147.33 | 1.85 | Simferopol | 44.73 | 34.00 | 5.40 |
| Hong Kong | 22.42 | 114.20 | 16.11 | Socorro | 34.04 | 253.44 | 4.51 |
| Huancayo | -12.05 | 284.67 | 12.91 | South Pole | -89.98 | 0.00 | 0.09 |
| Inuvik | 68.35 | 226.27 | 0.16 | Swerdlovsk | 56.73 | 61.07 | 2.23 |
| Irkutsk | 52.47 | 104.03 | 3.63 | Sydney | -33.60 | 151.10 | 4.53 |
| Jungfraujoch | 46.55 | 7.98 | 4.63 | Takeyama | 35.22 | 139.62 | 11.97 |
| Kerguelen Island | -49.35 | 70.22 | 1.14 | Tashkent | 41.33 | 69.62 | 7.48 |
| Khabarovsk | 48.50 | 135.20 | 5.45 | Tbilisi | 41.72 | 44.80 | 6.74 |
| Kiel | 54.33 | 10.13 | 2.33 | Thule | 76.55 | 291.16 | 0.00 |
| Kiev | 50.72 | 30.30 | 3.57 | Tixie Bay | 71.55 | 128.90 | 0.45 |
| Kochi | 33.57 | 133.55 | 12.99 | Tokyo-Itabashi | 35.75 | 139.72 | 11.61 |
| Koenji | 35.71 | 139.64 | 11.63 | Tsumeb | -19.20 | 17.58 | 9.15 |
| Leeds | 53.82 | 358.45 | 2.25 | Turin | 45.07 | 7.67 | 5.01 |
| Lomnicky Stit | 49.20 | 20.22 | 4.00 | Uccle | 50.80 | 4.36 | 3.13 |
| Los Cerrillos | -33.50 | 289.30 | 10.57 | Vostok | -78.47 | 106.87 | 0.00 |
| Macul Station | -33.45 | 289.40 | 10.59 | Yakutsk | 62.02 | 129.72 | 1.65 |
| Magadan | 60.11 | 151.01 | 2.10 | Zugspitze | 47.42 | 10.98 | 4.36 |

The discontinuity noticeable for some stations at 1975 is a result of an undercorrection of the projected secular drift assigned to the original IGRF Epoch 1965.0 coefficients. Magnetic field data obtained in the last decade have shown that the observed secular changes in the geomagnetic field were, in general, larger in the forward direction than those predicted using the initial IGRF time derivatives in 1965.

Although the absolute accuracy of the 1975 vertical cutoff rigidities may be suspect, the general trend of the rigidity values is real. At the 12th ICRC Shea (1971) suggested that large decreases in the vertical cutoff rigidity for stations such as Huancayo should be measurable from neutron monitor measurements provided that the monitor itself was stable over an extended period and provided that the modulated cosmic ray intensity returned to the same value (such as similar solar minimum conditions). Cooper and Simpson (1979) later found it was necessary to correct the Huancayo long term neutron monitor data for vertical cutoff rigidity changes in their analysis of the magnetic rigidity dependence due to the ~ 11-year large scale solar modulation.

Using the vertical cutoff rigidity values calculated for Epoch 1980 and those calculated for Epoch 1955, we find that the counting rate of a neutron monitor at Huancayo should have increased by 1.9% and the counting rate of a neutron monitor at Mt. Norikura should have decreased by 1.1% over this 25-year period assuming that the galactic cosmic ray intensity returns to similar levels over the time interval.

## 5. Conclusions

Vertical cutoff rigidities for cosmic ray stations using the International Geomagnetic Reference Field for Epoch 1980 have been determined by the trajectory-tracing method. Significant changes between the vertical cutoff rigidities calculated using Epoch 1975 field coefficients and those calculated using Epoch 1980 field coefficients have been found for some locations. Specifically, decreases in vertical cutoff rigidities were calculated for Central and South America, South Africa and India; increases were calculated in Europe and Japan. However, long term changes, i.e. those between 1955 and 1980, are present, and these changes are the direct result of secular changes in the geomagnetic field. If stable neutron monitors were located at places where there are significant changes in the vertical cutoff rigidity, such as at Huancayo, Mexico City and Mt. Norikura, they should detect a change in long term counting rate as a direct consequence of the change in vertical cutoff rigidity.

## References

Cooper, J.F., and J.A. Simpson, (1979), 16th ICRC, Conference Papers, 12, p. 176.
Peddie, N. W., (1982), PAGEOPH, 120, p. 197.
Shea, M.A., (1971), 12th ICRC, Conference Papers, 3, p. 859.
Shea, M.A., and D.F. Smart, (1983), Paper MG10-3, this conference.
Shea, M.A., D.F. Smart, and H. Carmichael, (1976), AFGL-TR-76-0115, ADA028978.

JOURNAL OF GEOPHYSICAL RESEARCH, VOL. 92, NO. A3, PAGES 2551–2554, MARCH 1, 1987

# On the Correlation Between Asymptotic Directions of Cosmic Ray Particles and Cutoff Rigidities in the Evolving Geomagnetic Field

E. O. FLÜCKIGER

*Physikalisches Institut, Universität Bern, Switzerland*

D. F. SMART AND M. A. SHEA

*Air Force Geophysics Laboratory, Hanscom Air Force Base, Bedford, Massachusetts*

L. C. GENTILE

*Emmanuel College, Boston, Massachusetts*

The concept of geomagnetic optics, as described by the asymptotic directions of approach, is extremely useful in the analysis of cosmic radiation data. However, when changes in cutoff rigidities occur as a result of evolution in the geomagnetic field, there are corresponding changes in the asymptotic cones of acceptance. It has been demonstrated that the effect of geomagnetic disturbances on asymptotic directions of approach can be estimated for nonpolar locations from the corresponding change in the cutoff rigidity. In this paper we show that the same procedure is applicable with respect to the secular evolution in the geomagnetic field, and that with this procedure it is possible to adjust reference published asymptotic directions to other epochs if the change in cutoff rigidity is known.

## 1. INTRODUCTION

Cosmic ray particles reaching a location on or near the earth travel along specific allowed trajectories through the geomagnetic field. In order to relate cosmic ray intensity variations observed by the worldwide network of cosmic ray stations to the cosmic ray flux in space the concept of asymptotic directions of approach was developed (see *McCracken et al.* [1968] for a review). Using the asymptotic directions of approach one can relate any specific cosmic ray particle arrival direction with a unique direction in space. For a cosmic ray particle with rigidity $R$, arriving at a specific location (characterized by the geographic latitude, $\Lambda$, and the geographic longitude, $\Phi$) from a direction of incidence (described by the zenith angle $\theta$ and the azimuthal angle $\phi$) the asymptotic direction of approach is given by the unit vector $\mathbf{A}(R, \Lambda, \Phi, \theta, \phi)$ pointing in the reverse direction to the particle's velocity vector prior to the particle's entry into the geomagnetic field. The vector $\mathbf{A}$ is specified in the geocentric coordinate system as asymptotic latitude, $\lambda(R)$, and asymptotic longitude, $\psi(R)$. Only vertical arrival directions are considered here.

The rigidity spectrum of cosmic ray particles arriving from a specific direction at any location in the geomagnetic field contains distinct fiducial marks. The exact rigidity values of these fiducial marks are in general determined by the arduous and computer intensive process of numerical simulation of cosmic ray trajectories. In this paper we refer to $R_1$ as the rigidity associated with the first discontinuity in asymptotic direction occurring when progressively lower rigidities are considered. The value of $R_1$ is always greater than or equal to the lowest rigidity at and above which all trajectory calculations yield allowed orbits. (For a detailed definition see, for example, *Cooke et al.* [1985].) The significance of $R_1$ is that the cosmic ray trajectories corresponding to rigidities larger than $R_1$ have a similar structure that facilitates comparisons between different configurations of the geomagnetic field.

*Flückiger et al.* [1983*a*, *b*, 1986] have shown that geomagnetic disturbances affect the cutoff rigidities in a predictable manner dependent on the strength and longitudinal structure of the magnetic perturbation and on the longitudinal difference between the magnetic perturbation and the observing location. Furthermore, the changes in asymptotic latitude and longitude (down to the first discontinuity) also behave in a similarly predictable manner. Therefore the asymptotic directions of approach during perturbed geomagnetic conditions can be deduced with considerable accuracy from the asymptotic directions computed using the quiescent geomagnetic field if the associated change in cutoff rigidity is known.

For secular changes in the geomagnetic field it is possible to estimate the changes in cutoff rigidity from parameters that are more easily computed than cutoff rigidities, such as the $L$ parameter [*McIlwain*, 1961]. *Smart and Shea* [1967] showed that this parameter is well-correlated with the cutoff rigidity and *Shea et al.* [1985] demonstrated that the change in the L parameter is closely associated with the change in the geomagnetic cutoff. In this paper we show that the concept of deducing the asymptotic directions from a known reference set can also be applied to changes resulting from the secular evolution of the geomagnetic field.

## 2. GENERAL CONCEPT

In order to describe changes in the asymptotic directions we have defined the terms $\Delta\lambda^*(R) = \lambda'(R) - \lambda(R - \Delta R_1)$ and

$$\Delta\psi^*(R) = \psi'(R) - \psi(R - \Delta R_1)$$

where $\Delta R_1 = R_1' - R_1$ represents the change in vertical cutoff rigidity, and where the primed values refer to the evolved or perturbed geomagnetic field and the unprimed values refer to the reference geomagnetic field. For geomagnetic disturbances



Paper number 6A8615.
0148-0227/87/006A-8615$02.00

TABLE I. Comparison (According to Equation (2)) of Asymptotic Longitudes Calculated for Epochs 1965.0 and 1980.0

| | Geographic Latitude, deg | Geographic Longitude, deg | 1965 $R_1$, GV | Asymptotic Longitude for Epoch 1965 | | | | | | 1980 $R_1$, GV | $\Delta R_1$, GV | Asymptotic Longitude for Epoch 1980 | | | | | |
|---|---|---|---|---|---|---|---|---|---|---|---|---|---|---|---|---|---|
| | | | | $\delta R$ = 0.0 GV | $\delta R$ = 0.1 GV | $\delta R$ = 0.2 GV | $\delta R$ = 0.5 GV | $\delta R$ = 0.75 GV | $\delta R$ = 1.0 GV | | | $\delta R$ = 0.0 GV | $\delta R$ = 0.1 GV | $\delta R$ = 0.2 GV | $\delta R$ = 0.5 GV | $\delta R$ = 0.75 GV | $\delta R$ = 1.0 GV |
| Ahmedabad, India | 23.01 | 72.61 | 15.92 | 406 | 336 | 311 | 276 | 260 | 248 | 15.78 | −0.14 | 394 | 333 | 310 | 275 | 259 | 247 |
| Alma Ata, USSR | 43.20 | 76.94 | 6.93 | 396 | 319 | 295 | 261 | 245 | 234 | 6.82 | −0.11 | 375 | 313 | 291 | 258 | 243 | 232 |
| Brisbane, Australia | −27.50 | 153.01 | 7.42 | 481 | 405 | 385 | 354 | 337 | 325 | 7.18 | −0.24 | 466 | 401 | 382 | 351 | 334 | 322 |
| Buenos Aires, Argentina | −34.58 | 301.50 | 10.61 | 627 | 545 | 519 | 484 | 470 | 459 | 10.13 | −0.48 | 600 | 539 | 514 | 481 | 467 | 456 |
| Chacaltaya, Bolivia | −16.31 | 291.85 | 12.87 | 618 | 547 | 522 | 488 | 472 | 460 | 12.55 | −0.32 | 597 | 541 | 518 | 485 | 469 | 458 |
| Deep River, Canada | 46.10 | 282.50 | 1.19 | 530 | 449 | 423 | 393 | 378 | 368 | 1.30 | 0.11 | 507 | 449 | 427 | 399 | 381 | 373 |
| Dourbes, Belgium | 50.10 | 4.60 | 3.44 | 298 | 224 | 200 | 167 | 153 | 141 | 3.54 | 0.10 | 282 | 225 | 203 | 169 | 153 | 141 |
| Durham, United States | 43.10 | 289.16 | 1.69 | 557 | 475 | 443 | 418 | 400 | 389 | 1.84 | 0.15 | 531 | 472 | 453 | 421 | 404 | 397 |
| Gulmarg, India | 34.07 | 74.42 | 12.35 | 404 | 332 | 309 | 274 | 257 | 244 | 12.20 | −0.15 | 392 | 329 | 307 | 273 | 256 | 244 |
| Hermanus, South Africa | −34.42 | 19.22 | 5.06 | 307 | 239 | 215 | 180 | 166 | 156 | 4.83 | −0.23 | 287 | 233 | 210 | 177 | 163 | 154 |
| Huancayo, Peru | −12.05 | 284.67 | 13.25 | 626 | 544 | 520 | 494 | 467 | 455 | 12.94 | −0.31 | 596 | 538 | 515 | 481 | 465 | 453 |
| Mexico City, Mexico | 19.33 | 260.82 | 10.24 | 617 | 515 | 494 | 458 | 436 | 423 | 9.91 | −0.33 | 587 | 514 | 494 | 459 | 437 | 424 |
| Mildura, Australia | −34.23 | 142.22 | 4.59 | 457 | 379 | 357 | 312 | 293 | 280 | 4.38 | −0.21 | 429 | 376 | 356 | 314 | 295 | 282 |
| Mt. Washington, United States | 44.30 | 288.70 | 1.50 | 526 | 459 | 442 | 408 | 398 | 384 | 1.63 | 0.13 | 546 | 482 | 446 | 417 | 401 | 388 |
| Pic du Midi, France | 42.93 | 0.25 | 5.61 | 294 | 228 | 204 | 169 | 153 | 143 | 5.76 | 0.15 | 280 | 227 | 204 | 170 | 155 | 144 |
| Potchefstroom, South Africa | −26.70 | 27.10 | 7.72 | 346 | 270 | 245 | 206 | 189 | 178 | 7.49 | −0.23 | 320 | 264 | 241 | 203 | 187 | 176 |
| Sydney, Australia | −33.60 | 151.10 | 5.19 | 447 | 381 | 355 | 314 | 297 | 285 | 5.04 | −0.15 | 434 | 380 | 355 | 314 | 297 | 285 |
| Tbilisi, USSR | 41.72 | 44.80 | 7.00 | 357 | 287 | 265 | 233 | 217 | 206 | 6.88 | −0.12 | 344 | 283 | 262 | 231 | 215 | 204 |
| World Grid | 30.00 | 315.00 | 6.72 | 634 | 576 | 556 | 526 | 510 | 498 | 7.92 | 1.20 | 648 | 583 | 562 | 530 | 512 | 498 |
| World Grid | 35.00 | 315.00 | 5.06 | 590 | 539 | 514 | 478 | 463 | 453 | 5.43 | 0.37 | 595 | 544 | 521 | 487 | 472 | 463 |
| World Grid | 40.00 | 315.00 | 3.50 | 598 | 546 | 525 | 492 | 476 | 463 | 4.13 | 0.63 | 606 | 552 | 528 | 484 | 465 | 451 |
| World Grid | 45.00 | 315.00 | 2.34 | 571 | 516 | 496 | 468 | 450 | 434 | 2.69 | 0.35 | 596 | 539 | 509 | 462 | 444 | 434 |
| World Grid | 30.00 | 300.00 | 5.12 | 575 | 524 | 499 | 463 | 448 | 438 | 5.42 | 0.30 | 582 | 530 | 507 | 471 | 457 | 447 |
| World Grid | 35.00 | 300.00 | 3.73 | 599 | 540 | 519 | 479 | 458 | 444 | 4.30 | 0.57 | 592 | 533 | 507 | 464 | 446 | 433 |
| World Grid | 40.00 | 300.00 | 2.56 | 569 | 522 | 498 | 452 | 431 | 418 | 2.93 | 0.37 | 570 | 507 | 477 | 442 | 430 | 423 |

The table refers to cosmic ray particles with vertical direction of incidence and includes locations where the absolute change in geomagnetic cutoff rigidity, $|\Delta R_1|$, between 1965 and 1980 is greater than or equal to 0.1 GV. For details, see text.

*Flückiger et al.* [1983*b*, 1986] found that $\Delta\lambda^* \approx 0°$ for low, middle and high (but not polar) latitudes. For $\Delta\psi^*$ only small values on the order of several degrees were found down to rigidities approaching the value of $R_1'$. We describe the correspondence between the asymptotic directions in any evolved geomagnetic field and the asymptotic directions in a reference geomagnetic field by

$$\lambda'(R) = \lambda(R - \Delta R_1) + \Delta\lambda^*(R) \quad (1)$$

and

$$\psi'(R) = \psi(R - \Delta R_1) + \Delta\psi^*(R) \quad (2)$$

The residuals $\Delta\lambda^*(R)$ and $\Delta\psi^*(R)$ are discussed in the next section. It turns out that for nonpolar locations and for rigidities from the value of $R_1'$ up to several GV above this value $\Delta\lambda^*(R)$ is approximately zero and that $\Delta\psi^*(R)$ is, in general, on the order of a few degrees.

At rigidities below $R_1'$ no similar relations have been found, although coherent clusters of trajectories may be distorted uniformly by magnetic changes. It has been shown that the main features of allowed and forbidden regions in the penumbra are conserved to a certain extent in a perturbed geomagnetic field [*Flückiger et al.*, 1979; *Flückiger*, 1982]. However, the asymptotic longitudes of the allowed trajectories of the fine detailed structure in the cosmic ray penumbra continue to be quasi-random.

## 3. Application

We have compared the asymptotic directions for cosmic ray stations and world grid locations calculated by the trajectory-tracing method [*McCracken et al.*, 1965] for the International Geomagnetic Reference Field epoch 1980.0 [*Peddie*, 1982] with those calculated for epoch 1965.0 [*IAGA Commission 2*, 1969]. We would expect a close correspondence between the asymptotic directions above the rigidity of the first discontinuity according to equations (1) and (2). In Table 1 we illustrate the comparison for locations where the absolute change in geomagnetic cutoff rigidity, $\Delta R_1$, between 1965 and 1980 is greater than or equal to 0.1 GV. Referring to equation (2) the asymptotic longitudes in this table are given for the rigidities $R = R_1 + \delta R$ for epoch 1965.0 and for $R = R_1' + \delta R$ for epoch 1980.0, with $\delta R = 0.0$, 0.1, 0.2, 0.5, 0.75 and 1.0 GV. An inspection of the table indicates that corresponding asymptotic longitudes for the specified rigidity values are quite similar. The differences have to be related to the absolute changes in asymptotic longitude for a given rigidity which at many locations are more than 100° near the value of $R_1$ (or $R_1'$ if $R_1' > R_1$).

Figure 1 shows, as a function of $\delta R$, the arithmetic mean of the absolute values of the residuals in asymptotic latitude, $|\overline{\Delta\lambda^*(\delta R)}|$, obtained by averaging

$$|\Delta\lambda^*(\delta R)| = |\lambda'(R_1' + \delta R) - \lambda(R_1 + \delta R)|$$

for each value of $\delta R$ over all locations in Table 1. The error bars represent the standard deviation of $|\Delta\lambda^*(\delta R)|$ for all stations in Table 1. We indeed find $\Delta\lambda^* \approx 0°$. Figure 2 shows the corresponding results for asymptotic longitude. We find that for the secular variations of the geomagnetic field between 1965 and 1980 the average absolute value of the residuals $\Delta\psi^*$ is on the order of a few degrees, a value which can be neglected in most applications.

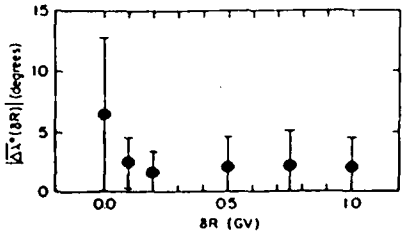


**Fig. 1. Mean of the absolute values of the residuals in asymptotic latitude, $|\overline{\Delta\lambda^*(\delta R)}|$, as a function of $\delta R$, obtained by averaging over all locations in Table 1. The error bars represent the standard deviation of $|\Delta\lambda^*(\delta R)|$ for all stations in Table 1.**

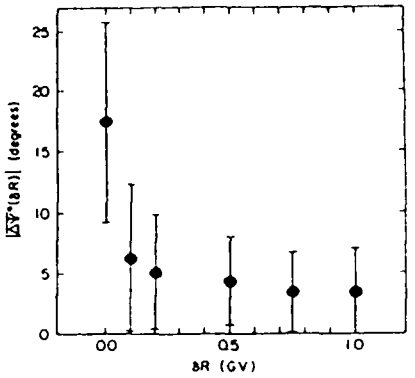


Fig. 2. Mean of the absolute values of the residuals in asymptotic longitude $|\overline{\Delta\psi^*(\delta R)}|$, as a function of $\delta R$, obtained by averaging over all locations in Table 1. The error bars represent the standard deviation of $|\Delta\psi^*(\delta R)|$ for all stations in Table 1.

For a few particular locations (e.g., world grid 45°N, 315°E) the residuals in asymptotic longitude are larger than 15° for $\delta R \geq 0.1$ GV. However, in an analysis, e.g., on pitch angle distributions during a solar particle event, this could have an effect only when the cosmic ray data from these specific locations are essential and when the energy spectrum is very steep.

## 4. Conclusions

We have illustrated that for cosmic ray particles of vertical incidence and for rigidities above the $R_1$ value (corresponding to the first discontinuity in asymptotic direction progressing down through the rigidity scale) the correspondence between asymptotic directions of cosmic ray particles and cutoff rigidities in the evolving geomagnetic field between epochs 1965.0 and 1980.0 is essentially the same as in a perturbed geomagnetic field. For nonpolar locations the asymptotic directions in an evolved geomagnetic field can therefore be obtained from a "known" reference set of asymptotic directions if the change in cutoff rigidity is known.

*Acknowledgments.* The authors wish to acknowledge helpful comments by the referees. E.O.F. acknowledges support by the Swiss National Foundation, grant 2.632-0.85, while L.C.G. acknowledges support from the U.S. Air Force Geophysics Laboratory under contract F19628-82-K-0039.

The Editor thanks H. H. Sauer and G. Wibberenz for their assistance in evaluating this paper.

## References

Cooke, D. J., J. E. Humble, M. A. Shea, D. F. Smart, N. Lund, I. L. Rasmussen, B. Byrnak, P. Goret, and N. Petrou, Re-evaluation of cosmic ray cutoff terminology, *19th Int. Cosmic Ray Conf., Conf. Pap.*, *5*, 328, 1985.

Flückiger, E. O., Effects of asymmetric magnetospheric currents on cosmic radiation, *Rep. AFGL-TR-82-0177*, Air Force Geophys. Lab., Bedford, Mass., 1982.

Flückiger, E., H. Debrunner, D. F. Smart, and M. A. Shea, Calculation of changes in cosmic ray cutoff rigidities due to a partial ring current system in the magnetosphere, *16th Int. Cosmic Ray Conf., Conf. Pap.*, *4*, 273, 1979.

Flückiger, E. O., D. F. Smart, and M. A. Shea, The effect of local perturbations of the geomagnetic field on cosmic ray cutoff rigidities at Jungfraujoch and Kiel, *J. Geophys. Res.*, *88*, 6961, 1983*a*.

Flückiger, E. O., D. F. Smart, and M. A. Shea, Procedure for estimating the change in asymptotic directions at a mid-latitude cosmic ray station resulting from a local change in cosmic ray cutoff rigidity, *18th Int. Cosmic Ray Conf., Conf. Pap.*, *3*, 431, 1983*b*.

Flückiger, E. O., D. F. Smart, and M. A. Shea, A procedure for estimating the changes in cosmic ray cutoff rigidities and asymptotic directions at low and middle latitudes during periods of enhanced geomagnetic activity, *J. Geophys. Res.*, *91*, 7925, 1986.

International Association of Geomagnetism and Aeronomy (IAGA) Commission 2, Working Group 4, International geomagnetic reference field 1965.0, *J. Geophys. Res.*, *74*, 4407, 1969.

McCracken, K. G., U. R. Rao, B. C. Fowler, M. A. Shea, and D. F. Smart, Cosmic ray tables: Asymptotic directions, variational coefficients and cut-off rigidities, *IQSY Instruction Manual 10*, International Quiet Sun Year Committee, London, 1965.

McCracken, K. G., U. R. Rao, B. C. Fowler, M. A. Shea, and D. F. Smart, Cosmic rays, in *Annals of the IQSY*, vol. 1, edited by C. M. Minnis, chap. 14, p. 198, MIT Press, Cambridge, Mass., 1968.

McIlwain, C. E., Coordinates for mapping the distribution of magnetically trapped particles, *J. Geophys. Res.*, *66*, 3681, 1961.

Peddie, N. W., International geomagnetic reference field: The third generation, *J. Geomagn. Geoelectr.*, *34*, 309, 1982.

Shea, M. A., D. F. Smart, and L. C. Gentile, The use of the McIlwain *L*-parameter to estimate cosmic ray vertical cutoff rigidities for different epochs of the geomagnetic field, *19th Int. Cosmic Ray Conf., Conf. Pap.*, *5*, 332, 1985.

Smart, D. F., and M. A. Shea, A study of the effectiveness of the McIlwain coordinates in estimating cosmic-ray vertical cutoff rigidities, *J. Geophys. Res.*, *72*, 3447, 1967.

E. O. Flückiger, Physikalisches Institut, Universität Bern, Sidlerstrasse 5, CH-3012 Bern, Switzerland.

L. C. Gentile, Emmanuel College, 400 The Fenway, Boston, MA 02115.

M. A. Shea and D. F. Smart, Air Force Geophysics Laboratory, Hanscom Air Force Base, Bedford, MA 01731.

(Received June 23, 1986;
revised October 22, 1986;
accepted October 22, 1986.)

JOURNAL OF GEOPHYSICAL RESEARCH, VOL. 90, NO. A7, PAGES 6251–6266, JULY 1, 1985

# Peak Flux Density Spectra of Large Solar Radio Bursts and Proton Emission From Flares

E. W. CLIVER

*Air Force Geophysics Laboratory, Hanscom Air Force Base, Massachusetts*

L. F. MCNAMARA

*Ionospheric Prediction Service, Darlinghurst, New South Wales, Australia*

L. C. GENTILE

*Emmanuel College, Boston, Massachusetts*

We have reexamined the relationship between "U-shaped" peak flux density microwave spectra and solar proton events for ~200 large ($Sp$ ($\geq$2 GHz) $\geq$ 800 solar flux units (sfu)) microwave bursts (1965–1979). The radio spectra fell into two basic classes: U-shaped, with two maxima ($\geq$800 sfu) in the range from 200 MHz to $\geq$10 GHz (59% of all events), and cutoff spectra, with a maximum $\geq$800 sfu at $f \geq 2$ GHz and $Sp$ (200 MHz) < 100 sfu (18%). Nine percent of the events had "intermediate" spectra with a maximum $\geq$800 sfu at $f \geq 2$ GHz and 100 sfu $\leq Sp$ (200 MHz) < 800 sfu. We were unable to classify 15% of the events because of incomplete data. The associations of the three classes of spectra with type II (and /or type IV) meter wavelength bursts and >10-MeV proton events of any size ($\geq$0.01 protons cm$^{-2}$ s$^{-1}$ sr$^{-1}$) are as follows: U-shaped: type II/IV (90% of large microwave bursts with U-shaped spectra are associated with type II/IV events), protons (77%); intermediate: type II/IV (78%), protons (73%), and cutoff: type II/IV (22%), protons (33%). These statistics affirm various lines of evidence linking coronal shock waves and interplanetary proton events. They also suggest that the meter wavelength branch of the U-shaped spectrum may be attributable to second-phase (versus flash phase) accelerated electrons. We have examined this latter supposition and find that it cannot be true in general. In our sample a type II event was in progress at the time of the peak of the low-frequency branch for only about half of the bursts with U-shaped spectrum (U bursts). For these events we cannot rule out a possible contribution to the peak 200-MHz flux from either the second harmonic of the type II burst or from flare continuum of the type FC II, provided that the starting frequency of the fundamental type II burst is $\gtrsim$100 MHz. The low-frequency branch of the U burst appears to be more closely related to impulsive phase type III emission. We note that the small sample of U bursts that lacked type II/IV association is also poorly associated with proton events. We conclude that the observed association between U bursts and proton events probably results from the big flare syndrome rather than a close physical link between these two phenomena. If the current National Oceanic and Atmospheric Administration prediction threshold of $J$ (>10 MeV) $\geq$ 10 protons cm$^{-2}$ s$^{-1}$ sr$^{-1}$ had been in effect during the period covered by our data base (1965–1979), the U burst "yes or no" forecast tool would have had a false alarm rate of 50–70% and would have failed to provide warning for 40–50% of the significant prompt proton events attributable to disk flares. We note that several (eight of 46) of the prompt proton events with $J$ (>10 MeV) $\geq$ 10 protons cm$^{-2}$ s$^{-1}$ sr$^{-1}$ observed from 1965 to 1979 originated in flares that had relatively weak ($\leq$300 sfu) burst emission at 200 MHz.

## 1. INTRODUCTION

*Castelli et al.* [1967] proposed that the "U-shaped" peak flux density radio spectrum with high flux densities ($\gtrsim$1000 solar flux units (1 sfu = $10^{-22}$ W m$^{-2}$ Hz$^{-1}$)) at meter and centimeter wavelengths and a minimum in the decimeter range is the "preferred spectrum" for major solar proton flares. This concept was investigated in a series of papers by Castelli and his coworkers [*Castelli*, 1968; *O'Brien*, 1970; *Castelli and Guidice*, 1972; *Castelli and Barron*, 1977; *Castelli and Tarnstrom*, 1978]. In the initial reports on this topic [*Castelli et al.*, 1967; *Castelli*, 1968], evidence was presented indicating that the U-shaped spectrum was a necessary or almost necessary condition for a solar flare to produce a polar cap absorption (PCA) event. Thus *Castelli et al.* [1967] found U-shaped radio spectra for the three visible hemisphere "PCA flares" of 1966.

In a verification of the utility of the U-shaped spectrum, *O'Brien* [1970] compiled a comprehensive list of 30 microwave events with this spectral shape (hereinafter, "U bursts") occurring from 1966 to 1968. O'Brien associated 13 of these flare bursts with principal ($\geq$2.0 dB of absorption measured by a 30-MHz riometer) PCA events and 14 with minor (<2.0 dB) PCA's or proton events detected only by satellites and was unable to associate the three remaining U bursts with a near-earth particle enhancement. Significantly, in the reverse association, O'Brien found no cases of principal PCA's during this period that were not associated with U bursts. *Castelli and Barron* [1977] compiled a comprehensive list of 81 U bursts in 1966–1976. For nine of these events a major proton event (PCA) was in progress at the time of the U burst, and no fresh injection of protons was observed. Seventy of the remaining 72 events were associated either with PCA's (27 of which had peak absorption $\geq$2.0 dB) or satellite proton events. For the same period, 1966–1976, *Castelli and Tarnstrom* [1978] published a catalog of 114 proton events that were associated with flares that did not have U-shaped microwave spectra. Seventy-six of these events could be identified with visible hemisphere flares, and of these only three were principal PCA events. Thus the current picture of the relation-



Paper number 4A8326.
0148-0227/85/004A-8326$05.00

ship between U bursts and proton events is that the U-shaped spectrum is (1) an almost sufficient condition (70/72 = 97%) for the occurrence of an interplanetary proton event of any size and (2) an almost necessary condition (27/30 = 90%) for the occurrence of a principal PCA ($\geq$ 2.0 dB).

Largely as a result of the efforts of Castelli and his colleagues, the presence or absence of a U-shaped spectrum is used as a "yes or no" indicator of significant proton acceleration in solar flare bursts at the U.S. space forecasting centers in Boulder and Omaha [*Heckman*, 1979; *Cliver et al*, 1978; *Thompson and Secan*, 1979]. Moreover, the successful application of the U burst as an indicator, coupled with the ability to view the sun through clouds at radio wavelengths, was a significant factor in the evolution of the worldwide solar radio patrol of the U.S. Air Force [*Castelli et al.*, 1973] and the establishment of the present-day Radio Solar Telescope Network [*Guidice et al.*, 1981] that monitors solar emissions in the frequency range from 245 MHz to 15.4 GHz.

Despite the use of the U-shaped spectrum as a forecasting aid, however, certain questions about its development, pragmatic application, and physical interpretation remain unanswered. S. W. Kahler (private communication, 1980) and G. M. Simnett (private communication, 1980) pointed out that certain events in Castelli and Barron's list of 81 events did not appear to satisfy the stated definition of a U burst, while other events whose peak flux density spectra conformed to the definition were omitted. Some of the difficulty lies in the definition of the U-shaped spectrum used by Castelli and Barron, because it contains no mention of the allowable separation in time between peaks at different frequencies. For certain events in *Castelli and Barron*'s [1977] (hereinafter CB) list (events 6, 17, 22, and 61) the low-frequency maximum occurs from 10 to 80 min after the ~10-GHz peak. In two of these events (events 17 and 61) the ~200-MHz emission did not begin until $\geq$15 min after the centimeter wavelength maximum. Constructing peak flux density spectra from discrete frequency peaks separated by tens of minutes strains the credibility of the U burst as a forecast tool (and as a meaningful physical construct), since given enough time and the relative high frequency of bursts at the longer wavelengths, unrelated microwave and meter wavelength bursts might be combined to give U-shaped spectra. While the appropriateness of the inclusion of these and other (events 10, 20, 25, 34, 36 and 55) events on the U burst list of CB is debatable, other events that satisfied the U-shaped spectral criteria were omitted from the list. Well-defined examples of such events occurred on September 4, 1966 (0417 UT), March 4, 1967 (1716 UT), March 21, 1969 (1334 UT), January 14, 1971 (1122 UT), and March 6, 1972 (1116 UT).

From our perspective a more fundamental question than the classification of individual events in previous studies of U-shaped spectra and proton events concerns the basic methodology of these studies. Despite the considerable effort that has been expended on investigations of the U burst-proton event relationship, no systematic study to classify the peak flux density spectra of large solar bursts into different types and then to compare the proton association of non-U types with that of the U bursts has been undertaken. Thus at present, we know neither (1) the approximate fraction of large radio bursts that have U-shaped spectra nor (2) the degree of association between large bursts with non-U spectra and proton events. Until these questions are addressed, it is difficult to assess the value of the U burst as a "yes or no" forecast tool, since it is not known how well it discriminates against large microwave bursts of different spectral type.

Finally, questions about the physical interpretation of the U-shaped peak flux density spectrum have persisted since its introduction. *Castelli et al.* [1967] and *Castelli* [1968] made little attempt to provide an explanation for the observed association between U bursts and proton events. Subsequently, *Castelli and Guidice* [1972] interpreted this relationship in terms of a two-stage acceleration process. In their model, flash phase electrons accelerated downward toward the solar surface (or trapped on low-lying loops) give rise to the centimeter wavelength branch of the U burst. The intensity of the microwave peak ($\gtrsim$ 1000 sfu in U bursts) served as an indicator that the energy release during the impulsive phase was sufficient to produce a coronal shock wave (inferred from a type II burst) through which the electrons accounting for the meter wavelength branch of the U burst and the protons observed at earth were accelerated by means of a Fermi-type process. The idea of two phases of particle acceleration in flares was proposed by *Wild et al.* [1963] and *De Jager* [1969]. The picture suggested by *Castelli and Guidice* [1972] for the relationship between the two stages is in qualitative agreement with the detailed model of *Lin and Hudson* [1976]. However, since *Cliver et al.* [1983*b*, *c*] have shown that significant ($J$( > 10 MeV) $\geq$ 10 protons cm$^{-2}$ s$^{-1}$ sr$^{-1}$) proton events can be associated with relatively small ($Sp$ (~9 GHz) < 100 sfu) microwave bursts, as was also indicated by *Castelli and Tarnstrom* [1978], the explanation of the U burst-proton relationship proposed by Castelli and Guidice is problematical. Nevertheless, *Lin* [1970] and *Svestka and Fritzova-Svestkova* [1974] have noted an association between type II bursts and interplanetary proton events, and it would be interesting to see if large flare bursts with the U-shaped spectrum are preferentially associated with type II bursts in comparison with large non-U bursts. Without such additional evidence for a physical link between U bursts and proton events the inclination is to dismiss the U burst-proton event association as an example of the big flare syndrome [*Kahler*, 1982*a*], perhaps useful for forecasting purposes but incapable of providing insights on the problem of proton acceleration in flares. In essence the big flare syndrome states that a flare that is prominent in one energy or wavelength range tends to be prominent in all and cautions about overinterpreting associations/correlations observed in samples of big flares.

In this study we classify the peak flux density spectra of all large ($Sp$ ($\geq$2 GHz) $\geq$ 800 sfu) radio bursts observed from 1965–1979 and compare the associations of bursts of different spectral classes with interplanetary proton events and type II/IV bursts. In addition, we examine the nature of the low-frequency branch of the U-shaped spectrum and conduct a search for necessary conditions in the radio domain for the occurrence of a significant ($J$ ( > 10 MeV) $\geq$ 10 protons cm$^{-2}$ s$^{-1}$ sr$^{-1}$) proton event.

In section 2 we discuss our data sources, event selection criteria, and burst classification procedures. The various statistical associations are presented in section 3, and a summary and discussion of results are contained in section 4.

## 2. Radio and Proton Data (1965–1979)

### *Radio Data Sources*

For both discrete and sweep frequency radio data we relied primarily on the Quarterly Bulletin of Solar Activity (QBSA) for events occurring before 1969 and Solar Geophysical Data (SGD) for subsequent years. It is important to note that, for consistency, only tabulated data were used. Reference was not made either to published burst profiles or to the Sagamore

Hill strip chart data, which we have archived for the years 1966–1981.

*Selection Criteria*

In our search for large microwave bursts occurring during this period we used the following selection criteria: (1) $Sp \geq 800$ sfu at $f \geq 2$ GHz, and (2) 85 E $\geq \phi \leq 85°$W, where $Sp$ is the peak radio flux density and $\phi$ is the longitude of the associated Hα flare. We considered only frequencies ≥2 GHz, since this frequency serves as a nominal divider between the decimetric wavelengths, where intense narrow band features often occur without significant associated microwave emission, and the centimetric wavelengths, where spectral variations are typically smoother [cf. *Kundu*, 1965]. The ≥800 sfu level is roughly equivalent to Castelli and Barron's ≥1000 sfu level. The solar longitude criterion was adopted to screen out events occurring close to, or beyond, the limb for which the radio source may have been partially occulted. A complete listing of the 193 microwave events satisfying these selection criteria and their associated Hα, sweep frequency radio, and proton data are given by *Cliver et al* [1985].

*Constructing Spectra*

Several of the 193 events had more than one reported peak in their flux density time profiles that satisfied our $Sp$ (≥2 GHz) ≥ 800 sfu selection criterion (e.g., two of the large bursts in the August 1972 sequence). For such events we constructed spectra at the time of the largest peak at the highest frequency for which observations were reported. Since secondary (late) peaks in microwave outbursts tend to have their maxima at progressively lower frequencies [*Kai*, 1968; *Kahler*, 1982*b*], this procedure was designed to select the initial major peak in the listed events. While this tactic did not always, in fact, identify the first reported centimeter wavelength peak ≥800 sfu, it did ensure a consistent approach to the data. We *considered only* those lower-frequency flux density maxima that fell within a 5 min sliding window containing the highest-frequency highest-flux "anchor time." No two discrete frequency maxima that were used to determine the peak flux density spectrum could be separated in time by more than 5 min. The 5 min width of the time window was arbitrarily chosen, and while it still may be too large to provide physically meaningful spectra, it is an improvement on the relatively open-ended approach of CB. In practice, large microwave bursts often have their maxima occurring within 1–2 min at frequencies across the spectrum.

The reported peak flux densities in the 5-min window were plotted as a function of frequency on log-log graph paper (Figures 1–6). We considered only frequencies ≥200 MHz with the exception of Boulder (184 MHz). Visual fits were made through the plotted points for each event. At frequencies >2 GHz it was relatively easy to construct a consensus peak flux density spectrum from the plotted points, owing both to the smoother spectral and temporal variations at these frequencies and to the reasonably good (10–20% variations [*Tanaka et al.*, 1973; *Kahler*, 1982*a*]) intercalibration of the worldwide patrol. Below 2 GHz, and especially near 200 MHz, the situation becomes more difficult. The narrow band features in the decimeter range present a particular problem, since one cannot be sure whether an apparent pronounced spectral variation is real or the result of an erroneous report by a single observatory. The procedure we eventually adopted at decimeter wavelengths was close to a "connect the dots" approach, smoothing out minor variations that could be due to calibration differences but following exactly large variations that we had no reason to doubt. Examples of events with relatively narrow band decimetric features in their spectra are given in Figures 2*b*, 2*c*, 3*b*, 3*c*, 4*b*, 6*b*, and 6*c*. At $f \sim 200$ MHz, peak flux densities reported by different stations observing at closely spaced frequencies can vary by a factor of 2–5 or more (Figures 1*c*, 3*b*, 3*d*, and 4*a*). It seems doubtful that variations of this size could be due to faulty calibration, since the difference would also appear in the daily measurement of the quiet sun flux. Rapid spectral variations in the burst emission at these lower frequencies may play a role, although for certain cases, large discrepancies were noted in the reported peak flux densities of observatories monitoring the same nominal frequencies. We suggest that the significant differences often observed near 200 MHz result from the effects of different time constants on bursts with fast time structure or from nonlinear receiver response for large events. Since both of these effects will tend to reduce observed peak flux densities (assuming that one does not over correct for nonlinearity), we favored the higher reported values in events with widely divergent peak flux densities at 200 MHz. This decision affected the spectral classifications of 12 events.

While observatories may report the times/peak flux densities of several maxima at a given frequency in a complex burst, this practice is by no means standard and often only the largest peak is reported. This is a particular problem at the lower (<1 GHz) frequencies, where the largest peak may not occur until late in the event. For 10 events with insufficient spectral data at the anchor time, however, it was possible to infer the spectral shape by using peak fluxes reported later (or earlier) in the event as upper limits.

*Spectral Classes*

Despite the occasional complexity that may present itself in the peak flux density spectrum of any given event, we found that we were able to classify the spectra of the 193 events listed by *Cliver et al* [1985] into two basic groups and an intermediate type. The dominant spectral type was the U shape that composed 59% (113/193) of the sample. For a peak flux density spectrum to be classified as U-shaped, we required (1) a spectral maximum ≥800 sfu at some frequency $f \geq 2$ GHz, (2) a second maximum ≥800 sfu at some frequency (≥200 MHz) below that of criterion 1 and (3) a spectral *minimum at some frequency between* that of the maxima in criteria 1 and 2 (but <10 GHz) with a flux density value significantly (≥40%) below those of criteria 1 and 2.

The above definition allows a variety of spectra to be classified as U-shaped. A number of examples of this spectral type are shown in Figures 1–3. Figure 1 contains examples of the "classic" U burst spectrum with the low-frequency flux density maximum occurring from ~200 to 500 MHz. Approximately 75% of the U bursts in our sample had this type of spectrum; ~20% had their lower-frequency maximum in the range from >500 MHz to 2 GHz. Figures 2*a*, 2*c*, 2*d*, and 3*a*–3*d* give seven of the 15 cases of U bursts that had their low-frequency peak at $f \geq 1$ GHz. The events in Figure 2 were on CB's list, while those in Figure 3 were not.

At this point it is of interest to compare our list of events with U-shaped spectra to that of CB for the period in common from 1966 to 1976. Of the 85 previously identified U bursts during this period (81 from CB and four added by *Castelli and Tarnstrom* [1978]), 11 occurred either at or behind the solar limb ($\phi > 85°$), and were not considered for our list. For 15 other events on CB's list we were either unable to classify the peak flux density spectrum because of insufficient data in the 5-min window (10 cases) or arrived at a

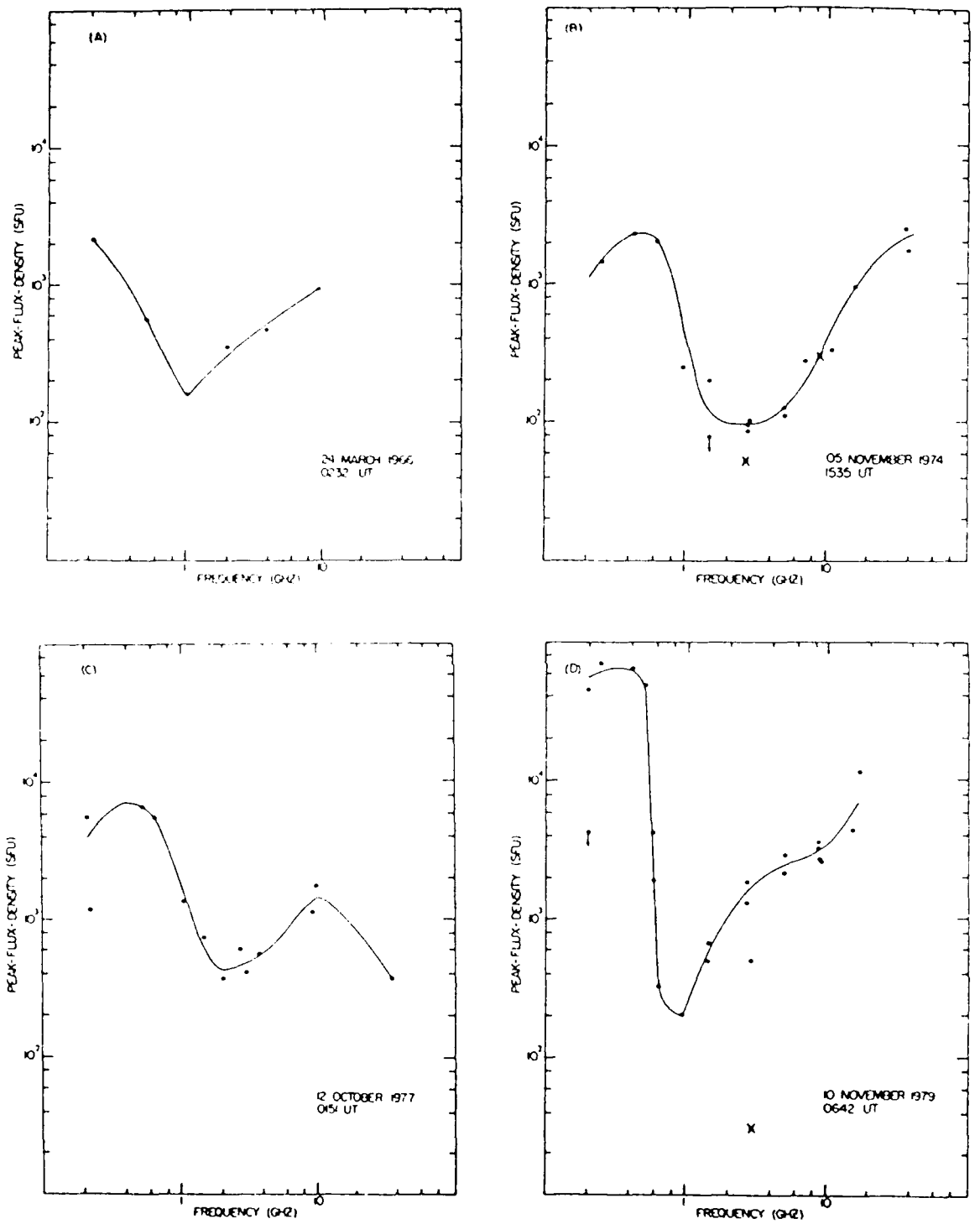


Fig. 1. Examples of the classic U-shaped spectrum with the low-frequency maximum occurring near 200 MHz. Events in Figures 1*a* and 1*b* were on *Castelli and Barron*'s [1977] list of U-bursts, while events in Figures 1*c* and 1*d* occurred after the period they considered. In Figures 1–6, crosses indicate doubtful or uncertain flux density values, and downward pointing arrows indicate upper limits. Uncertainties in measured peak fluxes at frequencies >2 GHz are typically < ± 20%. Differences in reported values at $f \leq 2$ GHz may be substantially larger (factors of 2–10), as can be seen from these figures. Note that the origin of the *y* axis of the plots in Figures 1–3 is at 10 sfu compared to 1 sfu in Figures 4–6.

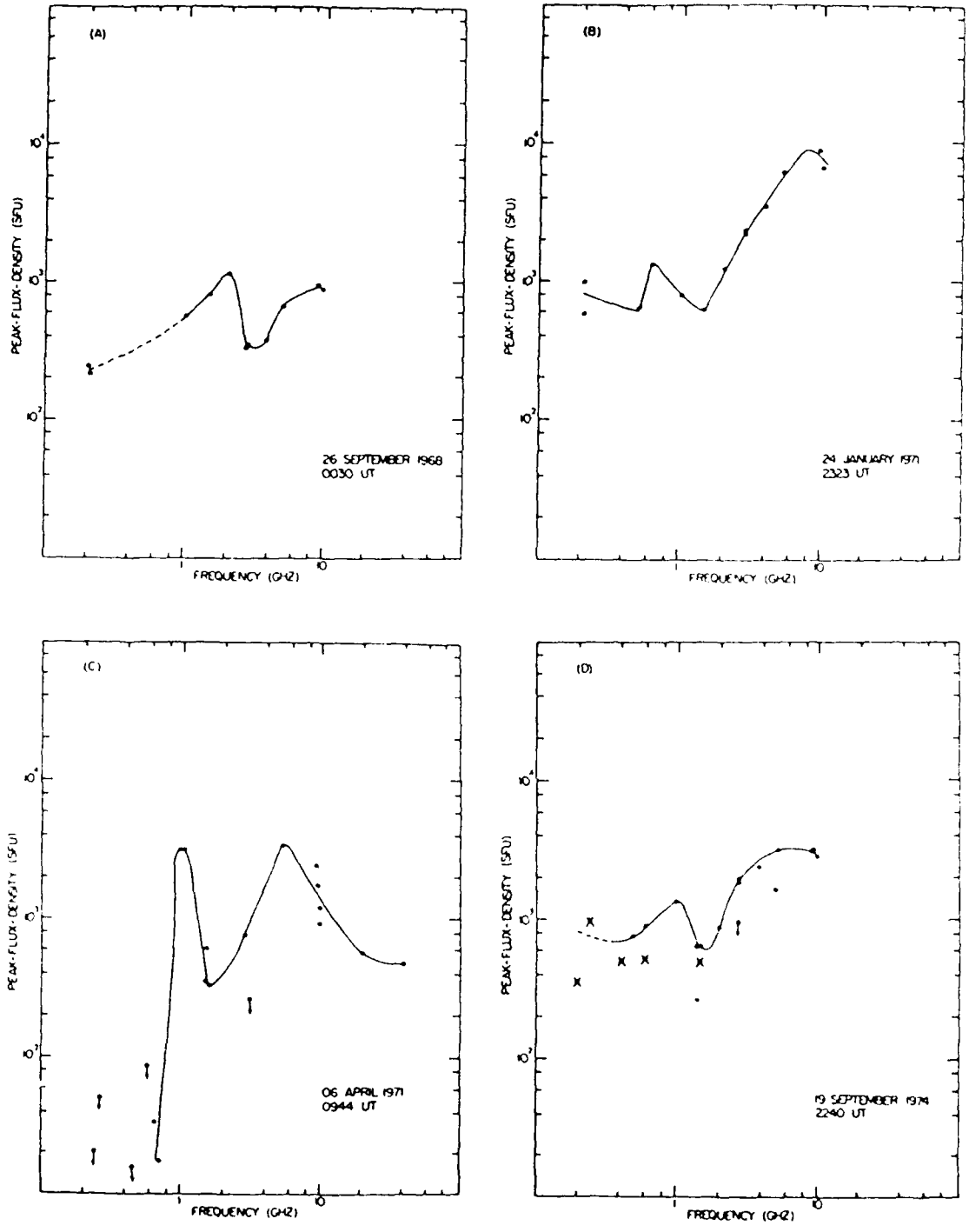


Fig. 2. Examples of U-shaped peak flux density spectra that had their lower-frequency maximum in the decimetric range. Each of these events was on *Castelli and Barron*'s [1977] U burst list.

different classification (five cases). Thus there were 59 events in the intersection of our U burst data sets for the common years of these studies. In addition, we identified 25 events during this period that were not included on the U burst list compiled by CB and Castelli and Tarnstrom but satisfied the U-shaped spectral criteria that we adopted. We point out that 13 of these 25 events would not have been classified as U bursts if spectral maxima $\geq$ 1000 sfu (versus $\geq$ 800 sfu) in the meter/decimeter and centimeter wavelength ranges had been required. This would account for their absence from the CB list. By the same standard, however, three other events on their list might be excluded.

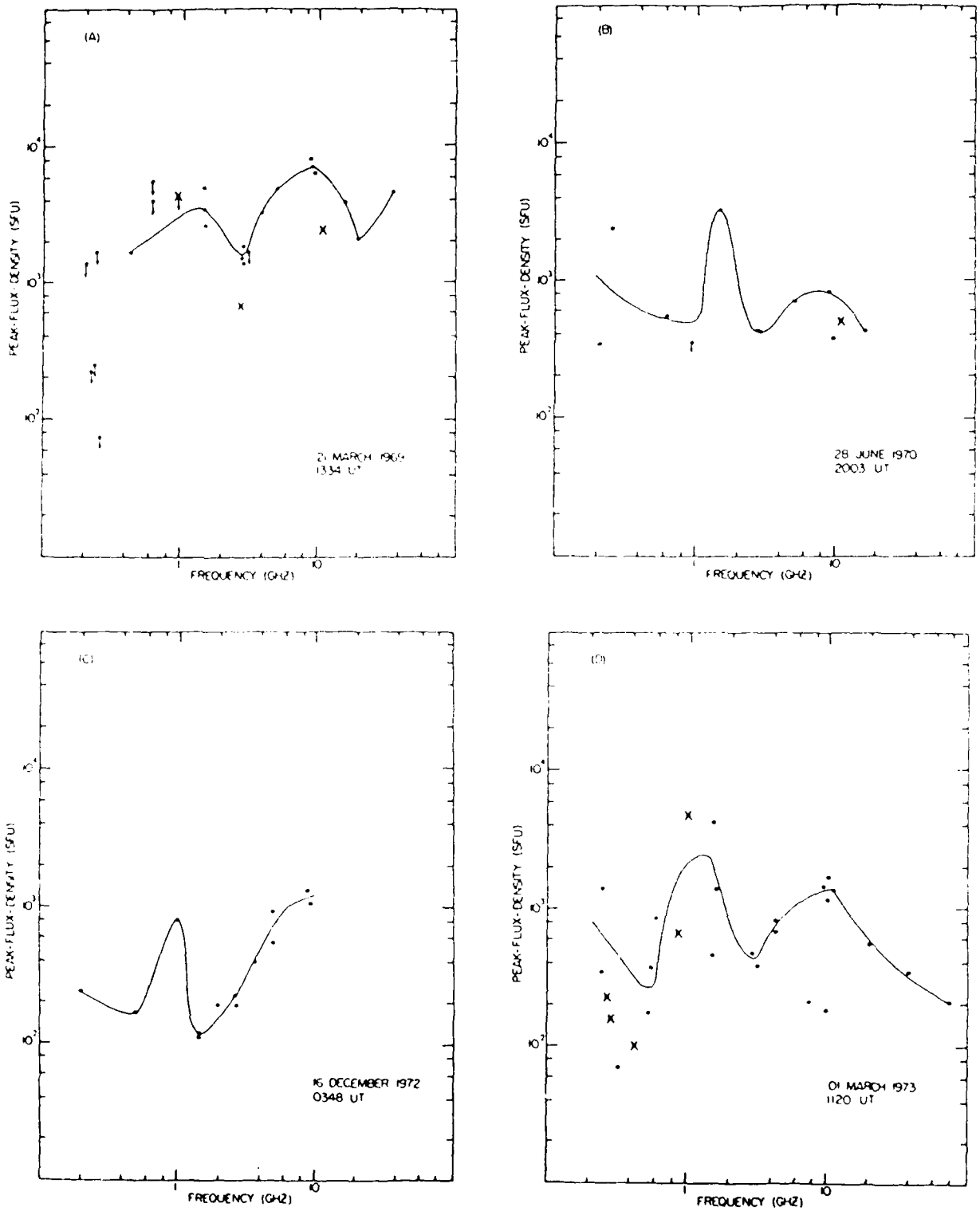


Fig. 3. Examples of U-shaped peak flux density spectra that had their lower-frequency maximum in the decimetric range. These events were not on *Castelli and Barron's* [1977] list.

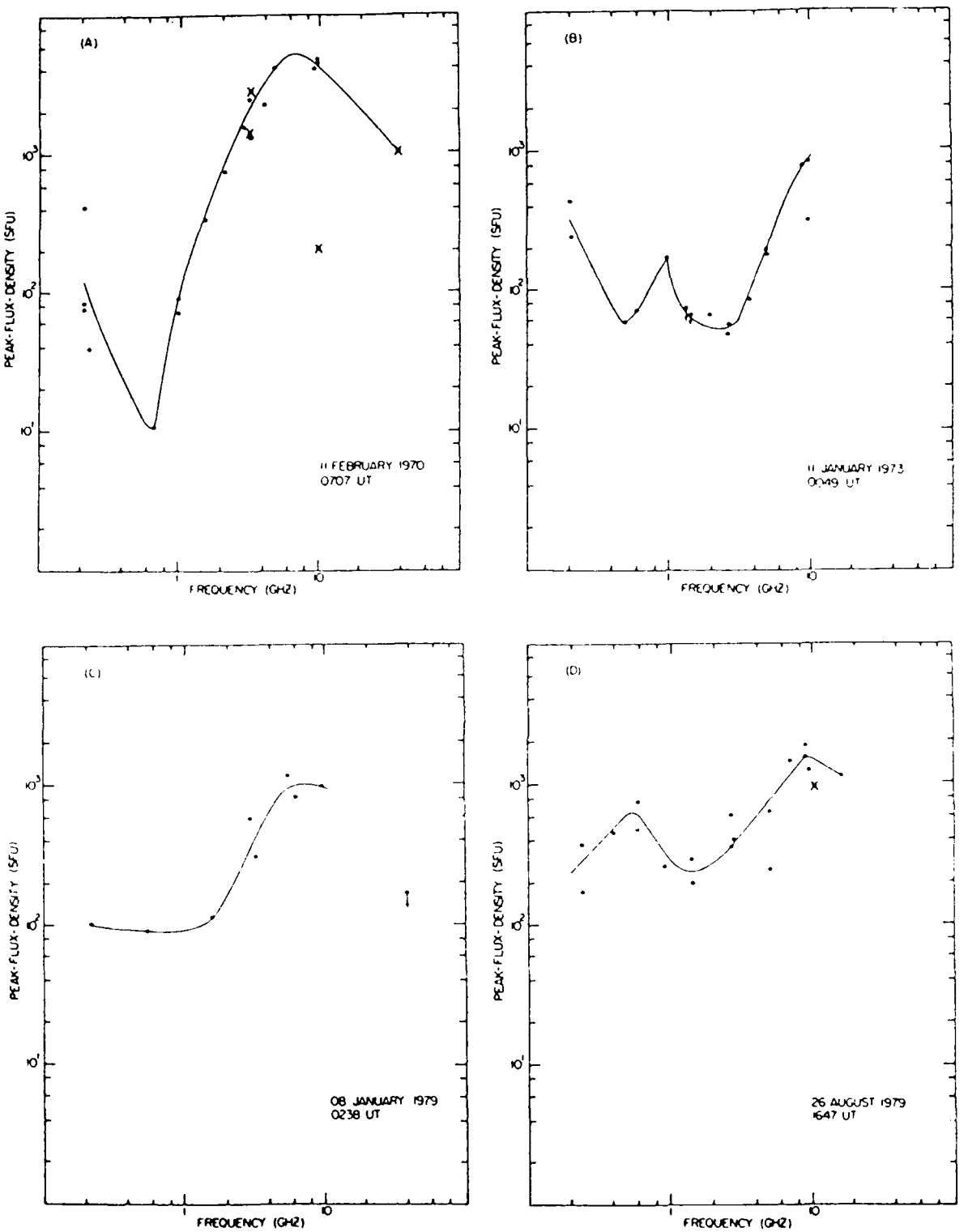


Fig. 4. Examples of microwave bursts with what we have termed "intermediate" peak flux density spectra. The classification of the event on February 11, 1970 (Figure 4*a*), was affected by our decision to favor the higher reported flux values near 200 MHz. The spectrum of the event on January 11, 1973 (Figure 4*b*), has a decimetric component, while that of January 8, 1979 (Figure 4*c*), is relatively flat in the meter and decimeter range.

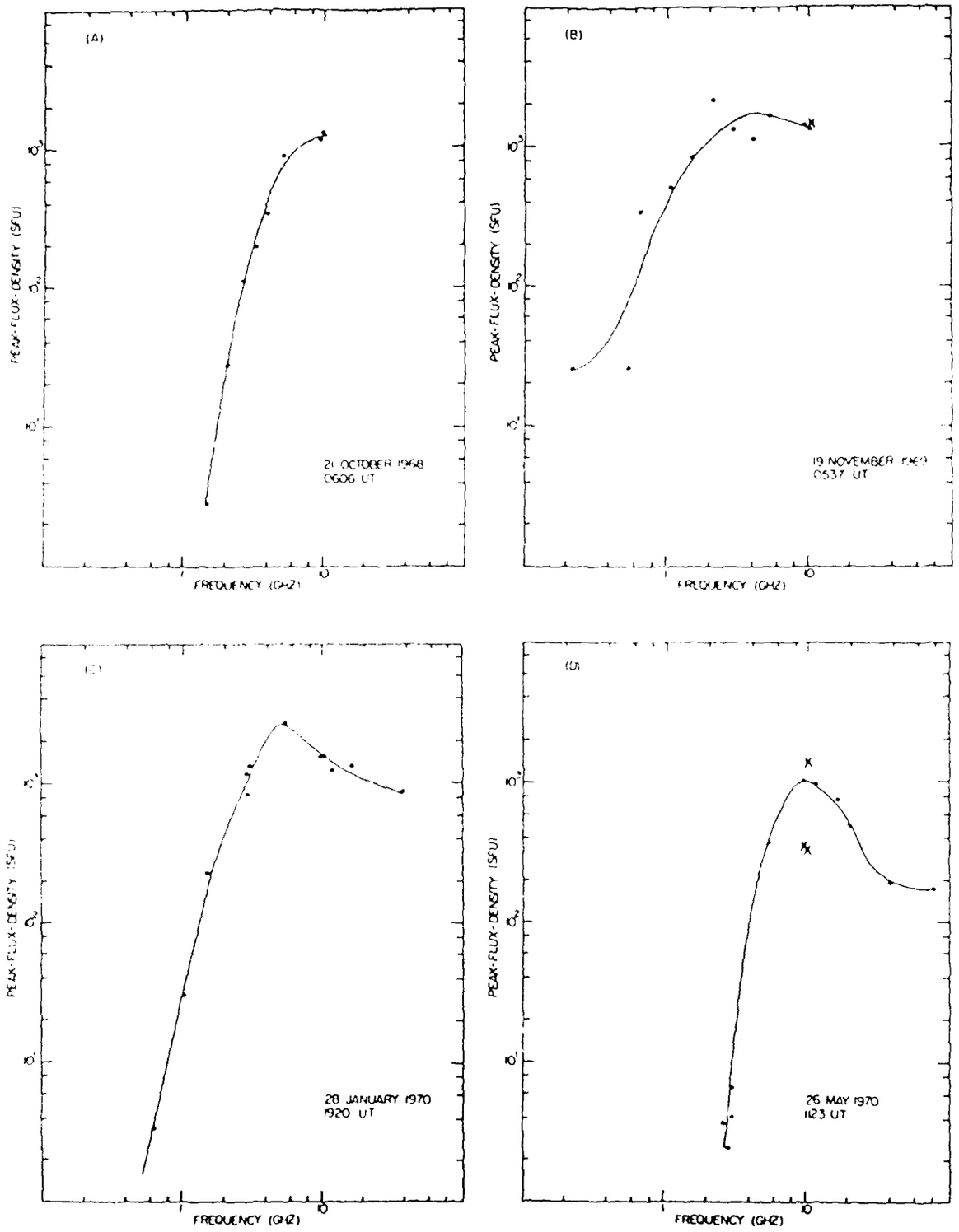


Fig. 5. Examples of large microwave bursts with cutoff or quasi-cutoff spectra.

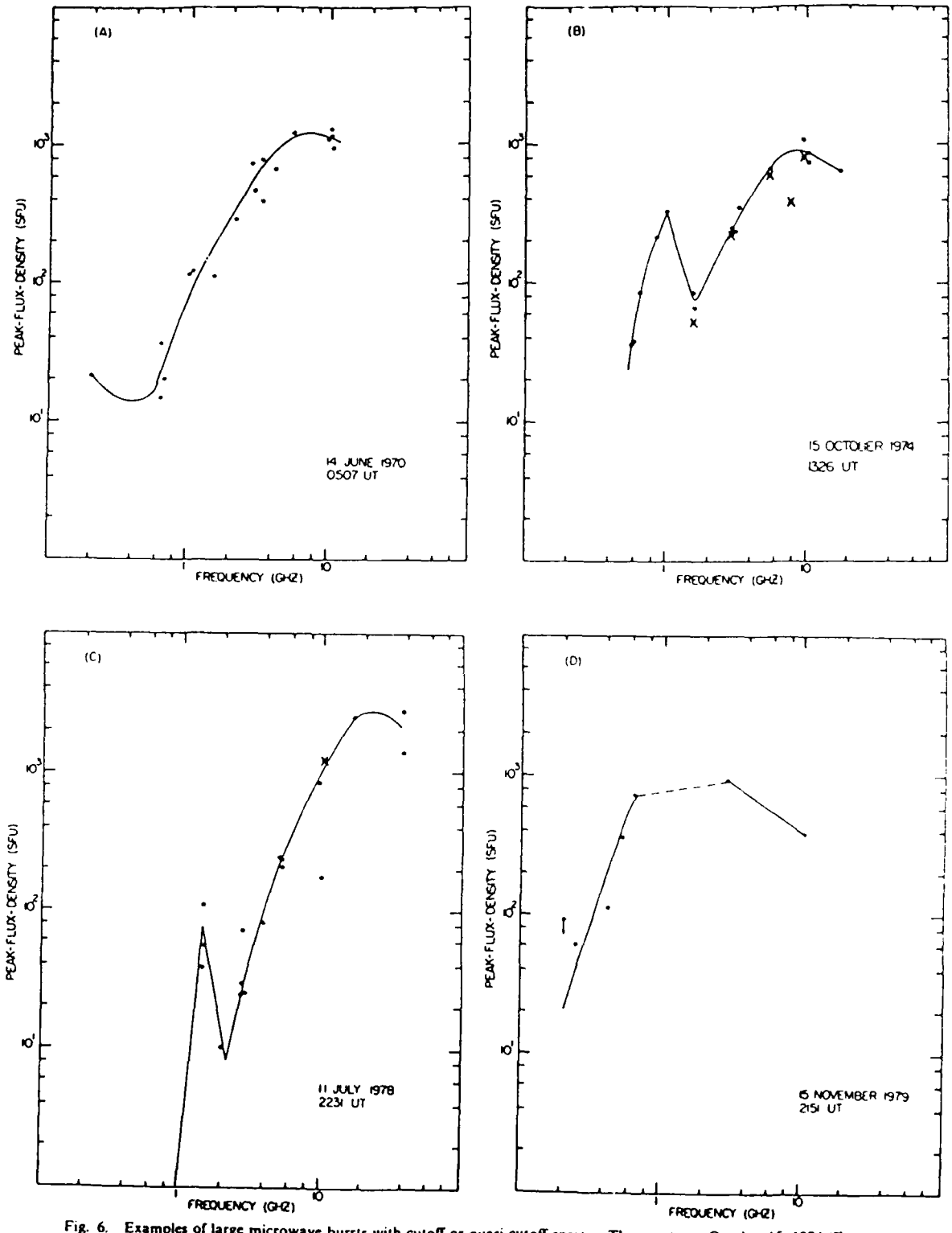


Fig. 6. Examples of large microwave bursts with cutoff or quasi-cutoff spectra. The events on October 15, 1974 (Figure 6*b*), and July 11, 1978 (Figure 6*c*), exhibited a decimetric component in their spectra.

For 52 of the 165 events for which we were able to determine spectra a $\geq$800 sfu maximum at $f \geq 2$ GHz was not accompanied by a maximum with $Sp \geq 800$ sfu at a lower frequency. In many cases the high-frequency emission was apparently unaccompanied by any emission at lower frequencies, and emission would appear to taper smoothly down from the centimeter wavelength maximum and cut off at frequencies $\gtrsim$ 1 GHz. In other cases the spectrum was U-shaped, but the lower-frequency maximum did not have $Sp \geq 800$ sfu. Still, in a few other cases the spectrum below the centimeter wavelength peak neither cut-off completely nor turned back up but remained relatively flat at a given flux-density level. To distinguish between these various types of events, we adopted the following classification scheme. We classified events as having intermediate peak flux density spectra for which: (1) a spectral maximum $\geq$ 800 sfu occurred at $f \geq 2$ GHz, (2) no significant ($Sp \geq 800$ sfu) spectral maximum occurred at a frequency lower than that of criterion 1 (down to 200 MHz), and (3) $Sp$(200 MHz) $\geq$ 100 sfu. This set of criteria distinguishes these intermediate events from those having "cutoff" or "quasi-cutoff" spectra for which criteria 1 and 2 also apply, but for which criterion 3 becomes $Sp$ (200 MHz) $<$ 100 sfu. Thus microwave bursts of the intermediate spectral class have peak 200 MHz emission between that of U bursts and cutoff events. We point out, however, that the occurrence of a decimeter wavelength peak with $Sp \geq 800$ sfu automatically qualified an event as a U burst in our classification scheme (assuming that it met the other stated criteria) regardless of the peak flux density of any reported 200-MHz burst.

While for many of the events having cutoff spectra, emission appeared to be cut off well above 200 MHz, we know from experience that many and perhaps a majority of the smaller events ($Sp <$ 100 sfu) at 200 MHz go unreported [cf. *Roelof et al.*, 1983]. Thus the cutoff events are not necessarily those for which no low-frequency emission was observed but rather are events for which the peak 200-MHz emission was significantly down (a factor of 8 or more) from its centimeter wavelength maximum. In all cases where no event was reported near 200 MHz (184–328 MHz) we checked the published patrol times to see if a station (e.g., Hiraiso, Gorky, Sagamore Hill) was, in fact, observing in this frequency range. If a station were observing and did not report an event, we assumed that $Sp$ ($\sim$ 200 MHz) $<$ 100 sfu.

Eighteen of the 193 events in our data set (9%) had intermediate peak flux density spectra and 34 (18%) had cutoff spectra. Examples of intermediate spectra are shown in Figure 4, and examples of cutoff spectra are given in Figures 5 and 6. Examples of intermediate and cutoff spectra with decimetric peaks are shown in Figures 4*b*, 6*b*, and 6*c*, respectively.

We were unable to classify the peak flux density spectra of 28 (15%) of the events in our data sample. The most common reason (20 cases) for our inability to construct a meaningful spectrum was the lack of data points, particularly at low frequencies, within the 5-min sliding window.

*Proton Data*

For the proton associations of the 193 events we used the work by *Svestka and Simon* [1975], reports by *Dodson et al.* [1977, 1978], and the published list of *van Hollebeke et al.* [1975] for the years 1965–1972. We made the associations ourselves for the subsequent years. We considered only increases for which the logarithm of the peak near-earth $>$10 MeV flux had a characteristic $\gtrsim -2$. Somewhat smaller increases, with log ($J$) $< -2$, can be observed by existing satellite sensors, but fluctuations at this level are common, and it is difficult to confidently associate these small increases with flares [cf. *Kahler*, 1982*b*; *van Hollebeke et al.*, 1975]. For the period from January 1965 to May 1967 we relied on the proton event classification of *Smart and Shea* [1971], as used by *Svestka and Simon* [1975], to determine the logarithm of $J$ ($>$10 MeV). For the period from May 1967 to May 1973 we were able to make this determination directly from the $>$10 MeV data acquired by the Johns Hopkins University Applied Physics Laboratory (JHU APL) experiments aboard IMP-F, -G, and -I and published in SGD. For the years 1973–1979 we worked with the 20–40 MeV data collected by the JHU APL sensors aboard IMP-H and -J. For this differential channel a peak flux of $\geq 10^{-4}$ protons cm$^{-2}$ s$^{-1}$ sr$^{-1}$ MeV$^{-1}$ corresponds to a peak $>$10-MeV flux of $J \geq 10^{-2}$ protons cm$^{-2}$ s$^{-1}$ sr$^{-1}$ if one assumes a spectral slope of $-3$ [*van Hollebeke et al.*, 1975]. We subtracted the background due to earlier events when determining log ($J$). We made note of all cases where a fresh injection of protons from a given event might have been masked by a proton event already in progress or where an injection of particles near the time of the flare in question may have, in fact, been due to a more likely candidate parent flare.

We note that for the period May 1967 to May 1973, *Svestka and Simon* [1975] and *Dodson et al.* [1977, 1978] listed 7 of the 193 events as only being sources of low-energy ($<$10 MeV), low-flux ($< 10^{-2}$ protons), or non-near-earth ($>60°$ from the earth-sun line) proton events. Four of these particle events were associated with U bursts, two with cutoff events, and one with an unclassified event.

*Major Proton Events, 1965–1979*

By examining the proton association of the 113 U bursts in our sample we can determine a false alarm rate for the U burst forecast tool for predicting proton events above a given threshold. To determine the fraction of major proton events that are associated with U bursts, we compiled a list of the 46 prompt proton events with $J$ ($>$ 10 MeV) $\geq$ 10 protons cm$^{-2}$ s$^{-1}$ sr$^{-1}$ (above preevent background) occurring from 1965 to 1979 that had unambiguous visible hemisphere ($85°E \geq \phi \leq 85°W$) parent H$\alpha$ flare associations. The $J$ ($>$10 MeV) $\geq$ 10 protons cm$^{-2}$ s$^{-1}$ sr$^{-1}$ threshold is currently in use at the National Oceanic and Atmospheric Administration (NOAA) Boulder forecast center [*Heckman*, 1979]. This is the same list of events that was used in the study by *Cliver et al.* [1983*c*]. A complete listing of these events with their associated data is given by *Cliver et al.* [1985].

## 3. Data Analysis

*Peak Flux Density Spectral Type Versus Proton Events*

In Table 1 we present our results on the association of proton events with large radio bursts of different spectral types for the 193 events in our sample. To allow for particle propagation effects, we have divided Table 1 into two parts, corresponding to western hemisphere and eastern hemisphere events. We have further divided the events from each hemisphere into "clean" and masked or ambiguous cases. The clean events are those in which the flare association is unambiguous, and a fresh injection of $>$10-MeV protons is observed above the flux background, either quiet or disturbed, existing at the time of the flare. In the right-hand section of Table 1 the associated value of the logarithm of the $>$10-MeV peak flux refers either to the level of the enhanced $>$10-MeV flux at the

TABLE 1. Peak Flux Density Spectral Class Versus Proton Event Size

| | Logarithm of > 10-Mev Peak Flux | | | | | | | | | | |
|---|---|---|---|---|---|---|---|---|---|---|---|
| | "Clean" Cases | | | | | | Ambiguous or Masked Events | | | | |
| Spectral Type | ≥2 | 1 | 0 | −1 | −2 | < −2 | ≥2 | 1 | 0 | −1 | −2 |
| *Western Hemisphere** | | | | | | | | | | | |
| U-shaped | 10 | 12 | 4 | 3 | 2 | 3 | 2 | 6 | 3 | 4 | 2 |
| Intermediate | | | 2 | 2 | 1 | 2 | | 1 | 1 | 1 | 1 |
| Cutoff | | 1 | | 2 | | 1 | | 1 | | 2 | 5 |
| Unclassified | 1 | 2 | | 1 | | | 1 | 2 | 3 | 1 | |
| *Eastern Hemisphere†* | | | | | | | | | | | |
| U-shaped | 2 | 4 | 4 | 7 | 8 | 14 | 1 | 1 | 6 | 7 | 8 |
| Intermediate | | | 1 | | 2 | 1 | 1 | | 2 | | |
| Cutoff | | | | 1 | 1 | 9 | | 3 | 3 | 2 | 3 |
| Unclassified | | 1 | 1 | 1 | 1 | 4 | 1 | | | 2 | 6 |

*Total of 49 "clean" cases and 36 ambiguous or masked events.
†Total of 62 "clean" cases and 46 ambiguous or masked events.

time of the microwave burst in question (masked events) or to the peak level of the time-related proton event that, in our judgment, was probably not due to the burst under consideration (ambiguous events).

Considering the clean cases only, the percentage association of protons with the three spectral types is given in Table 2. The high degree of association between U bursts and proton events for western hemisphere flares supports the evidence presented by CB, indicating that the U burst is an "almost sufficient" condition for the occurrence of a proton event of any size. However, we note that the large western hemisphere flare bursts with intermediate and cutoff spectral classifications also have significant proton association (71 and 75%, respectively). Since the number of western hemisphere events of these two spectral types is small, it may be appropriate to increase our sample size by considering the percentage association of the three spectral types with protons for flares occurring anywhere on the visible disk (85°E ≥ $\phi$ ≤ 85°W). As expected, the percentage association for U bursts is smaller when the whole sun is considered. The proton association for the intermediate events is constant over the full disk, although the total number of cases (11) is still not large. For the entire sun, however, the percentage association of the cutoff events (33%) begins to distinguish itself from that of the U bursts (77%) and the intermediate events (73%). Although we cannot rule out the propagation effect as the cause of the weak proton association of the eastern hemisphere cutoff events versus that of the U bursts, we note that the longitudinal distribution in this hemisphere of flare bursts of the three spectral types with "clean" proton circumstances does not appear to favor either the U bursts or the intermediate events compared to the bursts with cutoff spectra. The median eastern hemisphere longitude for such events in each spectral class is as follows: U bursts (38°E, 39 events), intermediate events (50°E, 4), and cutoff events (29°E, 11). Thus in a consideration of the relationship of microwave peak flux density spectra to proton events of any size the U-shaped spectrum is differentiated primarily from the cutoff spectrum that is deficient, and in many cases apparently lacking, in 200-MHz emission.

### *The U Burst as a Forecast Tool*

To derive a false alarm rate for the U burst forecast tool, we counted as successes only those cases in which a U burst was followed by a proton event with $J$ (> 10 MeV) ≥ 10 protons cm$^{-2}$ s$^{-1}$ sr$^{-1}$ [*Heckman*, 1979]. If we consider only western hemisphere events, we have 22 successes versus 21 false alarms for a false alarm rate of 49% (21/43). To determine the number of false alarms, we added the number of U bursts without proton association to the number of U bursts with clean and ambiguous/masked proton associations for which the characteristic of log ($J$ > 10 MeV) was ≤ 0. We did not consider the eight masked or ambiguous cases for which the peak > 10-MeV flux was above the prediction threshold. Only 48% (22/46) of the large $J$ (> 10 MeV) ≥ 10 protons cm$^{-2}$ s$^{-1}$ sr$^{-1}$ proton events would have been successfully forecast by the U burst tool. We note that even if the longitude range from 85°E to 85°W comprising all of the 46 large events is considered, the success rate is still only 61% (28/46), while the false alarm rate is 73% (75/103).

### *Radio Signatures of Major Proton Events*

While *Cliver et al.* [1983*c*] demonstrated that a strong centimeter wavelength emission peak (i.e., $Sp$ > 100 sfu) is not a requirement for a prompt proton event with $J$ (> 10 MeV) ≥ 10 protons cm$^{-2}$ s$^{-1}$ sr$^{-1}$ to occur, it might be supposed that a prominent (≳1000 sfu) lower-frequency (200 MHz) emission peak remains as a necessary observable for significant particle acceleration in (or escape from) flares. That this is not the case is shown in Figure 7, where a histogram of $Sp$ (~200 MHz) for the parent flares of the 46 large proton events is presented. Even though we used the largest ~200-MHz flux density peak reported by any observatory on patrol (and occurring at any time during the listed Hα flare), eight events (seven, if we ignore March 7, 1970 [cf. *Cliver et al.*, 1983*c*]) had $Sp$ (~200 MHz) ≤ 300 sfu. Thus neither the high-frequency (~9 GHz) nor the low-frequency (~200 MHz) branch of the classical (i.e., $Sp$ ≳ 1000 sfu) U burst appears to be a requirement for the occurrence of a large, prompt proton event.

Work by *Pick-Gutmann* [1961], *Harvey* [1965], and *Castelli and Tarnstrom* [1978] indicated that the integrated microwave flux density $E_\mu$, obtained by taking the product of the burst mean flux density and duration, might be an important parameter in regard to proton acceleration in flares [cf. *Kundu and Haddock*, 1960]. In particular, the Pick-Gutmann and Castelli and Tarnstrom studies suggest that an integrated flux density $E_\mu \gtrsim 10^{-17}$ J m$^{-2}$ Hz$^{-1}$ is a requirement (or threshold) for the observation of a PCA event. However, this value of $E_\mu$ is relatively small and can be achieved by a predominantly thermal burst (gradual rise and fall or postburst increase) with a mean flux density of 15 sfu and a duration of 2 hours. In fact, with the possible exception of the August 21, 1979, event [*Cliver et al.*, 1983*b*] the weak impulsive phase proton events discussed by *Cliver et al.* [1983*c*] had values of $E_\mu > 10^{-17}$, primarily because of their long durations. Since there is no apparent close physical link between thermal microwave emission and nonthermal energetic protons [cf.

TABLE 2. Percentage Association of Protons With the Three Spectral Types

| Spectral Type | West | East | Total |
|---|---|---|---|
| U burst | 91% (31/34) | 64% (25/39) | 77% (56/73) |
| Intermediate | 71% (5/7) | 75% (3/4) | 73% (8/11) |
| Cutoff | 75% (3/4) | 18% (2/11) | 33% (5/15) |

Values in parentheses are associated events out of total number of events.

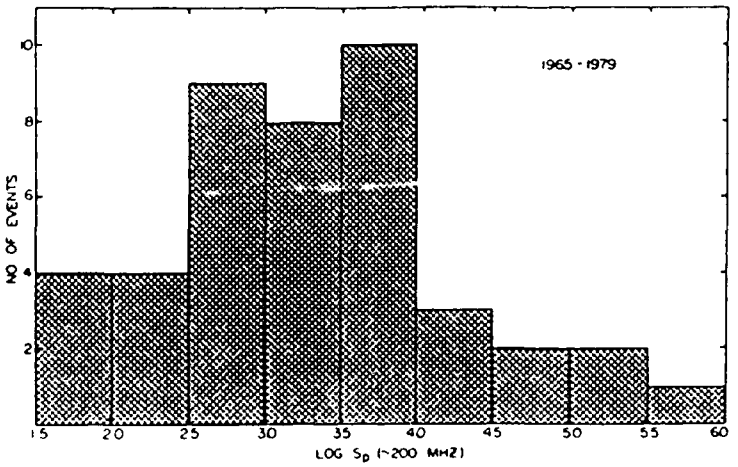


Fig. 7. Histogram of the reported peak flux density at ~200 MHz for the parent flares of the large ($J$ (>10 MeV) ≥ 10 protons cm$^{-2}$ s$^{-1}$ sr$^{-1}$) prompt proton events that were observed from 1965 to 1979. For each event we took the largest flux density reported by any observatory on patrol near 200 MHz (184–328 MHz) during the time of the associated Hα disk (85 E ≥ $\phi$ ≤ 85 W) flare. Note that several (8 of 46) of these events have relatively weak (≤300 sfu) emission at ~200 MHz.

*Kahler*, 1982*a*], the concept of an integrated microwave flux density "threshold" for proton acceleration in flares may be misleading [cf. *Cliver et al.*, 1983*c*]

At this point it is of interest to compare the U-shaped spectrum as an "almost necessary" or favorable condition for a significant proton event with meter wavelength phenomena that have been linked to proton acceleration, specifically type II bursts [*Lin*, 1970; *Svestka and Fritzova-Svestkova*, 1974] and type IV bursts [*Bell*, 1963, and references therein; *Maxwell et al.*, 1964; *Kahler*, 1982*b*] We find that type II and type IV bursts are associated with the 46 large $J$ (>10 MeV) > 10 protons cm$^{-2}$ s$^{-1}$ sr$^{-1}$ proton events in the following percentages: type II, 80% (35/44); type IV, 84% (36/43); and U burst, 65% (28/43) We emphasize that these percentage associations were obtained strictly on the basis of data reported in SGD and QBSA A reexamination of the sweep frequency records might reveal possible type II events (e.g., *Maxwell* [1973] and *Böhme and Krüger* [1973] reported possible type II bursts for two flares in the August 1972 sequence for which no type II burst was initially reported in SGD). Nevertheless, in view of the perceived link between type II bursts and proton events it is interesting that 20% of the largest proton events observed from 1965 to 1979 did not have obvious associated metric type II bursts.

### *Microwave Spectral Class and Type II/IV Bursts*

Because of the statistical relationship between U bursts and proton events and between type II/IV bursts and proton events we have examined the associations of type II/IV bursts with large microwave bursts of different peak flux density spectral types. In Table 3 it can be seen that the percentage association of microwave bursts of different spectral classes with type II/IV bursts parallels their association with proton events (85°E ≥ $\phi$ ≤ 85°W). We note that the microwave events with cutoff peak flux density spectra also appear to be deficient in type III bursts. The statistical results in Table 3 are consistent with the current picture [e.g., *Lin and Hudson*, 1976; *Kahler et al.*, 1978; *Cliver et al.*, 1982; *Mason et al.*, 1984] that the protons observed at earth are accelerated at a shock front, and it appears that the U bursts are preferentially related to protons in contrast to cutoff events because of their higher-percentage association with type II/IV events. We should be able to check this supposition directly by comparing the proton association of U bursts (and cutoff events) that were accompanied by type II and/or type IV emission with those that were not. However, as can be seen from Table 3, the control group of U bursts without type II/IV association is relatively small. We found only 11 U bursts that lacked both type II and type IV associations. Nine of these 11 events were associated with eastern hemisphere flares. For two of these nine events, possible proton events were masked by small (log $J$ ≤ −1) events in progress, while only one of the remaining seven events was associated with protons (−2) at the level (≥ −2) considered. Of the two western hemisphere events, one was masked (−1) and one was unassociated. Thus only one of the eight clean control events (albeit seven of these from eastern hemisphere flares) was associated with a >10-MeV proton event. For comparison we note that 74% (23/31) of the clean eastern hemisphere U bursts with type II and/or type IV bursts had proton association. The seven clean eastern hemisphere U bursts without type II/IV association had a median longitude of 45°, slightly less favorable than the 31 clean eastern hemisphere U bursts with type II/IV associ-

TABLE 3. Association of Sweep Frequency Bursts and Proton Events With Peak Flux Density Spectral Classes

| Spectral Type | Associated Phenomena | | | | |
|---|---|---|---|---|---|
| | Type III | Type II | Type IV | Type II and/or IV | Full Disk Protons "Clean" Cases |
| U-shaped | 93% (109) | 70% | 73% | 90% | 77% (73) |
| Intermediate | 72% (18) | 61% | 67% | 78% | 73% (11) |
| Cutoff | 34% (32) | 12% | 19% | 22% | 33% (15) |
| Unclassified | 80% (25) | 68% | 68% | 80% | 67% (12) |

Numbers in parentheses equal total number of events.

ation, 38°. A consideration of the associations of cutoff events with and without type II/IV bursts and proton events is also hampered by small numbers, although the results are consistent with the overall statistics presented in Table 3; three of the five clean cutoff events (16°E median longitude) with type II/IV association were related to >10-MeV events as opposed to two of 10 clean cut-off events (20°E median longitude) without type II/IV association.

At this point it is instructive to consider some of the cutoff events that have proton association in greater detail. For the event on October 27, 1968 (log $(J) = -1$), H. Tanaka [see *Svestka and Simon*, 1975, part 2) reports type IV emission beginning at 1307 UT, ~30 min after the initial peak ≥800 sfu and near the start of a major ($Sp$ (5 GHz) = 860 sfu) burst that we consider to be a secondary peak [cf. *Cliver*, 1983] in an extended flare event. Similarly, for the event on November 16, 1970 (log $(J) = -1$), the type II/IV event begins at 0112 UT, ~20 min after the initial ≥800 sfu peak but near the maximum of a significant ($Sp$ (9.4 GHz) = 1030 sfu) burst apparently associated with the same Hα flare. For both of these events, 200-MHz bursts were reported only in association with the later peak. These events indicate that it may be misleading to expect the spectrum of a single peak in a complex microwave burst to tell the entire story in regard to a flare's association with type II/IV bursts and protons. For the above cases it is tempting to speculate that the flares evolved from a compact to an open magnetic field structure [cf. *Pallavicini et al.*, 1977].

*Timing of Type II Burst and 200-MHz Peak*

Given the statistical associations between type II bursts, protons, and U bursts (and the relative deficiency of type II emission and proton association in the cutoff events), it seems logical to ask if the shock wave observed by way of the type II burst, and, presumably, accelerating the protons, might in some way account for the low-frequency branch of the U-shaped spectrum, particularly the high fluxes often observed near 200 MHz. There are two possible ways that the type II burst could account for, or contribute to, the 200-MHz radiation. First, the type II itself is generally an intense emission with flux densities ranging from ~50 to several thousand solar flux units [*Kundu*, 1965]. For those events with relatively high starting frequencies, emission at the second harmonic would be in the 200-MHz range and thus might contribute to the low-frequency branch of the U-shaped spectrum. About one third of type II bursts have fundamental starting frequencies >100 MHz [*Maxwell and Thompson*, 1962], and ~60% of type II bursts exhibit harmonic structure [*Kundu*, 1965]. Second, a possible way in which a shock wave might contribute to the 200-MHz emission that often comprises the low-frequency branch of the U-shaped spectrum is through the flare continuum emission designated as FC II by *Robinson and Smerd* [1975]. This emission follows the type II burst at any frequency and is thought to be due to shock-accelerated electrons trapped in a large-scale magnetic loop [*Robinson*, 1978]. To see if either the type II or FC II could contribute to the 200-MHz emission in U bursts, we determined if the associated (if any) type II burst was in progress at the time of the 200-MHz peak (within the sliding 5-min window) for each of the U bursts in our sample. We counted as concomitant those cases in which type II bursts were in progress or began within ≤0.5 min after the average peak time at 200 MHz. Since the low-frequency branch of the U-shaped spectrum may be due to flash phase accelerated electrons, we also looked to see if a type III burst was in progress during the low-frequency maximum (or ended ≤0.5 min before the 200-MHz maximum or began ≤0.5 min after it), since these emissions are a characteristic component of the impulsive phase [*Kane*, 1974]. The results of the timing comparisons were as follows:

| | In Progress at Time of 200-MHz Peak |
|---|---|
| Type II only | 19% (20/103) |
| Type II and type III | 30% |
| Type III only | 44% |
| Neither | 7% |

We caution that as pointed out by *Svestka and Fritzova-Svestkova* [1974], it is impossible to tell if type III and the 200-MHz emission maxima are exactly coincident without examining the sweep frequency records because typically these large type III bursts last for several minutes and are composed of tens of individual bursts.

From these figures it can be seen that the FC II and type II emission could contribute to the peak 200-MHz emission in U bursts in at most ~50% of the cases, assuming that the starting frequency of the fundamental type II emission is ≳100 MHz. For the 21 U bursts in our sample that occurred during Culgoora observing hours we were able to check the starting frequencies of the associated type II bursts from a compilation by *Robinson et al.* [1983]. Harmonic emission started at $f \gtrsim$ 200 MHz for only about half of these events, (11/21 = 52%) [cf. *Maxwell and Thompson*, 1962], although for those events where the type II was in progress at the time of the 200-MHz peak, harmonic emission began at $f \gtrsim 200$ MHz in 71% (10/14) of the cases. For 51% of the U bursts in our sample a type II burst was either not observed, ended prior to, or began ≳0.5 min after the peak of the 200-MHz emission. A comparison of the peak 200-MHz flux densities of these U bursts (51%) with those of the type II coincident events revealed no marked differences between the two distributions. The median 200-MHz flux value of the type II coincident events (3400 sfu) is larger, as might be expected, but the median value for the noncoincident events (2000 sfu) is also well above the minimum value (≳1000 sfu) required for the classical U burst. Since the 200-MHz peak is coincident with type III emission for 74% of the U bursts examined, it appears that flash phase electrons are primarily responsible for the low-frequency branch of the U-shaped spectrum.

## 4. DISCUSSION

*Summary*

From this study of the peak flux density spectra of nearly 200 large ($Sp$ ($\geq 2$ GHz) ≥ 800 sfu) microwave bursts and their associated proton and sweep frequency emissions we have found the following:

1. There appear to be two basic peak flux density spectral types: (1) U-shaped, with two maxima ≥ 800 sfu in the range from 200 MHz to ≥10 GHz (59% of all events) and (2) cutoff, with a spectral maximum ≥ 800 sfu at $f \geq 2$ GHz and $Sp$ (200 MHz) < 100 sfu (18%). Nine percent of the events had what we termed intermediate spectra with a spectral maximum ≥ 800 sfu at $f \geq 2$ GHz and 100 sfu ≤ $Sp$ (200 MHz) < 800 sfu. We were unable to classify 15% of the events in our data sample.

2. If the current NOAA proton prediction threshold of $J(>10$ MeV) ≥ 10 protons cm$^{-2}$ s$^{-1}$ sr$^{-1}$ had been in effect during the period covered by our data base (1965–1979), the U burst "yes or no" proton event forecast tool would have had a

false alarm rate of ~50% and would have failed to provide a warning for ~50% of the significant prompt proton flares attributable to disk flares during this period. These figures apply if proton event warnings had been issued only following U bursts associated with western hemisphere flares. If warnings had been made following U bursts from anywhere on the sun (85°E ≥ $\phi$ ≤ 85°W), the false alarm rate would have been 73%, and 39% of the significant proton events would not have been predicted by this method.

3. The associations of flare bursts (85°E ≥ $\phi$ ≤ 85°W) of different peak flux density spectral type with type II and/or type IV bursts and with > 10-MeV proton events of any peak intensity (≥0.01 protons cm$^{-2}$ s$^{-1}$ sr$^{-1}$) are as follows: U-shaped, type II/IV (90%), protons (77%); intermediate, type II/IV (78%), protons (73%); cutoff type II/IV (22%), protons (33%).

4. In 74% of the microwave bursts with U-shaped spectra the 200-MHz emission peak occurred during a type III event. For 49% of the U bursts a type II was in progress during, or began ≤ 0.5 min after, the peak 200-MHz emission.

5. Several (eight of 46) of the proton events with $J$ (> 10 MeV) ≥ 10 protons cm$^{-2}$ s$^{-1}$ sr$^{-1}$ (1965–1979) originated in visible hemisphere flares with relatively weak ($Sp$ < 300 sfu) associated 200-MHz emission.

### *The U Burst as a Prediction Tool*

The pessimistic picture of the U-shaped peak flux density spectrum as a proton prediction tool that we have presented in this study contrasts with that of earlier studies [e.g., *Castelli and Barron*, 1977]. We point out, however, that the differences in our results stem primarily from (1) the use of a lower event prediction threshold than was previously used, i.e., $J$(> 10 MeV) ≥ 10 protons cm$^{-2}$ s$^{-1}$ sr$^{-1}$ [*Heckman*, 1979] versus $J$ ≥ 40 protons cm$^{-2}$ s$^{-1}$ sr$^{-1}$ [*Castelli*, 1968; *Juday and Adams*, 1969; *Castelli and Tarnstrom*, 1978] and (2) the observation after 1976, the final year considered in studies by *Castelli and Barron* [1977] and *Castelli and Tarnstrom* [1978], of four large ($J$ ≥ 40) proton events that originated in flares with non-U microwave spectra. Despite differences in the basic approach (and the classification of several individual events) between ours and the earlier studies, our results pertaining to the U burst as a forecast tool are in general agreement with those of Castelli and his coworkers for the prediction threshold and the time period they considered. Moreover, until a more reliable early indicator of proton acceleration/escape in flares is identified the U burst tool (or variants [cf. *Akinyan et al.*, 1979]) will likely continue to be used in combination with H$\alpha$ and sweep frequency radio signatures at solar forecast centers.

Nevertheless, the recent observation of four large ($J$ ≥ 40) proton events associated with microwave bursts with non-U spectra underscores suspicions raised in other studies [e.g., *Kahler*, 1982*a*,*b*; *Cliver et al.*, 1983*c*] that the U-shaped spectrum may not have a strong physical connection with the process by which the protons observed at earth are accelerated. Even for the $J$ ≥ 40 events that were preceded in ~80% of the cases by bursts with U-shaped spectra, the wide variation in spectral shape among events like April 6, 1971 (Figure 2*c*), with a large decimetric peak and weak 200-MHz emission, events like July 7, 1966, [*Svestka*, 1976, p. 193], and January 24, 1971 (Figure 3*b*), that are classified as U bursts because of relatively sharp spectral variations in the decimetric range, and the more classic types such as March 24, 1966, and November 5, 1974 (Figures 1*a* and 1*b*), make it difficult to embrace U bursts as a special class of microwave bursts that are somehow uniquely related to interplanetary proton events. We attribute the high percentage association (31 of 34 western hemisphere cases) of these phenomena to the fact that U bursts are generally (90% of the time) accompanied by type II and/or type IV bursts indicative of a second-stage process involving a shock wave.

### *The Low-Frequency Branch of the U-shaped Spectrum*

*Kundu and Vlahos* [1982] have suggested that the U-shaped spectrum is a reflection of nothing more than the fact that there are two different sources of burst radiation, one for centimeter wavelengths and one for decimeter wavelengths, with different electron energy distributions and different magnetic fields. In this study we asked whether the two emission maxima might not also reflect different acceleration processes for the radiating electrons that give rise to the separate branches of the U-shaped spectrum. In particular, we entertained a picture in which a shock wave might account for the low-frequency (~200 MHz) branch of the U-shaped spectrum, either through emission from the second harmonic of the type II burst or through flare continuum (FC II) radiation [*Robinson*, 1978] in those cases where the starting frequency of the fundamental type II burst is ≳100 MHz. We found that this picture cannot obtain, in general, since a type II burst was in progress at the time of the low-frequency maximum (nominally at 200 MHz) for only about half of the U bursts in our sample. This conclusion is based on the assumption that the shock either does not exist or is incapable of accelerating electrons prior to the occurrence of a type II burst. In 74% of the cases the peak 200-MHz emission in U bursts occurred at the time of reported type III emission, suggesting that the low-frequency branch of the U-shaped spectrum is primarily due to radiation from flash phase electrons. In fact, since both the starting frequency and intensity of type III emission can be expected to increase with the size of the associated microwave (hard X ray) burst [*Kane*, 1981], it seems likely that for the U bursts the low-frequency branch is often due to the type III burst itself. In this context we note that in addition to having relatively weak proton and type II associations the cutoff events in our sample were also deficient in type III emission.

### *U Bursts and the Big Flare Syndrome*

The large ($Sp$ (≥ 2 GHz) ≥ 800 sfu) microwave bursts examined in the study tend to have U-shaped peak flux density spectra (59%, 113/193) and to be associated with type II/IV bursts (76%, 139/184) and > 10-MeV proton events (69%, 77/111). However, the small number of events with U-shaped spectra that lacked both type II and type IV emission were poorly associated with interplanetary protons. This argues that the type II/IV burst is the critical observable for particle acceleration and not the U-shaped spectrum. The fact that the statistical association of the cutoff bursts with proton events parallels their associations with type II/IV bursts provides additional support for this contention. In addition, we note that for the majority of the U bursts in our sample the high fluxes often observed near 200 MHz appear to be more closely related to type III emission than to the shock wave (type II burst) that is presumably accelerating the protons. Thus we conclude that the U-shaped spectrum at both high (~10 GHz) and low (~200 MHz) frequencies is primarily an impulsive phase phenomenon and that the observed statistical U burst-proton association is probably due to the big flare syndrome [*Kahler*, 1982*a*] rather than the result of a direct physical connection between these two phenomena. The observation that the

cutoff events are deficient in type III as well as type II emission relative to the U bursts, however, suggests that a less direct or "once-removed" connection may exist between the U-shaped spectrum and proton acceleration in that the probability of shock formation (type II/protons) in these large flares apparently increases in more open magnetic field structures (type III/U burst).

*Impulsive Phase Proton Acceleration*

*Forrest* [1983] and *Forrest and Chupp* [1983] have recently presented gamma ray evidence indicating that ions are accelerated along with electrons in the impulsive phase of all flares. However, *Cliver et al.* [1983*a*] have shown that the correlation between gamma ray line fluences and interplanetary proton fluxes is poor. This leaves open the possibility that the ions observed at the sun via gamma ray line emission are accelerated by a different process than the bulk of the protons detected at 1 AU. In particular, we favor a picture, as indicated above, in which the protons observed at earth are accelerated in a second-stage process involving a shock wave [cf. *Kahler et al.*, 1984].

*Proton Flares With Weak 200-MHz Emission*

As a final comment, we note that in the largest disk flare associated proton events ($J > 10$) observed from 1965 to 1979 the 200-MHz emission was often relatively weak, $\lesssim 300$ sfu in eight of 46 cases. While either type II or type IV emission was lacking in a comparable number of cases, the identification of these sweep frequency events is more subject to interpretation, and it is possible that upon reexamination of the original records the missing phenomenon might be noted. The 200-MHz records should be less ambiguous, however, and we considered the highest flux density reported by any observatory during the associated Hα flare. Moreover, even several of the events with $J$ (>10 MeV) $\gtrsim 40$ protons cm$^{-2}$ s$^{-1}$ sr$^{-1}$ had relatively weak emission at $f \sim 200$ MHz, the lowest frequency currently monitored on a 24-hour per day basis by the ground-based solar radio patrol. Thus the low-frequency ($\sim$200 MHz) branch of the classical (i.e., $Sp \gtrsim 1000$ sfu) U burst does not appear to be a requirement for the occurrence of a large, prompt proton event. The lack of a radio response at this frequency, commensurate with the observed intensities of these large proton events, indicates that for certain flares a radio signature of particle acceleration/escape may only exist at lower frequencies (<200 MHz), as was the case for the October 4, 1965, proton flare [*Böhme*, 1972*a*,*b*], the ground level event parent flare on August 21, 1979 [*Cliver et al.*, 1983*b*], and the eruptive filament event on December 5, 1981 (S. W. Kahler et al., unpublished manuscript, 1985).

*Acknowledgments.* We thank R. E. McGuire for providing proton data plots and S. W. Kahler and M. A. Shea for critical readings of the manuscript. L. I. McNamara was supported by a Senior Research Associateship from The National Research Council while at AFGL. We are grateful to A. Novak for typing and editing assistance.

The Editor thanks R. P. Lin and another referee for their assistance in evaluating this paper.

## REFERENCES

Akinyan, S. T., I. M. Chertok, and V. V. Fomichev, Quantitative forecasts of solar protons based on solar flare radio data, in *Solar Terrestrial Predictions Proceedings*, edited by R. F. Donnelly, vol. 3, p. D-14, National Oceanic and Atmospheric Administration, Boulder, Colo., 1979.

Bell, B., Type IV solar radio bursts, geomagnetic storms, and polar cap absorption (PCA) events, *Smithson. Contrib. Astrophys.*, *8*, 119, 1963.

Böhme, A., The time behavior of the continua during the initial stage of type IV bursts, *Sol. Phys.*, *24*, 457, 1972*a*.

Böhme, A., Spectral behaviour and proton effects of the type IV broad band continua, *Sol. Phys.*, *25*, 478, 1972*b*.

Böhme, A., and A. Kruger, On the type IV bursts of August 2, 4 and 7, 1972, Collected Data Reports on August 1972 Solar-Terrestrial Events, *Rep. UAG-28*, part 1, p. 260, World Data Cent. A for Sol.-Terr. Phys., Boulder, Colo., 1973.

Castelli, J. P., Observation and forecasting of solar proton events, *Rep. AFCRL-68-0104*, Air Force Cambridge Res. Lab., Hanscom AFB, Mass., 1968.

Castelli, J. P., and W. R. Barron, A catalog of solar radio bursts 1966–1976 having spectral characteristics predictive of proton activity, *J. Geophys. Res.*, *82*, 1275, 1977.

Castelli, J. P., and D. A. Guidice, On the classification, distribution, and interpretation of solar microwave burst spectra and related topics, *Rep. AFCRL-72-0049*, Air Force Cambridge Res. Lab., Hanscom AFB, Mass., 1972.

Castelli, J. P., and G. L. Tarnstrom, A catalog of proton events 1966–1976 having non-classical solar radio burst spectra, *Rep. AFGL-TR-78-0121*, Air Force Geophys. Lab., Hanscom AFB, Mass., 1978.

Castelli, J. P., J. Aarons, G. A. Michael, Flux density measurements of radio bursts of proton-producing flares and nonproton flares, *J. Geophys. Res.*, *72*, 5491, 1967.

Castelli, J. P., J. Aarons, D. A. Guidice, and R. M. Straka, The solar radio patrol network of the USAF and its application, *Proc. IEEE*, *61*, 1307, 1973.

Cliver, E. W., Secondary peaks in solar microwave outbursts, *Sol. Phys.*, *84*, 347, 1983.

Cliver, E. W., J. A. Secan, E. D. Beard, and J. A. Manley, Prediction of solar proton events at the Air Force Global Weather Central's space environmental forecasting facility, in *Proceedings, Conference on Effect of the Ionosphere on Space and Terrestrial Systems*, edited by J. M. Goodman, p. 393, U.S. Government Printing Office, Washington, D. C., 1978.

Cliver, E. W., S. W. Kahler, M. A. Shea, and D. F. Smart, Injection onsets of ~2 GeV protons, ~1 MeV electrons, and ~100 keV electrons in solar cosmic ray flares, *Astrophys. J.*, *260*, 362, 1982.

Cliver, E. W., D. J. Forrest, R. E. McGuire, and T. T. von Rosenvinge, Nuclear gamma rays and solar proton events, *Cosmic Ray Conf. Pap. Int. Conf. Cosmic Rays 18th*, *10*, 342, 1983*a*.

Cliver, E. W., S. W. Kahler, H. V. Cane, M. J. Koomen, D. J. Michels, R. A. Howard, and N. R. Sheeley, Jr., The GLE-associated flare of 21 August, 1979, *Sol. Phys.*, *89*, 181, 1983*b*.

Cliver, E. W., S. W. Kahler, P. S. McIntosh, Solar proton flares with weak impulsive phases, *Astrophys. J.*, *264*, 699, 1983*c*.

Cliver, E. W., L. F. McNamara, and L. C. Gentile, Peak-flux-density spectra of large solar radio bursts and proton emission from flares, Air Force Geophys. Lab., Hanscom AFB, Mass., *Rep. AFGL*, in press, 1985.

De Jager, C., Solar flares: properties and problems, in *Proceedings of COSPAR Symposium on Solar Flares and Space Research*, edited by C. De Jager and Z. Svestka, p. 1, North Holland, Amsterdam, 1969.

Dodson, H. W., E. R. Hedeman, and O. C. Mohler, Survey and comparison of solar activity and energetic particle emission in 1970, *Rep. AFGL-TR-77-0222*, Air Force Geophys. Lab., Hanscom AFB, Mass., 1977.

Dodson, H. W., E. R. Hedeman, and O. C. Mohler, Solar and geophysical associations with the principal energetic particle events in 1971 and 1972, *Rep. AFGL-TR-78-0266*, Air Force Geophys. Lab., Hanscom AFB, Mass., 1978.

Forrest, D. J., Solar γ-ray lines, *AIP Conf. Proc.*, *101*, 3, 1983.

Forrest, D. J., and E. L. Chupp, Simultaneous acceleration of electrons and ions in solar flares, *Nature*, *305*, 5932, 1983.

Guidice, D. A., E. W. Cliver, W. R. Barron, and S. Kahler, The air force RSTN system, *Bull. Am. Astron. Soc.*, *13*, 553, 1981.

Harvey, G. A., 2800 megacycle per second radiation associated with type II and type IV solar radio bursts and the relation with other phenomena, *J. Geophys. Res.*, *70*, 2961, 1965.

Heckman, G., Predictions of the space environment services center, in *Solar Terrestrial Predictions Proceedings*, vol. 1, edited by R. F. Donnelly, p. 322, National Oceanic and Atmospheric Administration, Boulder, Colo. 1979.

Juday, R. D., and G. W. Adams, Riometer measurements, solar proton intensities and radiation dose rates, *Planet Space Sci.*, *17*, 1313, 1969.

Kahler, S. W., The role of the big flare syndrome in correlations of

solar energetic proton fluxes and associated microwave burst parameters, *J. Geophys. Res.*, *87*, 3439, 1982*a*.

Kahler, S. W., Radio burst characteristics of solar proton flares, *Astrophys. J.*, *261*, 710, 1982*b*.

Kahler, S. W., E. Hildner, and M. A. I. van Hollebeke, Prompt solar proton events and coronal mass ejections, *Solar Phys.*, *57*, 429, 1978.

Kahler, S. W., N. R. Sheeley, Jr., R. A. Howard, M. J. Koomen, D. J. Michels, R. E. McGuire, T. T. von Rosenvinge, and D. V. Reames, Associations between coronal mass ejections and solar energetic proton events, *J. Geophys. Res.*, *89*, 9683, 1984.

Kai, K., Evolutional features of solar microwave type IV bursts, *Publ. Astron. Soc. Jpn.*, *20*, 140, 1968.

Kane, S. R., Impulsive (flash) phase of solar flares: Hard x-ray, microwave, euv and optical observations, in *Coronal Disturbances*, edited by G. Newkirk, Jr., p. 105, D. Reidel, Hingham, Mass., 1974.

Kane, S. R., Energetic electrons, type III radio bursts, and impulsive solar flare x-rays, *Astrophys. J.*, *247*, 1113, 1981.

Kundu, M. R., *Solar Radio Astronomy*, Wiley Interscience, New York, 1965.

Kundu, M. R., and F. T. Haddock, A relation between solar radio emission and polar cap absorption of cosmic noise, *Nature*, *186*, 610, 1960.

Kundu, M. R., and L. Vlahos, Solar microwave bursts—A review, *Space Sci. Rev.*, *32*, 405, 1982.

Lin, R. P., The emission and propagation of 40 keV solar flare electrons, I, The relationship of 40 keV electron to energetic proton and relativistic electron emission by the sun, *Sol. Phys.*, *12*, 266, 1970.

Lin, R. P., and H. S. Hudson, Non-thermal processes in large solar flares, *Sol. Phys.*, *50*, 153, 1976.

Mason, G. M., G. Gloeckler, and D. Hovestadt, Temporal variations of nucleonic abundance in solar flare energetic particle events, II, Evidence for large scale shock acceleration, *Astrophys. J.*, *280*, 902, 1984.

Maxwell, A., Dynamic spectra of four solar radio bursts during the period 1972 August 2–7, Collected Data Reports on August 1972 Solar-Terrestrial Events, *Rep. UAG-28*, part 1, p. 255, World Data Cent. A for Sol.-Terr. Phys. Boulder, Colo., 1973.

Maxwell, A., and A. R. Thompson, Spectral observations of radio bursts, II, Slow drift bursts and coronal streamers, *Astrophys. J.*, *135*, 138, 1962.

Maxwell, A., R. J. Defouw, and P. Cummings, Radio evidence for solar corpuscular emission, *Planet. Space Sci.*, *12*, 435, 1964.

O'Brien, W. E., The prediction of solar proton events based on solar radio emission, *Rep. AFCRL-70-0425*, Air Force Cambridge Res. Lab., Hanscom AFB, Mass., 1970.

Pallavicini, R., S. Serio, and G. S. Vaiana, A survey of soft x-ray limb flare images: The relation between their structure in the corona and other physical parameters, *Astrophys. J.*, *216*, 108, 1977.

Pick-Gutmann, M., Evolution des emissions radioelectriques solaires de type IV et leur relation avec d'autres phenomenes solaires et geophysiques, *Ann. Astrophys.*, *24*, 183, 1961.

Robinson, R. D., A study of solar flare continuum events observed at metre wavelengths, *Aust. J. Phys.*, *31*, 533, 1978.

Robinson, R. D., and S. F. Smerd, Solar flare continua at the metre wavelengths, *Proc. Astron. Soc. Aust.*, *2*, 374, 1975.

Robinson, R. D., J. M. Tuxford, K. V. Sheridan, and R. T. Stewart, A catalogue of major metre-wavelength solar events recorded by the DAPTO and Culgoora solar radio observatories (1961–1981), *Proc. Astron. Soc. Aust.*, *5*, 84, 1983.

Roelof, E. C., H. W. Dodson, and E. R. Hedeman, Dependence of radio emission in large Hα flares 1967–1970 upon the orientation of the local solar magnetic field, *Sol. Phys.*, *85*, 339, 1983.

Smart, D. F., and M. A. Shea, Solar proton event classification system, *Solar Phys.*, *16*, 484, 1971.

Svestka, Z., *Solar Flares*, D. Reidel, Hingham, Mass., 1976.

Svestka, Z., and L. Fritzova-Svestkova, Type II radio bursts and particle accelera ion, *Sol. Phys.*, *36*, 417, 1974.

Svestka, Z., and P. Simon (Eds.), *Catalog of Solar Particle Events, 1955–1969*, D. Reidel, Hingham, Mass., 1975.

Tanaka, H., J. P. Castelli, A. E. Covington, A. Kruger, T. L. Landecker, and A. Tlamicha, Absolute calibration of solar radio flux density in the microwave region, *Sol. Phys.*, *29*, 243, 1973.

Thompson, R. L., and J. A. Secan, Geophysical forecasting at AFGWC, in *Solar Terrestrial Predictions Proceedings*, vol. 1, edited by R. F. Donnelly, p. 350, National Oceanic and Atmospheric Administration, Boulder, Colo., 1979.

van Hollebeke, M. A. I., L. S. M. Sung, and F. B. McDonald, The variation of solar proton energy spectra and size distribution with heliolongitude, *Sol. Phys.*, 41, 189, 1975.

Wild, J. P., S. F. Smerd, and A. A. Weiss, Solar bursts, *Ann. Rev. Astron. Astrophys.*, *1*, 291, 1963.

E. W. Cliver, Air Force Geophysics Laboratory, Space Physics Division (PHP), Hanscom Air Force Base, MA 01731.

L. C. Gentile, Physics Research Division, Emmanuel College, 400 The Fenway, Boston, MA 02115.

L. F. McNamara, Ionospheric Prediction Service, P.O. Box 702, Darlinghurst, New South Wales 2010, Australia.

(Received September 11, 1984;
revised November 29, 1984;
accepted February 18, 1985)